Cyclic and Post-Cyclic Behavior of Silt-Rich, Transitional Soils of the Pacific Northwest:

A Data Archive for Geo-professionals in Practice and Research

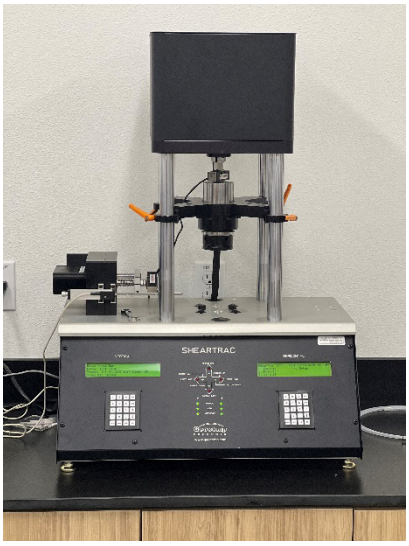

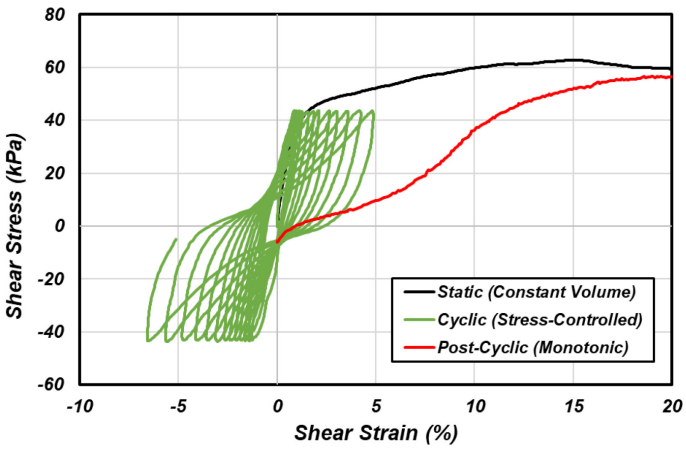

August 2022

Prepared for

Oregon Department of Transportation

Bridge Engineering Section

Salem, Oregon

Prepared by

NEW ALBION
Geotechnical, Inc.

Title: **Cyclic and Post-Cyclic Behavior of Silt-Rich, Transitional Soils of the Pacific Northwest: A Database for Geo-professionals in Practice and Research**

Authors: Stephen E. Dickenson[1], Arash Khosravifar[2], Michael Beaty[3], Jason Bock[4], Diane Moug[2], Scott Schlechter[4], and Jan Six[5]

Principal Investigator: Stephen E. Dickenson, Ph.D., P.E. (CA, OR, NV, WA), D. PE

sed@newalbiongetotechnical.com

Performing Organization: New Albion Geotechnical, Inc.

3400 San Juan Drive

Reno, NV 89509

ABSTRACT

As a resource for researchers and practitioners focused on the seismic performance of major civil infrastructure, including surface and maritime transportation systems, the project team has developed a large, publicly accessible database of static, cyclic, and post-cyclic laboratory test data for predominantly silt-rich (transitional) soils with properties and dynamic behaviors typically lying between, or transitioning from, "sand-like" behavior and "clay-like" behavior. Silt-rich soil deposits are prevalent in the Pacific Northwest, and in regions of British Columbia and Alaska. This database has been established with laboratory data and supporting documentation from geotechnical project reports and applied research investigations for soil units primarily located within these three regions, and supplemented to a lesser degree with data from other regions. The collection of laboratory test data, supporting documentation, and meta-data are curated by the second author at the Department of Civil & Environmental Engineering, Portland State University and managed as a "living data repository" that is being continually updated with new data from projects throughout the Pacific Northwest.

The database is comprised of the results of predominantly Direct Simple Shear (DSS) tests with supplementary data from Triaxial compression (TX) tests, and currently includes the results of over 450 cyclic tests. The focus of the cyclic testing included evaluation of the progressive accumulation of cyclically induced shear strain, generation of excess pore pressure, and strain-dependent stiffness and damping, and post-cyclic behavior. Data from stress-controlled and strain-controlled tests have been collected. On many projects, post-cyclic tests were performed to evaluate one-dimensional volumetric strain associated with post-cyclic reconsolidation of the specimens (55 tests) and constant-volume monotonic tests to evaluate the cyclic degradation of stiffness and strength of the fine-grained soils (151 tests). The data is presented in this report as plots of cyclic resistance and post-cyclic behavior, accompanied by supporting tabulation of index properties, stress history, and static stress-strain behavior, when available. The data compilation includes silt

from a variety of depositional environments primarily from the three regions of interest, thus the samples support assessment of the influence of factors such as mineralogy, fabric, composition, consistency, density, stress-history, and aging on the cyclic and post-cyclic behavior of the soil.

This database of over 450 tests provides researchers and practitioners with a basis for laboratory-based evaluation of the following: (i) cyclic resistance for a range of reference shear strains, (ii) post-cyclic stress-strain-strength behavior, and (iii) post-cyclic one-dimensional volumetric strain. The cyclic resistance of the silt has been evaluated following well-established procedures accounting for parameters such as soil consistency, stress history, effective stress, and to a lesser degree (due to limited data availability) static shear stress bias. This report primarily serves as a summary of the collected data. General observations and limited interpretation of the data trends for cyclic resistance, post-cyclic stress-strain behavior, and volumetric strain of silt and low-plasticity clay are presented; however, it should be noted that the general interpretations are merely provided to provide background for ongoing research being completed by the authors.

KEY WORDS

Silt, cyclic tests, cyclic strength, residual strength, volume changes

REFERENCE CITATION

The contents of this report are public domain, and the project team encourages the use of this data for research on the cyclic behavior of transitional soils and as a supplement to site-specific data in engineering practice (subject to the Limitations provided in this data report). The co-authors request that appropriate attribution be provided for the use of the data collected and presented in this report. The following citation should be provided in technical reports and publications making use of the data presented in this report:

Dickenson, S. E., Khosravifar, A., Beaty, M. H., Bock, J., Moug, D., Schlechter, S. M., and Six, J. (2021). "Cyclic and Post-Cyclic Behavior of Silt-Rich, Transitional Soils of the Pacific Northwest; A Database for Geo-professionals in Practice and Research," Data report prepared for the Oregon Department of Transportation, Bridge Engineering Section, Salem, Oregon, by New Albion Geotechnical, Inc., Reno, NV

[1] New Albion Geotechnical, Inc., Reno, NV

[2] Portland State University, Dept. of Civil & Environmental Engineering, Portland, OR

[3] Beaty Engineering, LLC, Beaverton, OR

[4] GRI, Tigard, OR

[5] Shannon & Wilson, Lake Oswego, OR

DISCLAIMER

This research effort was initiated with sponsorship provided by the Oregon Department of Transportation. Ongoing development of the database has been made possible by direct funding or in-kind support provided by the following organizations: New Albion Geotechnical, Inc., the Department of Civil and Environmental Engineering, Portland State University, and GRI.

The extensive collection of project data would not have been possible without additional, significant in-kind contributions from several organizations. This support has been provided by Beaty Engineering, LLC (Beaverton, OR), GRI (Tigard, OR), Jacobs (Corvallis and Portland, OR, and Seattle, WA), Shannon & Wilson, Inc. (Lake Oswego, OR, and Seattle, WA), and the Washington State Department of Transportation (WSDOT). This in-kind support included, but was not limited to, the following: (i) geologic, geophysical, and geotechnical documentation at project sites, (ii) cyclic test data on silt-rich soil, (iii) personnel time provided throughout the project for input, writing, reviewing, and final editing of the data report, and (iv) assistance with the evaluation of cyclic and post-cyclic data.

LIMITATIONS

This data report, which contains preliminary observations and interpretations of data trends, provides the summary of a multi-year investigation involving the collection and synthesis of cyclic and post-cyclic test data for predominantly silt-rich soils primarily obtained at sites in the Pacific Northwest. The data repository has been supplemented with project data from sites in Alaska, British Columbia, and central California. The laboratory data and project reports were initially assembled from project files provided by the project team. This archive was supplemented with project data generously provided by ODOT, WSDOT, and numerous practicing geotechnical engineers. The data summary, project narrative, and recommendations provided in this data report are based on the information provided by the agencies and geotechnical practitioners as part of this applied research investigation. The project team encourages the use of this data for research on the cyclic behavior of transitional soils and as a supplement to site-specific data in engineering practice with consideration of the limitations discussed herein. With respect to the latter, this data report provides information that may be useful for initial assessment of silt behavior for project-specific applications; however, the project team strongly recommends that seismic analysis leading to design be made on the basis of site-specific data including the use of project specific cyclic testing as appropriate.

The project team highlights potential limitations associated with utilization of data trends provided in this report for both research and practice. These observations and issues should be considered for project-specific applications. Specific limitations include the following:

- Beyond screening of the static, cyclic, and post-cyclic data, and trends, for each project data set, the project team did not reevaluate aspects of field sampling, degree of sample disturbance, methods of specimen preparation in the lab, calibration of instrumentation, other testing protocols, or quality control practices. Due to the range of likely variation of these aspects across the test results included in the database, some additional variability in the data compilations and interpretations should be anticipated.
- The findings of this investigation are based on project reports obtained from numerous sources. The cyclic testing data was performed and interpreted by others; therefore, the validity and quality of data obtained by a large group of independent practitioners cannot be guaranteed by the project team.
- The project team did not participate in the implementation of the work by other consultants and did not independently verify the accuracy or completeness of the information contained in the project reports.
- This work has been performed by the project team to comply with the standards of care and skill ordinarily exercised by professionals of the geologic and geotechnical profession practicing in the same or similar localities of western North America. Within the limitations imposed by scope, schedule, budget, and provided information, or as described in this report, the information presented in this report was prepared in accordance with generally

accepted professional engineering principles and practice at the time this report was prepared. No other representation, and no warranty or guarantee, is provided.

ACKNOWLEDGEMENTS

On behalf of the project team, the lead author greatly appreciates the contributions made by numerous geo-professionals who generously donated their time, data reports, and encouragement throughout the development of this database. The database, reporting, and on-line access in its current format would not have been possible without the tremendous assistance of the geotechnical community in the Pacific Northwest. The project team, researchers, and practicing engineers in the region owe a debt of gratitude to the following individuals and organizations for providing the project data summarized in this report.

This investigation was made possible by the interest, commitment, and support of the Oregon Department of Transportation, Bridge Engineering Section. The project was initiated under the guidance of Jan Six, PE, GE, Sr. Geotechnical Engineer, Bridge Engineering Section (retired), currently with Shannon & Wilson, Inc., and continued with the encouragement and insights provided by Susan Ortiz, PE, GE, Sr. Geotechnical Engineer, Bridge Engineering Section.

Laboratory data from many of the project sites in Washington was made available by Tony Allen, P.E., State Geotechnical Engineer, WSDOT (retired). The project team is grateful to Tony for providing access to a wealth of data obtained in support of WSDOT projects involving silt-rich soil. We also greatly appreciate the substantial contributions made by many members of the design engineering teams on those numerous WSDOT projects.

In addition to the data provided from ODOT and WSDOT projects, the collection of project files for the database required significant contributions by numerous individuals. The usefulness of the laboratory archive was significantly enhanced by the generous contributions of project reports by the regional engineering community. The project team wishes to thank the following individuals for their tremendous support and contributions throughout the execution of this project:

Donald Anderson, Jacobs	Ender Parra, MEG Consulting (Tetra Tech)
Monique Anderson, Shannon & Wilson, Inc.	Nick Paveglio, NV5
Alan Bean, Northwest Geotech, Inc.	Bill Perkins, Shannon & Wilson, Inc.
King Chin, GeoEngineers, Inc.	Park Piao, Shannon & Wilson, Inc.
Sam Christie, Kleinfelder, Inc.	Seungcheol Shin, Jacobs
Karen Dawson, Jacobs	Brett Shipton, NV5
Michael Eller, Kleinschmidt Associates	Sam Sideras, Shannon & Wilson, Inc.
Jack Gordon, GRI	Wes Spang, GRI
Mike Greenfield, Greenfield Geotechnical	James Struthers, WSDOT

Ben Haines, FHWA	John Sully, MEG Consulting Ltd. (Tetra Tech)
Nason McCullough, Jacobs	Paul Sully, MEG Consulting Ltd. (Tetra Tech)
Reda Mikhail, Golder	Deanne Takasumi, Jacobs
Scott Mills, NV5	Andy Vessely, Cornforth Consultants, Inc. (retired)
Robert Mitchell, Shannon & Wilson, Inc.	Rick Wentz, Wentz Pacific, Ltd.
Todd Mooney, WSDOT	Allison Pyrch, Hart Crowser (now Haley & Aldrich)
Travis Munson, Jacobs	Joseph Harmon, Hart Crowser (now Haley & Aldrich)
David Hemstreet, Alaska DOT & PF	Brice Exley, Hart Crowser (now Haley & Aldrich)

The significant contributions made to this project by the geotechnical practitioners previously acknowledged have been complemented by two active researchers who, as principal investigators, have completed valuable laboratory and field-based investigations of the cyclic behavior of silt-rich, transitional soils. Both have produced seminal work on the topic that has been adopted by geotechnical practitioners on major projects worldwide. The first author is grateful to Professor Ross Boulanger (Department of Civil and Environmental Engineering, University of California, Davis) for his tremendous support and contribution of research reports, graduate student theses and dissertations prepared under his guidance, and other technical documents that have contributed to the understanding of the cyclic resistance of fine-grained soils. This project, and others led by the first author also focused on the dynamic behavior of silt and clay, have greatly benefited from his insights, freely shared research reports, and high-quality lab data.

The project team is also grateful to Professor Dharma Wijewickreme (Department of Civil Engineering, University of British Columbia) for his generosity with shared technical materials from his library of applied research in support of the project. Dr. Wijewickreme has also provided research reports, graduate student theses and dissertations prepared under his guidance, and technical publications addressing the cyclic and post-cyclic behavior of silt.

The project team would also like to recognize the notable contributions that were made by Portland State University students Robert Schomp and Tanner Bryantt. Both students helped extract cyclic testing and in-situ testing data from the geotechnical reports.

The research team is also especially grateful to Christina Villeneuve, RG (GRI, Director of Business Development & Marketing, Geologist), for her tremendous effort, patience, and support with the production of this data report through multiple working drafts, input from 7 active co-authors, and work provided over weekends and evenings. She has been a valuable member of the research team by leading efforts on the assembly, formatting, and presentation of the final report.

CONTENTS

Chapter 1: Introduction

Chapter 2: Cyclic Shear Strain Accumulation and Resistance in Stress-Controlled Tests

Chapter 3: Post-Cyclic Stress-Strain Behavior and Cyclic Degradation of Undrained Shear Strength

Chapter 4: Post-Cyclic One-Dimensional Volumetric Strain

Chapter 5: Excess Pore Pressure Generation in Strain-Controlled Cyclic Tests

Chapter 6: Cone Penetration Test and Cyclic Shear Resistance Data

APPENDICES

Appendix A: Alaska Project Sites

Appendix B: British Columbia Project Site

Appendix C: Oregon Project Sites

Appendix D: Washington Project Sites

Appendix E: Considerations for Testing and Interpretation of Results on Reconstituted Specimens of Silt

CHAPTER 1

Introduction

CHAPTER 1 CONTENTS

1-1 INTRODUCTION 2
1-1.1 Background and Purpose 2
1-1.2 Characteristic of the Data Set 3
1-1.3 Data Management and Curation of the Archive 5
1-1.4 Development of the On-line, Publicly Accessible Database 6
1-2 CHAPTER 1 FIGURES 7

1-1 INTRODUCTION

This report accompanies the extensive database of laboratory cyclic and post-cyclic data collected and processed by the project team on silt-rich soil primarily from the Pacific Northwest, and regions of British Columbia and Alaska. This database has been established with laboratory data and supporting documentation from geotechnical project reports and applied research investigations in these three regions. The objective of this effort has been the development of a comprehensive, publicly accessible database of cyclic and post-cyclic laboratory data on silt deposits at sites predominantly located in the Pacific Northwest. The primary goal has been the preparation of this data report and on-line data repository that serve as resources for researchers and practitioners focused on the cyclic behavior of silt and the seismic performance of structures underlain by silt deposits.

This document serves as a Data Report, with tabulation of geotechnical index properties, supporting in-situ and laboratory geotechnical parameters, and summary plots and figures for each project data set. The interpretation of test results, trends in stress- or strain-dependent behavior, implications or guidelines for practice are currently the focus of interrelated investigations by members of the project team and collaborators, and are not provided in this data report. Technical documents and publications developed using material from the database and focusing on applications in geotechnical practice will be posted at the on-line data repository (refer to Section 1.2) immediately following publication.

1-1.1 BACKGROUND AND PURPOSE

Silt-rich soil deposits are prevalent in the Pacific Northwest and in regions of British Columbia and Alaska. The cyclic and post-cyclic behavior of silt has been well-documented as intermediate between the generalized, and short-hand, characterization of soil behavior as either "sand-like" or "clay-like", thereby adding a level of complexity to projects focused on the seismic performance of earth retention systems, deep foundations, and slope stability involving silt. Laboratory-based investigations of the cyclic resistance, and perhaps more importantly, the post-cyclic stress-strain behavior of this intermediate, or "transitional", soil have contributed to the understanding that the practice-oriented procedures for evaluating the cyclic resistance and potential for triggering of liquefaction of "sand-like" soil are not appropriate for transitional soil, even with the application of standard fines-correction factors used in the former. The evolution of perspectives on post-cyclic behavior (i.e., volumetric strain, residual undrained shearing resistance, vulnerability of lateral spread and ground failure) of silt is similar in the sense that laboratory-based procedures developed for clean sands and silty sands must be applied judiciously, if at all, for transitional soil. The potentially significant differences in cyclic shear strain accumulation, progressive development of excess pore pressure, strain-dependent behavior of silt, and the implications for the seismic performance of embankments, bridge foundations and appurtenant structures have warranted the development of this database of cyclic test results for regional silt deposits.

This project was initiated by a need for practical guidance on the characterization of cyclic and post-cyclic behavior of silt for use in design of bridge foundations in Oregon and Washington. The requisite first step in this process was the collection of laboratory data from project reports and research investigations from which trends could be developed for the various silt deposits in the Pacific Northwest. With direct support from the Oregon Department of Transportation (ODOT) and substantial in-kind support from the Washington State Department of Transportation (WSDOT), the first author established a database of geotechnical reports and cyclic laboratory reports obtained for bridge projects and supplemented with additional data from applied research investigations and regional projects from consulting practice. The research and practicing communities generously supported the initial effort and made it clear that the investigation should be expanded. In response to the regional desire for a comprehensive archive of data the research team was established, which provided a wealth of experience, numerous additional project reports, and keen insights on evolving needs for additional data. From the start, the project research team has been committed to the continuing collection, synthesis, and interpretation of new data sets, and very importantly, to the development of an open, easily accessible on-line resource for researchers and practicing geo-professionals in the Pacific Northwest. The on-line repository is curated and available at the Department of Civil and Environmental Engineering, Portland State University at: https://silt.cee.pdx.edu/

1-1.2 CHARACTERISTIC OF THE DATA SET

The database is comprised of the results of predominantly Direct Simple Shear (DSS) tests with supplementary data from Triaxial compression (TX) tests, and currently includes the results of over 450 cyclic tests. The focus of the cyclic testing included evaluation of the progressive accumulation of cyclically induced shear strain, generation of excess pore pressure, and strain-dependent stiffness and damping. Data from stress-controlled and strain-controlled tests have been collected. On many projects, post-cyclic tests were performed to evaluate volumetric strain associated with post-cyclic reconsolidation of the specimens and constant-volume monotonic tests to evaluate the cyclic degradation of stiffness and strength of the fine-grained soils. An overview of the tests collected to date is provided in Table 1-1. The data is presented in this report in the form of plots of cyclic resistance and post-cyclic behavior, accompanied by supporting tabulation of index properties, stress history, and static stress-strain behavior, when the data is available.

Table 1-1: SUMMARY OF TESTS COMPILED IN THE DATABASE

Test Type	Approximate Number of Tests
Cyclic DSS (stress-controlled)	180
Cyclic DSS (strain-controlled)	52
Cyclic TX (stress-controlled)	68
Post-cyclic shear resistance (DSS)	151
Post-cyclic 1D volumetric strain (DSS + TX)	55

The database includes silt from a variety of depositional environments in the three broad geographical regions of interest (Figure 1.1), thus the testing supports assessment of the influence of factors such as composition, density, fabric, stress-history, and aging on the cyclic and post-cyclic behavior of the soil. For the sake of this data report, the depositional environment for each of the samples has been generalized as one of the following:

- Fluvial (e.g., overbank, floodplain, glacial outwash),
- Estuarine (e.g., mudflat, slough, inter-tidal zone),
- Coastal Near-shore (in shallow to intermediate water depths),
- General Alluvial,
- Mine Tailings (e.g., gravel processing and wash tailings)

At this time, the database does not include, or apply to, the following deposits:

- Loess (aeolian deposits),
- Silt-rich residual soils,
- Mine tailings,
- Deposits of silt-sized diatomaceous soil.

In addition to the general geologic description of depositional environment, the deposit is described with a reference to the general project location and, where applicable, with a name commonly used in the region. Examples include Willamette Silt, Portland Hills Silt, Lower Columbia River Silt, Lower Willamette River Silt, Seattle – Elliott Bay (Duwamish) Silt, Fraser River Silt, and Bootlegger Cove Formation. The variability in composition, consistency, and engineering properties in these various silt deposits is significant. The differences are often evident in laboratory index tests, particle size distribution, and consolidation tests routinely performed in geotechnical practice. These tests have been supplemented at several locations represented in the database with imaging and testing that is less commonly performed in engineering practice (e.g., Scanning Electron Microscopy, X-Ray Diffraction).

This collection of over 450 tests provide researchers and practitioners with a basis for evaluation of the following supporting performance-based evaluation of civil infrastructure founded on, or through, silt deposits: (i) cyclic resistance for a range of reference shear strains, (ii) post-cyclic undrained stress-strain-strength behavior, and (iii) post-cyclic one-dimensional volumetric strain. The cyclic resistance of the silts has been evaluated from the data collection following well-established procedures accounting for parameters such as soil consistency, stress history, effective stress, and to a lesser degree (due to limited data availability) static shear stress bias. The test results cover a range of fine-grained soil, which is predominantly silt, although clay-like soils have been included in the database for the sake of identifying trends in cyclic and post-cyclic behavior. The data set can be generalized as applying to predominantly ML or CL soil-types, with Plasticity Index (PI) ranging from NP to in excess of 30 (Figure 1.2), Over-Consolidation Ratio (OCR) in the laboratory testing apparatus prior to cyclic loading of 1.0 to 3.0 (as high as 8 for Anchorage, AK), and specimens from most depths ranging between 15 and 100 ft (with some down to 250 ft). It is acknowledged that the database includes test results on soils that would be typically classified as "clay-like" based on gradation and plasticity.

While this report primarily serves as a summary of the collected data, practice-oriented procedures for evaluating the cyclic resistance, post-cyclic stress-strain behavior, and volumetric strain of silt and low-plasticity clay are presented. Interpretation of the data trends and implications for performance-based seismic design in engineering practice are topics of on-going investigation by the project team.

1-1.3 DATA MANAGEMENT AND CURATION OF THE ARCHIVE

The collection of laboratory test data, supporting documentation, and meta-data are curated by Professor Khosravifar at the Department of Civil & Environmental Engineering, Portland State University, and managed as a "living archive" that is being continually updated with new data from projects throughout the Pacific Northwest. The summary geotechnical data sheets, plots, figures, and selected meta-data will be openly available for researchers and practitioners; however, the project-specific Geotechnical Data Reports, Geotechnical Design Reports, and Laboratory reports will not be made available by the project team. This is due in part to the time and effort required to maintain an open-access repository of reports and associated requests for information, and also due to confidentially agreements with numerous project owners, developers, and agencies that have generously agreed to the use of the data but have requested or required that the project site and reports not be made available.

The project team encourages regional practitioners to contribute to the expansion of the data set by providing cyclic test data and supporting geotechnical documentation, as may be permitted on a project-specific basis. All contributors will be acknowledged with credit for the data provided. Again, the long-term objective of this investigation is the creation and continuing development

of a robust dataset benefiting the research and geotechnical practice communities in the Pacific Northwest.

1-1.4 DEVELOPMENT OF THE ON-LINE, PUBLICLY ACCESSIBLE DATABASE

The data presented in this report are available through an online repository that can be accessed using the following URL address: https://silt.cee.pdx.edu/ This online tool is intended to be a live database and data will be added as they become available.

1-2 CHAPTER 1 FIGURES

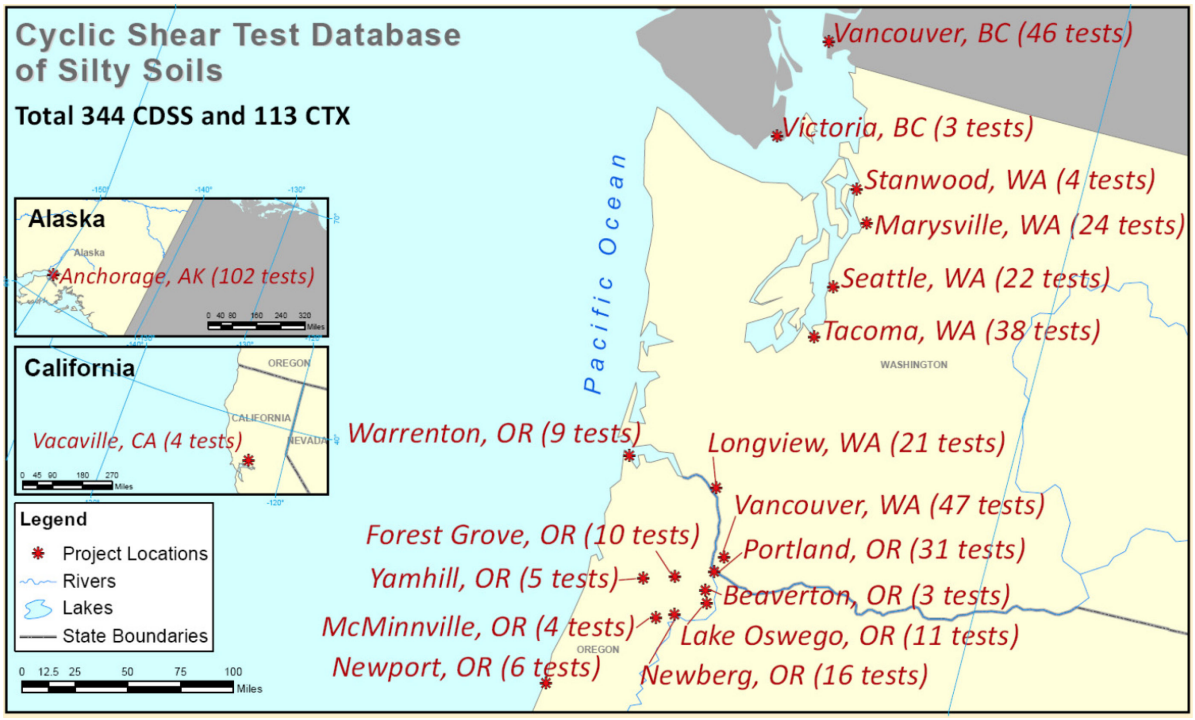

Figure 1.1: Project Site Locations

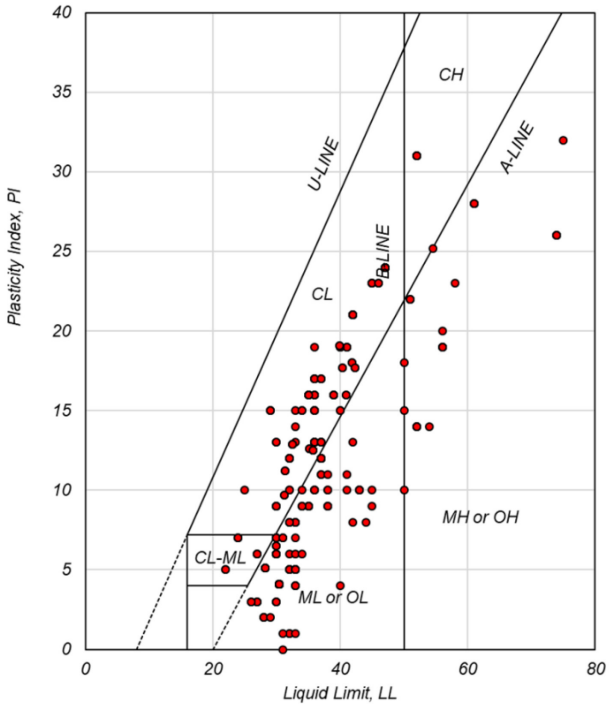

Figure 1.2: Plasticity Characteristics of the Test Soils

CHAPTER 2

Cyclic Shear Strain Accumulation and Resistance in Stress-Controlled Tests

CHAPTER 2 CONTENTS

2-1 INTRODUCTION 10

2-2 OBSERVATIONS ON DIFFERENCES BETWEEN ACCUMULATION OF SHEAR STRAIN IN LOOSE SANDS AND SILT SOILS 11

2-3 CYCLIC RESISTANCE RATIO (CRR) FOR DIFFERENT REFERENCE SHEAR/AXIAL STRAINS 12

2-3.1 Effect of Stress History on Cyclic Resistance Ratios 13

2-3.2 Cyclic Resistance Ratios for Columbia River Silt and Willamette River Silt 14

2-3.3 Cyclic Resistance Ratios for Willamette Silt (Missoula Flood Deposits) 14

2-3.4 Cyclic Resistance Ratios for Tidal/Estuarine Silts in Puget Sound, WA 15

2-3.5 Cyclic Resistance Ratios for Port of Anchorage Tidal Silts and Bootlegger Cove Formation 15

2-3.6 Correlations between Cyclic Resistance Ratios and Plasticity Index 17

2-3.7 Correlations between Cyclic Resistance Ratios and Liquid Limit 17

2-3.8 Effects of Test Type of on Cyclic Resistance Ratios 18

2-3.9 Effects of Reference Shear and Axial Strains on Cyclic Resistance Ratios 18

2-4 REFERENCES 19

2-5 CHAPTER 2 FIGURES 21

2-1 INTRODUCTION

This chapter summarizes the results of the stress-controlled tests that are included in this database. The dataset in this chapter includes over 120 stress-controlled cyclic direct simple shear (CDSS) and cyclic triaxial (CTX) tests on intact soil samples from 27 projects covering different index properties, gradation, and depositional environments. The test results are supplemented by CTX testing of reconstituted samples from three silt deposits.

Table 2-1 lists key soil properties and test parameters for the stress-controlled tests included in this chapter. The soil specimens are characterized as low-plasticity silt (ML), low plasticity clay (CL), high plasticity silt (MH), high plasticity clay (CH), and silty sand (SM) based on USCS classification. The fines contents (FC) for the soils that are included in this chapter range from 18% to 100% and the PI values range from nonplastic (NP) to 47. The soil samples were extracted from shallow depths down to a depth of 248 ft and were tested at an initial vertical effective stress ranging from 292 psf to 20885 psf. The overconsolidation ratios (OCR) generally ranged from 1 to 3. In most of the tests the OCR was recreated in the lab following the SHANSEP approach where the specimens were consolidated to a vertical effective stress higher than the estimated preconsolidation stress in the device and then unloaded to recreate OCR in the lab. However, in three sets of tests (Projects W_07, O_10 and O_12) the consolidation phase followed the recompression approach where the samples were consolidated to a stress that was close to the in situ vertical effective stress followed by cyclic loading. The effect of the recompression approach is discussed in the following sections.

Table 2-1: Stress-controlled cyclic DSS and cyclic TX tests used in this study

Project ID	Soils*	USCS classification	PI	OCR
O_01: Warrenton, OR	CRS	ML	9-12	1
O_02: Columbia River Crossing Longview	CRS	N/A	N/A	1-3
O_03: N. Marine Dr, Bybee Lake/Hayden Island	CRS	ML	10	1-2
O_07: Tilikum Crossing	WRS	ML	NP-10	1-1.3
O_08: Port of Portland T5	WRS	SM	27	2
O_09: St. Johns Crossing	WRS	N/A	N/A	1-3
O_10: Swan Island	WRS	MH	20-32	1.2-2.4
O_12: Forest Grove	WS	ML	5	3
O_18: Newport	Yaquina Bay Silt	MH	22-47	1.6
W_01: Stanwood WS SR-532	Tidal/Estuarine Silt	ML	8-10	1
W_02: Marysville WS SR-529, Ebey Slough	Tidal/Estuarine Silt	ML	7-23	1
W_07: Port of Tacoma	Tidal/Estuarine Silt	ML	N/A	1

Project ID	Soils*	USCS classification	PI	OCR
W_09: WS I-5/I-205 Salmon Creek Interchange	Lacustrine Silt	ML	NP-6	1
W_10: Vancouver, WA	Wash Tailing	ML/MH	12-13	2
W_11: Longview Riverfront	CRS	MH	14-32	1
W_12: Port of Vancouver	CRS	CL	13	1-3
W_13: Vancouver, WA	CRS	CH	NP	1
A_01: Port of Anchorage	Tidal Silt	CL/ML	12	1.9-2.6
A_02: Port of Anchorage	Tidal Silt	ML/CL	NP-24	1-1.9
A_04: Port of Anchorage	BCF	CL/CH	16-31	1-2
B_01: Victoria, BC	Estuarine Silt	CL	23	1
O_05_CTX: N. Marine Dr.	CRS	ML	1-14	1-2
O_11_CTX: Lake Oswego	Lacustrine Silt	ML/ML-MH	NP-18	1
O_13_CTX: Yamhill, OR	Completely Weathered Basalt	N/A	N/A	1
O_14_CTX: Forest Grove, OR	WS	ML	NP-3	1
O_19_CTX: Hayden Island, OR	CRS	ML	NP-25	1.2-1.9
O_22_CTX: Corvallis, OR	Reconstituted Corvallis Silt	ML	9	1-1.5
O_23_CTX: Adair Village, OR	Reconstituted Adair Silt	ML	9	1-2
W_14_CTX: Port of Tacoma	Reconstituted Tacoma Silt	N/A	N/A	1
A_03_CTX: USGS	BCF	CL	10-19	1

Note:

*CRS = Columbia River Silt, WRS=Willamette River Silt, WS=Willamette Silt (Missoula Flood Deposits), BCF=Bootlegger Cove Formation

2-2 OBSERVATIONS ON DIFFERENCES BETWEEN ACCUMULATION OF SHEAR STRAIN IN LOOSE SANDS AND SILT SOILS

Past earthquakes demonstrated that large ground deformations and ground "failures" may occur as a result of liquefaction in loose sands. The large ground deformations are associated with dramatic degradation of shear stiffness and strength in sands once the pore water pressure ratio (Ru) approaches values near 100%. Triggering of liquefaction in loose sand under level or moderately sloping ground results in nearly zero shear stiffness intervals during which shear strains develop very rapidly. An example of this behavior is shown in Figure 2.1a for Sacramento River sand by Boulanger and Idriss (2006). The accumulation of cyclically induced shear strains per cycle after the onset of liquefaction are usually very large in sands, ranging on average 2% and

higher for sands with relative densities smaller than Dr = 40% as reported by Gingery (2014) and interpreted from data by Wu (2002) as shown in Figure 2.1b.

The data presented in this database suggest differences between the cyclic behavior of silts that classify as ML, CL, MH and CH based on USCS classification and loose sands. The silt soils do not exhibit such dramatic degradation of stiffness even after developing shear strains of ~3% and larger. The shear strains in silt soils continue to accumulate during cyclic loading; however, the magnitude of accumulated shear strains per cycle are generally smaller than those reported for sand soils. This behavior is shown in Figure 2.2 as an example from a CDSS test performed on a Columbia River Silt specimen from Warrenton, OR (Project ID: O_01). This specimen is classified as ML and has a plasticity index PI = 9 and an OCR of 1. The specimen was extracted from 130 ft depth, consolidated to a vertical effective stress of 8350 psf, and cyclically loaded for 39 uniform cycles at a CSR of 0.15 at a loading frequency of 0.1 Hz. The sample continues to show a dilative response past the shear strain of 3% and accumulates approximately 0.7% per cycle with no sign of "failure" with unbounded accumulation of shear strain until the test stopped at a single amplitude shear strain of 7% after 39 loading cycles. In light of the behavior observed in these tests, the cyclic resistance ratios of silts in this database are evaluated at reference shear strains up to 9% when data were available.

2-3 CYCLIC RESISTANCE RATIO (CRR) FOR DIFFERENT REFERENCE SHEAR/AXIAL STRAINS

Data from 311 cyclic direct simple shear (CDSS) and 85 cyclic triaxial (CTX) tests are presented in this chapter to develop cyclic resistance ratios and their potential correlations with various loading conditions and soil properties, such as overconsolidation ratio (OCR), PI, etc. The cyclic stress ratio (CSR) was defined in CDSS tests and CTX tests using the following equations:

$$CSR = \frac{\tau_{cyc}}{\sigma'_{vc}} \text{ in CDSS} \qquad \text{(Equation 2-1)}$$

$$CSR = \frac{(\sigma_{dev,cyc})/2}{\sigma'_{3c}} \text{ in CTX} \qquad \text{(Equation 2-2)}$$

The CSR values for tests that were performed at a loading frequency of 0.1 Hz were increased by 9% to convert to equivalent 1 Hz loading assuming the typical loading rate behavior observed for clay soils (Idriss and Boulanger, 2008). For tests performed at other frequencies the adjustment factor to equivalent 1 Hz loading was interpolated based on the natural log relationship between CSR and loading frequency.

The cyclic resistance ratios (CRR) were calculated based on the number of uniform cycles (N) required to reach a reference strain. For CDSS tests the following reference single-amplitude (SA) shear strains were considered: γ_{ref} = 1%, 3%, 5%, 7% and 9%. For CTX tests, reference double-amplitude (DA) axial strains of ε_{ref} = 5% and 10% as well as pore pressure ratio of Ru = 100% were

considered. A power equation was fit to the data from each set of tests to interpolate $CRR_{M=7.5}$ defined as the cyclic stress ratio (CSR) required to reach the reference shear strain, reference axial strain, or Ru=100% in 15 uniform loading cycles using the equation below. The calculation of cyclic shear resistance based on 15 cycles is typically used for sand soils with a relatively large b value and corresponds to the equivalent number of uniform cycles in a magnitude 7.5 earthquake (Idriss and Boulanger 2008). The b value for silt soils is usually smaller than those for sand. The cyclic shear resistances in this study are reported for 15 cycles as a reference and can be easily converted to other values of uniform cycles using the equation below. The fit parameters (a and b) and the corresponding $CRR_{M=7.5}$ is provided for each set of tests in the plots that are presented in Appendix A through D.

$$CSR = a \times N^{-b} \qquad \text{(Equation 2-3)}$$

For example, Figure 2.3 shows the derivation of CRR for different reference shear strains for test data from Columbia River silt samples (Project ID: O_01). Six CDSS tests were performed on six specimens that were obtained from 130 ft and 248 ft depths and were consolidated to OCR=1 at vertical effective stresses of 8350 psf and 16710 psf respectively. The six specimens tested had a plasticity index (PI) ranging from 9 to 12 and were classified as ML material based on USCS classification. The figure shows CSR versus number of loading cycles to reach reference single amplitude shear strains of 1%, 3%, 5%, and 7%. The $CRR_{15cycles}$ values were interpolated at 15 cycles using the power fit and range from 0.17 to 0.20 for the different reference shear strains shown in this figure. The b-value of the power fit defines the slope of CSR with respect to the log of the number of cycles to reach the reference strain. This parameter can be used to calculate CRR corresponding to different numbers of loading cycles to evaluate the effects of earthquake magnitude (e.g., the larger number of cycles in long-duration earthquakes and its importance to magnitude scaling factor) or to estimate the relative response of loading cycles with various amplitudes that may occur during an earthquake. It is noticeable that the b-value for silt samples shown in this figure ranges from 0.12 to 0.19 which is smaller than the b-value of 0.34 reported for undisturbed frozen samples of clean sand (Yoshimi et al., 1984).

2-3.1 EFFECT OF STRESS HISTORY ON CYCLIC RESISTANCE RATIOS

The effect of stress history on cyclic resistance ratios were evaluated using a subset of data where tests were performed on soil samples with different overconsolidation ratios (OCR). In these tests, the OCR was recreated in the lab by consolidating the specimens to a higher confining stress (slightly larger than the in situ preconsolidation stress) and then unloaded to a smaller confining stress prior to cyclic loading. Figures 2.4a to 4h show the CRR plots for a reference shear strain of γ_{ref} = 3% (or 3.75% for Figure 2.4h) for projects where cyclic tests were performed at different OCR values. As clearly suggested by these plots, CRR increases with increasing OCR. Figure 2.5a

shows the CRR vs. OCR which also supports the increasing trend between CRR and OCR. Figure 2.5b shows the CRR values normalized by CRR at OCR=1 suggesting that CRR is proportional to $OCR^{0.8}$ for silt soils. This relationship is used in the following sections where OCR-normalized CSR values are provided for different soil units. Figure 2.5c compiles the test results in terms of $CSR/OCR^{0.8}$ versus number of cycles and shows this approach produces relatively consistent results across the range of OCRs included in the data set.

2-3.2 CYCLIC RESISTANCE RATIOS FOR COLUMBIA RIVER SILT AND WILLAMETTE RIVER SILT

Figure 2.6a shows the cyclic stress ratio (CSR) versus number of uniform cycles for samples obtained from Columbia River Silt and Willamette River Silt. This figure clearly shows that CRR for overconsolidated samples (shown with red symbols) is larger than the CRR for normally consolidated samples (shown with blue symbols). Figure 2.6b shows CSR normalized by OCR^0.8 for the same tests. This figure suggests that the cyclic resistance of silt soils can be better characterized (and predicted) if normalized by OCR. As a preliminary guidance for practitioners, a power equation is fit to the data using the equation below. The "a" and "b" parameters are reported in this figure and subsequent figures in this section.

$$\frac{CSR}{OCR^{0.8}} = a \times N^{-b} \qquad \text{(Equation 2-4)}$$

It is worth noting that while there is considerable scatter in the data due partly to inherent variabilities in natural soils, some trends are identifiable among the outlier data points. For example, the outlier data point from Swan Island (Project O_10) in Figure 2.6a pertains to a test where the in situ OCR (2.4) was not recreated in the lab; instead, the recompression approach was used where the sample was consolidated to the in situ vertical effective stress of 2200 psf followed by cyclic loading. This pattern is also observed in other samples where OCR was not recreated in the lab, such as the Forest Grove samples (Project O_12) shown in later figures. On the basis of this observation, it is recommended to perform consolidation tests prior to cyclic tests to get a reasonable estimate of OCR in the field. When possible, SHANSEP approach can be followed to consolidate specimens to a confining stress that is slightly higher than the preconsolidation stress (~20% larger) to reduce sample disturbance and then unloaded to a smaller stress to recreate OCR in the lab prior to cyclic loading.

2-3.3 CYCLIC RESISTANCE RATIOS FOR WILLAMETTE SILT (MISSOULA FLOOD DEPOSITS)

Figure 2.7a shows the cyclic stress ratio (CSR) versus number of uniform cycles for samples obtained from Willamette Silt (Missoula Flood deposits). Most of the tests performed on samples

from Forest Grove (Project O_12), Beaverton (Project O_16), and McMinnville (Project O_17) did not reach 3% shear strain by the end of the cyclic loading phase (after 50 to 200 cycles.) These data points are shown in the plot but should be considered qualitatively for characterizing the cyclic resistance ratios of Willamette Silt samples. To supplement data points from tests on intact samples that reached 3% shear strain, data from tests on reconstituted samples from Corvallis (Project O_22) with similar plasticity indices are added as a reference. Figure 2.7b shows CSR normalized by OCR^0.8 for the same tests and the corresponding power fit to the data. It is worth noting that the OCR-normalized cyclic resistance ratio, interpolated at 15 loading cycles as a reference, is approximately $(CRR/OCR^{0.8})_{15\ cycles} = 0.23$ for Willamette Silt which is slightly larger than $(CRR/OCR^{0.8})_{15\ cycles} = 0.21$ for the alluvial soils from Columbia River Silt and Willamette River Silt. It is important to note that the cyclic shear stresses in this study are reported as recorded in CDSS or CTX tests. No additional conversions are applied to convert the CTX data to equivalent-DSS values. The conversion between CTX and CDSS may make up some of the differences observed between data for Willamette Silt and alluvial silts from Columbia River and Willamette River silts.

2-3.4 CYCLIC RESISTANCE RATIOS FOR TIDAL/ESTUARINE SILTS IN PUGET SOUND, WA

Figure 2.8a shows the cyclic stress ratio (CSR) versus number of uniform cycles for samples obtained from tidal/estuarine silty soils in Puget Sound area in Washington. To supplement the data on intact samples, data from cyclic tests on reconstituted samples from Port of Tacoma (Project O_14) are added for reference. Figure 2.8b shows CSR normalized by OCR^0.8 for the same tests and the corresponding power fit parameters are reported in the figure. The OCR-normalized CRR, interpolated at 15 loading cycles as a reference, is approximately $(CRR/OCR^{0.8})_{15\ cycles} = 0.19$, which is slightly smaller than the alluvial silt soils from Willamette River and Columbia River samples. However, it should be noted that only one specimen with OCR > 1 is represented in this dataset.

2-3.5 CYCLIC RESISTANCE RATIOS FOR PORT OF ANCHORAGE TIDAL SILTS AND BOOTLEGGER COVE FORMATION

Figure 2.9a shows the cyclic stress ratio (CSR) versus number of uniform cycles for samples obtained from Port of Anchorage for tidal silt samples and Bootlegger Cove Formation (BCF). Figure 2.9b shows CSR normalized by OCR^0.8 for the same tests. Once normalized with OCR, the data shows clear differences between tidal silt samples and BCF samples. Consequently, the power fit is developed separately for each soil unit. The OCR-normalized CRR, interpolated at 15 loading cycles as a reference, is approximately $(CRR/OCR^{0.8})_{15\ cycles} = 0.15$ for the tidal silts which is noticeably smaller than the values calculated for the tidal/estuarine silts in Puget Sound and the

alluvial silts from Willamette and Columbia rivers. The OCR-normalized CRR values for BCF are estimated as $(CRR/OCR^{0.8})_{15\ cycles} = 0.22$.

Table 2-2 summarizes the OCR-normalized cyclic resistance ratios for different soil units presented in this section.

Table 2-2: OCR-normalized cyclic resistance ratios for silts soils in PACNW

Soil Unit	PI	OCR	Number of tests	a	b	CRR/(OCR$^{0.8}$) at 15 cycles
Columbia River Silt and Willamette River Silt	NP-44	1-3	55	0.26	0.08	0.21
Willamette Silt (Missoula Flood Deposits)	NP-12	1-3	11	0.32	0.13	0.23
Tidal/Estuarine Silts in Puget Sound, WA	NP-23	1-1.5	18	0.28	0.15	0.19
Port of Anchorage Tidal Silts	NP-24	1-2.6	14	0.25	0.19	0.15
Bootlegger Cove Formation	10-31	1-2	18	0.29	0.1	0.22

2-3.6 CORRELATIONS BETWEEN CYCLIC RESISTANCE RATIOS AND PLASTICITY INDEX

The data scatter in Figures 2.6 to 2.9 is partly related to variations in soil properties within each soil unit. Some of this scatter can be explained by the relationship between the cyclic resistance ratio and plasticity index (PI). Various studies have shown that the cyclic behavior of fine-grained soils changes from liquefaction (sand-like behavior) to cyclic softening (clay-like behavior) over a narrow range of plasticity index (PI). Figure 2.10a shows the criteria proposed by Idriss and Boulanger (2008), where the cyclic resistance of fine-grained soils changes (increases) from sand-like CRR to clay-like CRR at PI of 7. Figure 2.10b shows the criteria proposed by Bray and Sancio (2006) where the fine-grained soils transition between susceptible, moderately susceptible, and not susceptible at PI values of 12 and 18. Both studies suggest that the cyclic resistance ratio increases with PI. Similar trend is shown by Wijewickreme et al. (2019) for Fraser River Silt and other silt soils in British Columbia as shown in Figure 2.11.

Figure 2.12 shows the CRR normalized with OCR^0.8 versus PI from CDSS tests in this study. The CRR is calculated as the cyclic stress ratio required to reach 3% single amplitude shear strain in 15 cycles using the power relationship shown in Equation 2-4. The data suggests an increasing trend between CRR/OCR^0.8 and PI. For comparison, data on Fraser River Silt and other fine-grained soils from Wijewickreme et al. (2019) were analyzed and plotted on Figure 2.13 showing a similar increasing trend between cyclic resistance ratio and PI.

2-3.7 CORRELATIONS BETWEEN CYCLIC RESISTANCE RATIOS AND LIQUID LIMIT

Similar increasing trends are observed between cyclic resistance ratios and the liquid limit (LL). Figure 2.14 shows the OCR-normalized cyclic resistance ratios (CRR/OCR^0.8) versus LL for the data included in this study as well as the data presented by Wijewickreme et al. (2019) for Fraser River Silt and other fine-grained soils.

2-3.8 EFFECTS OF TEST TYPE OF ON CYCLIC RESISTANCE RATIOS

The CRR values calculated from CTX tests in this study are somewhat larger than those calculated from CDSS tests. This is graphically shown in Figure 2.15 where data from CTX tests are added to data from CDSS tests shown in previous figures. For a similar range of PI values, the CRR from CTX tests are approximately 40% larger than the CRR from CDSS tests. As mentioned earlier, it is important to note that the CSR and CRR values reported in this study are calculated from recorded data in CTX and CDSS tests without applying any conversion.

2-3.9 EFFECTS OF REFERENCE SHEAR AND AXIAL STRAINS ON CYCLIC RESISTANCE RATIOS

The CRR in previous figures were shown for a reference single amplitude shear strain of 3% for CDSS tests and a reference double amplitude axial strain of 5% for CTX tests. While these reference shear and axial strains are commonly used in evaluating liquefaction susceptibility of loose sands where 3% shear strain is usually accompanied by a pore pressure ratio of approximately 100% followed by "failure", the cyclic response of silt soils included in this study exhibit considerable stiffness and strength beyond 3% shear strain. Figure 2.16a shows the CRR normalized by $OCR^{0.8}$ to reach different reference strains in 15 cycles including single amplitude shear strain γ = 1%, 3%, 5%, 7% and 9% for CDSS tests. Figure 2.16b shows the ratio of CRR at a given reference shear strain normalized by CRR at a single amplitude shear strain γ = 3%. The data suggest an increasing trend between CRR and reference shear strain for CDSS tests; for example, CRR at a single amplitude shear strain of 7% can be up to 50% larger than CRR at a single amplitude shear strain of 3%. Contrary to the CDSS tests results, the CTX test results do not show a strong increasing trend between CRR and the reference axial strain. Figure 2.17a shows the OCR-normalized CRR ($CRR/OCR^{0.8}$) to reach different reference axial strains in 15 cycles versus double amplitude (D.A.) axial strains of ε = 2%, 5%, 10%, and 20%. Figure 2.17b shows the ratio of CRR at a given reference axial strain normalized by CRR at a double amplitude axial strain of ε = 5%. The data suggest no significant increase in CRR with respect to the reference axial strain. This difference needs to be studied further in future studies.

2-4 REFERENCES

Bray, J. D., & Sancio, R. B. (2006). Assessment of the liquefaction susceptibility of fine-grained soils. Journal of Geotechnical and Geoenvironmental Engineering, 132(9), 1165-1177.

Boulanger, R. W., & Idriss, I. M. (2006). Liquefaction susceptibility criteria for silts and clays. Journal of Geotechnical and Geoenvironmental engineering, 132(11), 1413-1426.

Gingery, J. R. (2014). Effects of liquefaction on earthquake ground motions (Doctoral dissertation, UC San Diego).

Idriss, I. M., & Boulanger, R. W. (2008). Soil liquefaction during earthquakes. Earthquake Engineering Research Institute.

Wijewickreme, D., Soysa, A., & Verma, P. (2019). Response of natural fine-grained soils for seismic design practice: A collection of research findings from British Columbia, Canada. Soil Dynamics and Earthquake Engineering, 124, 280-296.

Wu, J. (2002). Liquefaction triggering and post-liquefaction deformation of Monterey 0/30 sand under unidirectional cyclic simple shear loading. University of California, Berkeley.

2-5 CHAPTER 2 FIGURES

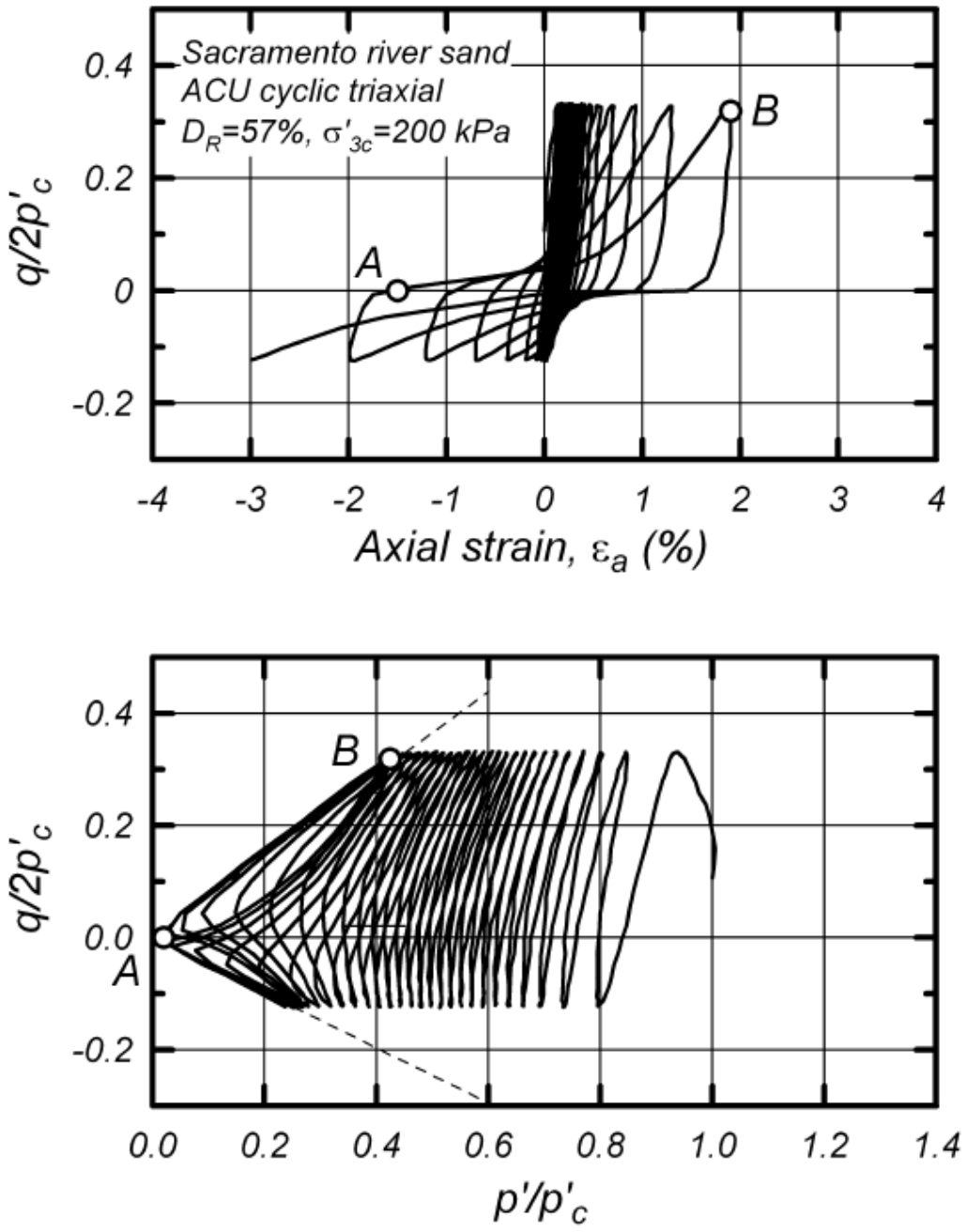

Figure 2.1a: Example cyclic undrained response of sand (Sacramento rover sand) from Boulanger and Idriss (2006).

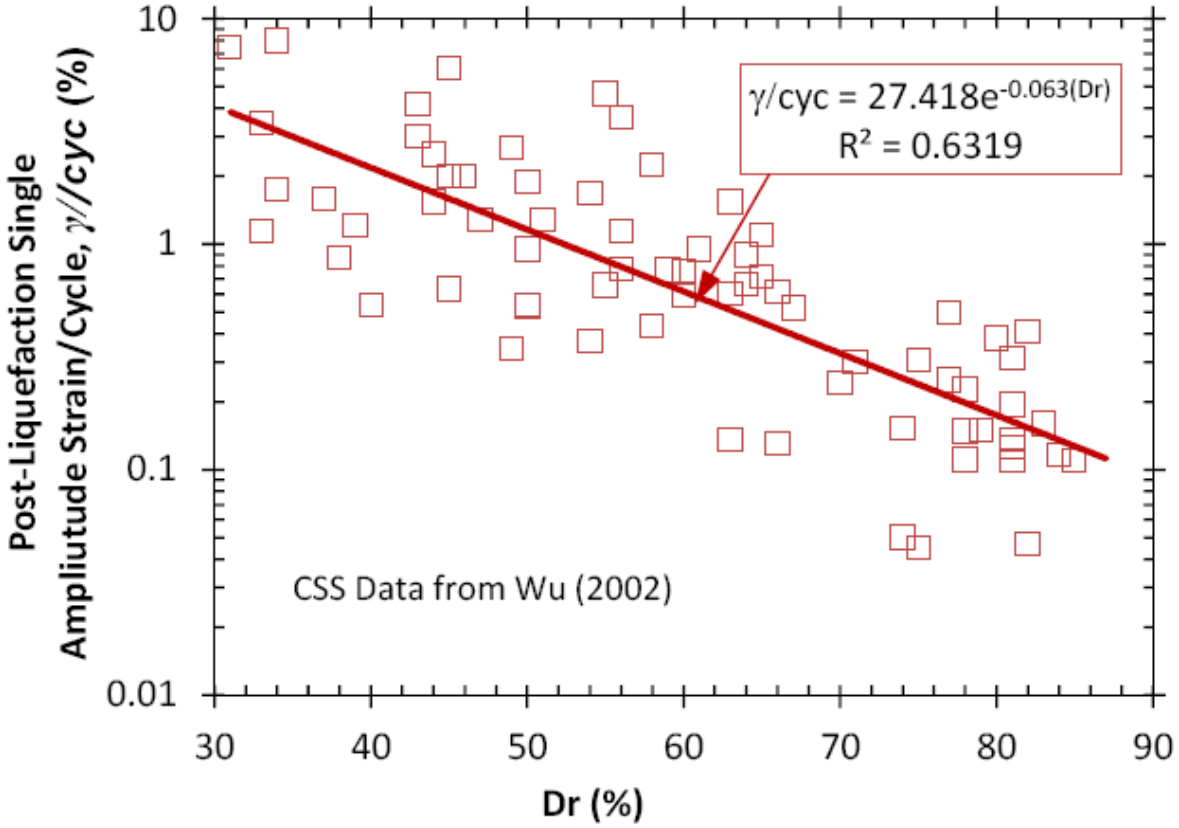

Figure 2.1b: Accumulation of post-liquefaction shear strains per cycle in sands (from Gingery, 2014 interpreted from undrained cyclic tests data by Wu, 2002)

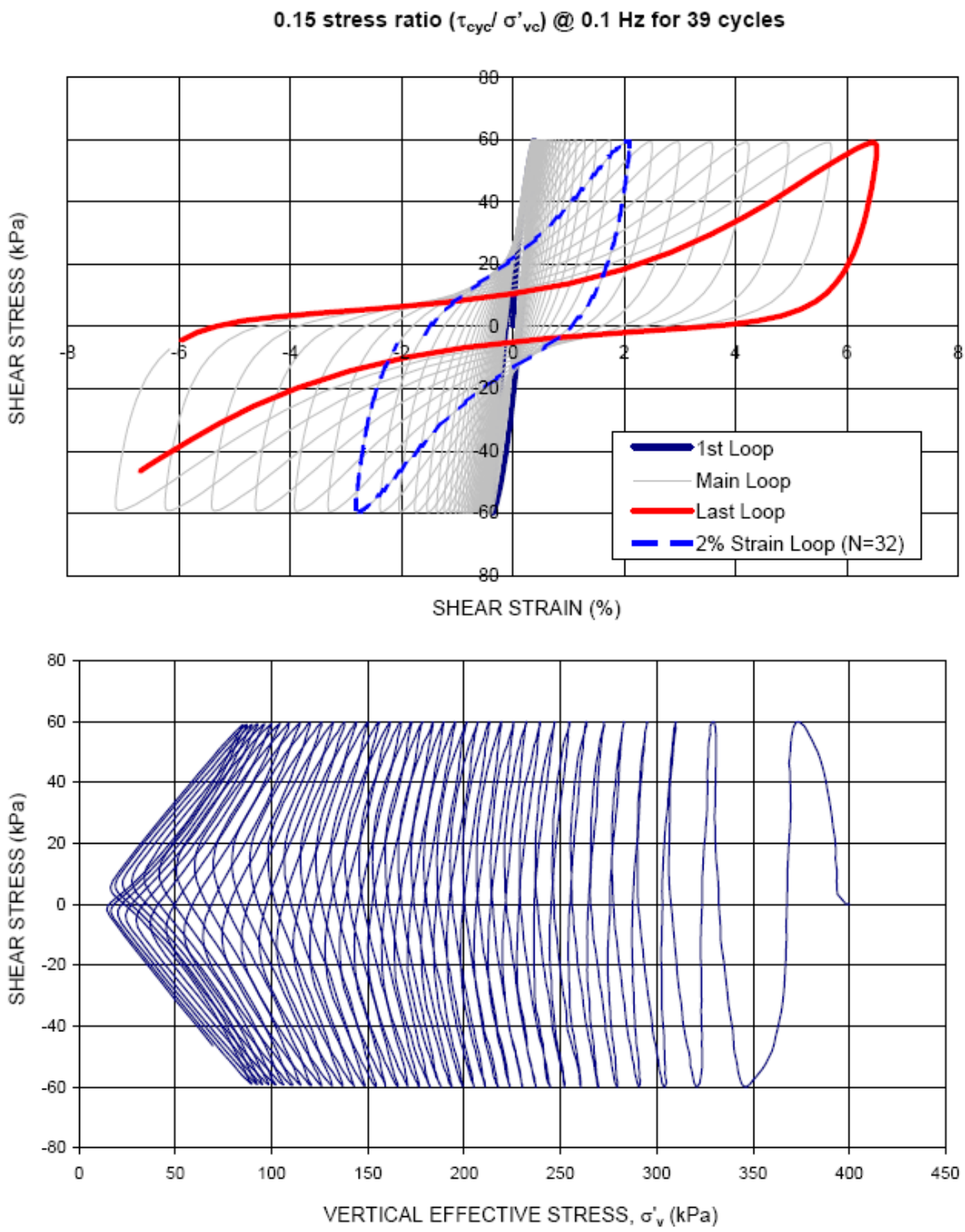

Figure 2.2: Example cyclic response of silt (PI=9) from Warrenton, OR (Project ID: O_01).

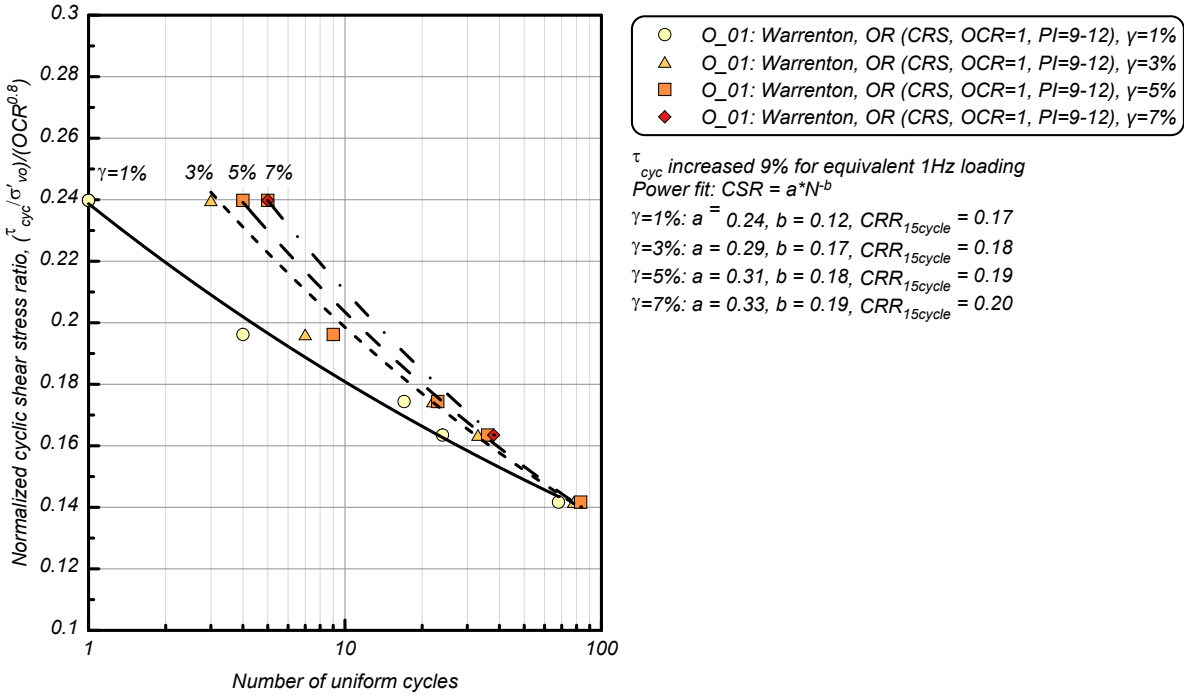

Figure 2.3: Cyclic stress ratio versus number of loading cycles to reach different reference single amplitude shear strains – Columbia River Silt from Warrenton, OR (Project ID: O_01)

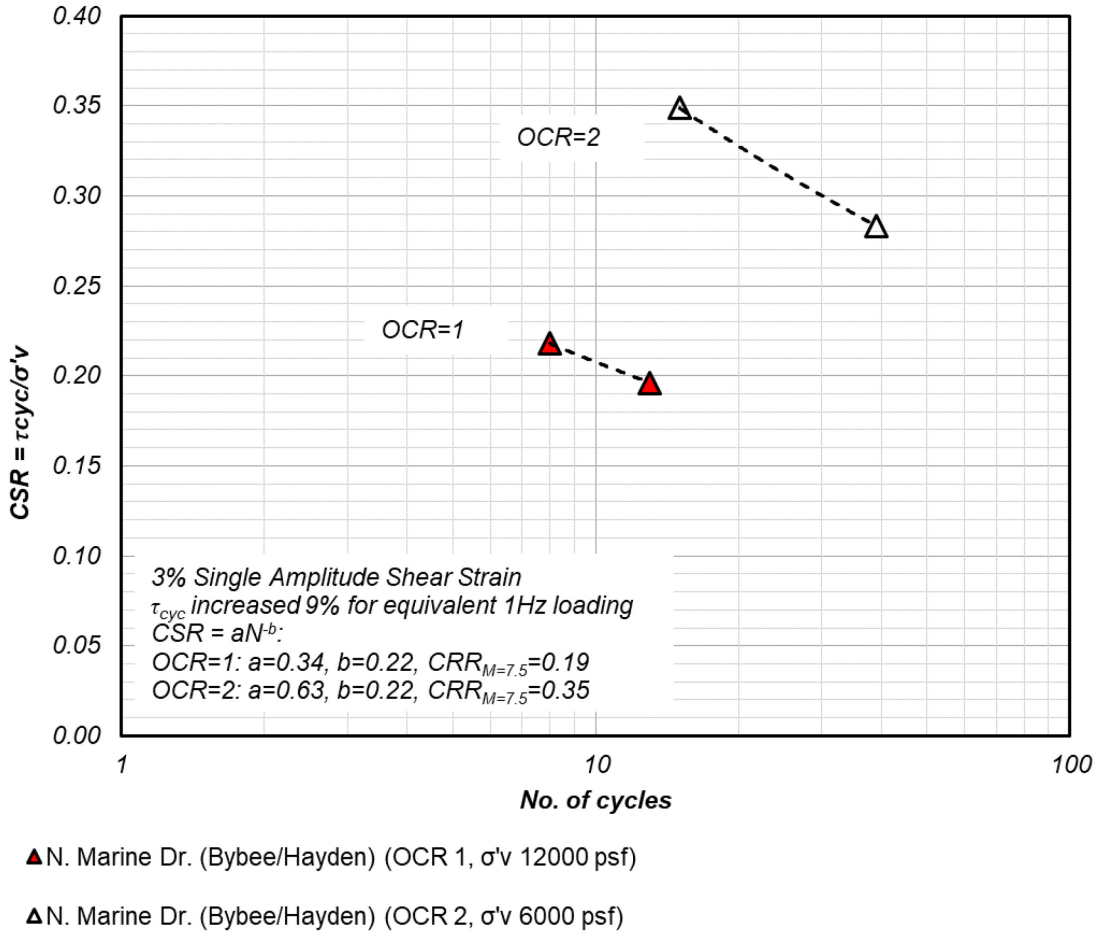

Figure 2.4a: Effects of OCR on cyclic resistance ratio – Columbia River Silt (ML; PI = 10) from BPA Seismic Performance Evaluation Project / N. Marine Drive Bybee Lake/Hayden Island in Portland, OR (Project ID: O_03)

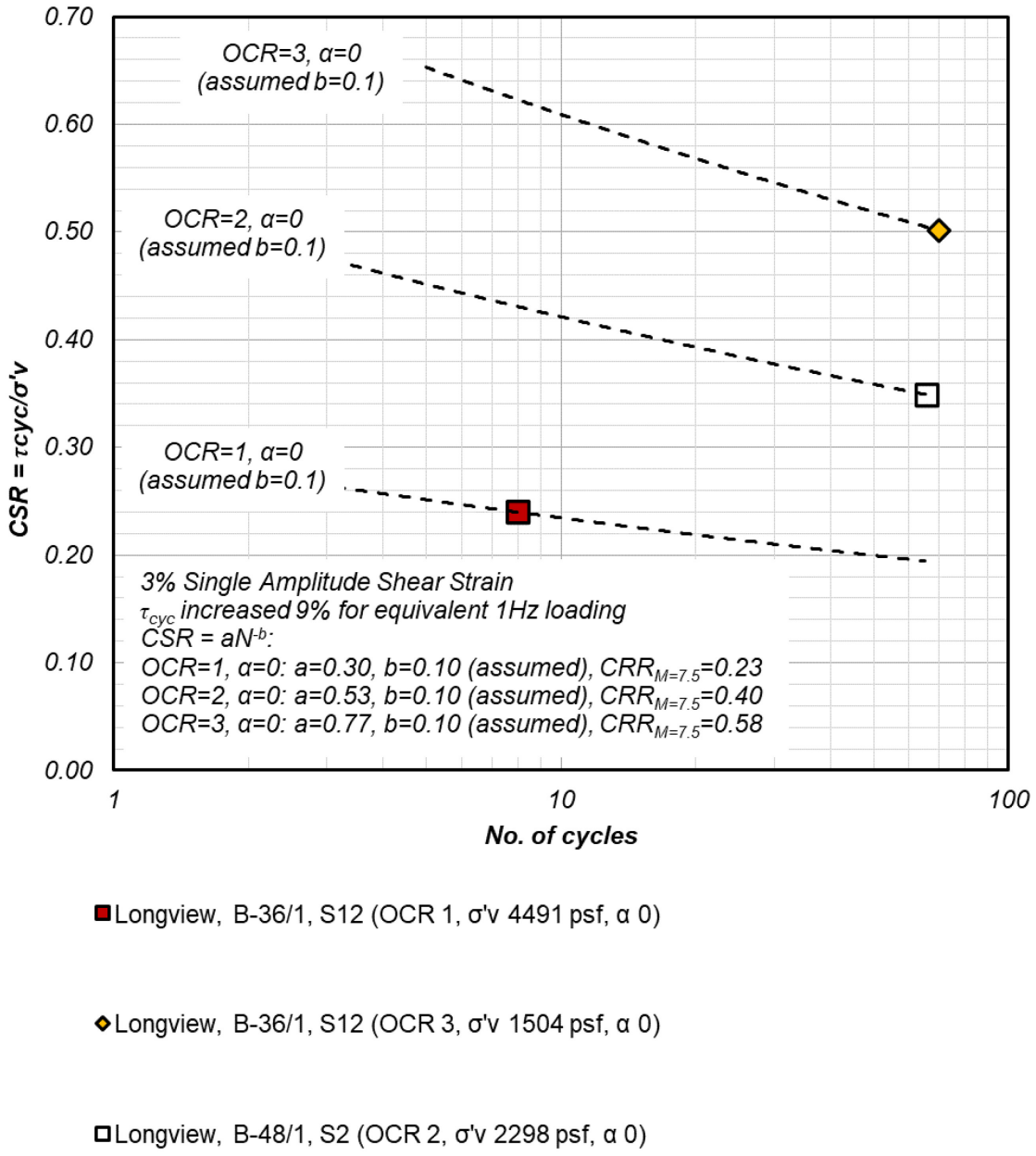

Figure 2.4b: Effects of OCR on cyclic resistance ratio –Columbia River Silt from BPA Seismic Performance Evaluation project / Columbia River Crossing, Longview, WA (Project ID: O_02)

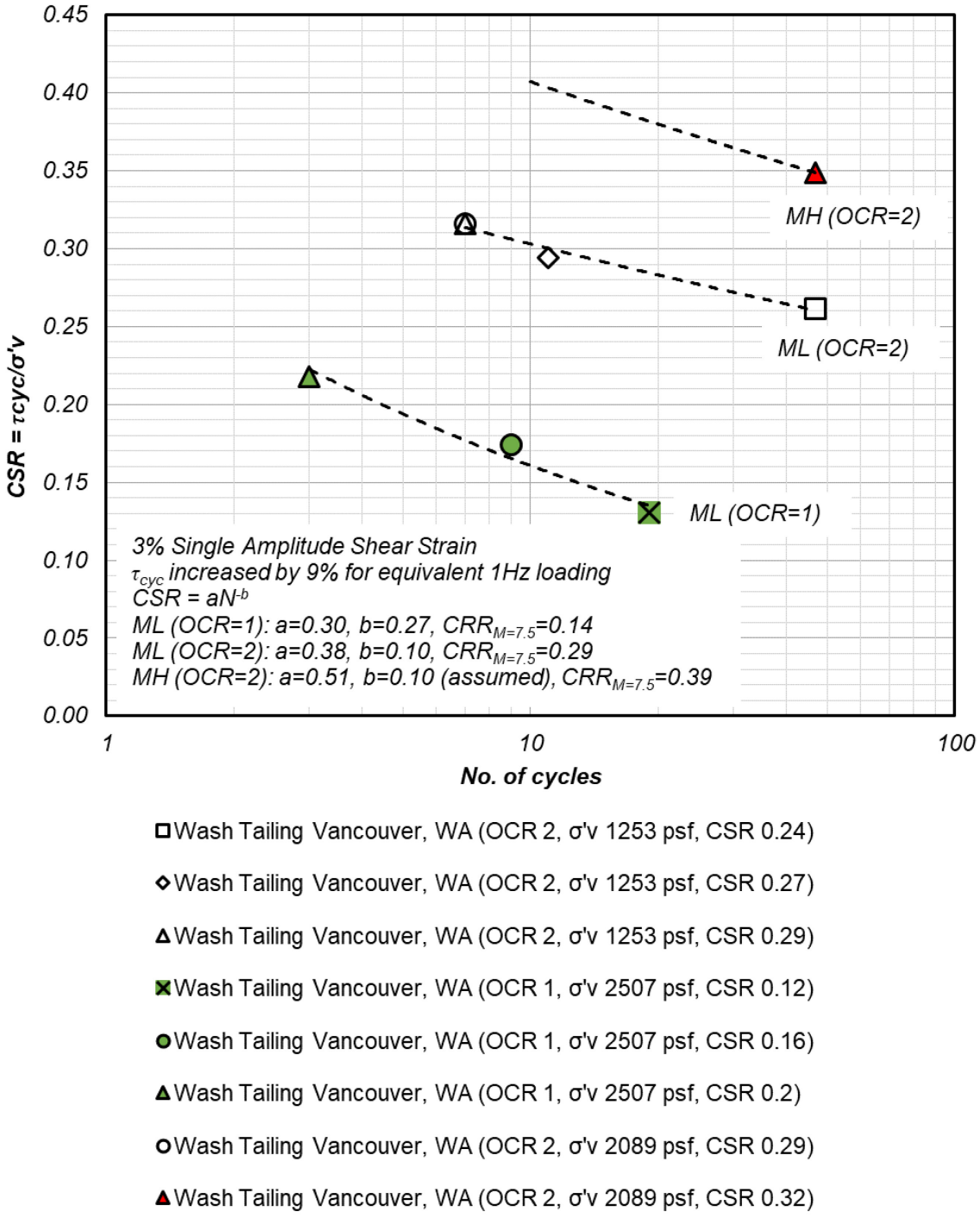

Figure 2.4c: Effects of OCR on cyclic resistance ratio – Wash Tailing (ML and MH; PI = 12 to 28) from Vancouver, WA (Project ID: W_10)

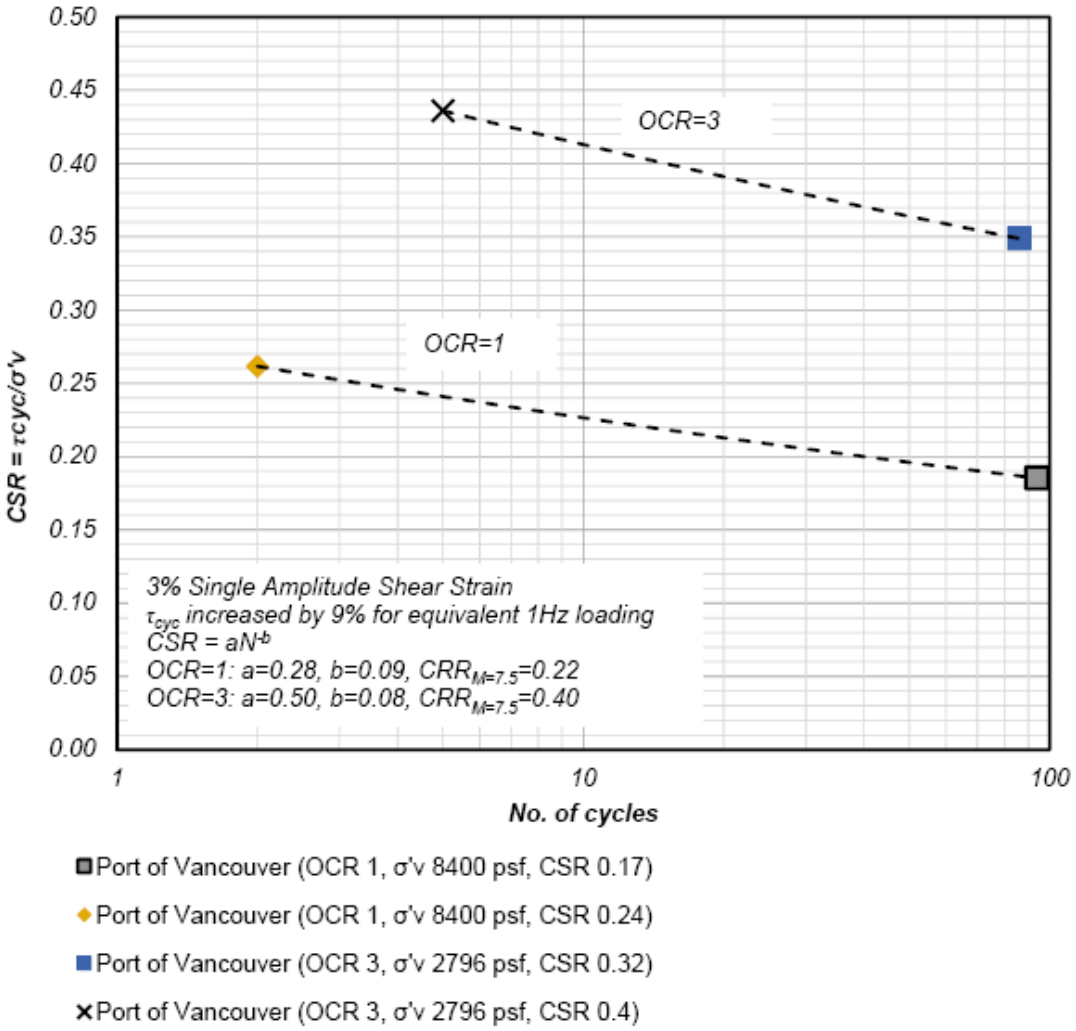

Figure 2.4d: Effects of OCR on cyclic resistance ratio – Columbia River Silt (CL; PI = 13) from BPA Seismic Performance Evaluation Project / Port of Vancouver, Vancouver, WA (Project ID: W_12)

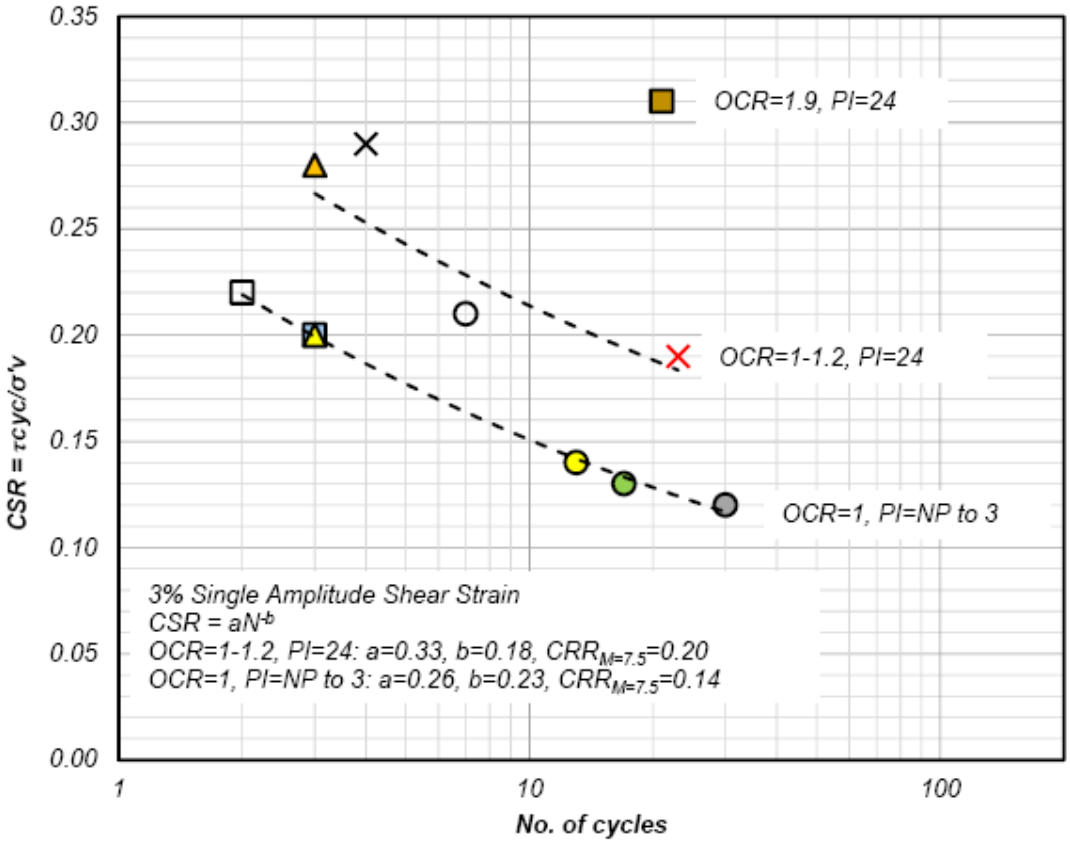

Figure 2.4e: Effects of OCR on cyclic resistance ratio – Tidal Silt (ML and CL; PI = NP to 24) from Port of Anchorage Intermodal Expansion project, Anchorage, AK (Project ID: A_02)

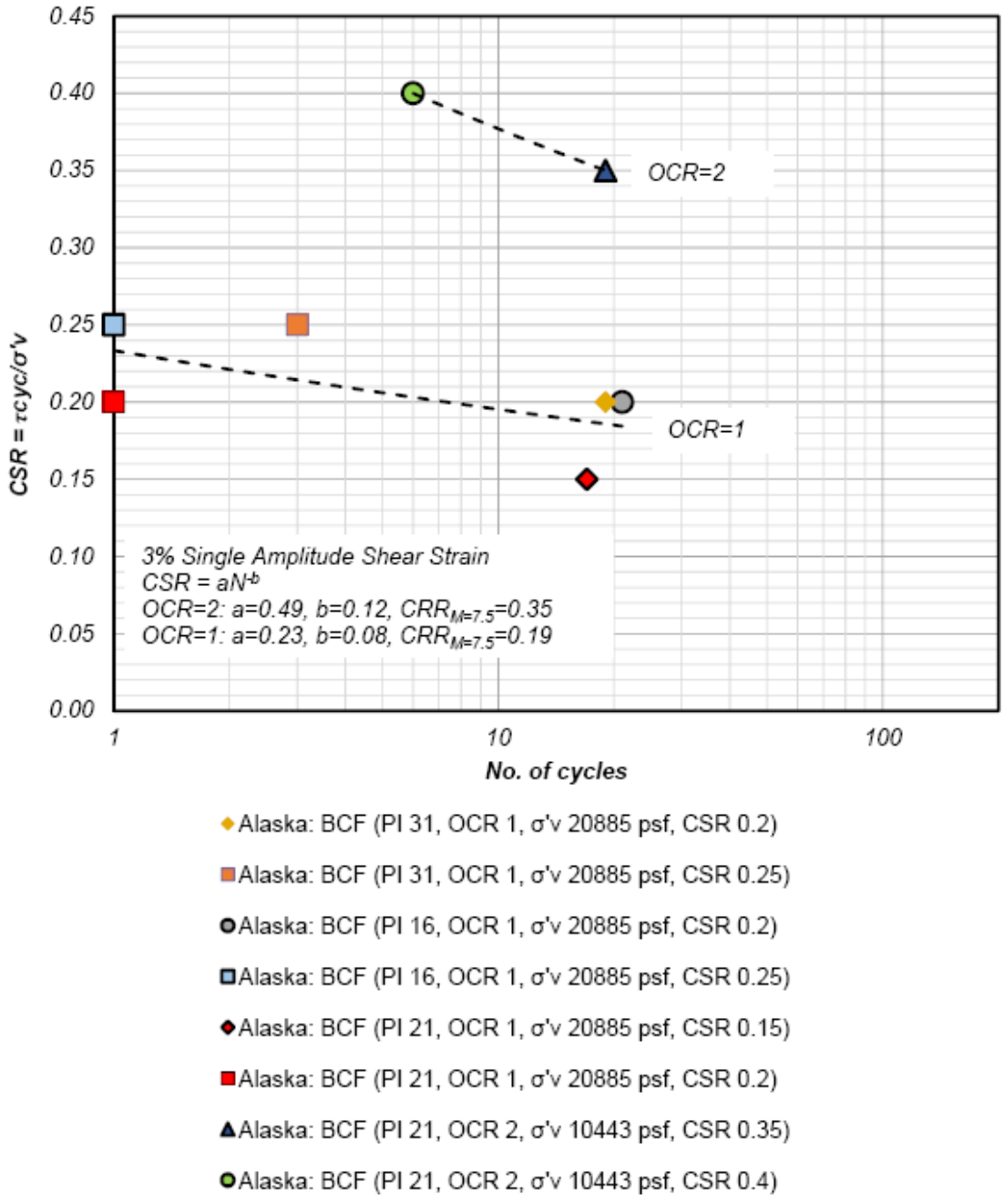

Figure 2.4f: Effects of OCR on cyclic resistance ratio – Bootlegger Cove Formation (CL and CH; PI = 16 to 31) from Port of Anchorage Intermodal Expansion project, Anchorage, AK (Project ID: A_04)

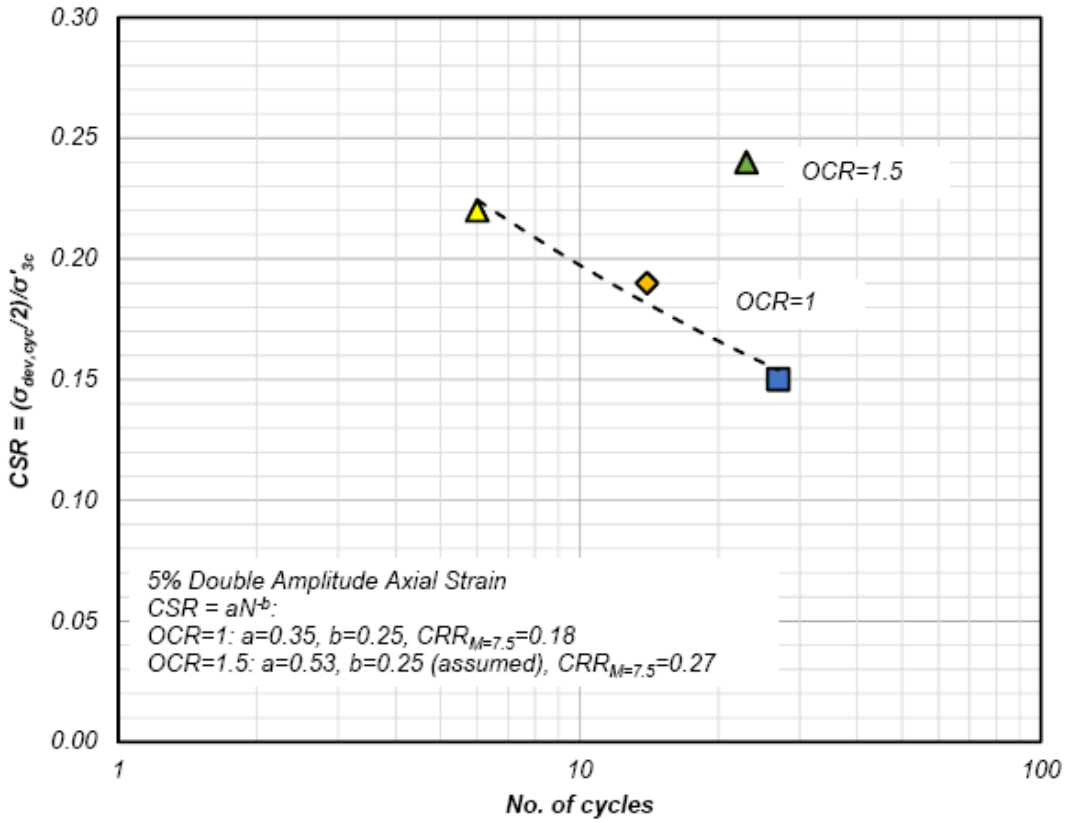

Figure 2.4g: Effects of OCR on cyclic resistance ratio – Reconstituted Tacoma Silt from Tacoma, WA (Project ID: W_14)

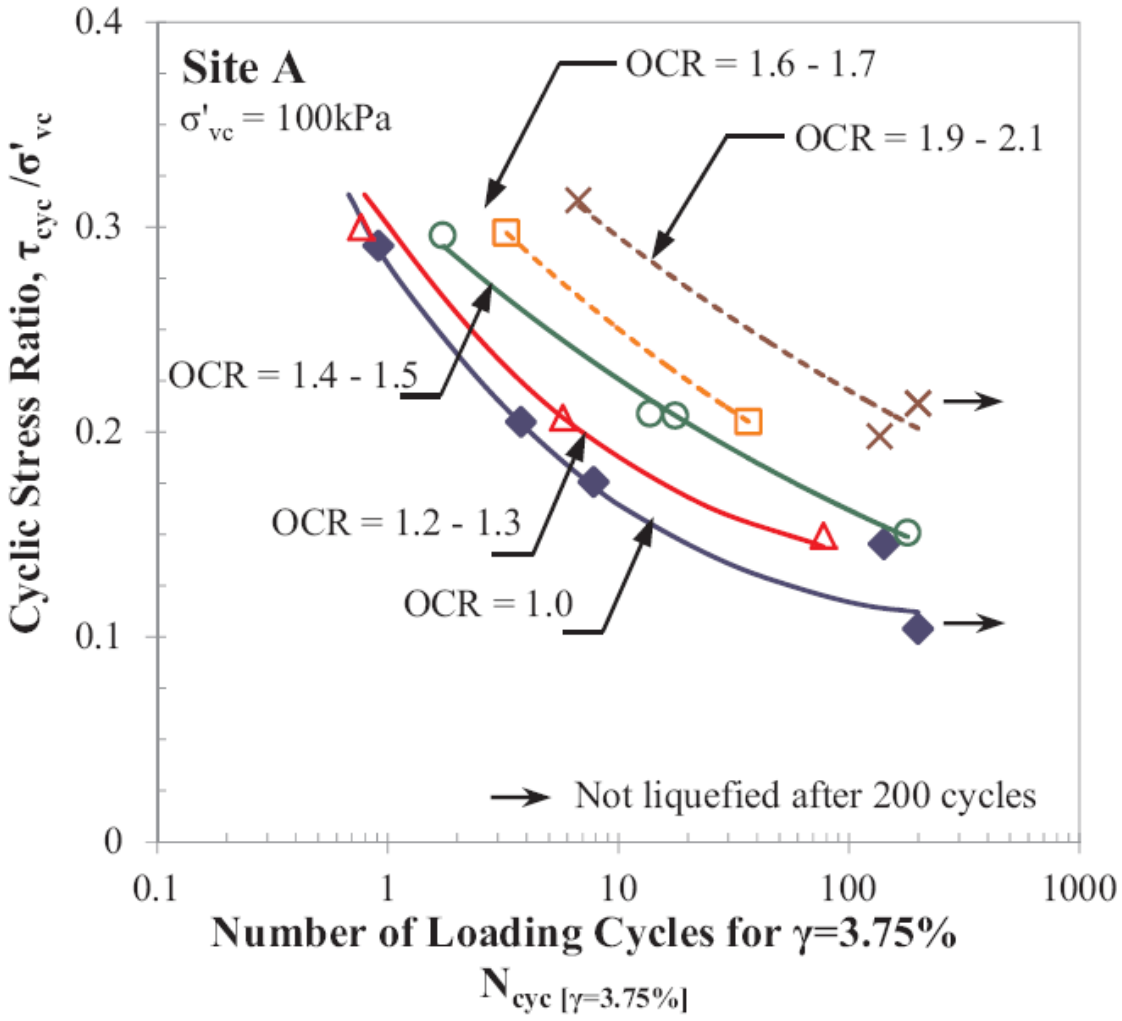

Figure 2.4h: Effects of OCR on cyclic resistance ratio – Fraser River Silt (ML; PI=4) from Vancouver, BC (Wijewickreme et al., 2019)

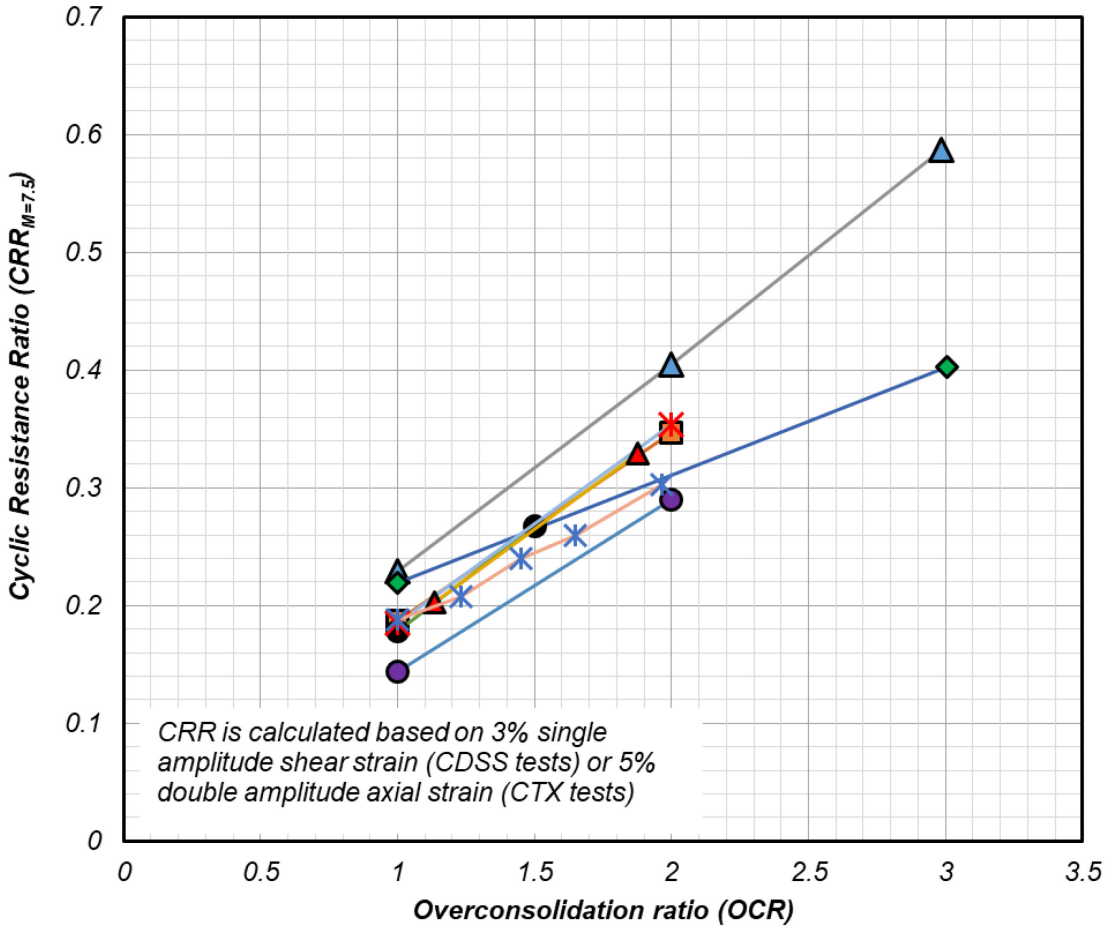

Figure 2.5a: Effect of OCR on cyclic resistance ratio

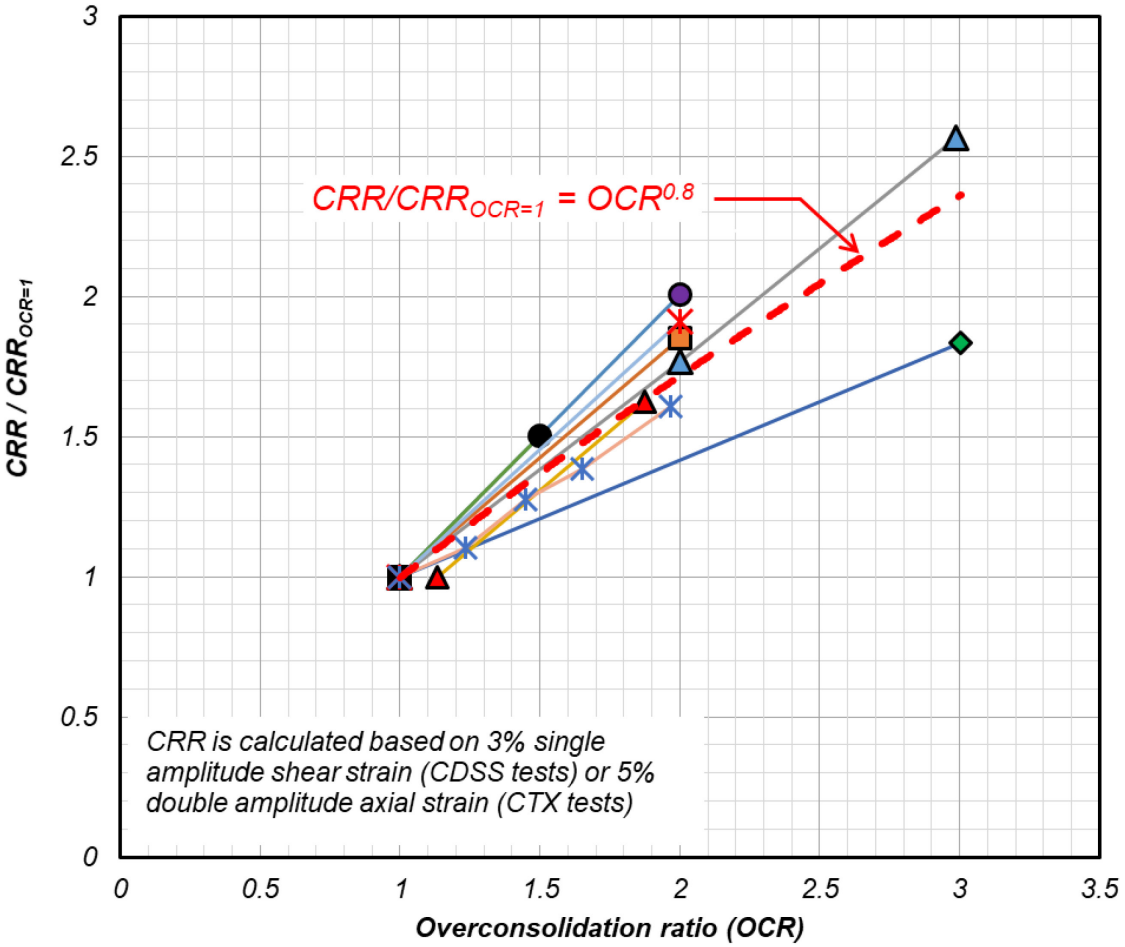

Figure 2.5b: Effect of OCR on cyclic resistance ratio

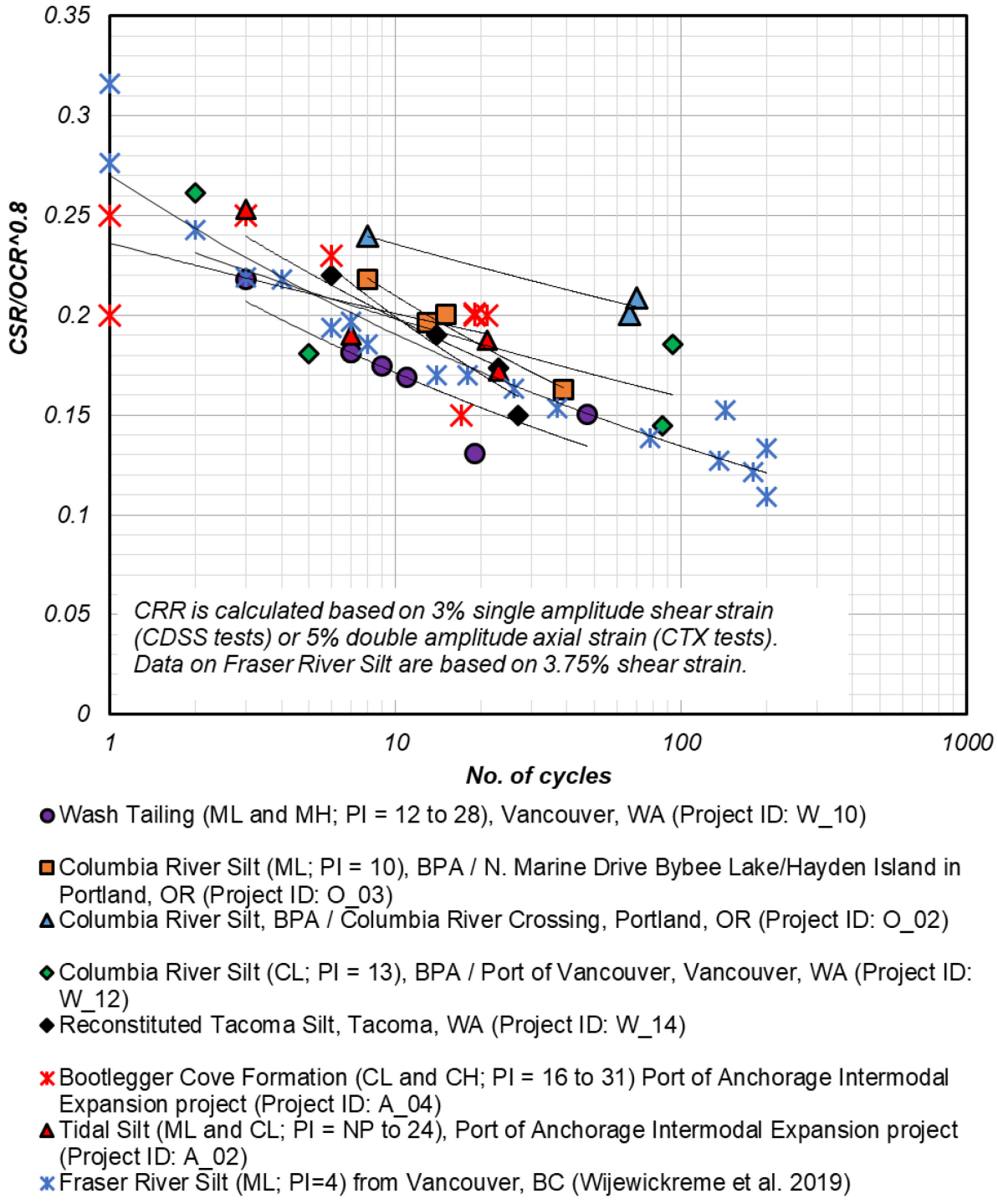

Figure 2.5c: Cyclic stress ratio normalized by OCR^0.8 versus number of cycles to reach a reference shear strain (CDSS) or axial strain (CTX)

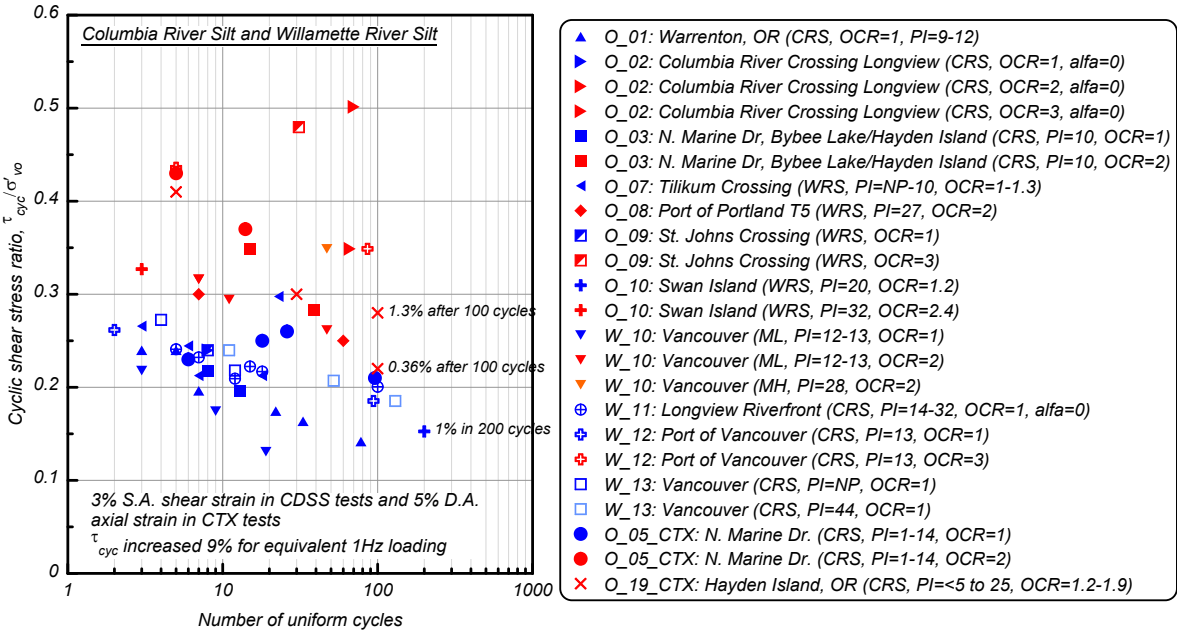

Figure 2.6a: Cyclic stress ratio versus number of loading cycles for Columbia River Silt and Willamette River Silt samples.

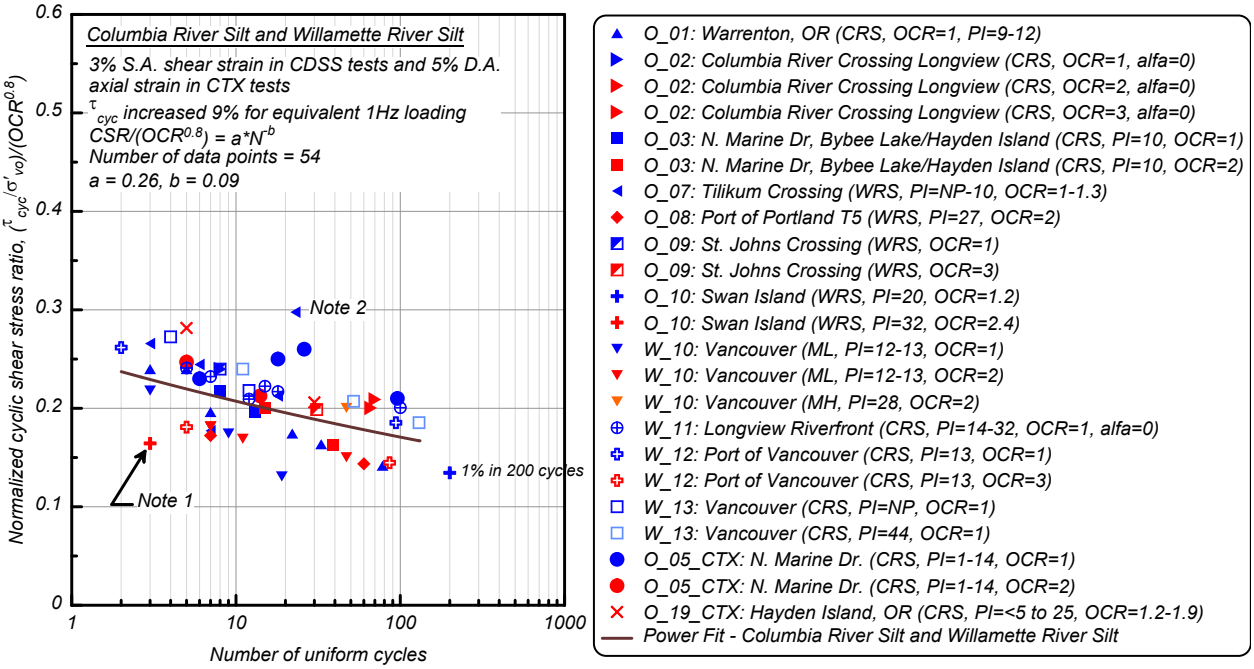

Note 1: OCR of 2.4 for Swan Island samples (O_10) is field value.
Lab created OCR is 1.
In situ σ'vp=5200 psf
in situ σ'vo=2277 psf
lab σ'vc=2200 psf (consolidation stress)
lab σ'vo=2200 psf (stress prior to cyclic)

Note 2: Excluded from fit. 3rd test from staged cyclic loading.

Figure 2.6b: OCR-normalized cyclic stress ratio versus number of loading cycles for Columbia River Silt and Willamette River Silt samples.

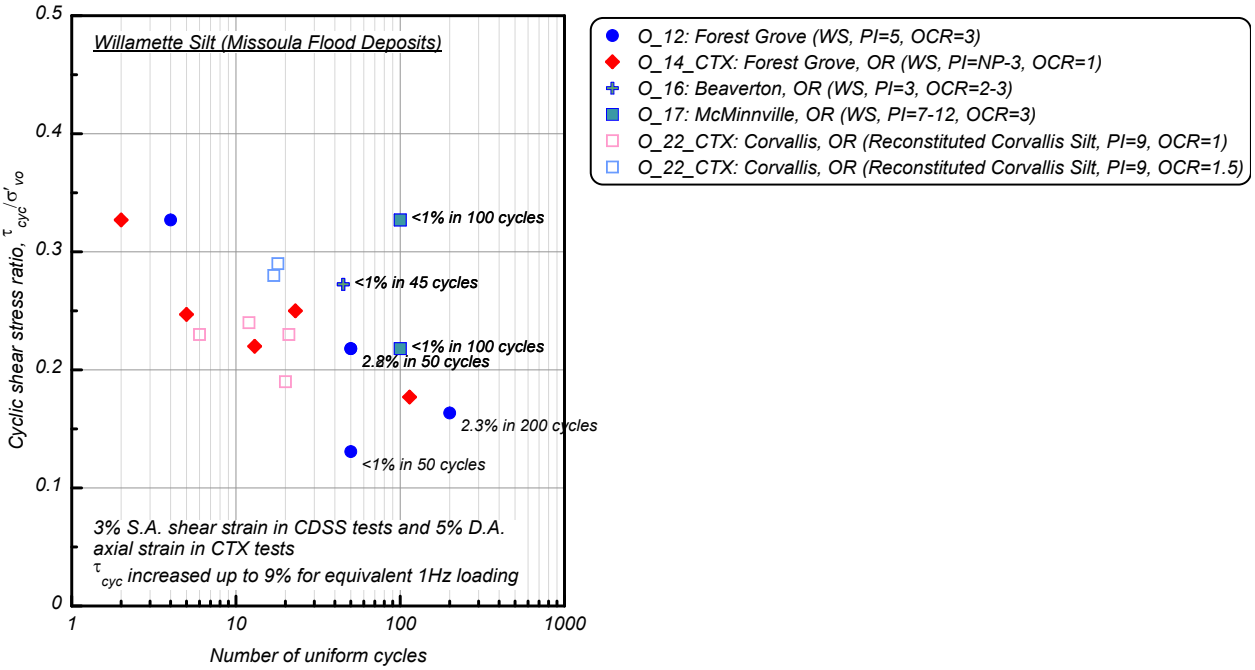

Figure 2.7a: Cyclic stress ratio versus number of loading cycles for Willamette Silt (Missoula Flood Deposit) samples.

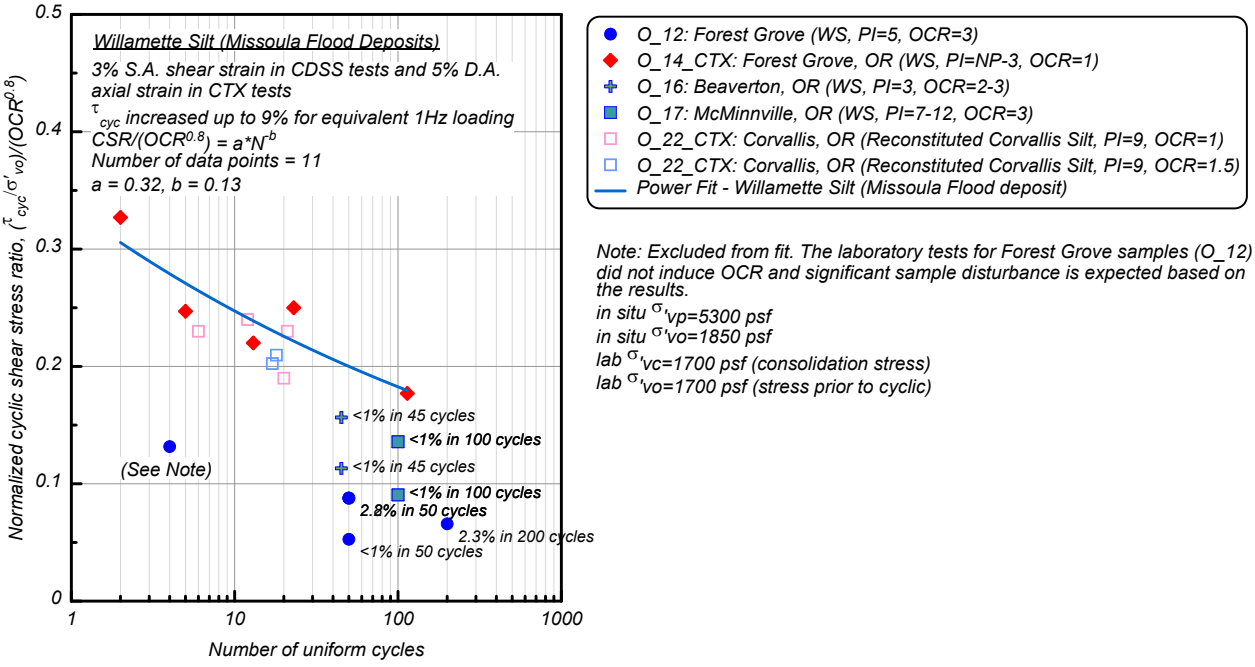

Figure 2.7b: OCR-normalized cyclic stress ratio versus number of loading cycles for Willamette Silt (Missoula Flood Deposit) samples.

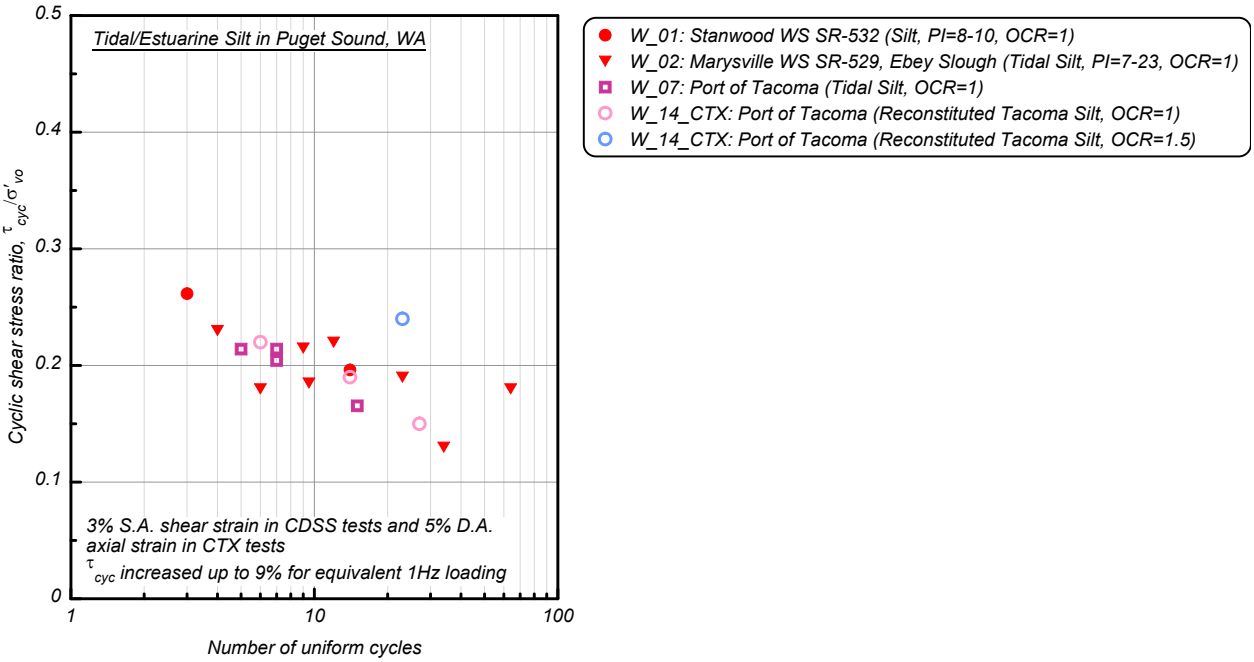

Figure 2.8a: Cyclic stress ratio versus number of loading cycles for Tidal/Estuarine silt soils in Puget Sound, Washington

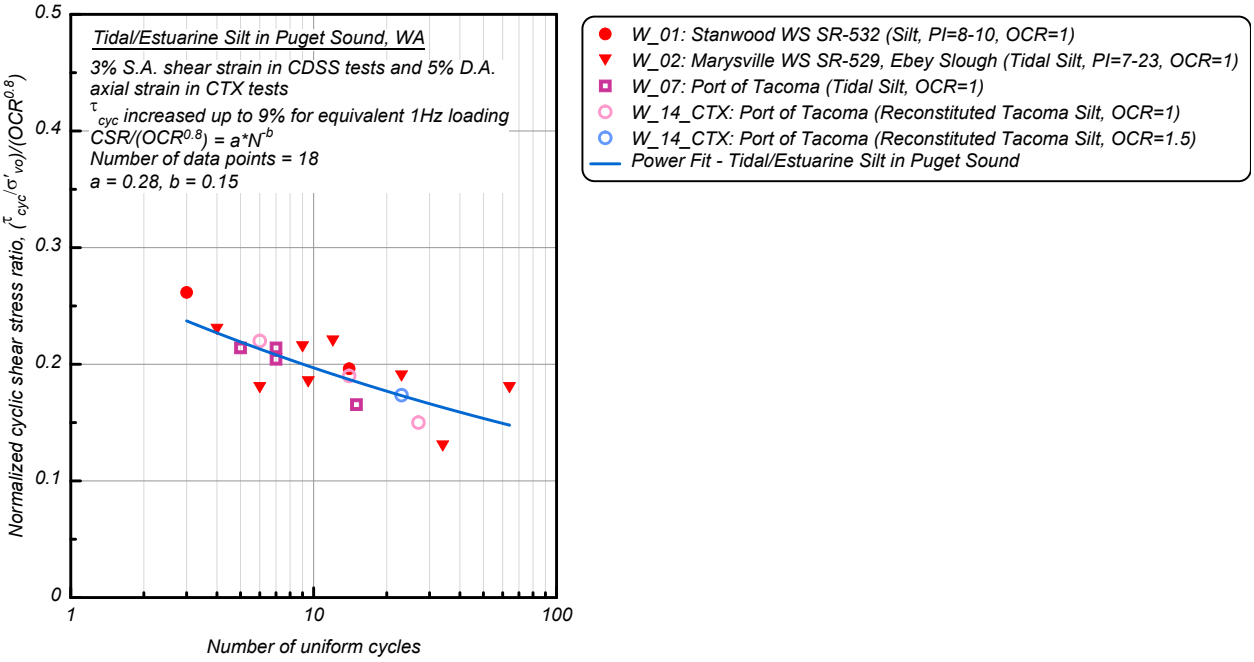

Figure 2.8b: OCR-normalized cyclic stress ratio versus number of loading cycles for Tidal/Estuarine silt soils in Puget Sound, Washington

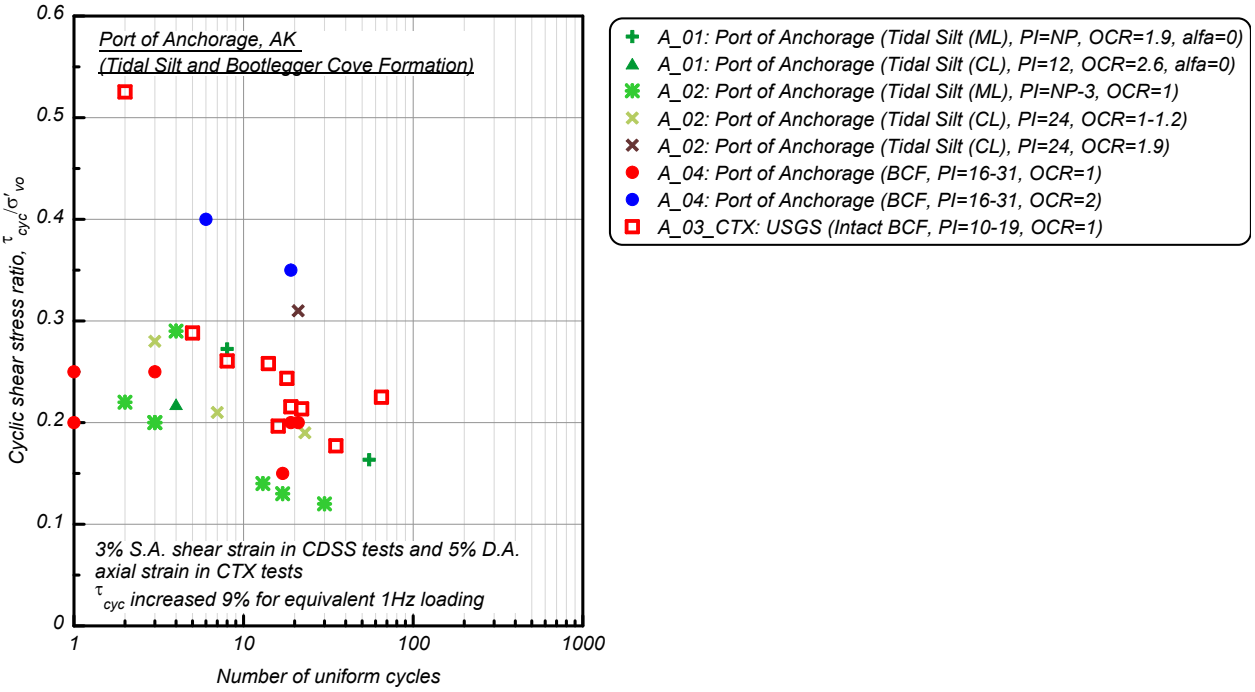

Figure 2.9a: Cyclic stress ratio versus number of loading cycles for Tidal Silt and Bootlegger Cove Formation in Port of Anchorage

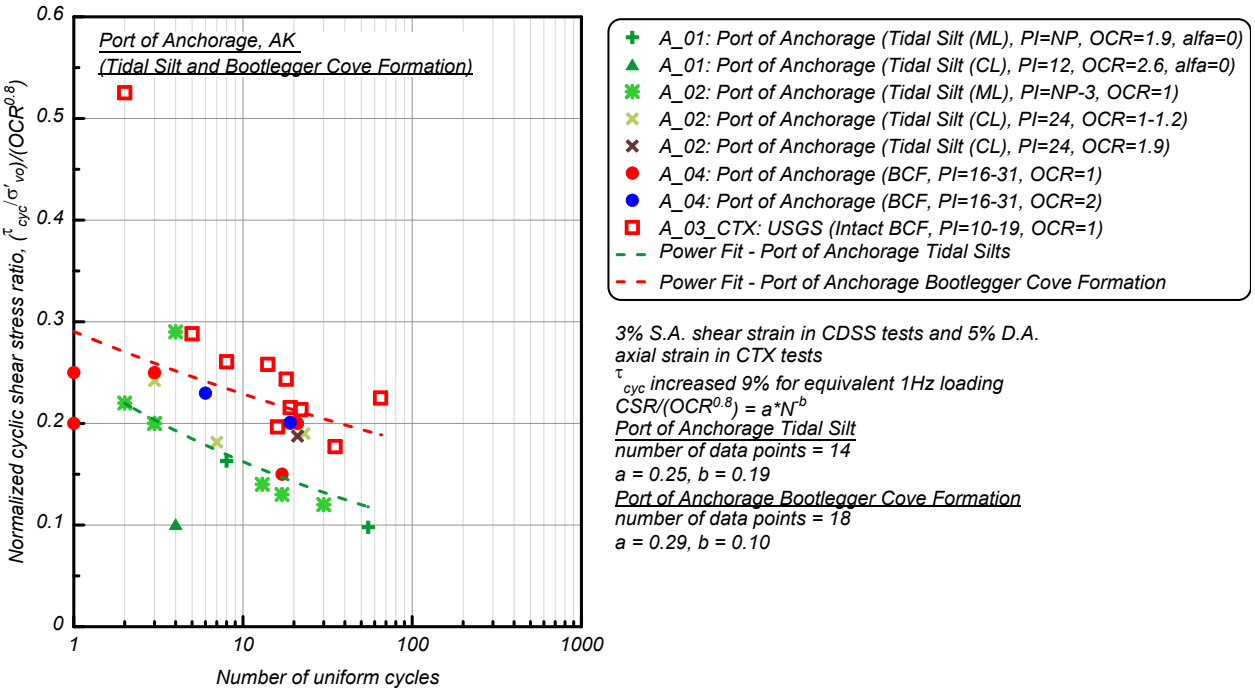

Figure 2.9b: OCR-normalized cyclic stress ratio versus number of loading cycles for Tidal Silt and Bootlegger Cove Formation in Port of Anchorage

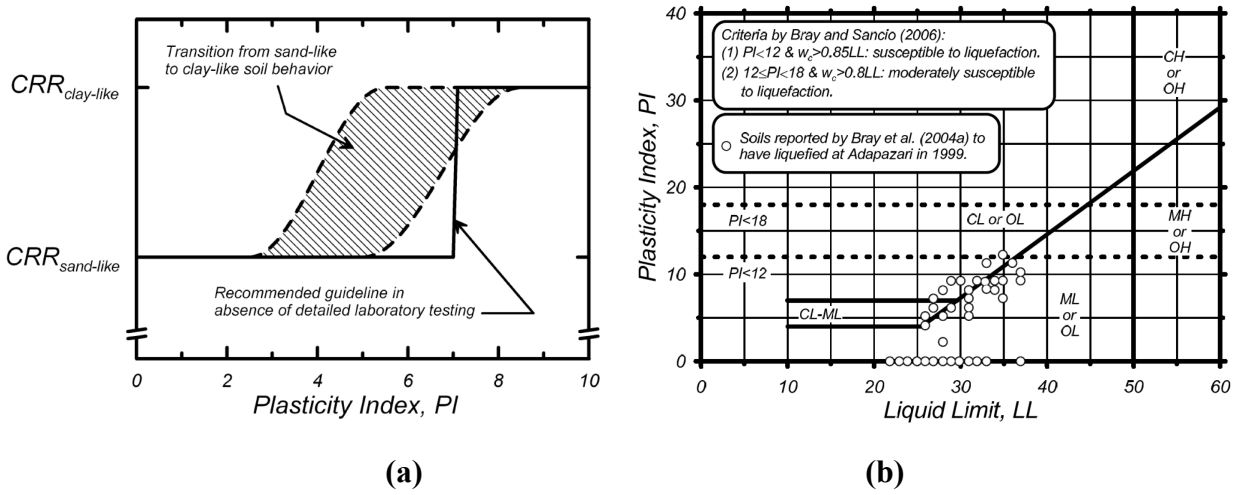

Figure 2.10: Liquefaction susceptibility of fine-grained soils (a) proposed criteria by Idriss and Boulanger (2008), (b) proposed criteria by Bray and Sancio (2006) reproduced by Boulanger.

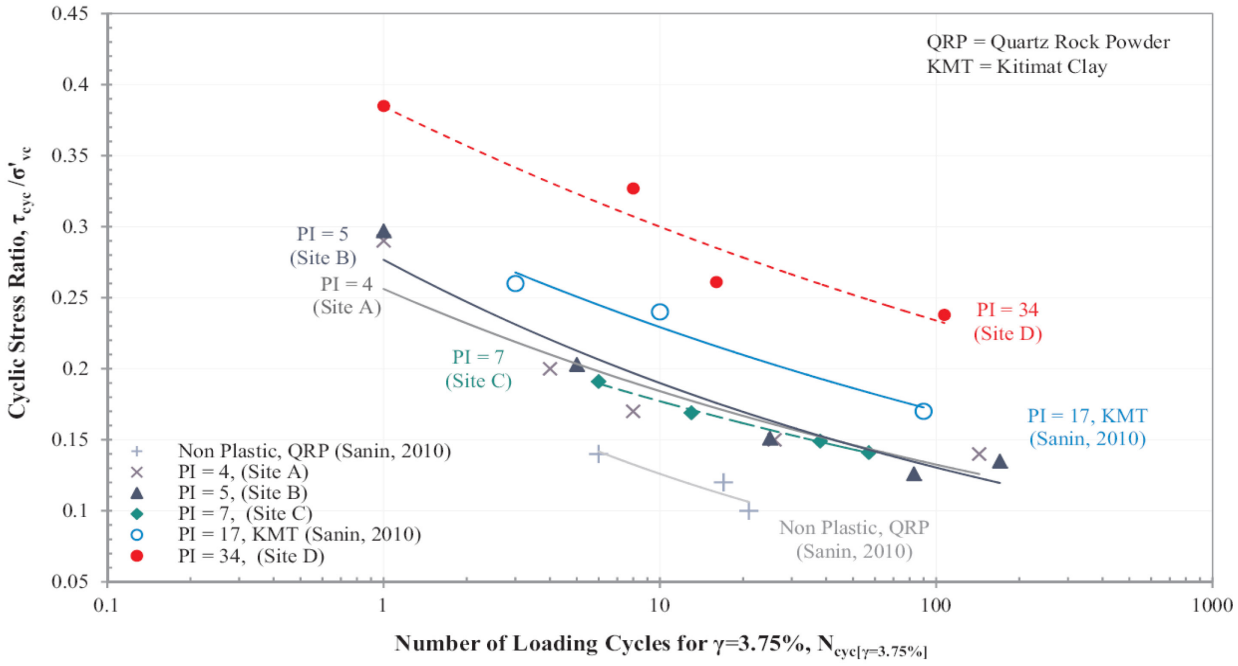

Figure 2.11: Cyclic stress ratio versus number of loading cycles to shear strain of 3.75% for fine grained soils with different plasticity indices (Wijewickreme et al., 2019)

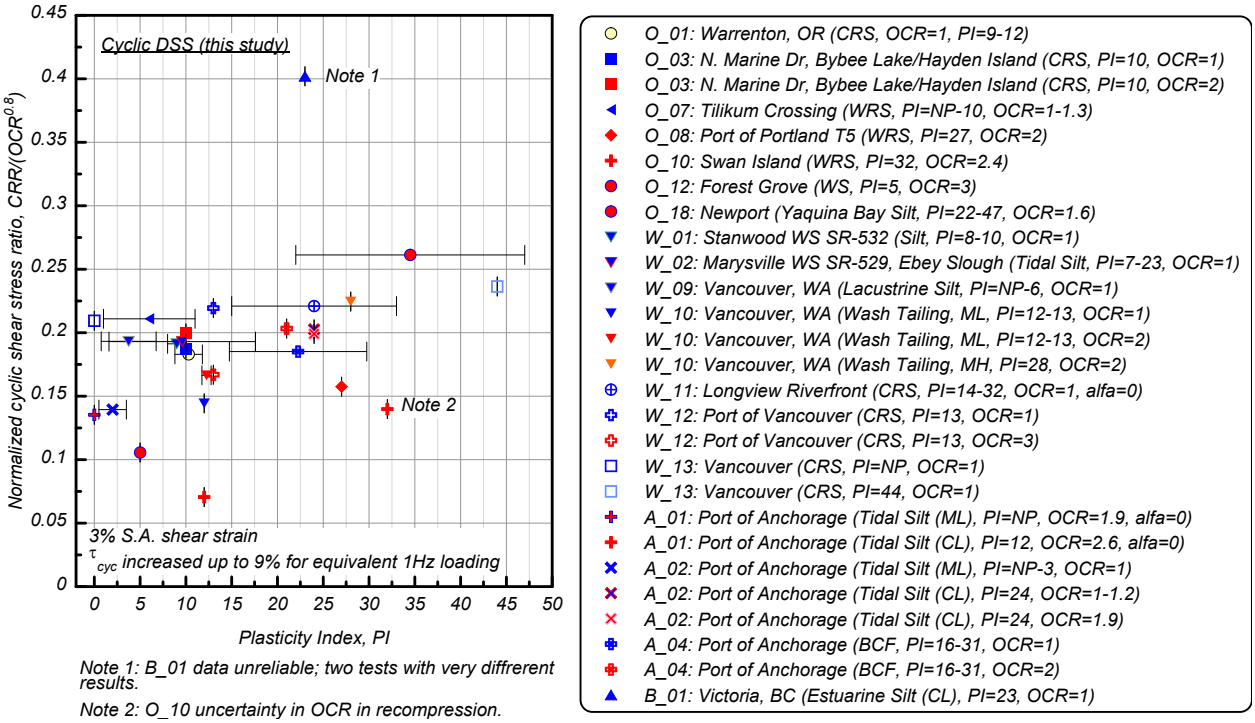

Figure 2.12: OCR-normalized cyclic stress ratio versus plastic index from CDSS tests. Error bars show the range for tested samples.

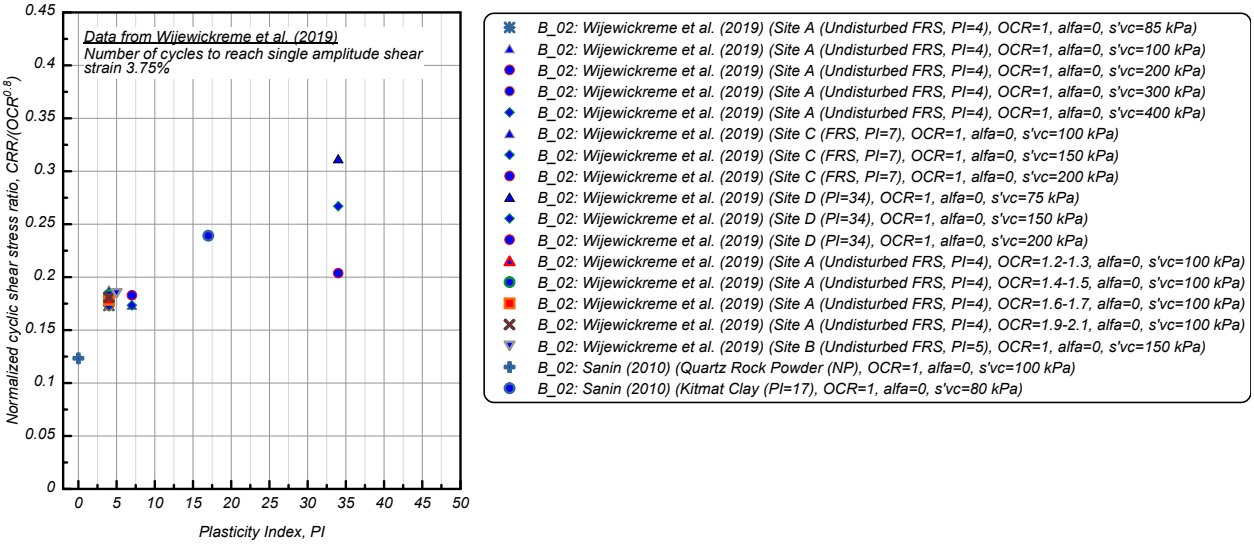

Figure 2.13: OCR-normalized cyclic stress ratio versus plastic index analyzed from data in Wijewickreme et al. (2019)

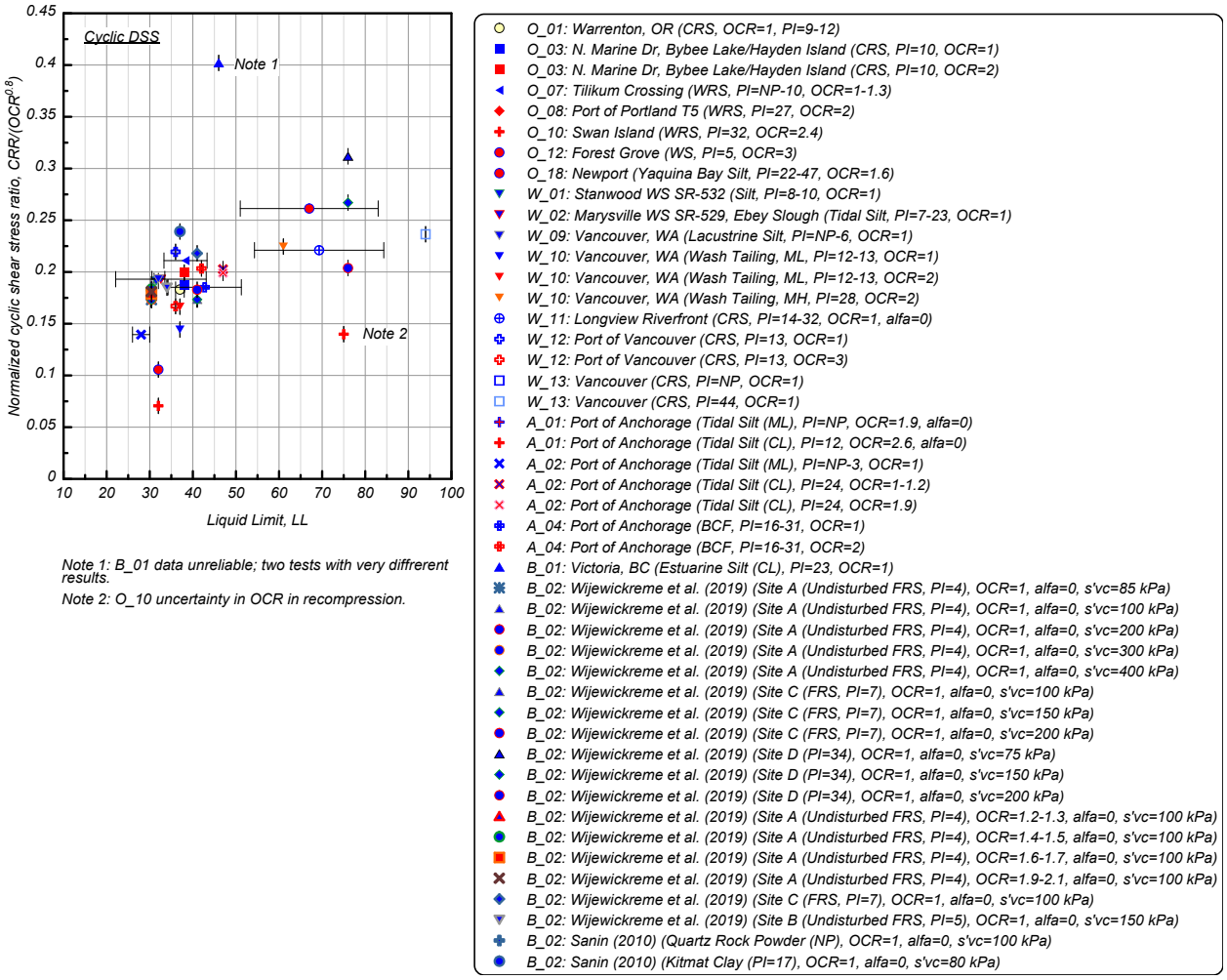

Note 1: B_01 data unreliable; two tests with very diffrerent results.

Note 2: O_10 uncertainty in OCR in recompression.

Figure 2.14: OCR-normalized cyclic stress ratio versus liquid limit

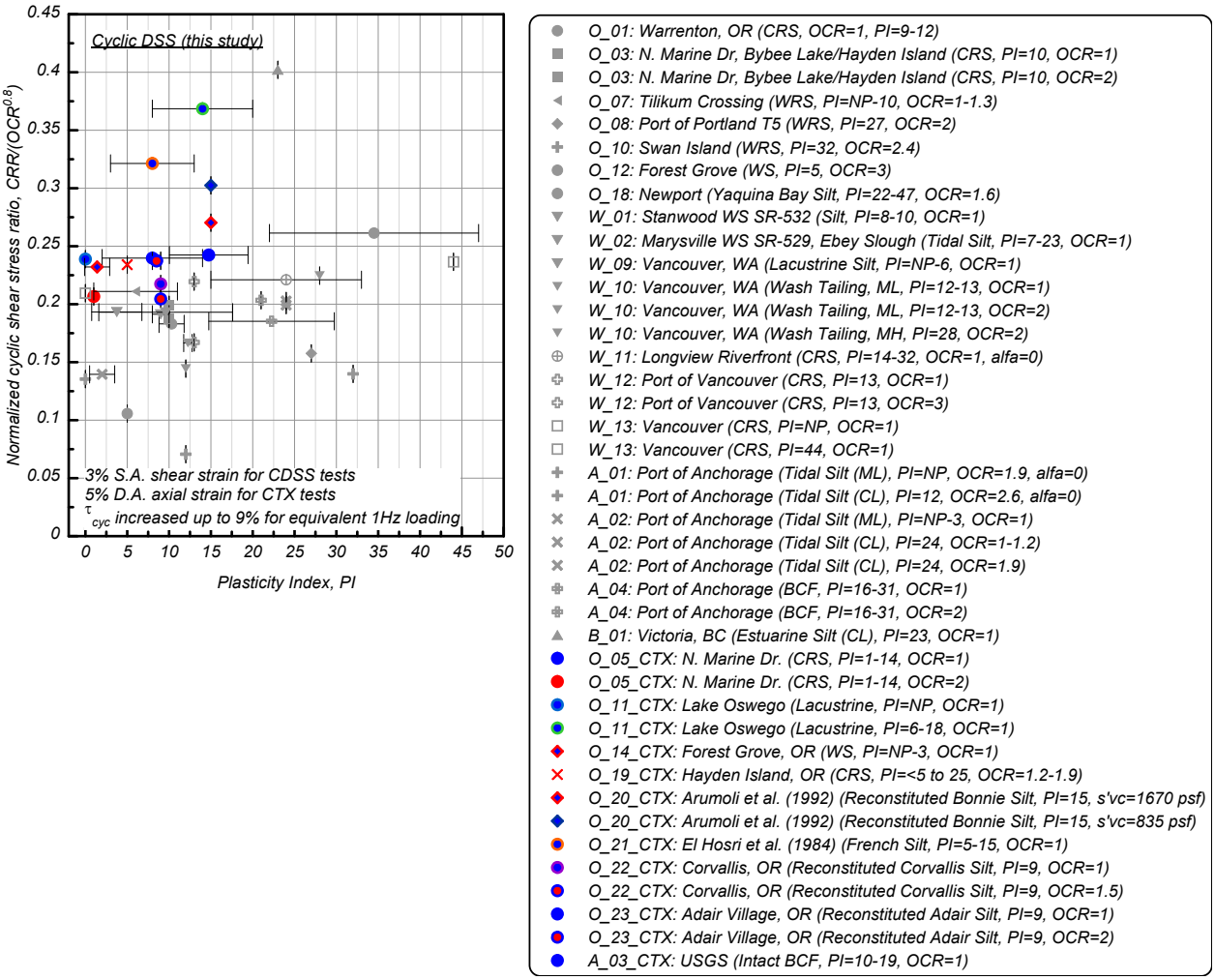

Figure 2.15: OCR-normalized cyclic stress ratio versus plastic index from CDSS and CTX tests

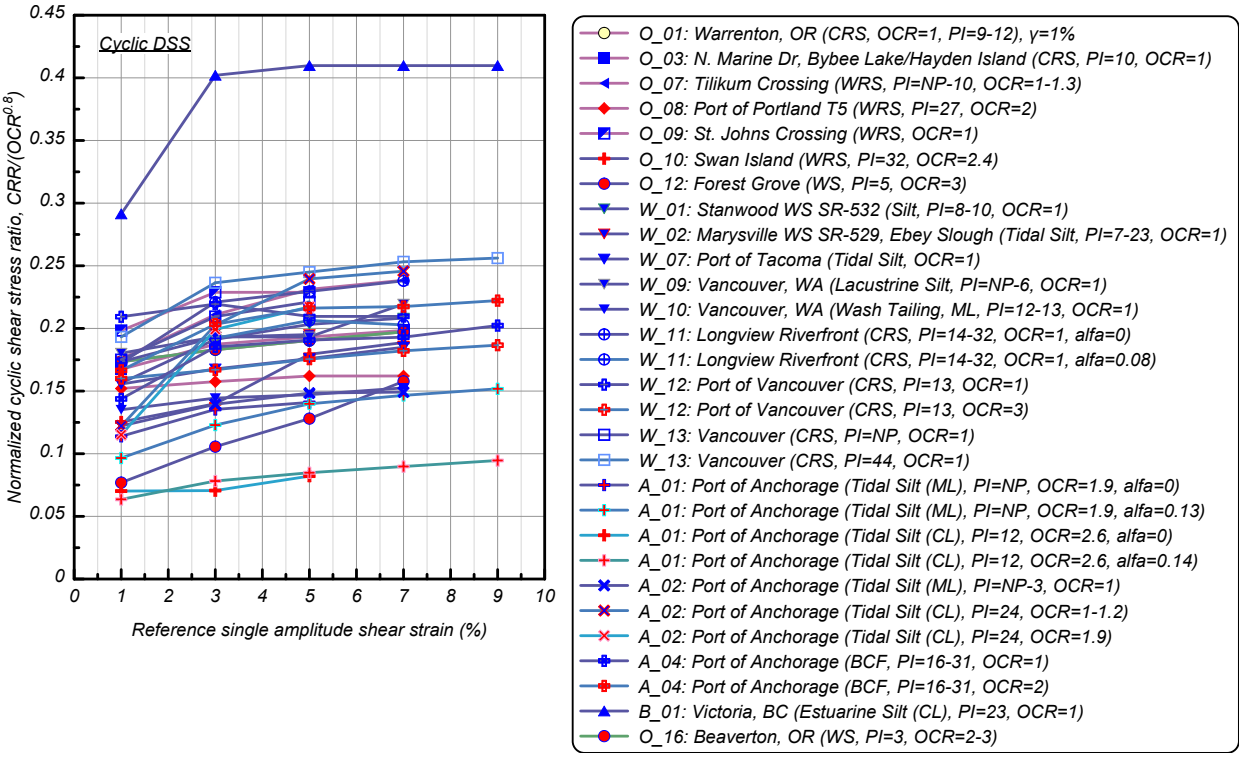

Figure 2.16a: OCR-normalized cyclic resistance ratio to reach different reference shear strains in 15 cycles - CDSS tests

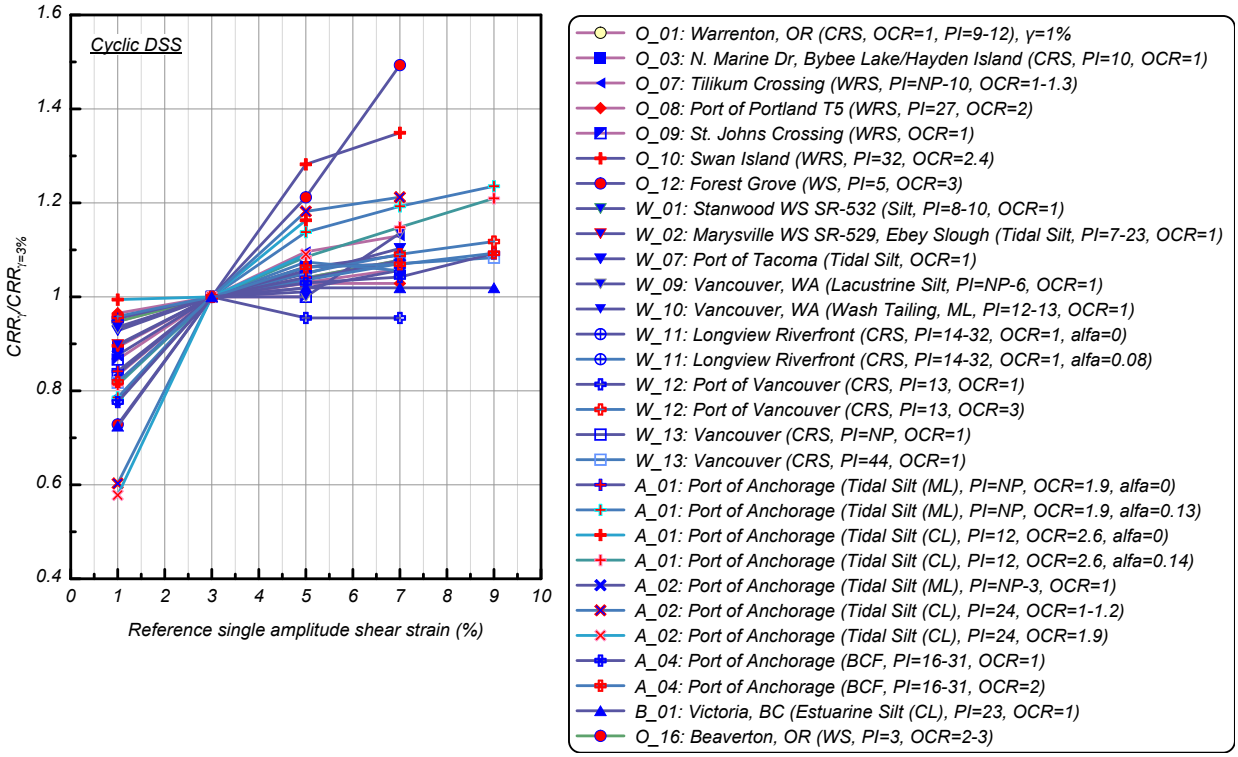

Figure 2.16b: CRR at a given reference shear strain normalized by CRR at a single amplitude shear strain of 3% - CDSS tests

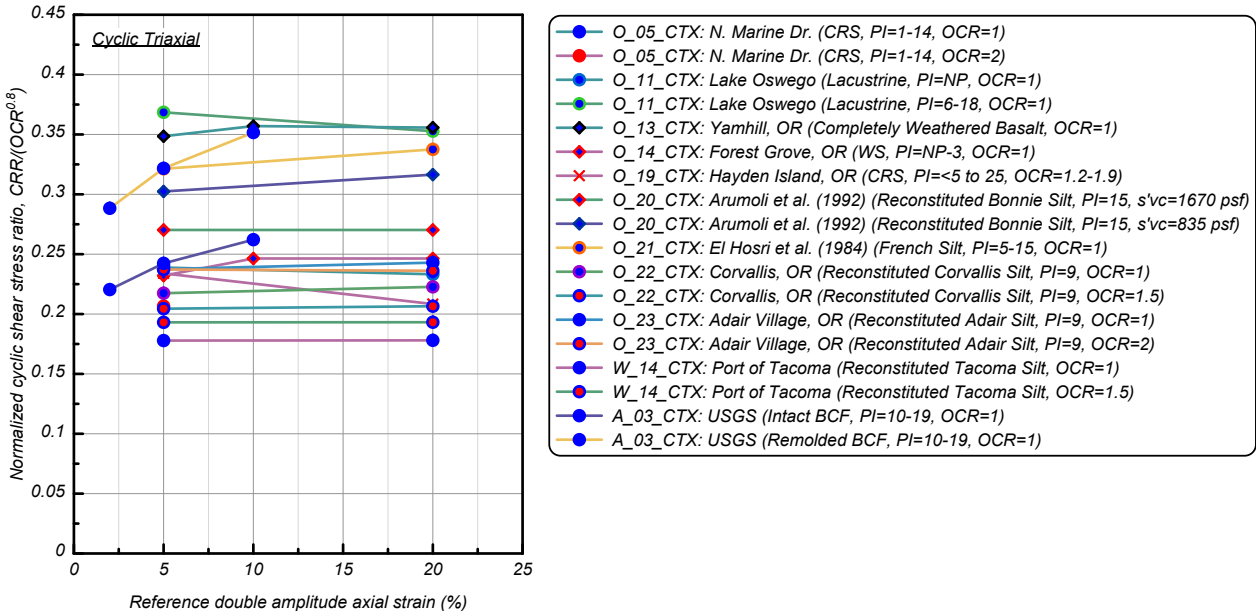

Figure 2.17a: OCR-normalized cyclic resistance ratio to reach different reference axial strains in 15 cycles - CTX tests

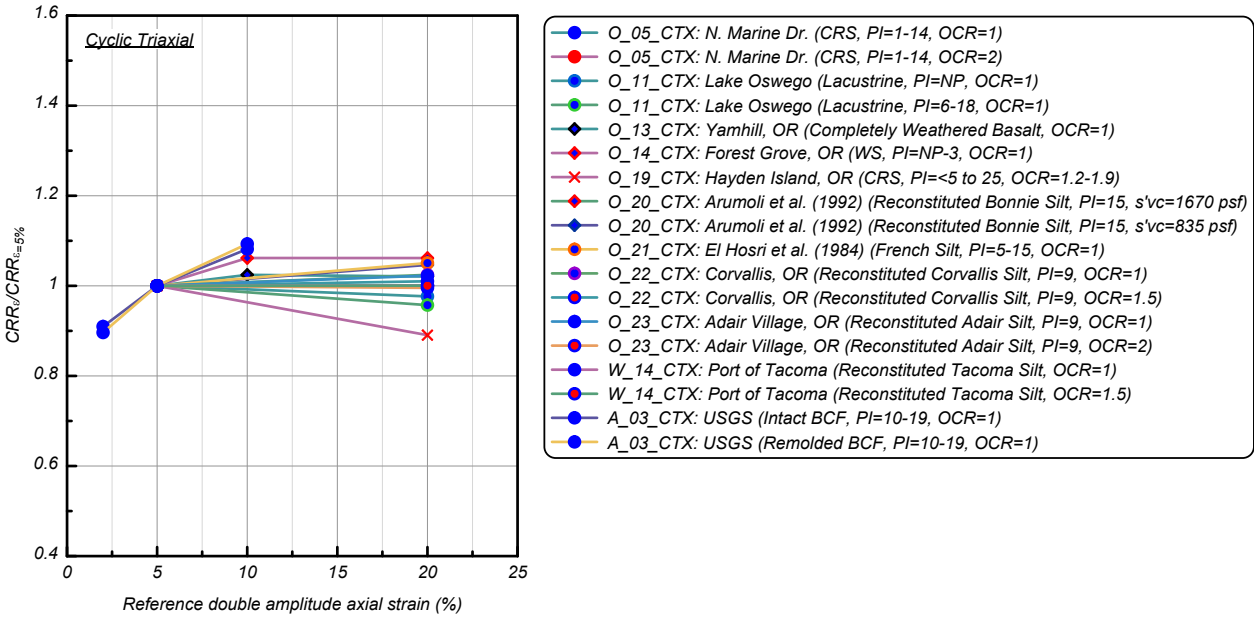

Figure 2.17b: CRR at a given reference axial strain normalized by CRR at a double amplitude axial strain of 5% - CTX tests

CHAPTER 3

Post-Cyclic Stress-Strain Behavior and
Cyclic Degradation of Undrained Shear Strength

CHAPTER 3 CONTENTS

3-1 INTRODUCTION 46

3-2 STATIC UNDRAINED SHEAR STRENGTH 46

3-3 POST-CYCLIC STRESS-STRAIN-STRENGTH BEHAVIOR 49

3-3.1 General Observations from Constant Volume DSS Tests 49

3-3.2 Influence of Maximum Accumulated Shear Strain and Excess Pore Pressure on the Post-Cyclic Strength Ratio 52

3-3.3 Cyclic Degradation of Undrained Shear Strength 57

3.4 OBSERVATIONS AND GENERAL CONSIDERATIONS BASED ON THE TRENDS PRESENTED 62

3.5 REFERENCES 65

3-1 INTRODUCTION

The accumulation of shear strain and excess pore pressure during cyclic loading of saturated silt (addressed in chapters 2 and 5, respectively) can result in a progressive softening of the stress – strain behavior, with degradation of both stiffness and strength. This behavior is commonly evaluated in laboratory testing following a three-step procedure that includes; (i) consolidation phase to the defined vertical effective stress and target over-consolidation ratio (OCR), (ii) cyclic loading phase intended to bracket the amplitude and number of loading cycles to be representative of the regional seismic hazard, and (iii) the post-cyclic loading phase, wherein a static, monotonic load is applied immediately after the cyclic load to minimize the dissipation of excess pore pressure between the final two-steps of the testing sequence. The stress-strain-strength behavior of the silt immediately after cyclic loading is compared to the results of static tests to quantify the reduction in stiffness and strength as a function of maximum accumulated shear strain or residual (i.e., average of peak-to-peak) excess pore pressure generated during cyclic loading. This practice-oriented approach of evaluating post-cyclic behavior provides trends in the post-cyclic strength of the silt used in seismic deformation analyses, including straightforward Newmark analysis using a strain- or displacement-dependent shear strength to define k_y, or in calibration of constitutive models for the progression from moderate to large-strain behavior (e.g., PM4Sand, PM4Silt, UBCHYST, Hyper-U).

The post-cyclic behavior of the silt deposits examined in this regional investigation has been evaluated using all of the triaxial and Direct Simple Shear (DSS) data collected; however, this chapter focuses on a synthesis of the results of only the constant-volume, stress-controlled DSS tests. The influence of depositional environment, soil composition, consistency, and stress history on the stress-strain behavior of the silt deposits was investigated for the broad range of cyclic loading conditions represented in the database (e.g., stress history [OCR], Cyclic Stress Ratio, number of cycles, maximum cyclic shear strain and excess pore pressure development). The subsections of this chapter generally follow the steps previously outlined for the evaluation of cyclic degradation, with a focus on the comparison of the post-cyclic stress-strain behavior to the static tests, the latter used as the benchmark. The tables and figures provided in this chapter represent a small subset of the data provided in the appendices of this data report. Representative trends in post-cyclic stress-strain behavior are plotted for several of the project sites, providing ranges in the degree of degradation of stiffness and strength, and highlighting the variability associated with the data sets for similar silt deposits.

3-2 STATIC UNDRAINED SHEAR STRENGTH

The static undrained shear strength in constant volume DSS tests serves as the initial condition, or pre-cyclic benchmark, for the assessment of strength degradation due to cyclic loading. The static tests are routinely performed in general conformance with standard procedures (ASTM D 6528); however, it should be noted that different methods for consolidating the specimen to a prescribed OCR have been applied in the projects covered in the database (e.g., consolidation to

the current vertical effective stress in the field, or to a value greater than the maximum past pressure from consolidation testing then unloading to the target OCR). The latter procedure (SHANSEP) has been well presented in the technical literature (e.g., Ladd and Foote, 1974; Koutsoftas and Ladd, 1985; Ladd, 1991).

The undrained shear strength ratio (s_{u_st}/σ'_{vc}) increases with increasing OCR, and this trend is expressed as:

$$s_{u\_st}/\sigma'_{vc} = S \times (OCR)^m \qquad \text{Equation 3-1}$$

Where:

s_{u_st}	:	Static undrained shear strength at a defined shear strain, or within a defined range
σ'_{vc}	:	Vertical effective consolidation stress
S	:	Undrained shear strength ratio, $(s_{u\_st}/\sigma'_{vc})_{nc}$, for the normally consolidated state
OCR	:	Overconsolidation ratio, $(\sigma'_{v,max}/\sigma'_{vc})$
m	:	Curve fitting parameter for the slope of s_{u_st}/σ'_{vc} versus OCR

As an example, the trend of undrained shear strength with OCR for fine-grained soils from the Columbia River and Willamette River in the Portland-Vancouver-Longview region is provided in Figure 3.1. The parameters S and m for this data set are 0.25 and 0.9, respectively. It is important to note that the undrained strength ratio in Figure 3.1 has been defined on the basis of the peak mobilized shearing resistance mobilized at a shear strain of 15%, or less. The reference shear strain can have a significant influence on the reported shear strength, especially for overconsolidated silt that can exhibit strain-hardening stress-strain behavior. The reference shear strain commonly used in research reports ranges from 10% to 15%.

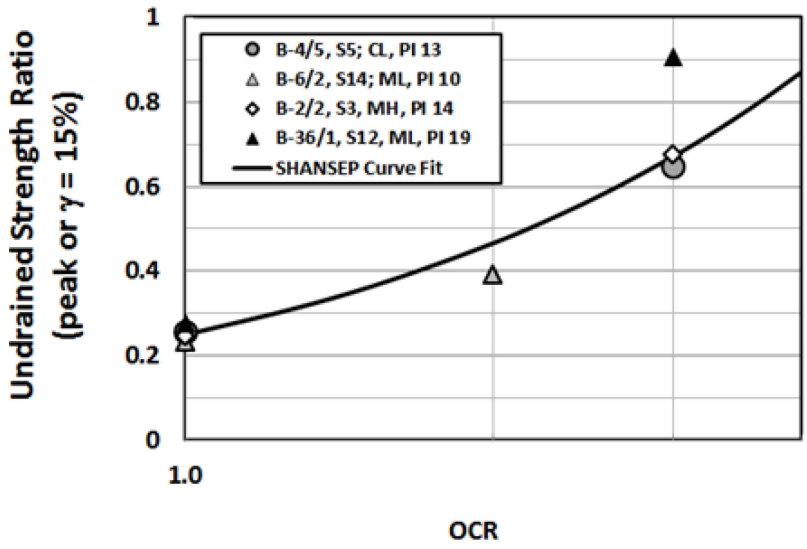

Figure 3.1: Static undrained strength ratio (Beaty et al., 2014).

Static DSS data for sites throughout the regions addressed in this investigation has been evaluated and a summary of the shear strength ratio parameters from selected sites is provided in Table 3-1. All of the undrained shear strengths have been defined as the shearing resistance at 10% shear strain, with the exception of the Columbia and Willamette Rivers (first row of the table), as previously addressed. In the absence of site-specific DSS data a range of likely undrained shear strength values can be established from the trends for similar silt deposits provided in Table 3-1.

Table 3-1: Supporting Data to Compute the Undrained Strength Ratio for Various Silt Deposits

SOIL	DEPTH RANGE (ft)	WATER CONTENT (%)	PI	USCS	CURVE-FITTING PARAMETERS S	m
Columbia & Willamette Rivers[1]	16 – 80	33 - 60	10 - 19	ML - CL	0.25	0.90
Willamette River: Portland	23 - 65	42 - 51	6 - 10	ML	0.25	0.85
Wash-Tailings: Silt		39 - 42	12 - 28	ML - MH	0.29	0.80
Willamette Silt (Site 1)	15 - 30	36 - 43	5 - 16	ML - CL	0.24	0.80
Willamette Silt (Site 2)	10 – 28	n/a	n/a	ML - CL	0.27	0.70
Willamette Silt (Site 3)	14 - 55	31 – 40	2 – 9	ML	0.31	0.75

SOIL	DEPTH RANGE (ft)	WATER CONTENT (%)	PI	USCS	CURVE-FITTING PARAMETERS S	m
General Mark Clark Bridge: Estuarine Silt	34 - 87	33 - 35	8 - 10	ML	0.29	n/a
Fraser River Silt (Site A[2])	18 - 29	34 -39	4	ML	0.26	n/a
Fraser River Silt (Site B[2])	16 - 23	34 - 44	5	ML	0.22	0.76
Fraser River Silt (Site C[2])	14 - 18	38 - 53	7	ML	0.24	0.79
Anchorage: Bootlegger Cove Formation Silty Clay (waterfront site, AK-04)	49 - 142	19 - 31	10 - 31	CL	0.26	0.75
Anchorage: Bootlegger Cove Formation Silty Clay (upland site)[3]	41 - 68	25 - 38	12 - 16	CL	0.21	0.70
Anchorage: Tidal Silt[4]	11 – 26	26 – 29	NP - 12	ML - CL	0.22	0.79

Notes:
[1] Beaty et al. (2014).
[2] Wijewickreme et al. (2019).
[3] WCC (1982), Egan et al. (1984).
[4] Christie, et al. (2019).

3-3 POST-CYCLIC STRESS-STRAIN-STRENGTH BEHAVIOR

3-3.1 GENERAL OBSERVATIONS FROM CONSTANT VOLUME DSS TESTS

The post-cyclic shear strength of fine-grained soils is reported in the form of a post-cyclic strength ratio $(\tau_{cyc} / S_{u\text{-}st})_{Y=x}$, where:

τ_{cyc} : Shearing resistance at a reference shear strain in the post-cyclic monotonic test,
S_{u_st} : Static undrained shear strength at the same reference shear strain

Note that the rate of strain in the static and post-cyclic monotonic tests should be equivalent to eliminate the influence of rate effects on the measured shearing resistance. While this approach provides a useful measure of strength reduction due to cyclic degradation it does not provide an indication of the associated reduction in soil stiffness and overall post-cyclic stress-strain behavior, an aspect of post-cyclic characterization that is important for calibration of constitutive models used in nonlinear deformation analysis. An example of the influence of cyclic degradation on post-cyclic behavior of a silt from the Ebey Slough project site is provided in Figure 3.2. The post-cyclic

reduction in both stiffness and strength is evident in the stress-strain curves. The following trends are noted in the post-cyclic behavior:

1. The results of three static tests are highlighted with red curves as the benchmark,
2. The stress-strain curves for the six post-cyclic monotonic tests are provided with the cyclic loading amplitude (CSR), maximum accumulated shear strain and residual excess pore pressure ratio due to the cyclic loading listed in the legend.
3. For the sake of a general comparison of the influence of residual excess pore pressure on the post-cyclic stress-strain behavior in the six tests can be grouped into three pairs, with Ru ranges of 22% to 24%, 52% to 66%, and 88% to 92%. The variability in post-cyclic stress-strain for each of these three pairs is evident and it is helpful to consider the average of the two tests within each pairing.
4. The average post-cyclic stress-strain behavior of the first pair (Ru 22% to 24%) is similar, yet slightly greater than the upper bound of the trends from the static test. The slight increase is likely due to the inherent variability in the specimens and a trend that is equivalent to the static tests would be recommended for analysis. It is important to note that the generation of minor to nominal excess pore pressure has had a negligible influence on the post-cyclic shear strength at 10% shear strain (i.e., post-cyclic strength ratio ≈ 1.0).
5. The average post-cyclic stress-strain behavior of the second pair (Ru 52% to 66%) is also within the bounds of the static tests, indicating that this moderate excess pore pressure has not resulted in significant cyclic degradation of strength at 10% shear strain.
6. The generation of high excess pore pressures (88% to 92%) results in a significant reduction in the stiffness and shearing resistance of the soil at post-cyclic shear strains less than roughly 7.5%. The two specimens then exhibit strain-hardening behavior with shearing resistance increasing to the maximum shear strain of the test at 20%. This demonstrates the significant influence of the higher Ru on post-cyclic behavior and again highlights the desire to define the shear strength at a prescribe shear strain.
7. Although the trends are subtle in this data set, it is apparent that the average strain to peak shearing resistance for the three pairs increases with Ru. This behavior is common for the silt deposits represented in this database.
8. The post-cyclic stress-strain behavior plotted in Figure 3-2 is soil-specific and provided for the sake of illustration. The influence of cyclically induced excess pore pressure on the post-cyclic strength varies with soil type and factors such as: soil composition, consistency, and stress history as previously noted. Post-cyclic strength ratios as a function of Ru for various soils are addressed in subsection 3-3.2.

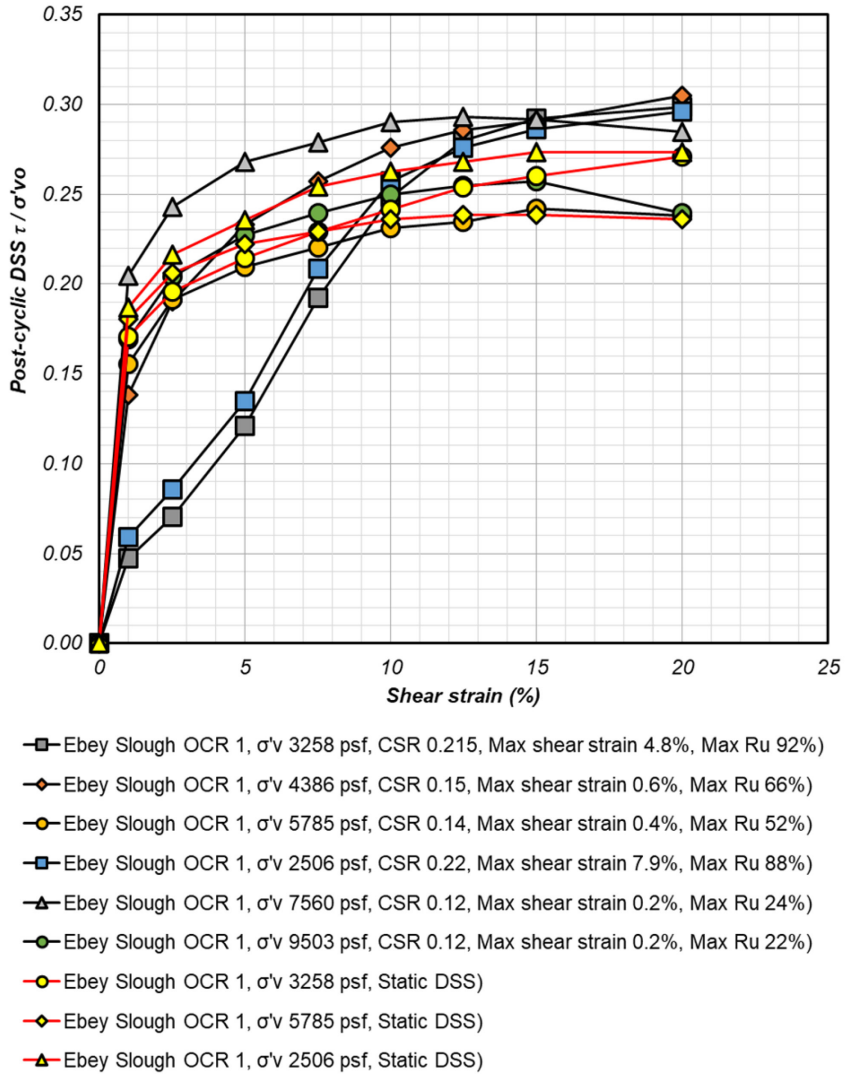

Figure 3.2: Comparison of static and post-cyclic stress – strain behavior in undrained, constant volume, DSS tests on silt from the Ebey Slough site (Project ID: WA-02).

The influence of the maximum Ru on post-cyclic stress-strain behavior is also illustrated for silt from the Lower Columbia River in Figure 3-3. The post-cyclic behavior is similar to that shown in Figure 3.2, with the specimens loaded to Ru in the 0.90 to 0.92 range exhibiting much greater degradation that the specimen loaded to Ru 0.47. The stress-strain curves in Figures 3.2 and 3.3 also highlight the importance of defining a reference shear strain for assigning the post-cyclic shear strength of the silt (i.e., strain-dependent, or strain-limited, strength). When utilizing the post-cyclic data to define the ratio τ_{cyc} / S_{u_st} it is recommended for the sake of consistency to use the same reference shear strain for both strength values. However, in situations where the geotechnical feature (e.g., slope, earth structure, foundation) is sensitive to cyclic and post-cyclic

deformations, it may be prudent to evaluate the post-cyclic shearing resistance at a smaller shear strain (e.g., 5% to 10%).

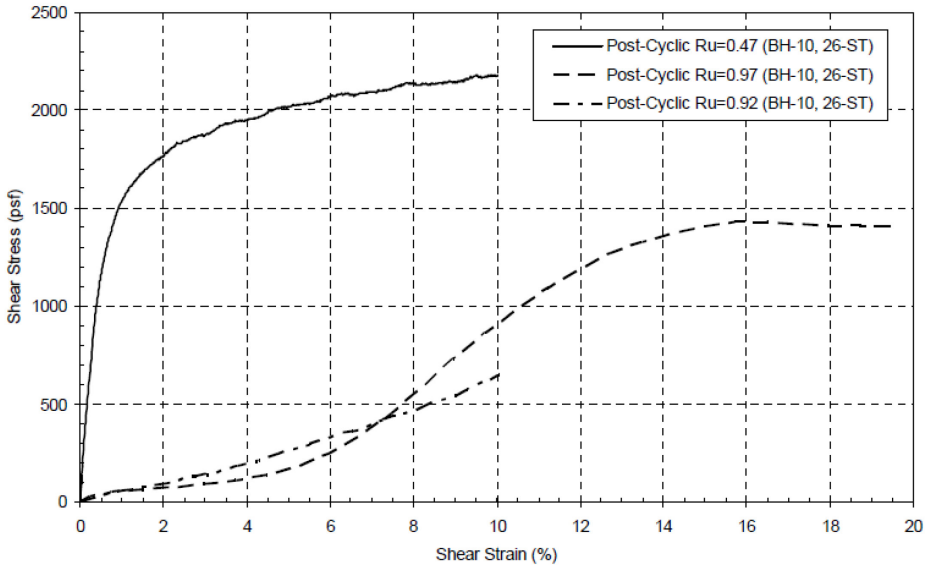

Figure 3.3: Post-Cyclic Stress – Strain curves for Silt from the Lower Columbia River (Site ID: OR-01) (McCullough et al., 2009).

3-3.2 INFLUENCE OF MAXIMUM ACCUMULATED SHEAR STRAIN AND EXCESS PORE PRESSURE ON THE POST-CYCLIC STRENGTH RATIO

The reduction in undrained shear strength due to cyclic loading has been found in this investigation, and in numerous others, to be related to the maximum shear strain mobilized and excess pore pressure exhibited during cyclic loading. Both reflect the amplitude and number of loading cycles, and are associated with the general disruption of the undisturbed fabric of the soil due to shearing. The influence of maximum accumulated shear strain on the post-cyclic monotonic stress-strain behavior for specimens from the Columbia River near Portland and Vancouver is illustrated in Figure 3.4. Three specimens were cyclically loaded to maximum shear strains of 0.7%, 4.2%, and 6.4%. The reduction in post-cyclic strength and stiffness as a function of the maximum cyclic shear strain is evident; however, it is noted that the specimen loaded to a maximum cyclic strain of 0.7% did not exhibit a reduction in undrained shearing resistance relative to the static behavior, as indicated by the peak normalized, cyclic strength ratio of 1.0. It is also noted that the strain required to reach the peak, post-cyclic shearing resistance increased with increasing cyclic shear strains of 4.2% and 6.4%. The maximum residual excess pore pressure ratios (Ru) exhibited in the cyclic tests are provided in the legend of Figure 3.4. As is commonly observed for inherently contractive specimens, the maximum Ru increased with maximum cyclic strain

indicating that either response characteristic could be used in correlations with post-cyclic strength and stiffness.

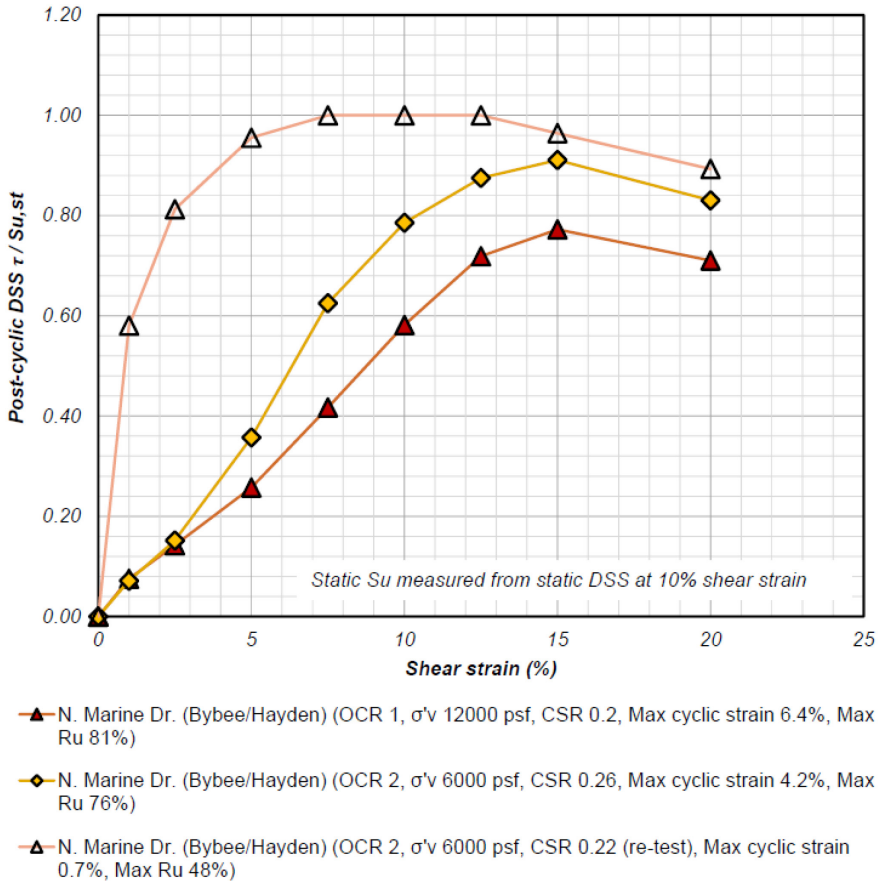

Figure 3.4: Post-Cyclic Normalized Stress – Strain Behavior for Three Specimens of Columbia River Silt (Site ID OR-03).

The post-cyclic monotonic behavior of a silty clay from the Bootlegger Cove Formation (BCF) at a waterfront site in Anchorage, Alaska (Site ID: AK-04) is provided as an additional example of the influence of maximum cyclic shear strain and Ru on cyclic degradation. The post-cyclic behavior of 16 specimens of the BCF silt is plotted in Figure 3.5, with the maximum cyclic shear strain and Ru provided in the legend. The influence of cyclic shear strain and Ru on post-cyclic monotonic behavior is again evident and inherent variability noted in the correlation with cyclic degradation defined on the basis of the post-cyclic strength ratio at 10% shear strain. The stress-strain curves are clustered in three general groups (i.e., three general ranges of observed cyclic degradation); the upper 6 tests, the intermediate 4 tests, and the lower 6 tests. The mean values of the maximum shear strain and residual Ru (Y_{cyc}, Ru) for these three groupings are (0.7%, 22), (6.9%, 45), and (11.9%, 77), respectively. The mean values for each of the three groups have been found to be

well-correlated with the cyclic degradation model for undrained shear strength addressed in section 3-3.3.

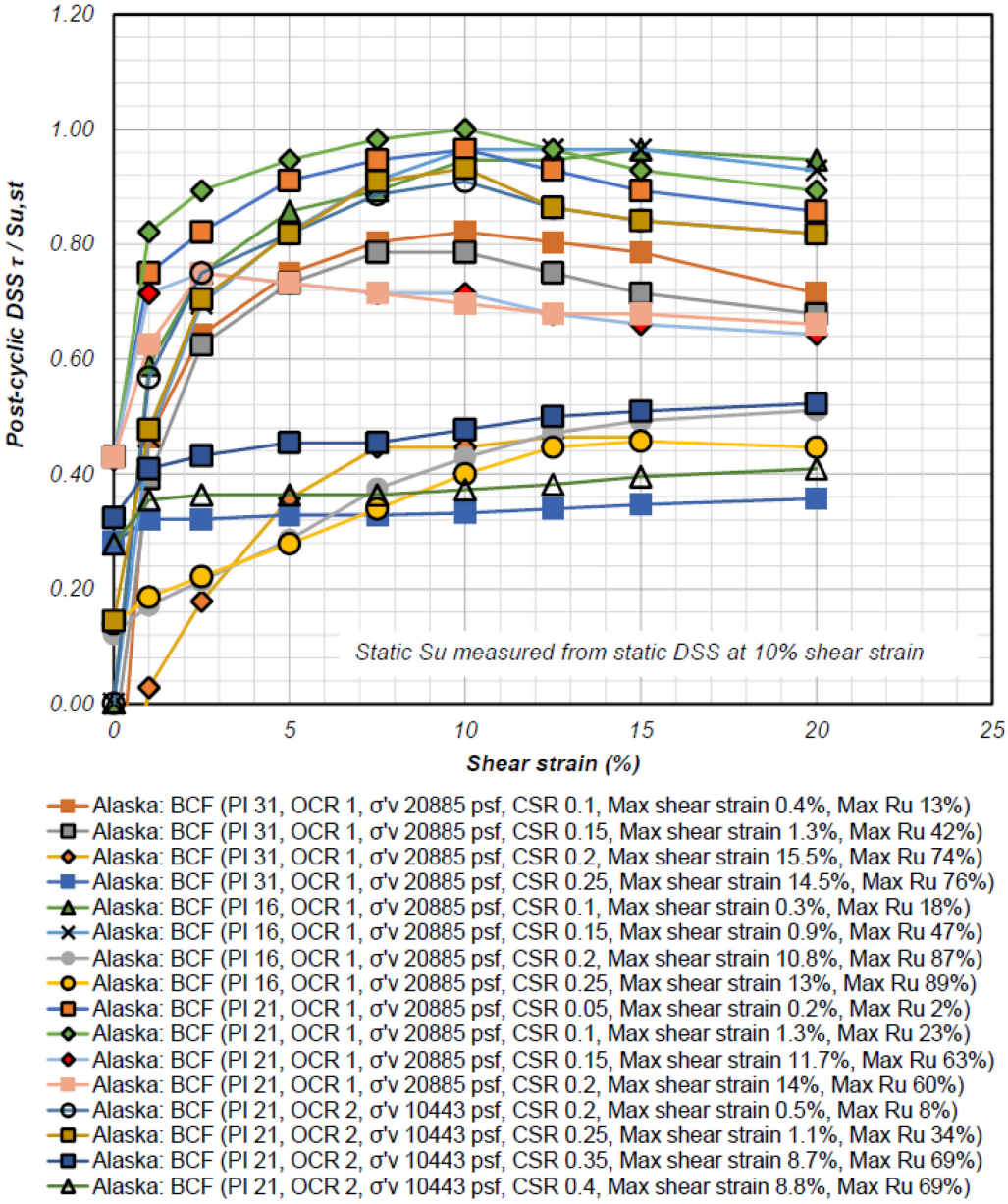

Figure 3.5: Post-Cyclic Normalized Stress – Strain Behavior for 16 Specimens of Predominantly Silty Clay from the Bootlegger Cove Formation, Anchorage, Alaska (Site ID: AK-04).

The relationship between cyclic shear strain and maximum residual Ru is provided in Figure 3.6a for the stress-strain curves plotted for specimens from two sites along the Columbia Rivers (Figures 3.3 and 3.4), and for the Bootlegger Cove Formation (Figure 3.5), demonstrating the general trends and inherent variability associated with specimens of native soil. The trends for all data collected in this investigation are illustrated in Figure 3.6b, providing a range for the various

silt deposits and sites evaluated. The trends provide the basis for a correlation between peak shear strain and peak Ru, a useful relationship for calibration of constitutive models for cyclic loading of silt and for bracketing a range of likely Ru values from the results of dynamic site response using Total Stress Analysis in which the cyclic shear strain is computed, and Ru must be estimated in an uncoupled manner. In the remainder of this chapter post-cyclic degradation of both stiffness and strength is related to excess pore pressure generation during cyclic loading as this was found to provide slightly improved correlation with the post-cyclic strength ratio and has been used in numerous investigations of post-cyclic behavior of fine-grained soils. This is likely due to influence of cyclic strain amplitude, number of load cycles, and stress history (OCR) on Ru and the post-cyclic behavior. The focus on Ru as the basis for estimating post-cyclic behavior necessitates practical procedures for estimation of Ru on projects that do not include cyclic laboratory testing. The following methods are suggested for consideration; however, each should be evaluated in terms of the method of approximation and inherent uncertainty associated with a specific approach. The estimation of Ru could be made in one or more ways, including:

1. Excess pore pressure computed in 1D site response using Effective Stress Analysis (e.g., DEEPSOIL) with the Pore Pressure Parameters provided in Chapter 5.
2. Compute the maximum shear strain in 1D site response using Total Stress Analysis (e.g., DEEPSOIL, SHAKE), convert the maximum shear strain to the equivalent, uniform shear strain to be consistent with laboratory testing, and apply a suitable correlation between the maximum shear strain and maximum Ru, such as provided in Figure 3-6.

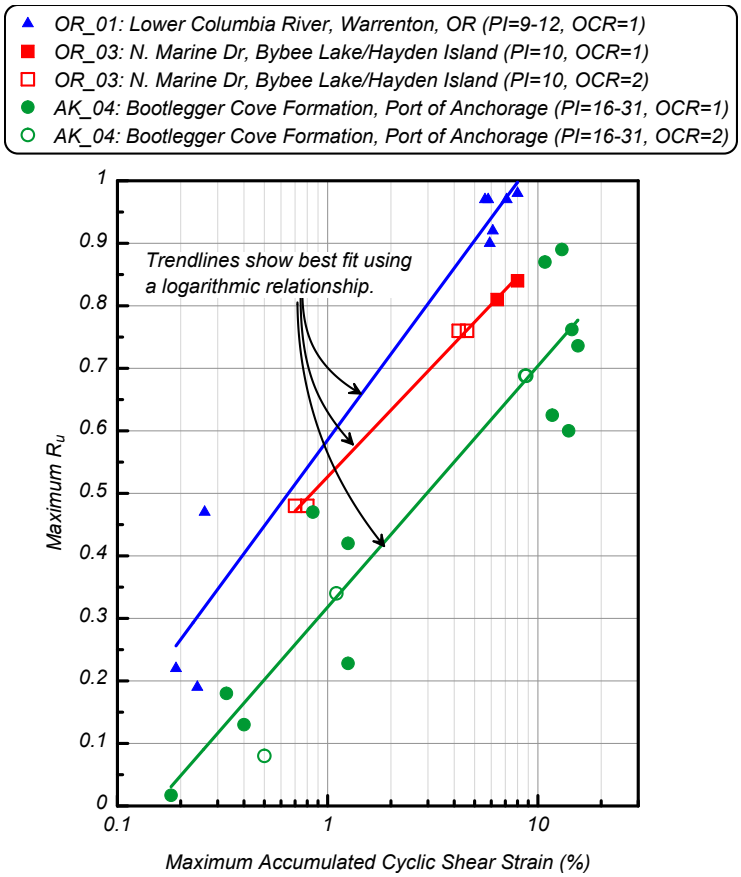

Figure 3.6a: Relationship between Maximum Ru and Maximum Accumulated Shear Strain in Constant Volume Cyclic DSS Tests on Two Columbia River Soils and the Bootlegger Cove Formation.

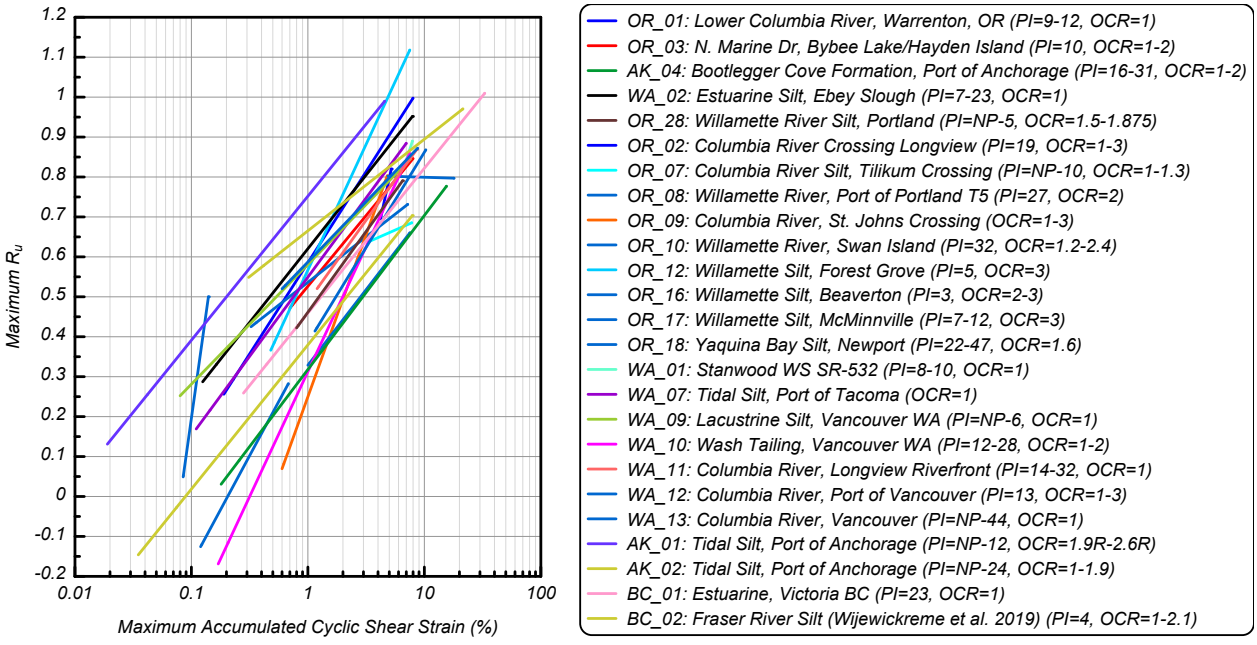

Figure 3.6b: Relationship between Maximum Ru and Maximum Accumulated Shear Strain in Constant Volume Cyclic DSS Tests on Silt from Various Sites.

The post-cyclic stress-strain curves, with maximum cyclic shear strain and Ru values, are provided in Appendices A to D for all of the available data sets.

3-3.3 CYCLIC DEGRADATION OF UNDRAINED SHEAR STRENGTH

The reduction in cyclic stiffness and post-cyclic undrained shear strength in fine-grained soil due to cyclic loading has been related to excess pore pressure generation in numerous investigations (e.g., Matasovic and Dobry, 1995; Vucetic, 1988; Egan et al., 1985; Beaty et al., 2014; Ajmera et al., 2019). Three examples of the trends in post-cyclic strength ratio (i.e., post-cyclic undrained strength / static undrained strength) as a function of Ru are provided in Figures 3.7 through 3.9 to illustrate the following key aspects of the post-cyclic behavior of the silt deposits evaluated:

1. The influence of residual Ru on cyclic degradation,
2. The influence of reference strain on the post-cyclic strength ratio (i.e., strain-dependency), and
3. The scatter inherent in the lab testing of specimens of native, intact soil (i.e., not reconstituted specimens).

The results of the extensive DSS testing program presented by Beaty and others (2014) are provide in Figure 3.7. The post-cyclic strength ratios at shear strains mobilized in the post-cyclic, monotonic tests of 5% and 10% are plotted against the maximum Ru during cyclic loading. Several aspects of the general trends are useful for practical applications. First, the reduction in undrained shearing resistance (i.e., cyclic degradation) is minor for Ru values less than 0.4, generally less than 5% for these fine-grained soils. The influence of Ru on the post-cyclic strength ratio becomes more pronounced at Ru values in the range of 0.5 to 0.7. As previously noted, the strength reduction is a function of the reference shear strain selected, with the influence of Ru greater at smaller post-cyclic shear strains. This observation may be important for sensitive structures and utilities founded on, or embedded in, silt deposits such as these, where strain-dependent strength and stiffness control seismic design. Finally, the scatter in the trends at for 5% and 10% reference shear strains is evident. This inherent variability should be evaluated on a project-specific basis and ranges of post-cyclic strength used in sensitivity or parametric analysis.

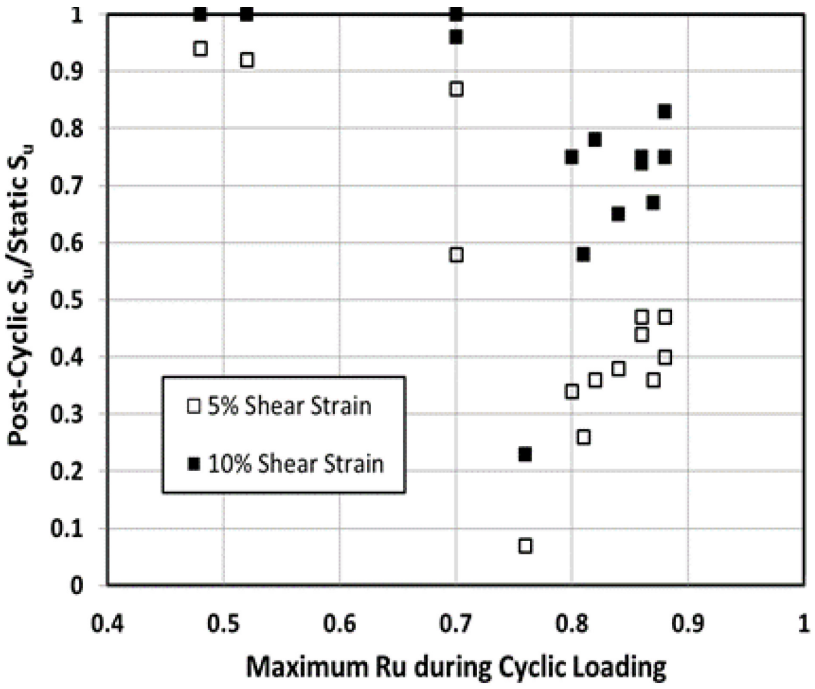

Figure 3.7: Relationship between Ratio of Post-Cyclic Strength and Maximum Excess Pore Pressure Ratio (R_u) for Fine-Grained Soil from the Columbia and Willamette Rivers (Beaty et al., 2014).

A second example of the trends in post-cyclic strength is provided in Figure 3.8 for Willamette Silt from of the northern Willamette Valley – Portland region. Similar post-cyclic behavior is noted in the importance of reference strain on the strength reduction, the general influence of Ru on the cyclic degradation, and the scatter in the laboratory data. With a focus on the strength reduction for 10% shear strain, it appears that the post-cyclic strength ratio remains in the 0.9 range until Ru reaches roughly 0.4 to 0.5, beyond which the increase in Ru has a progressively greater impact on the cyclic degradation of undrained strength.

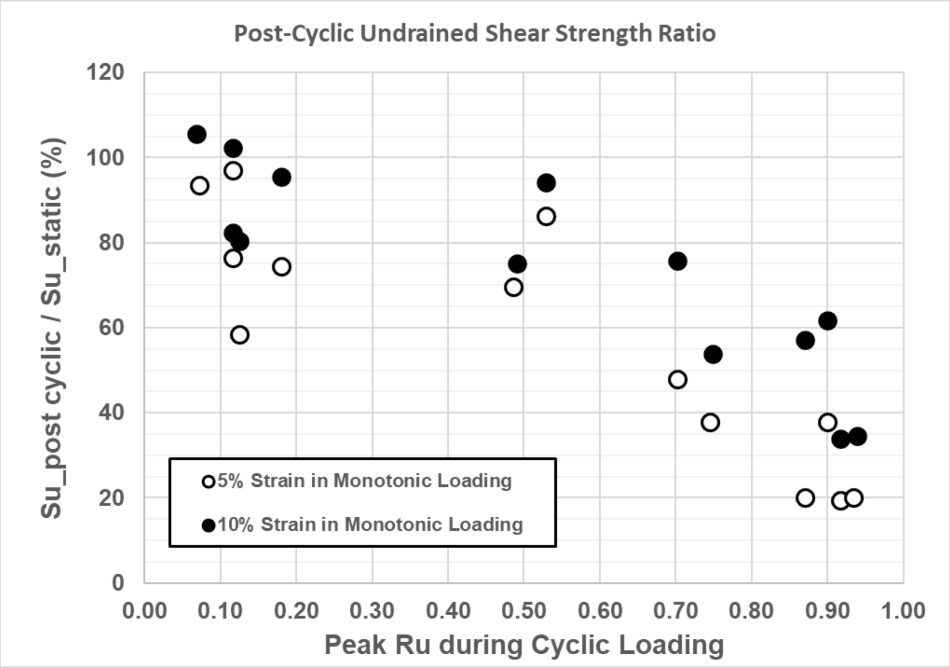

Figure 3.8: Relationship between Ratio of Post-Cyclic Strength and Maximum Excess Pore Pressure Ratio (R_u) for Willamette Silt.

A third example of the post-cyclic strength trends with Ru is provided for silty clay of the Bootlegger Cove Formation, and presented for the sake of comparison across a range of depositional environments, soil composition, and soil consistency. The trends are plotted from the same data set presented in Figure 3.5. The post-cyclic strength ratio is plotted for the reference strain of 10% only. For this soil and testing sequence the post-cyclic strength ratio remains in the 0.9 range until Ru reaches roughly 0.4, indicating minor strength reduction to moderate values of Ru. The significant influence of Ru beyond a value of 0.4 to 0.5 is evident.

The general trends in post-cyclic strength with Ru presented for three silt deposits selected from the regional database represent varying regions and depositional environments, with associated differences in composition and post-depositional effects (e.g., stress history, aging, possible cementation). The intent of the brief summary is to highlight general trends in post-cyclic behavior that warrant consideration for project-specific applications. Key points include the application of a reference strain for defining the strength reduction and the relative influence of Ru on the cyclic degradation.

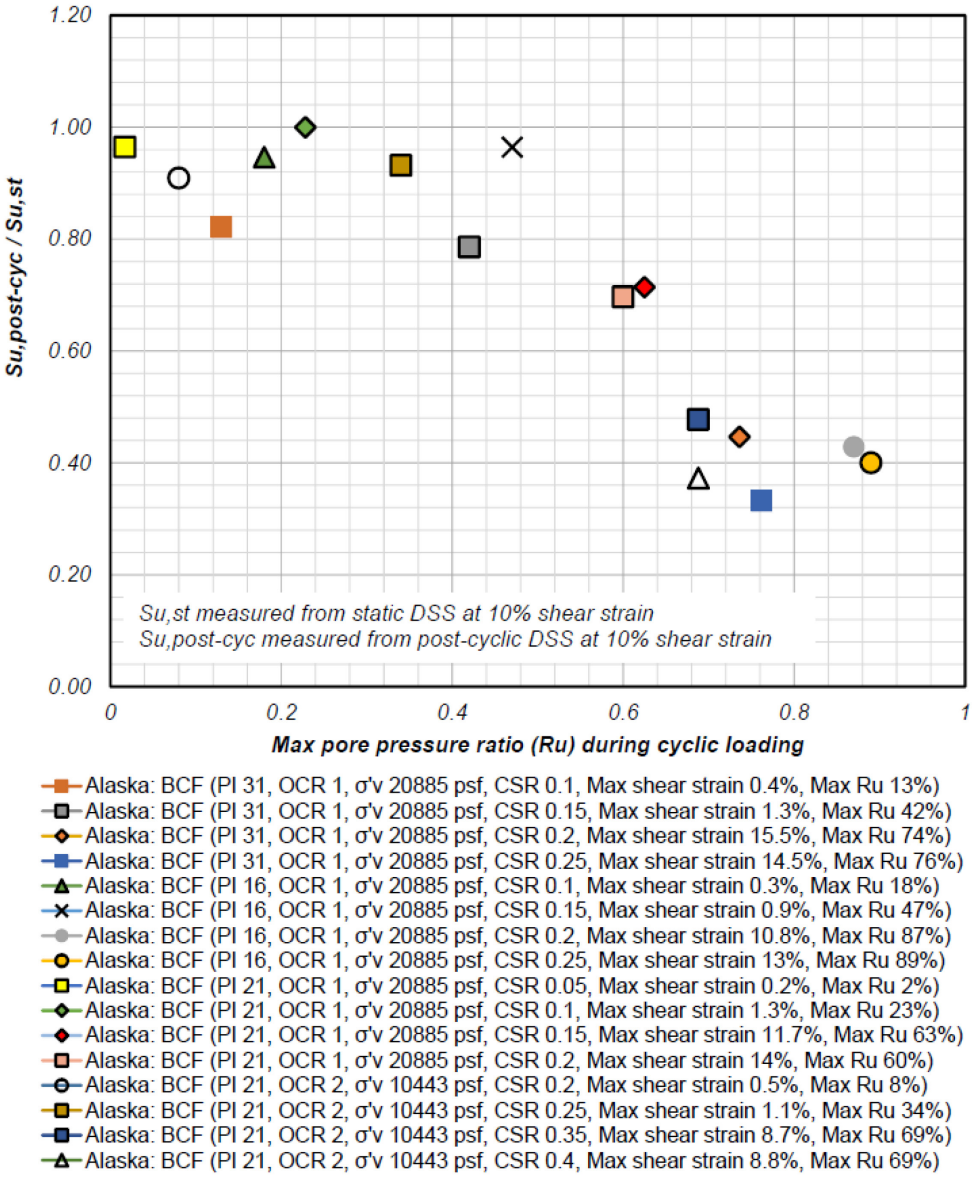

Figure 3.9: Relationship between Ratio of Post-Cyclic Strength and Maximum Excess Pore Pressure Ratio (R_u) for Specimens of Silt from the Bootlegger Cove Formation, Anchorage, Alaska (Site ID: AK_04).

In project applications, it is considered useful to develop a practice-oriented formulation for the reduction in post-cyclic undrained strength with cyclically induced excess pore pressure. The influence of excess pore pressure generation during cyclic loading on the post-cyclic undrained strength of the various silt deposits catalogued in this investigation has been evaluated using a model based on the SHANSEP procedure for undrained strength and the change in effective vertical stress immediately after cyclic loading. As outlined by Egan and others (1984) and Ajmera and others (2019), the post-cyclic effective stress ratio ($\sigma'_{vc} / \sigma'_{vpc}$) is equal to the ratio (1 / (1- Ru)), therefore Ru provides a convenient scaling factor for post-cyclic strength reduction using a

SHANSEP-based method of post-cyclic characterization. The three parameters listed are defined as follows:

σ'_{vc}: Consolidation stress (pre-cyclic loading vertical effective stress)
σ'_{vpc}: Effective vertical stress immediately after cyclic loading
Ru: Excess pore pressure ratio (cyclically induced pore pressure / σ'_{vc})

The following formulation (Equation 3-2) for estimation of post-cyclic undrained strength has been slightly modified from that presented by Egan and others (1985), yet it yields the same post-cyclic shear strength for a given value of Ru.

$$(\tau_{cyc} / S_{u\_st})_{Y=x} = (1 - Ru) \times [(1 / 1 - Ru)^{c}]^{m} \qquad \text{Equation 3-2}$$

Where:

τ_{cyc} : Shearing resistance at a reference shear strain in the post-cyclic monotonic test,
S_{u_st} : Static undrained shear strength at the same reference shear strain,
m : Curve fitting parameter for the slope of s_{u_st}/σ'_{vc} versus OCR (as applied in Equation 3-1)
c : Curve fitting parameter for the trend of the post-cyclic strength ratio with Ru

This method was applied by Egan and others (1985) on a silty clay from the Bootlegger Cove Formation (BCF) in an upland portion of Anchorage, Alaska. Very good agreement with the cyclic and post-cyclic DSS testing was obtained for the BCF clay using m and c values of 0.70 and 1.15, respectively. The resulting curve-fit for the variation of post-cyclic strength ratio with Ru is provided in Figure 3.10. The BCF clay relationship is supplemented with the trends developed for the following soils; (BCF tidal silty clay [Site ID AK_04], refer to Figure 3.9], Willamette Silt [refer to Figure 3.8], Columbia & Willamette Rivers [Beaty et al., 2014], Willamette River silt [Portland], reconstituted specimens of 18 fine-grained soils [Ajmera et al., 2019], and a marine clay [San Francisco Bay Mud, SFBM, PI 29 – 50 (average = 38)] provided to broaden the range of soil plasticity represented in the figure. The curve-fit coefficients, m and c, are listed in the legend of the figure, providing a range of values that provides a useful range of post-cyclic strength for a broad array of fine-grained soils.

The approximation for post-cyclic undrained strength as a function of Ru provided in Equation 3-2 is considered a practical, adequate method for estimating the effects of cyclic degradation on undrained strength, in the absence of site-specific cyclic laboratory data. It is noted; however, that the smoothed trends provided for the native, intact specimens plotted in Figure 3.10 provide a "best fit" to the lab data using the simple formulation. A review of the full data set compiled for this investigation demonstrates that a closer fit may be obtained using a bilinear approximation that is similar to that shown for the "Fine-Grained Soils (Reconstituted)", as reported by Ajmera

and others (2019). In general, the use of the bilinear trend reduces the influence of Ru on the post-cyclic strength for values of Ru less than 0.40 to 0.50, as observed in several of the data sets in this investigation, yet results in approximately the same post-cyclic strength ratios for Ru ranging from 0.70 to 0.90. In the absence of project-specific data, the method used to estimate the likely trend of post-cyclic undrained strength should be selected to be representative of the estimated range of interest for Ru (e.g., Ru ≤ 0.4 to 0.5, or ≥ 0.6 to 0.7).

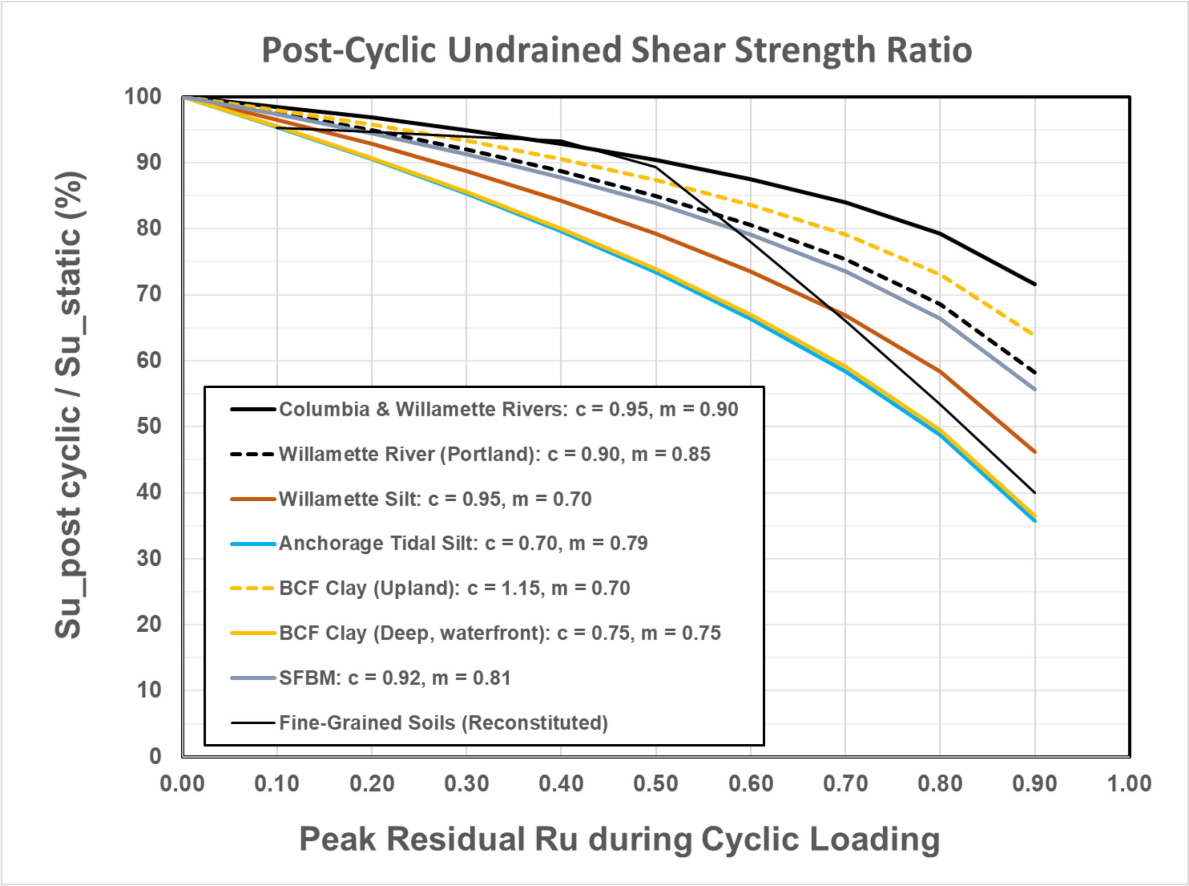

Figure 3.10: Trends of post-cyclic strength ratio and maximum residual excess pore pressure ratio (R_u) for various fine-grained soils.

3.4 OBSERVATIONS AND GENERAL CONSIDERATIONS BASED ON THE TRENDS PRESENTED

Cyclic degradation of soil stiffness and undrained strength is an important consideration for post-seismic stability and ground deformation. The cyclic data collected in this investigation has been supplemented with data from the technical literature for the sake of examining trends in the post-cyclic stress-strain-strength behavior of silt-rich soil deposits. The general trends in strength reduction due to cyclic loading are summarized in this data report to assist practitioners and researchers in bracketing representative ranges of the post-cyclic undrained strength ratio as

functions of Ru or maximum accumulated shear strain during cyclic loading. Although the trends provided in this report are useful for application in preliminary evaluations of cyclic degradation the variability and uncertainty inherent in the various data sets highlight the benefits of project-specific cyclic testing.

The data sets from selected projects considered representative of the array of silt deposits in the database have been presented to provide a useful summary of the influence of cyclic response, most notably Ru, on the post-cyclic strength of the silt units examined. A practical formulation for estimating post-cyclic strength as a function for Ru is presented, with the intent that the trends provide the basis for determination of a suitable range of undrained shear strengths that may be applied in deformation-based analysis of native slopes, embankment and levees, earth retention systems, and foundations underlain by silt-rich soil. On the basis of the data presented in this report the following general observations are provided for consideration by practitioners and researchers. These observations are intended to cover general aspects of the data collection and synthesis performed to date; however, they do not represent standards for practice, guidelines, or "Rules of Thumb."

1. The results of constant volume DSS tests have been used to examine trends in the reduction of undrained shear strength due to cyclic loading. The post-cyclic, static monotonic stage of the test sequence is performed immediately after the cyclic stage to minimize the dissipation of excess pore pressure and partial re-consolidation of the specimen. This testing procedure provides post-cyclic undrained strengths that can be significantly less than the post-cyclic strengths obtained in tests where the specimen is allowed to fully re-consolidate (i.e., no excess pore pressure) prior to the static monotonic test stage. Clearly, the difference in strength provided by these differing test sequences is a function of the maximum Ru in the cyclic testing stage.
2. The post-cyclic strength ratio, $(\tau_{cyc} / S_{u\text{-}st})_{Y=x}$, of the silts addressed in this data report is correlated with both the maximum accumulated shear strain and maximum excess pore pressure during the cyclic loading phase of the test. On this basis, estimation of post-cyclic undrained strength of silt should be made with consideration of both aspects of the soil behavior during cyclic loading.
3. Dilative, strain-hardening behavior was observed in many of the static and post-cyclic monotonic DSS tests evaluated in this investigation. In light of the progressive increase in shearing resistance at large strains, it is recommended that the peak strength be defined at a prescribed reference shear strain. It has been noted that shear strain values of 10% and 15% are commonly used in research and in practice.
4. The post-cyclic, strain-hardening behavior of silt observed in many of the DSS tests suggests that the stress-strain behavior is consistent with cyclic mobility, and not the rapidly increasing rate of shear strain accumulation associated with liquefaction of sand.
5. Although the influence of rate effects (i.e., rate of shear strain) on undrained shear strength warrants additional investigation, especially for low PI silt, the rate of loading in static and

post-cyclic monotonic stages of the test sequence should be constant to reduce variability on the measured shearing resistance.

6. Trends in the post-cyclic strength ratio with maximum excess pore pressure during cyclic loading have been provided for the sake of bracketing representative ranges for various silt deposits. In the absence of project-specific laboratory data, these trends are useful for evaluation of the cyclic degradation in strength anticipated across the range of Ru values computed from site response analysis, or other methods of approximation.
7. The trends in post-cyclic strength ratio as a function of maximum residual Ru presented in Figure 3.10 indicate that a post-cyclic strength equal to 80% of the static strength generally occurs when Ru values range from approximately 0.40 to 0.80, with a mean of roughly 0.60. In all cases presented, the post-cyclic strength ratio drops significantly for accumulated Ru values greater than roughly 0.55 to 0.75. The use of the common approximation that the post-cyclic strength is 80% of the static, which was originally applied for clay, should be applied judiciously for analysis as this simple scaling ratio is a function of both maximum accumulated shear strain and maximum excess pore pressure during cyclic loading.
8. The reference shear strain for defining cyclic resistance (Chapter 2) is commonly 3.0 % to 3.75%, which was originally based on laboratory testing of clean sands and the onset of significant softening and liquefaction behavior. As demonstrated in this investigation, and others focused on silt behavior, the Ru at 3% accumulated shear strain in cyclic DSS testing is often in the range of 0.70 to 0.90, thus at an average value of 0.80 the post-cyclic strength ratio at "failure" is roughly 0.50 to 0.80 for a variety of silt deposits (Figure 3.10). On the basis of the post-cyclic tests evaluated in this investigation, the results of total stress site response analysis indicating either the accumulation of 3% shear strain or application of cyclic shear stresses (i.e., Cyclic Stress Ratio) reaching "failure" should not be interpreted as resulting in the liquefaction behavior associated with loose to medium dense sand. This is an important distinction for deformation-based analysis.
9. The observations summarized in (8) highlight the fact that the post-cyclic undrained "residual" strength of silt should not be estimated using methods developed for liquefied sand with associated fines corrections.

3.5 REFERENCES

Ajmera, B., Brandon, T., & Tiwari, B. (2019). Characterization of the reduction in undrained shear strength in fine-grained soils due to cyclic loading. *Journal of Geotechnical and Geoenvironmental Engineering*, *145*(5), 04019017.

ASTM D 6528-17 (2017). Standard Test Method for Consolidated Undrained Direct Simple Shear Testing of Fine Grain Soils, ASTM International, West Conshohocken, PA, 2017, www.astm.org.

Beaty, M., Schlechter S., Greenfield, M., Bock, J., Dickenson, S., Kempner Jr., L., and Cook, K. (2014). Seismic Evaluation of Transmission Tower Foundations at River Crossings in the Portland-Columbia River Region, Tenth U.S. National Conference on Earthquake Engineering, Vancouver, B.C., July 21-25.

Christie, S., Zhang, Y., Dickenson, S., and Pintner, B. (2019). Seismic Analysis and Ground Improvement Design for the PCT Marine Terminal at the Port of Alaska, Proc. Of Ports '19, Port Engineering volume, ASCE COPRI, Pittsburgh, PA, 538 – 549.

Egan, J.A., Moriwaki, Y., and Moses, T.L. (1984). Site Characterization for Seismic Hazards Evaluations, Proc. Of the 1984 Seminar on Earthquake Engineering in Alaska, Alaska Academy of Engineering and Sciences, Alaska Chapter of EERI and Artic Division of the American Assoc. for the Advancement of Science, 1600 – 1619.

Koutsoftas, D.C., and Ladd, C.C. (1985). Design Strength for an Offshore Clay, Jrnl. Of Geotechnical Engineering, ASCE, 111 (3), 337 – 355.

Ladd, C. C. (1991). Stability evaluation for staged construction. Jrnl. Of Geotech. Eng., ASCE, 117 (4), 540–615.

Ladd, C. C. and Foote, R. (1974). New design procedure for stability of soft clays. Jrnl. Of the Geotechnical Engineering Division, ASCE, 100(GT7), 763-786.

Matasovic, N. and Dobry, M. (1995). Generalized Cyclic-Degradation-Pore-Pressure Generation Model for Clays, Jrnl. Of Geotechnical Engineering, ASCE, 121 (1), 33 – 42.

McCullough, N.J., Hoffman, B., Takasumi, D.L., Anderson, D.G., Dickenson, S.E. (2009). Seismic Site Response for an LNG Facility – Analyses and Lessons Learned, Proc. Of the ASCE TCLEE National Conference, Oakland, CA.

Vucetic, M. (1988). Normalized behavior of offshore clay under uniform cyclic loading, Canadian Geotechnical Jrnl., Vol. 25, 33-14.

Wijewickreme, D., Soysa, A., and Verma, P. (2019). Response of natural fine-grained soil for seismic design practice: A collection of research findings from British Columbia, Canada, Soil Dynamics and Earthquake Engineering, 124, 280-296.

Woodward-Clyde Consultants (WCC), (1982). Anchorage Office Complex, Geotechnical Investigation, Anchorage, Alaska, Volume 3, Data Summary, prepared for the Alaska Department of Transportation and Public Facilities, Central Region, Design & Construction, December 1982.

CHAPTER 4

Post-Cyclic One-Dimensional Volumetric Strain

CHAPTER 4 CONTENTS

4-1 INTRODUCTION 68

4-2 ESTIMATION OF ONE-DIMENSIONAL VOLUMETRIC STRAIN FOR CLEAN SAND 68

4-3 ONE-DIMENSIONAL VOLUMETRIC STRAIN FOR SILT; PREVIOUS INVESTIGATIONS 73

4-4 ONE-DIMENSIONAL VOLUMETRIC STRAIN FOR SILT; DATA COMPILATION IN THIS INVESTIGATION 76

4-5 OBSERVATIONS AND GENERAL CONSIDERATIONS BASED ON THE TRENDS PRESENTED 78

4-6 REFERENCES 80

4-1 INTRODUCTION

The dissipation of excess pore water pressure developed during cyclic loading of saturated soil is accompanied by a reduction in void ratio of the vulnerable soil layers. The cumulative effect of reconsolidation throughout the deposits of interest results in ground surface settlement. In practice, the process of post-cyclic reconsolidation of soil is commonly evaluated for one-dimensional (1D) vertical strain, termed volumetric strain. The focus on 1D volumetric strain simplifies the assessment of cumulative strain and ground surface settlement, and is well-suited for evaluation by laboratory testing of the relationship between maximum excess pore pressure during cyclic loading and subsequent vertical strain during reconsolidation. It should be noted that the 1D constraint does not account for other important factors that may contribute to surface settlement and deformation during, and after, seismic loading (e.g., deviatoric strain, ejecta-induced surface displacement), thus these phenomena are often evaluated in an uncoupled manner. This chapter focuses on the post-cyclic, 1D volumetric strain behavior of silt-rich soil tested in the laboratory by direct simple shear (DSS) and triaxial (TX) methods. Laboratory-based procedures developed for sand-like soil have been applied, with necessary adjustments, for silts obtained from projects in the Pacific Northwest. The results of the post-cyclic tests compiled in this investigation have been summarized in the form of practice-oriented charts that are intended to be applied for bracketing the range of possible volumetric strain for silts and associated ground settlement.

4-2 ESTIMATION OF ONE-DIMENSIONAL VOLUMETRIC STRAIN FOR CLEAN SAND

The development and application of laboratory-based procedures for estimating 1D volumetric strain in sand have been well-presented in the technical literature (e.g., Idriss and Boulanger 2008) and will be briefly summarized to provide background for the development of practice-oriented relationships for silt. Several of the initial, well-documented procedures were established using DSS and TX testing of clean sands. Stress-controlled tests were used to characterize the post-cyclic reconsolidation of sand as a function of key factors such as: relative density, amplitude of cyclic loading (Cyclic Stress Ratio, CSR), number of load cycles, maximum accumulated cyclic shear strain, and maximum excess pore water pressure (pore pressure ratio; $R_u = \Delta u / \sigma'_{vc}$) experienced during the cyclic loading. Several of the most commonly applied practical procedures for estimating post-seismic settlement due to 1D volumetric strain have been presented by Tokimatsu and Seed (1987), Nagase and Ishihara (1988), and Ishihara and Yoshimine (1992). Subsequent refinements to these original procedures have been made to account for factors such as: fines content, large-strain accumulation ($\gamma_{max} \geq 10\%$), irregular cyclic loading, and depth-dependent volumetric strain (e.g., Shamoto et al., 1998, Tsukamoto et al., 2004; Duku et al. 2008; Cetin et al., 2009; Ishihara et al., 2016). These methods have also been used as the basis for CPT-based procedures for estimation of ground surface settlement by way of correlation between tip resistance, (qc1N)cs, and relative density for sand (e.g., Zhang et al., 2002).

The procedure developed by Ishihara and Yoshimine (1992) for estimating volumetric strain in clean sand is used as the framework for a similar approach in the silt-rich soils evaluated in this investigation. Their method for estimating ground surface settlement following seismic loading was initiated with a series of cyclic tests on clean Fuji River sand that provided the following general observations:

1. The post-cyclic volumetric strain is well-correlated with the maximum shear strain mobilized during the cyclic loading stage of the test.
2. Excess pore pressure development in cyclic tests can be correlated with accumulated shear strain.
3. The excess pore pressure ratio ($R_u = \Delta u / \sigma'_{vc}$) reaches 1.0 when the accumulated single-amplitude shear strain in CDSS testing is in the range of 2.5% to 3.5%, thus the onset of liquefaction can be correlated with maximum shear strain. After review of data sets developed using CDSS and cyclic Triaxial testing methods, Ishihara and his co-workers defined the single-amplitude shear strain of 3.5% as the criterion for initial liquefaction.
4. Trends were then developed for the factor of safety against liquefaction (FS_{liq}) versus the maximum amplitude of shear strain, as a function of the relative density of the sand. The relative density identified as a primary soil property for correlation with cyclic resistance.

One of the initial relationships for estimation of volumetric strain for clean sand is provided in Figure 4.1. The influence of maximum accumulated cyclic shear strain (related to cyclic demand) and the relative density of the sand (cyclic resistance) on the resulting volumetric strain is well established. This data set has been replotted by Idriss and Boulanger (2008) and is provided in Figure 4.2. The re-plotting of the laboratory data illustrates two useful aspects of the procedure; (i) the bi-linear approximation of the volumetric strain – maximum cyclic shear strain relationships can be easily incorporated into spreadsheets and used in conjunction with standard liquefaction triggering analyses, and (ii) the variability of the volumetric strain for carefully prepared, uniform, reconstituted specimens of clean sand is evident. The influence of this variability (i.e., uncertainty) should be acknowledged when interpreting the results of ground surface settlement estimated made using procedures such as this. It is also highlighted in Figures 4.1 and 4.2 that Initial Liquefaction (R_u = 100%) is correlated to maximum cyclic shear strain in the range of approximately 2.5% and 3.5%.

The trends in volumetric strain (Figure 4.1) were further developed by Ishihara and Yoshimine (1992) in the form of the commonly applied chart of volumetric strain as functions of factor of safety against the onset of liquefaction, provided in Figure 4.3. The factor of safety (FS_{liq}) used as the basis for this plot was defined as the ratio of the cyclic shear stress required to reach 3.5% single-amplitude shear strain in 20 cycles to the applied cyclic shear stress. The shear strain of 3.5% is the reference value for "failure", or as noted by Ishihara and Yoshimine (1992) *"…a criterion to define a state of cyclic softening at which the factor of safety is unity*." This chart has been applied in several investigations of field-case studies and found to provide reasonable estimates of total

ground surface settlement; however, calibration with field case histories has led to several recommendations for the application of the procedure and for scaling of the results in practice. Notable recommendations include the following:

1. The procedure, and more recent refinements, have been shown to result in total ground surface estimates that are slightly, yet systematically, greater than field observations. Several investigations have suggested that that the total settlement can be adjusted by scaling factors (e.g., 0.90 as recommended by Cetin et al., 2009).
2. The recommended maximum depth of application of the procedure for estimating the surface manifestation of settlement ranges from 15m to 18m (Ishihara et al., 2016; Cetin et al., 2009).

The 1D methods of evaluation for volumetric strain in clean sand have been found to provide simplified, yet adequate, estimation of ground surface settlement for many practical applications. The range of uncertainty and possible "error" has been noted by the originators of the procedures and bears repeating in this report. It is recommended in practice that settlement estimates be reported as ranges of likely settlement as opposed to a single value. Examination of the post-earthquake estimates of settlement and measured values suggests that the "best-estimate" of estimated settlement should be bracketed by bounds that are approximately 0.5 to 2 times the estimate (Tokimatsu and Seed 1987; Tsukamoto and Ishihara, 2010; Ishihara et al., 2016).

The practice-oriented and commonly applied procedures for estimating volumetric strain in clean sand outlined in this section have been summarized for the sake of comparison with trends for silt-rich soils. Test data on post-cyclic reconsolidation of relatively undisturbed specimens of silt has been compiled in this investigation and trends developed for volumetric strain as functions of the maximum accumulated shear strain and maximum excess pore pressure during the cyclic loading. These trends are subsequently presented in this chapter. Several pertinent differences between the procedures for clean sand outlined in this subsection and the silt trends that follow warrant consideration. The following should be noted when evaluating volumetric strain for silt-rich soil:

1. The trend of cyclic shear strain accumulation with excess pore pressure generation is commonly quite different between reconstituted specimens of clean sand and relatively undisturbed specimens of silt. The R_u value at peak mobilized cyclic shear strain of 3.0% to 3.5% is commonly in the range of 0.80 to 0.85, as opposed to the range of approximately 0.95 to 1.0 determined for clean sand.
2. The cyclic behavior of silt (e.g., cyclic strain increment per cycle of loading) at peak shear strain of roughly 3.5% and R_u of 0.85 has been noted in numerous investigations to be more similar to dense sand than to loose sand, thus exhibiting a cyclic mobility type response. On this basis, the behavior of the silt at reference strain values of 3.0% to 3.5% is not representative of "liquefaction" as applied to relatively loose sand therefore the use of the

factor of safety against liquefaction (FS_{liq}) should be replaced with other criteria such as reference peak shear strain or reference excess pore pressure.

3. The use of Relative Density is not appropriate for silt-rich soil and clean sand adjustment factors were not developed for transitional soil with greater than 50% fines by weight therefore converting void ratio in silt to an equivalent clean sand value for the sake of approximating Relative Density is not recommended.
4. The cyclic resistance of silt has been found to be well-correlated with static undrained shear strength and reasonably well-correlated with CPT measurements; however, SPT N-values are not recommended as the basis for estimating strength, cyclic resistance, or post-cyclic behavior of silt.
5. In light of the limitations associated with procedures developed for estimating volumetric strain for sand as applied for silt it is common to present the results of laboratory cyclic tests on the latter in the form of post-cyclic volumetric strain with maximum excess pore pressure or maximum shear strain during the cyclic potion of the test. This practical approach is adopted in this data report, as follows.

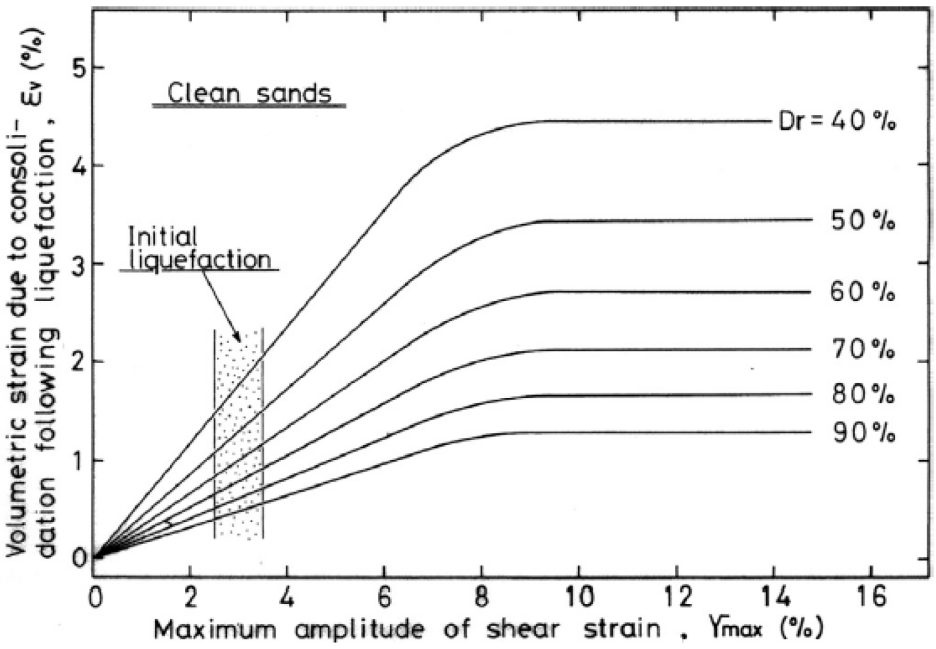

Figure 4.1: Summarized relationships between post-liquefaction volume change and shear strain (Ishihara and Yoshimine, 1992).

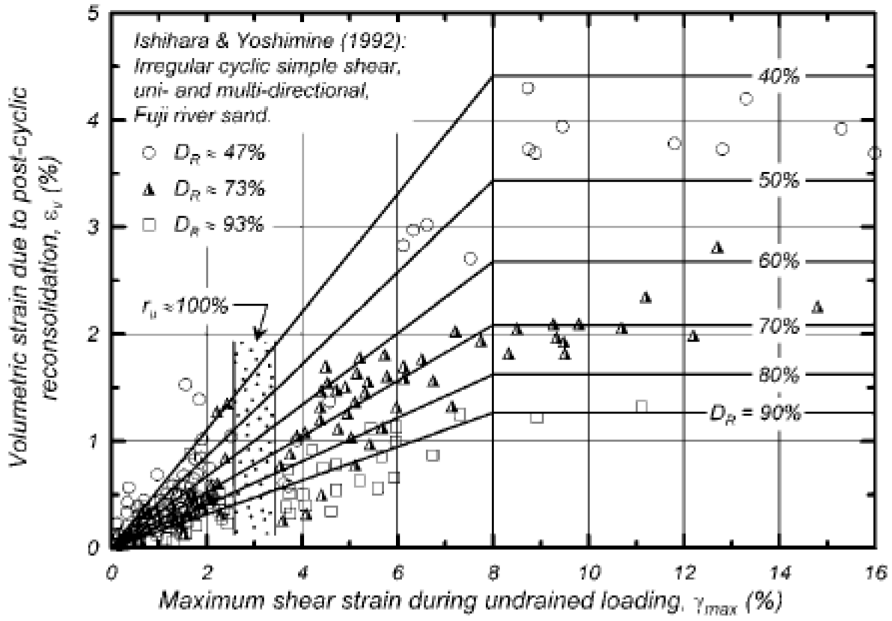

Figure 4.2: Relationship between post-liquefaction volumetric strain and the maximum shear strain induced during undrained cyclic loading of clean sand (after Ishihara and Yoshimine 1992; redrawn in Idriss and Boulanger 2008).

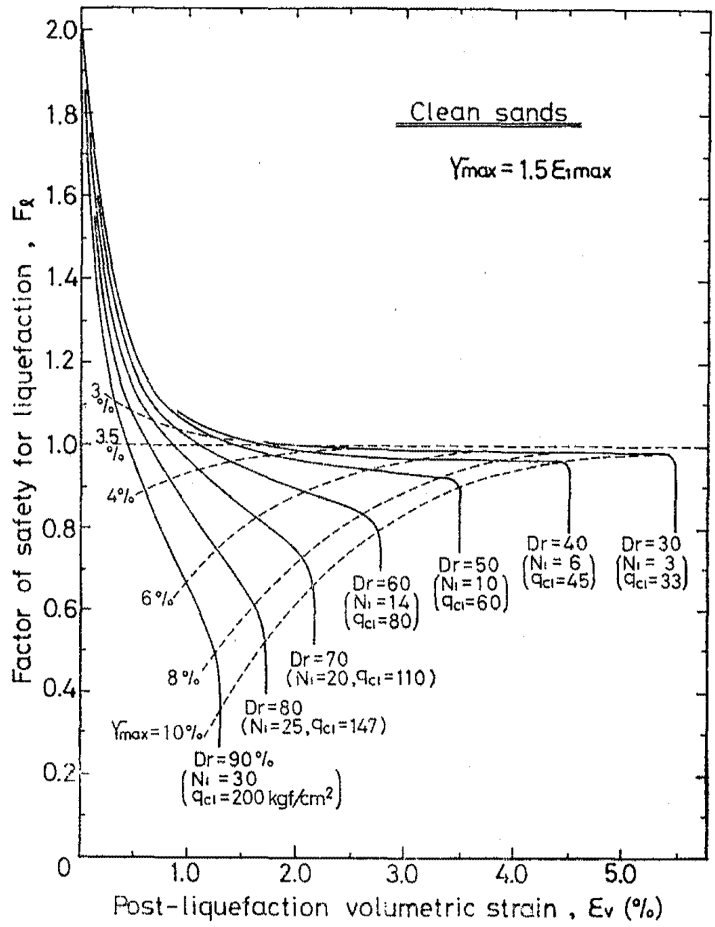

Figure 4.3: Chart for determining volumetric strain as functions of factor of safety (Ishihara and Yoshimine, 1992)

4-3 ONE-DIMENSIONAL VOLUMETRIC STRAIN FOR SILT; PREVIOUS INVESTIGATIONS

Volumetric strain in silt-rich soil has been the focus of several investigations in the Pacific Northwest and British Columbia. The results of pertinent investigations are summarized; one data set provided by a project involving the seismic performance of a major electric power transmission system in the Portland-Vancouver-Columbia River region (Beaty et al., 2014) and the second data set established from multiple research studies on Fraser River silt in British Columbia (Wijewickreme and Sanin, 2010; Wijewickreme et al., 2019). In both investigations trends in volumetric strain have been developed as a function of the maximum cyclic pore pressure ratio during cyclic loading in DSS tests. The trends provide practical guidance for estimation of volumetric strain in fine-grained soil, demonstrate the variability in strain values for relatively undisturbed specimens of the soils tested, and highlight differences in the post-cyclic volume change potential in silt and clean sand.

In the investigation summarized by Beaty and others (2014), CDSS tests were conducted on samples obtained along the lower Willamette River and Columbia River in the Portland-Vancouver-Longview region. The plasticity indices ranged from 0 (SM) to 32 (MH) and tests were performed on specimens consolidated to OCR values of 1.0 to 3.0. The relationship between the maximum Ru during cyclic loading and post-cyclic volumetric strain for the specimens tested for this project were plotted with data for various silt deposits from the Pacific Northwest (provided this data report) and this is provided in Figure 4.4. All of the data was obtained from CDSS tests by allowing the sample to consolidate following the cyclic loading. A reasonable trend can be established for the silt deposits represented in the figure. It is useful to note that the R_u value at the reference strain of 3.0%, is commonly 0.80 to 0.85 for the silts evaluated. This figure was used in the seismic performance investigation to bracket the likely range of volumetric strains used in computations of ground surface settlement.

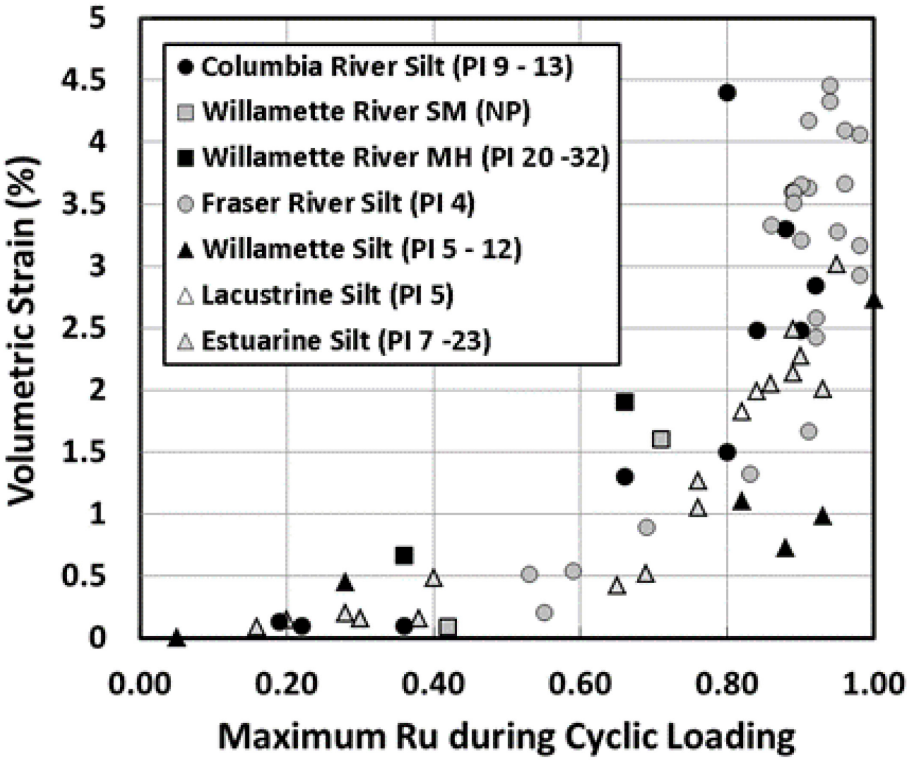

Figure 4.4: Relationship between post-cyclic 1D volumetric strain and R_u (Beaty et al., 2014).

The CDSS data obtained for soil deposits in the Pacific Northwest and plotted in Figure 4.4 was supplemented with similar data for low-plasticity (PI = 4) specimens of Fraser River silt tested in several applied research investigations at the University of British Columbia (Wijewickreme and Sanin, 2010; Wijewickreme et al., 2019). While the inherent scatter associated with relatively undisturbed specimens of fine-grained soils from different depositional environments and other

pertinent factors (i.e., mineralogy, fabric, void ratio, consistency, age, stress history) is evident, the overall, average trends provide reasonable agreement and useful guidance for practical applications. The post-cyclic DSS data on Fraser River silt plotted in Figure 4.4 was obtained from Wijewickreme and Sanin (2010). Additional data was provided in their paper that included testing on reconstituted specimens of the silt and a quart rock powder. The trend in volumetric strain for these specimens is provided in Figure 4.5.

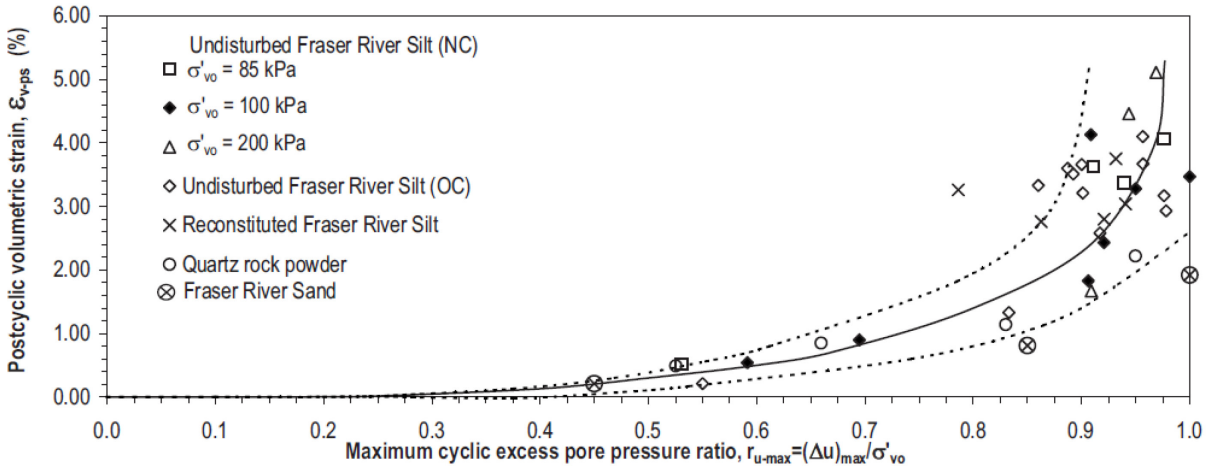

Figure 4.5: Post-cyclic volumetric strain versus maximum cyclic excess pore pressure ratio (Wijewickreme and Sanin, 2010).

Subsequent investigations of the post-cyclic behavior of fine-grained soils conducted by Wijewickreme and his co-workers have been summarized with additional data for silt specimens from other locations in British Columbia (Wijewickreme et al., 2019). Pertinent data for soil from four sites addressed in the paper is provided in Table 4.1. Soil from three of the sites is characterized as low plasticity silt (ML, PI 4 to 7) with the fourth site providing a high plasticity silt (MH, PI 34), which is useful for evaluating the possible influence of consistency on the post-cyclic volumetric strain. The results of the CDSS testing programs are plotted in Figure 4.6. The recommended trends provided in Figure 4.6 are similar to those plotted in Figure 4.5. These average trends also provide reasonable agreement with the data plotted in Figure 4.4 from numerous sites and a variety of different depositional environments, which supports the observation that the correlation between volumetric strain and maximum excess pore pressure does not appear to be greatly influenced by stress history (OCR), fabric, void ratio, or Plasticity Index, as noted by Wijewickreme et al. (2019).

Table 4-1: Characterization of the Test Specimens reported by Wijewickreme et al. (2019)

Site	Depth Range (m)	Water Content (%)	PI (%)	USCS	Estimated Preconsolidation Stress (kPa)
A. Fraser River 1	5.6 – 8.7	34 - 39	≈ 4	ML	85 – 95

B. Fraser River 2	5.0 – 7.0	35 - 44	≈ 5	ML	100 -125
C. Nicomekl River	4.2 – 5.5	38 - 53	≈ 7	ML	35 – 45
D. Fraser River 3	4.9 – 6.2	58 - 69	≈ 34	MH	75 - 85

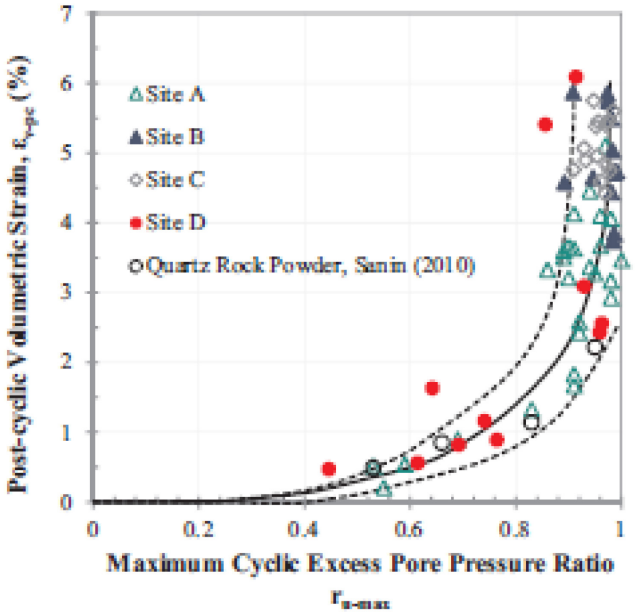

Figure 4.6: **Post-cyclic volumetric strain versus maximum cyclic pore water pressure ratio during cyclic DSS testing (Wijewickreme et al., 2019).**

4-4 ONE-DIMENSIONAL VOLUMETRIC STRAIN FOR SILT; DATA COMPILATION IN THIS INVESTIGATION

The data trends provided in Section 4-3 have been supplemented in this investigation with volumetric strain measurements made on specimens from numerous sites located throughout the Pacific Northwest. This greatly expands the application of the practice-oriented correlation of volumetric strain with maximum excess pore pressure generation to a variety of depositional environments and silt deposits. The data has been group into six general bins based on regional and depositional environment. The general groupings include: Columbia and Willamette River deposits, Willamette Silt associated with Missoula Floods, Tidal and Estuarine deposits in the Puget Sound region, Lacustrine deposits in the Portland-Vancouver region, "Other Silts" in the database (e.g., gravel pit wash tailings, residual soils), and incorporation of the Fraser River data obtained by Wijewickreme and his co-workers. The summary plot is provided in Figure 4.7. The combined data set provides a general trend that is in general agreement with the data trends in Figures 4.4 to 4.6; however, the range of scatter has increased. This increase in the range of volumetric strain values at a given R_u value may reflect inherent differences in the post-cyclic soil behavior of the various deposits, combined with variations in sample quality for various projects, and aspects of the testing conducted in the various laboratories from which the database has been compiled (e.g., type of test equipment, testing protocol, sample preparation techniques, application of

vertical stress(es) to prescribed consolidation state and OCR, etc.). Close inspection of the data trends for each of the six general groupings suggests that refinements in the volumetric strain estimation may be possible by developing deposit-, or environment-specific relationships. For example, it appears on the basis of limited data that the Willamette Silt deposits exhibit a lower vulnerability to post-cyclic reconsolidation and strain mobilization than estimated using an "average" trend. More data will be required to confirm this general observation. These observations support the benefit of site-specific data for major projects.

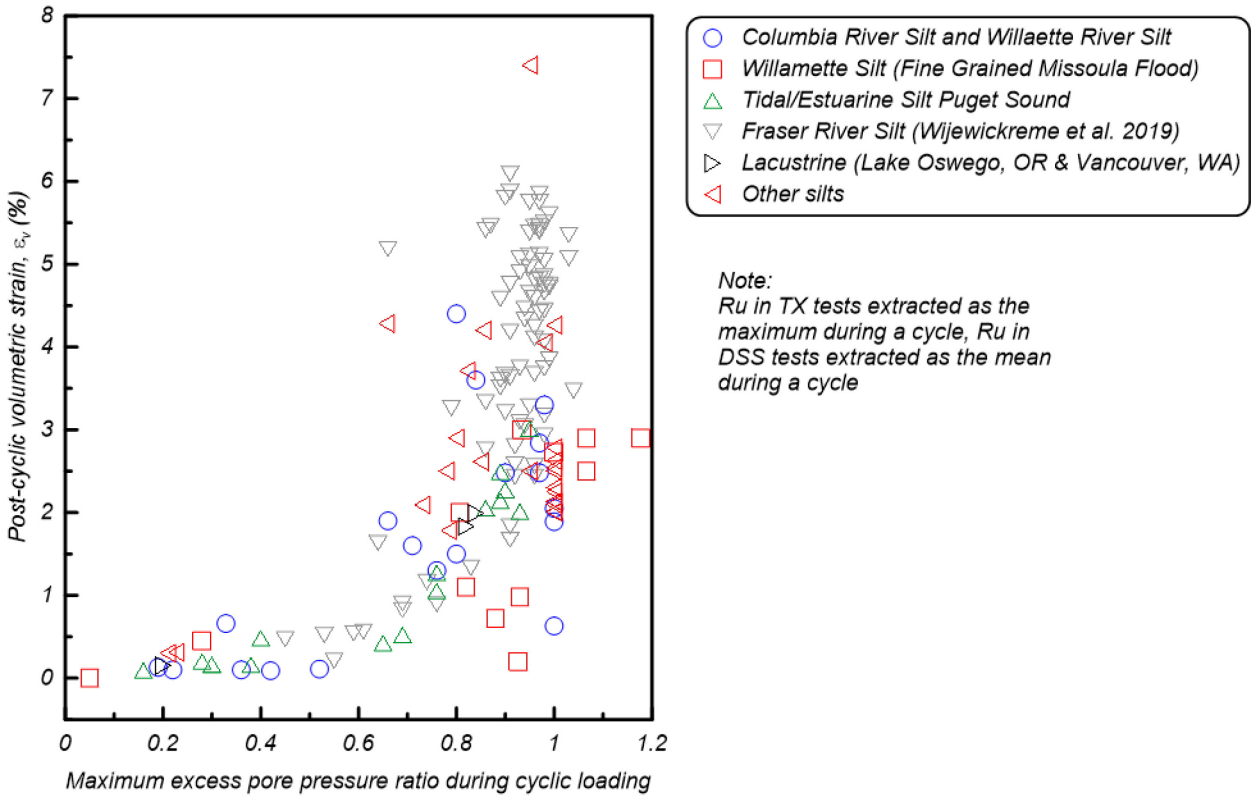

Figure 4.7: Post-cyclic Volumetric Strain versus Maximum Pore Pressure Ratio during Cyclic Loading

The results of the post-cyclic testing provided in Figure 4.7 have been re-plotted in the form of maximum accumulated shear strain during cyclic loading to the subsequent volumetric strain. This relationship was evaluated following the procedures developed for clean sand previously addressed and to provide another parameter for correlation to the volumetric strain. The maximum shear strain mobilized during cyclic loading was considered as this is routinely computed in 1D and 2D dynamic site response analyses, therefore the range of maximum strains at the depths of interest can be bracketed for the suite of input motions used in the site response analyses. The range of variability (i.e., uncertainty) associated with this relationship is clearly evident in Figure 4.8. The apparent lack of a correlation is especially pronounced for the array of

cyclic tests performed on Fraser River Silt. Wijewickreme et al. (2019) noted that a meaningful trend between volumetric strain and maximum cyclic shear strain levels could not be derived. This may be due, in part, to the consideration that the maximum amplitude of cyclic loading does not account for the duration of cyclic loading (i.e., number of loading cycles), whereas the maximum excess pore pressure reflects both the amplitude and the duration of loading.

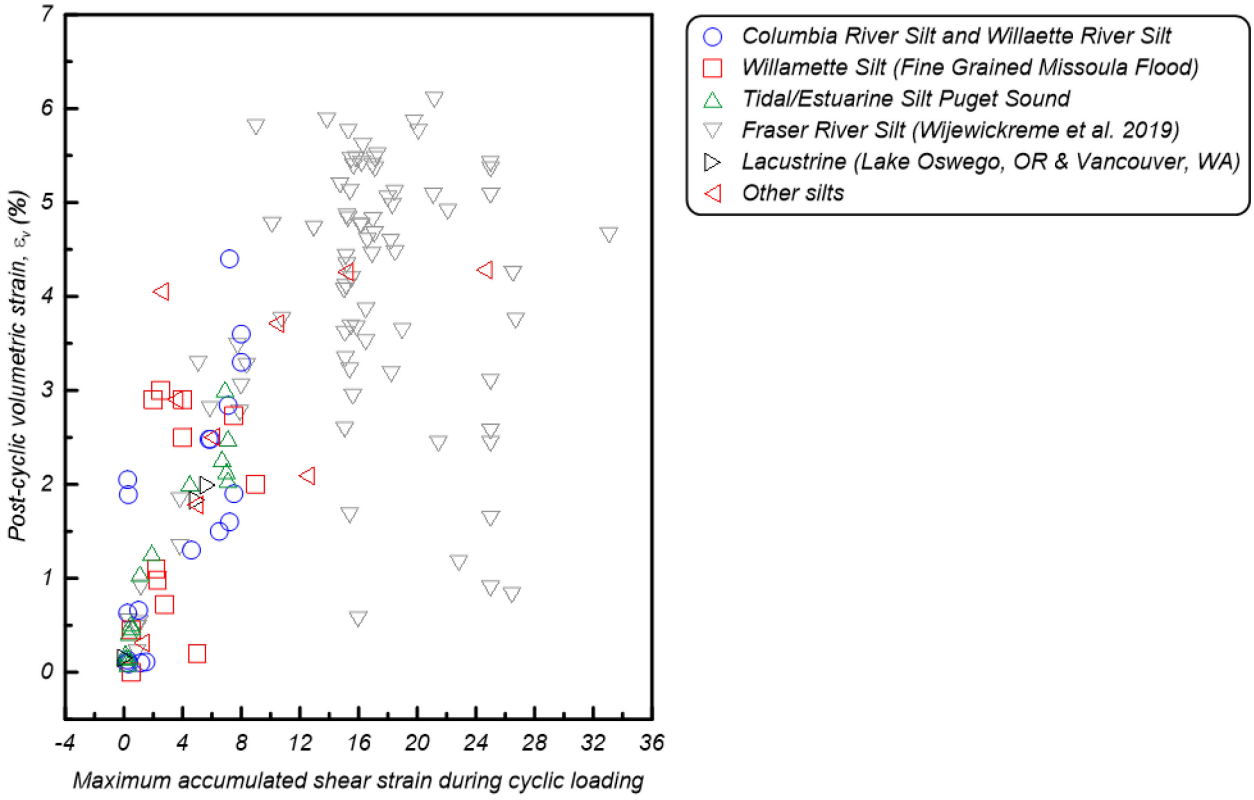

Figure 4.8: Post-cyclic Volumetric Strain versus Maximum Accumulated Shear Strain during Cyclic Loading

4-5 OBSERVATIONS AND GENERAL CONSIDERATIONS BASED ON THE TRENDS PRESENTED

A correlation between post-cyclic volumetric strain and the maximum excess pore pressure developed during cyclic loading has been evaluated and presented for use in the estimation of 1D settlement following seismic loading. Trends have been presented for test results on specimens from numerous sites and soil deposits located throughout the Pacific Northwest and British Columbia. The following general observations are provided for consideration by practitioners and researchers.

1. The trends provided in this investigation and in others provide a basis for evaluation of post-seismic settlement associated with “average” volumetric strain, and very importantly, for likely ranges in the volumetric strain values used for design.

2. The variability and uncertainty associated with estimating volumetric strain for relatively undisturbed specimens of silt have been noted. It is expected that specimens of native soil will inherently exhibit more variability than reconstituted specimens carefully prepared in the laboratory. The variability occurs at multiple scales, ranging from within the specimen itself (micro-scale), along the length of a sample tube, and between sample tubes obtained in the same deposits at a site.
3. In the summary provided for the assessment of volumetric strain in clean sand and estimation of settlement the following two issues were noted; (i) the application of a maximum recommended depth for the procedure (i.e., 15m to 18m), and the application of a scaling factor to calibrate the procedures for field case studies. In the absence of well-documented case histories in predominantly fine-grained soil no adjustments for silt-rich soil deposits are possible using the database compiled in this investigation.
4. The possible influence of effective confining stress on the volumetric strain has not yet been evaluated using the data set.
5. The trends provided in Figures 4.4 to 4.7 indicate that post-cyclic volumetric strain reaches 1.0% at R_u values ranging from roughly 0.60 to 0.75. At R_u of 0.6 the "average" trends are closer to 0.5% volumetric strain. These observations suggest that relatively high R_u values are required to produce volumetric strains exceeding 2%, which for the sake of comparison is roughly equivalent to the volumetric strain associated with clean sand having a relative density of 70% and low factor of safety against liquefaction.
6. The current investigation, and previous work by Wijewickreme and his co-workers, demonstrate that R_u is often approximately 0.80 to 0.85 when the specimens reach an accumulated cyclic shear strain of 3%, the value commonly associated with "failure." Post-cyclic volumetric strain for this reference "failure" shear strain can then be approximated as falling in the range of 1.0% to 2.0%.

4-6 REFERENCES

Beaty, M., Schlechter S., Greenfield, M., Bock, J., Dickenson, S., Kempner Jr., L., and Cook, K. (2014). Seismic Evaluation of Transmission Tower Foundations at River Crossings in the Portland-Columbia River Region, Tenth U.S. National Conference on Earthquake Engineering, Vancouver, B.C., July 21-25.

Cetin, K.O., Bilge, H.T., Wu, J., Kammerer, A.M., and Seed, R.B. (2009). Probabilistic Model for the Assessment of Cyclically Induced Reconsolidation (Volumetric) Settlements, *Jrnl. of Geotechnical and Geoenvironmental Engineering*, ASCE, 135(3): 387-398.

Duku, P.M., Stewart, J.P., Whang, D.H., and Yee, E. (2008). Volumetric Strains of Clean Sands Subject to Cyclic Loads, *Jrnl. of Geotechnical and Geoenvironmental Engineering*, ASCE, 134(8): 1073-1085.

Idriss, I.M., and Boulanger, R.W. (2008). Soil Liquefaction During Earthquakes, EERI Monograph, MNO-12, Earthquake Engineering Research Institute, Oakland, CA.

Ishihara, K., Harada, K., Lee, W.F., Chan, C.C., and Safiullah, A.M.M. (2016). Post-liquefaction settlement analyses based on the volume change characteristics of undisturbed and reconstituted samples, *Soils and Foundations*, Japanese Geotechnical Society, 56(3): 533-546.

Ishihara, K., and Yoshimine, M. (1992). Evaluation of settlements in sand deposits following liquefaction during earthquakes, *Soils and Foundations*, Japanese Geotechnical Society, 32(1): 173-188.

Nagase, H., and Ishihara, K. (1988). Liquefaction-induced compaction and settlement of sand during earthquakes, *Soils and Foundations*, Japanese Geotechnical Society, 28(1): 65-76.

Shamoto Y., Zhang, J-M, and Tokimatsu, K. (1998). Methods for Evaluating Residual Post-Liquefaction Ground Settlement and Horizontal Displacement, *Soils and Foundations*, Special Issue on Geotechnical Aspects of the January 17, 1995 Hyogoken-Nambu Earthquake, September, Japanese Geotechnical Society, 69-83. 8

Tokimatsu, K., and Seed, H.B. (1987). Evaluation of settlements in sands due to earthquake shaking, *Jrnl. of Geotechnical Engineering*, ASCE, 113(8): 861-879.

Tsukamoto, Y., and Ishihara, K. (2010). Analysis of settlement of soil deposits following liquefaction during earthquakes, *Soils and Foundations*, Japanese Geotechnical Society, 50(3): 399-411.

Tsukamoto, Y., Ishihara, K., and Sawada, S. (2004). Settlement of sand deposits following liquefaction during earthquakes, *Soils and Foundations*, Japanese Geotechnical Society, 44(5): 135-148.

Wijewickreme, D., and Sanin, M.V. (2010). Postcyclic Reconsolidation Strains in Low-Plasticity Fraser River Silt due to Dissipation of Excess Pore-Water Pressures, *Jrnl. of Geotechnical and Geoenvironmental Engineering*, ASCE, 136(10): 1347-1357.

Zhang, G., Robertson, P.K., and Brachman, R.W.I. (2002). Estimating liquefaction-induced ground settlements from CPT for level ground, Canadian Geotechnical Journal, 39: 1168-1180.

CHAPTER 5

Excess Pore Pressure Generation in Strain-Controlled Cyclic Tests

CHAPTER 5 CONTENTS

5-1 INTRODUCTION 84
5-2 CALIBRATION OF V&D MODEL PARAMETERS 85
5-3 REPRESENTATIVE RESULTS 86
5-4 CORRELATIONS BETWEEN CALIBRATED V&D SAND MODEL PARAMETERS AND OTHER SOIL PROPERTIES 86
5-4.1 Effects of overconsolidation ratio on calibrated F, s, and P parameters 86
5-4.2 Variations in F parameter and different fines content 87
5-4.3 Correlations between F parameter and shear wave velocity (Vs) 88
5-4.4 Variations in s parameter for different and fines content 89
5-4.5 Parameter γ_{tvp}: threshold shear strain for volumetric change 89
5-5 REFERENCES 92
5-7 CHAPTER 5 TABLES AND FIGURES 94

5-1 INTRODUCTION

The Vucetic-Dobry (V&D) pore pressure models are commonly used in practice to estimate cyclically induced pore pressure ratios as a function of cyclic shear strain. These models are typically implemented for effective-stress site response analysis using software programs such as D-MOD2000 (Matasovic and Ordonez 2012), DeepSoil (Hashash et al., 2016), etc. The model parameters for V&D sand and clay models have been provided in the literature primarily for sand and clay materials, e.g., Dobry et al. (1985), Vucetic and Dobry (1988), Matasovic (1993), Thilakarante and Vucetic (1987), Mei et al. (2018) for sand, and Matasovic and Vucetic (1995), Mortezaie and Vucetic (2016) for clay. Only a few studies have provided V&D model parameters for silt-rich soils, e.g., McCullough et al. (2009), Anderson et al. (2010), and Thilakarante and Vucetic (1987). Due to the scarcity of data on pore pressure generation in silt-rich soils, the V&D model parameters that are developed primarily for sands are often used by practitioners to evaluate the undrained cyclic response and the pore pressure development tendency of silt-rich soils. However, this approach tends to result in overestimation of the pore pressure development in silts, thereby resulting in an over-softening of the dynamic response of the silt in one-dimensional effective-stress site response analysis. This is shown in Figure 5.1a where the excess pore pressure ratio curves for a commonly used Wildlife Site Sand A (Vucetic and Dobry 1988) are compared with data on silty soils compiled in this study. The silt data in this study are obtained from 35 Cyclic Direct Simple Shear (CDSS) tests on silt samples from five different sites in the Pacific Northwest. As clearly shown in this figure, the cyclically induced pore pressure ratios in silt soils are significantly overestimated by typical sand curves. Similar conclusions were made by Hazirbaba and Rathje (2009) by comparing the pore pressure generations from sand samples by Dobry (1985) and cyclic tests performed on sands with various percentages of nonplastic silts as shown in Figure 5.1b.

This chapter contributes data on the excess pore pressure generation of transitional silty soils using strain-controlled CDSS tests performed on intact silt samples from five sites in the Pacific Northwest with different index properties, gradation, and depositional environment. Table 5.1 lists key soil properties and test parameters. The cyclic shear strains in these tests ranged from 0.1% to 2%. All of the tests were performed under constant-volume conditions and the pore pressures were back-calculated from the changes in the vertical stress. The cyclic loadings were applied mostly at 0.1 Hz frequency except for the tests performed at UCLA for the Alaskan Way Viaduct project (Project ID: W_03) where the loading frequency varied between 0.01 Hz and 0.1 Hz. Most of the tests were supplemented with bender element Vs measurements performed after consolidation and immediately prior to cyclic loading.

The dataset presented in this chapter includes 35 CDSS tests on samples characterized as low-plasticity silt (ML), low-plasticity clay (CL) or low-plasticity silty clay (CL-ML) based on their USCS classification. The fines content (FC) for these types of soil range from 54% to 100% and the silt

content ranges from 47% to 83%. The plasticity index (PI) for these types of soil range from NP to 16. Additionally, six CDSS tests on sand and silty sand soils (SP and SM) from WS SR-532 General Mark Clark Bridge project (Project ID: W_01) are included with FC ranging between 1% and 31%. These tests help identify the differences between pore pressure generation tendencies of sand soils and silt soils. All of the above-mentioned tests are strain-controlled CDSS tests except six stress-controlled CDSS tests on Columbia River silt from Warrenton, OR (Project ID: O_01) where the stress-controlled tests data were analyzed by McCullough et al. (2009) to develop V&D model parameters.

Figure 5.2a shows the dataset presented in this study on the plasticity chart. The soils presented in this study are characterized as being susceptible to cyclic softening based on screening methods by Idriss and Boulanger (2006) as shown in Figure 5.2b using the illustration method developed by Armstrong and Malvick (2016). It is important to note that the PI of these natural deposits generally increase with increasing fines content as shown in Figure 1b.

The soil samples were extracted from depths ranging from 15 ft to 248 ft and were tested at vertical effective stresses ranging from 1086 psf to 16708 psf. Most samples were normally consolidated prior to cyclic testing except the tests on Willamette Silt performed for SR18 Newberg-Dundee Bypass project (Project ID: O_15), which were tested at overconsolidation ratio (OCR) values of 1, 1.5 and 2.5. These tests were critical in identifying trends related to the effects of stress history and overconsolidation ratio on excess pore pressure generation potentials as described later.

5-2 CALIBRATION OF V&D MODEL PARAMETERS

The V&D model for sands (Dobry et al., 1985) was fit to the lab data in this database to characterize the tendency of silt-rich soils to develop excess pore pressure in undrained cyclic loading, and more specifically highlight the effects of stress history on pore pressure development tendency of silts. The model is provided in Equation 1. Details on the model parameters can be found in the corresponding reference. The model parameters (f, p, F, and γtvp) are presented in this chapter as they are reported in the corresponding Geotechnical Design Reports when those data were available. For projects where those data were not available, the V&D model parameters were calibrated in general accordance with the procedures outlines in Vucetic (1986), Matasovic (1993) and Mei et al. (2018). Table 5.2 summarizes the calibrated V&D parameters for all the tests/sites that are included in this study.

$$r_{u,N} = \frac{pfN_cF(\gamma_c - \gamma_{tvp})^8}{1 + fN_cF(\gamma_c - \gamma_{tvp})^8} \qquad \text{(Equation 1)}$$

5-3 REPRESENTATIVE RESULTS

Data from nine strain-controlled CDSS tests performed on Willamette Silt samples from SR18 Newberg-Dundee project (Project ID: O_15) are shown in Figure 5.3 as an example to highlight the effects of stress history on pore-pressure generation in silt soils. The tests were performed at shear strains of γ_c = 0.1%, 0.4%, and 1.6-2% on specimens consolidated to vertical effective stresses of 5000 psf, 7500 psf, and 12500 psf, and unloaded to 5000 psf creating laboratory–induced OCR of 2.5, 1.5 and 1, respectively. These samples had FC of 54% to 99%, silt contents of 46% to 79%, liquid limit (LL) of 30 to 33, PI of 5 to 9, and water contents of 32% to 36%. These samples are characterized as susceptible to liquefaction and/or cyclic softening based on screening procedures often used in practice (e.g., Bray and Sancio 2006, Idriss and Boulanger 2008).

Figure 5.3 shows the excess pore pressure ratios versus cyclic shear strain from strain-controlled CDSS tests (symbols) and the calibrated V&D sand model (straight lines). Data are presented for three sets of tests with OCR = 1, 1.5 and 2.5. The lab data clearly shows that as OCR increases, the tendency for developing excess pore pressure decreases.

Figure 5.4 shows the excess pore pressure versus loading cycles from CDSS tests and the calibrated V&D model for the same tests presented in the previous figure. The calibrated V&D model reasonably captures the excess pore pressures at larger shear strains (i.e., γ = 1.6% and 2%) and generally performs better for loading cycles greater than 5. The V&D model parameters can be controlled by the user to target a specific range of loading cycles and/or shear strains based on project specific requirements.

5-4 CORRELATIONS BETWEEN CALIBRATED V&D SAND MODEL PARAMETERS AND OTHER SOIL PROPERTIES

This section provides an overview of possible trends and correlations between V&D model parameters (F, p, f, s, γ_{tvp}) and other soil properties (e.g., OCR, FC, PI, and Vs) to help practitioners with the selection of V&D model parameters for project-specific applications.

5-4.1 EFFECTS OF OVERCONSOLIDATION RATIO ON CALIBRATED F, S, AND P PARAMETERS

The effects of stress history on pore pressure parameters are shown in Figure 5.5. Figure 5.5a shows the calibrated F parameter versus OCR for the data from Willamette Silt in OR18 Newberg-Dundee project where a series of tests were performed on specimens consolidated in lab to OCR values of 1, 1.5 and 2.5. Parameter F in the V&D model is one of the primary input parameters controlling the soil tendency to develop pore water pressure during cyclic loading (i.e., larger F values correspond to larger pore pressure ratios at a given cyclic shear strain). The data presented in this figure show the tendency for pore pressure generation to decrease as OCR increases.

It should be noted the strain-controlled testing database only includes one dataset (Willamette Silt from the OR18 Newberg-Dundee project) where OCR > 1, however, other supplementary data, not included in this database, confirm similar trends and behavior. The supplementary data is provided by CDSS tests performed on reconstituted samples for the Alaskan Way Viaduct project in Seattle, WA, as addressed in Appendix E, and test results on intact samples from Columbia River Silt (CRS) from Sunderland/Portland, OR (Preciado et al., 2021). The data from Columbia River Silt are obtained from field shaking, RCTS and CDSS tests (Preciado et al., 2021). Since the shear strains in the tests performed on Columbia River Silt were relatively small (less than 0.5%), curve fitting for calibrating V&D parameters could not be fully constrained at large strains; therefore, a range of calibrated parameters were developed that envelop the measured pore pressures which are shown in this figure with error bars.

A relationship is developed between F and OCR based on data presented in this figure. The decreasing trend between F and OCR (indicative of smaller pore pressures at higher OCR) is consistent with similar trends shown by other researchers (e.g., Mortezaie and Vucetic 2016; Jana and Stuedlein, 2021). The relationship between F and OCR is developed based on a limited number of data in this study and needs to be evaluated with more data in future studies. Figure 5.5b shows the increasing trend between calibrated s parameter and OCR. Figure 5.5c shows the decreasing trend between calibrated P parameter and OCR.

5-4.2 VARIATIONS IN F PARAMETER AND DIFFERENT FINES CONTENT

The calibrated F parameters are plotted against FC in Figure 5.6 to help illustrate the differences between pore pressure development tendencies in sand soils and silt soils. Only tests with OCR of 1 are plotted in this figure. Also shown in this figure are data from sandy soils (SP and SM) from WS SR-532 General Mark Clark Bridge project (Project ID: W_01) and other sandy soils reported by other researchers (Branding Sand reported by Dobry et al., 1985, Wildlife Site Sand A and B and Herber Road Site Sand PB and CF reported by Vucetic and Dobry, 1988, Santa Monica Beach Sand reported by Matasovic 1993, and Owi Island Sand reported by Thilakarante and Vucetic, 1987). Many previous studies have shown that the cyclic behavior of soil mixtures transitions from being governed by the course fraction to being governed by the fines fraction at FC between 35% to 50% (Polito and Martine 2001; Thevanayagam et al., 2003; Mitchell and Soga 2005). Figure 5.6 clearly illustrates this transition by highlighting the differences between pore pressure development tendencies in sand soils and silt soils. While the F parameters for sand soils (FC for data points in figure are all <40%) range from 0.75 to 10.9 (with a mean value of 2.3) the F parameters for silt soils (FC>50%) are significantly smaller and range from 0.3 to 1.1 (with a mean value of 0.9) for natural, intact NC (OCR=1) specimens presented in this study. The comparison between the calibrated F parameters for sand soils and silt soils suggests, as expected, that the

V&D model parameters developed for sands are generally not suitable to predict the pore pressure generation in silts.

It is noticeable that the two data points for sandy soils that are presented in this study (SP and SM from W_01 project) exhibited large F values that are similar to other sand soils reported in other studies. This observation confirms that there is no bias in the calibration procedure adopted in this study compared to other studies. The comparison between the calibrated F parameters for sand soils and silt soils suggests, as expected, that the V&D model parameters developed for sands are not suitable to predict the pore pressure generation in silts. There is no noticeable correlation between F parameter and FC for soils with FC>50%. Our investigation also showed no significant correlation between F parameter and other fundamental soil properties such as PI. Therefore, as a practical approach, a mean F parameter of 0.7 is proposed for NC silt soils with FC>50%.

5-4.3 CORRELATIONS BETWEEN F PARAMETER AND SHEAR WAVE VELOCITY (VS)

Figure 5.7 shows the relationship between calibrated F parameters and shear wave velocity (Vs). The Vs values for the data points in this database were measured using bender elements in the lab after consolidation and immediately prior to applying cyclic loading. Also shown in this plot are the commonly used sand data reported in other studies and a relationship proposed by Carlton (2014) as suggested in DeepSoil User Manual (Hashash et al., 2016). Note that Carlton's equation was developed based on sand data. As suggested by the figure, the F parameter does not seem to be well correlated with Vs. As such, Carlton's equation does not predict the F parameter accurately. The correlation seems to be consistently poor for both sand and silt soils. Similar observations were made by Mei et al. (2018) regarding the comparison between Carlton's equation with Vs data for sands. The F parameters for OC soils are well below the estimated values from Carlton's equation. The poor correlation between F parameter and Vs is somewhat surprising as it is expected that the cyclic resistance of soil should increase (and pore pressure and F parameter to decrease) with increasing soil stiffness (e.g., Andrus and Stokoe 2000; Baxter et al., 2008). More research is needed to explain the behaviors exhibited in this figure.

It is also noticed that the two sand data points in this study (SP and SM soils from Stanwood, WA, Project ID: W_01) exhibited noticeably larger F values compared to the silt soils (ML and CL-ML) with similar Vs values which indicates higher susceptibility to pore pressure generation for sand soils compared to silt soils with similar Vs values.

While the majority of data points included in this database are from tests performed on intact specimens, data from three cyclic tests on reconstituted specimens from Alaskan Way Viaduct project (AWV) (Project 04) are plotted for comparison. The calibrated F parameter for the

reconstituted samples fall within the range plotted for other intact silt specimens; however, the Vs values corresponding to these tests are significantly smaller than the Vs values for intact specimens.

Another set of outlier data points is highlighted in this figure corresponding to the tests performed on fluvial silts obtained from 16 ft depth in the I-5 Puyallup River Bridge in Tacoma, WA (Project ID: W_08). While the calibrated F parameters for these tests are within the range of values observed for other intact silt specimens, the Vs measured for one specimen is particularly low compared to other data points on intact samples. This difference could be attributed to various factors including different depositional environment, sample disturbance, etc. More research is required to find distinct soil characteristics that can explain this difference.

5-4.4 VARIATIONS IN S PARAMETER FOR DIFFERENT AND FINES CONTENT

Parameter s in the V&D sand model defines the curvature of the relationship between pore pressure ratio and cyclic shear strain. Carlton (2014) proposed a relationship between parameter s and FC. Figure 5.8 shows the relationship between the calibrated *s* parameters in V&D model and the fines content. In addition to the data from this database, data on sands and silts from other studies are also plotted for comparison. The silt data suggests a slightly increasing trend between parameter *s* and FC. While it is common to use an *s* parameter of 1 for clean sand with FC < 5% (e.g., Dobry and Abdoun 2015, Mei et al., 2018) the data points from silt soils in this study (FC greater than 50%) show *s* values larger than 1 (up to 2). The average calibrated *s* value for silt soils is approximately 1.6.

5-4.5 PARAMETER Γ_{TVP}: THRESHOLD SHEAR STRAIN FOR VOLUMETRIC CHANGE

The threshold shear strain for cyclically induced pore water pressure (γtp) was introduced by Dobry et al. (1982) and is defined as the shear strain below which no noticeable permanent pore pressure is developed with increasing number of cycles. Since then, various studies have investigated the influence of different soil properties on the threshold shear strain which for most part have concluded that the threshold shear strain is a fundamental cyclic soil property which is not affected by many factors. Dobry and Abdoun (2015) concluded that past research using lab and field tests show that the threshold shear strain is a robust soil property for sands which is mostly independent of the number of loading cycles, sand type, nonplastic fines content, relative density, depositional method, and the effective confining pressure between 20 kPa to 200 kPa. Vucetic (1994) showed that γtp slightly increases with PI for cohesive materials. His proposed range was further confirmed by Hsu and Vucetic (2006) as shown in Figure 5.9a and was slightly updated by Mortezaie and Vucetic (2016) based on data from two reconstituted clay soils. Jana and Stuedlein

(2021) showed that the range proposed by Mortezaie and Vucetic (2016) reasonably envelopes new data from natural, intact plastic silts with PI of 25 with OCR between 1.8 to 2. In this study we used data from in-situ field shaking (truck mounted shakers, T-Rex and Rattler, by NHERI@UTexas) to evaluate γtp for natural low-plasticity silts and its relationship to previously published relationships.

The potential of the intermediate soils to generate pore water pressure under cyclic loading was evaluated using in-situ cyclic testing with mobile field shakers from NHERI@UTexas (T-Rex and Rattler). These hydraulic shakers apply cyclic shear loading at the ground surface through a baseplate. The cyclic response of the soils was recorded using an array of pore pressure transducers (PPTs) and motion sensors (geophones). Horizontal and vertical displacements from the motion sensors were used to estimate shear strain (γc) imparted on the soil around the PPTs. The pore pressures are normalized with the initial effective stress adjusted for the weight of the shaker trucks. Cyclic testing was performed over multiple shaking events, where a single shaking event involved multiple, increasingly stronger shakes that subjected the ground to larger levels of γc. Each shaking event included N=36 equivalent uniform cycles applied at a frequency of 10 Hz. The maximum γ that was achieved using field cyclic testing was 0.25%. Additional details on testing procedures and instrumentation are provided in Preciado et al. (2021).

The results of excess pore pressure ratios versus shear strains (γc) from field cyclic tests are shown in Figure 5.10a. The incrementally increasing shaking amplitudes were used to identify the threshold shear strain for initiation of excess pore water pressure generation (γtp). The test results at sensor 1P (1.55 m bgs) showed that ru begins to increase at cyclic shear strain of γtp = 0.015%. The test results for sensor 2P (1.75 m bgs) showed that the threshold cyclic shear strain is γtp = 0.02%. The test results at 2.55 m bgs showed a threshold cyclic shear strain of γtp = 0.01%. Sensor P4 (4.55 m) produced very small negative pore pressures showing a dilative response due to a higher overconsolidation ratio. While the magnitudes of induced Δu were very small (due to the attenuation of waves with depth), the data suggest a threshold cyclic shear strain of γpp = 0.015% which is consistent with data from shallower sensors. These findings were generally consistent across different shaking events.

The threshold shears trains for pore pressure determined from Figure 5.10a are plotted against PI in Figure 5.10b. Data from tests on natural intact alluvial plastic silts by Jana and Stuedlein (2021) and reconstituted clay soils by Mortezaie and Vucetic (2016) and their recommended range is also plotted in this figure for comparison. The data by Jana and Stuedlein (2021) correspond to strain-controlled CDSS tests on natural intact alluvial plastic silts with OCR ranging from 1.8 to 2. Data by Mortezaie and Vucetic (2016) are from strain-controlled CDSS tests on reconstituted clay samples with OCR ranging from 1 to 4. The data points from natural low-plasticity silts from this study fall within the range proposed by Mortezaie and Vucetic (2016); therefore, it appears reasonable to continue using their proposed range in engineering applications. It is worth

mentioning that Dobry and Abdoun (2015) reported that overconsolidation of sand increases the threshold shear strain. While the authors believe that such correlations exist, the limited data shown in Figure 5.10b does not show that trend.

5-5 REFERENCES

Anderson, D. G., Shin, S., & Kramer, S. L. (2011). Nonlinear, Effective-Stress Ground Motion Response Analyses Following AASHTO Specifications for Load and Resistance Factor Design Seismic Bridge Design. *Transportation research record*, *2251*(1), 144-154.

Bray, J. D., & Sancio, R. B. (2006). Assessment of the liquefaction susceptibility of fine-grained soils. *Journal of geotechnical and geoenvironmental engineering*, *132*(9), 1165-1177.

Carlton, B. (2014). *An improved description of the seismic response of sites with high plasticity soils, organic clays, and deep soft soil deposits*. University of California, Berkeley.

Dobry, R., & Abdoun, T. (2015). Cyclic shear strain needed for liquefaction triggering and assessment of overburden pressure factor k σ. *Journal of Geotechnical and Geoenvironmental Engineering*, *141*(11), 04015047.

Dobry, R., 1985. *Liquefaction of soils during earthquakes. Rep. No*. CETS-EE-001, National Res. Council NRC, Committee on Earthquake Engineering, Washington, DC.

Dobry, R., Pierce, W. G., Dyvik, R., Thomas, G. E., & Ladd, R. S. (1985). Pore pressure model for cyclic straining of sand. *Rensselaer Polytechnic Institute, Troy, New York*.

Hashash, Y.M.A., Musgrove, M.I., Harmon, J.A., Groholski, D.R., Phillips, C.A., and Park, D. (2016) "DEEPSOIL 6.1, User Manual".

Hazirbaba, K., & Rathje, E. M. (2009). Pore pressure generation of silty sands due to induced cyclic shear strains. *Journal of geotechnical and geoenvironmental engineering*, *135*(12), 1892-1905.

Hsu, C. C., & Vucetic, M. (2006). Threshold shear strain for cyclic pore-water pressure in cohesive soils. *Journal of Geotechnical and Geoenvironmental Engineering*, *132*(10), 1325-1335.

Idriss, I. M., & Boulanger, R. W. (2008). *Soil liquefaction during earthquakes*. Earthquake Engineering Research Institute.

Matasovic, N. 1993. "Seismic response of composite horizontally-layered soil deposits," Ph.D. Thesis, University of California, Los Angeles.

Matasovic, N., & Ordonez, G. (2012). D-MOD2000–A computer program for seismic site response analysis of horizontally layered soil deposits, earthfill dams and solid waste landfills. *Geomotions, LLC*.

Matasović, N. and Vucetic, M., 1993. Cyclic characterization of liquefiable sands. *Journal of Geotechnical Engineering*, *119*(11), pp.1805-1822.

Matasović, N. and Vucetic, M., 1995. Generalized cyclic-degradation-pore-pressure generation model for clays. *Journal of geotechnical engineering*, *121*(1), pp.33-42.

McCullough, N. J., Hoffman, B., Takasumi, D. L., Anderson, D. G., & Dickenson, S. E. (2009). Seismic Site Response for an LNG Facility—Analyses and Lessons Learned. In *TCLEE 2009: Lifeline Earthquake Engineering in a Multihazard Environment* (pp. 1-12).

Mei, X., Olson, S.M. and Hashash, Y.M., 2018. Empirical porewater pressure generation model parameters in 1-D seismic site response analysis. *Soil Dynamics and Earthquake Engineering*, *114*, pp.563-567.

Mitchell, J. K., & Soga, K. (2005). *Fundamentals of soil behavior* (Vol. 3). New York: John Wiley & Sons.

Mortezaie, A.R. and Vucetic, M., 2013. Effect of frequency and vertical stress on cyclic degradation and pore water pressure in clay in the NGI simple shear device. *Journal of Geotechnical and Geoenvironmental Engineering*, *139*(10), pp.1727-1737.

Mortezaie, A., & Vucetic, M. (2016). Threshold shear strains for cyclic degradation and cyclic pore water pressure generation in two clays. *Journal of Geotechnical and Geoenvironmental Engineering*, *142*(5), 04016007.

Preciado, A. M., Sorenson, K., Khosravifar, A., Moug, D., Stokoe, K., Menq, F., & Zhang, B. (2021). Evaluating cyclic loading response of a low plasticity silt with laboratory and field cyclic loading tests. In *ASCE Lifelines 2021 Conference UCLA*.

Thilakaratne, V. and Vucetic, M., 1987. *Class-A Prediction of Accelerations and Seismic Pore Pressures at the Owi Island Site during Oct. 4 1985 Earthquake in Tokyo Bay-Part I*. Research Report, Civ. Eng. Dept., Clarkson Univ., Potsdam, NY, 60 p.

Vucetic, M. (1986). *PORE PRESSURE BUILDUP AND LIQUEFACTION AT LEVEL SANDY SITES DURING EARTHQUAKES (CALIFORNIA, JAPAN)* (Doctoral dissertation, Rensselaer Polytechnic Institute).

Vucetic, M. and Dobry, R., 1988. Cyclic triaxial strain-controlled testing of liquefiable sands. In *Advanced triaxial testing of soil and rock*. ASTM International.

5-6 CHAPTER 5 TABLES AND FIGURES

Table 5.1. Strain-controlled cyclic DSS tests used in this study

Project ID	Project / Location	Soils	Reference	Boring, Sample ID / Depth	Tests	Cyclic loading rate	D50 / D10 (mm)	Sand / Silt / Clay (%)	FC (%)	PL / LL (PI)	USCS classification	Natural water content (%)	Void ratio	Consolidation vertical stress / Vertical stress prior to cyclic loading (OCR)	Bender element Vs (ft/sec)
O_15	ODOT SR 18 Newberg-Dundee By-Pass / Oregon	Willamette Silt / Missoula Flood FF	GRI (2012)	B86, U3 / 15 ft	3 strain-controlled CDSS at γc = 0.1%, 0.4%, 1.6%	0.1 Hz	0.0065 / NA	0 / 64 / 36	100	23 / 39 (16)	CL-ML	37.9 - 43.1	1.02 - 1.16	5000 psf / 5000 psf (1)	797
				B153, U5 / 30 ft	3 strain-controlled CDSS at γc = 0.1%, 0.4%, 1.6%	0.1 Hz	0.008 / NA	1 / 79 / 20	99	21 / 30 (9)	CL-ML	32.4 - 36.3	0.88 - 0.98	5000 psf / 5000 psf (1)	1149
				B153, U4 / 20 ft	3 strain-controlled CDSS at γc = 0.1%, 0.4%, 1.6%	0.1 Hz	0.07 / 0.01	46 / 49 / 5	54	28 / 33 (5)	ML	33.3 - 35.3	0.90 - 0.95	7500 psf / 5000 psf (1.5)	1629
				B86, U4 / 20 ft	3 strain-controlled CDSS at γc = 0.1%, 0.4%, 2%	0.1 Hz	0.015 / 0.0015	3 / 77 / 20	97	24 / 30 (6)	ML	32.8 - 35	0.89 - 0.96	12500 psf / 5000 psf (2.5)	2632
W_01	WS SR-532, General Mark W. Clark Bridge / Stanwood, WA	Tidal Silt / Marine Estuarine	Anderson et al. (2011), CH2M (2009)	GMWC-1C-08, ST-2 (34 ft)	2 strain-controlled CDSS at γc = 0.1%, 0.7%	0.1 Hz	0.055 / 0.007	39 / 53 / 8	61	23 / 31 (8)	ML	32.3	0.88	3000 psf / 3000 psf (1)	840 - 924
				GMWC-1A-08, ST-5 (87 ft)	2 strain-controlled CDSS at γc = 0.1%, 0.7%	0.1 Hz	0.012 / 0.001	13 / 63 / 24	87	22 / 32 (10)	CL-ML	33	0.71	6700 psf / 6700 psf (1) and 7300 / 7300 (1)	1876 - 2044
O_01	Proposed Oregon LNG Facility / Warrenton, OR	Columbia River Silt	McCullough et al. (2009)	BH-6, 40-ST (248 ft)	3 stress-controlled CDSS at CSR 0.08, 0.16, 0.22	0.1 Hz	NA	1 / 81 / 18	99	25 / 37 (12)	ML	37.3	0.97	16708 psf / 16708 psf (1)	1086
				BH-10, 26-ST (131 ft)	3 stress-controlled CDSS at CSR 0.11, 0.13, 0.18	0.1 Hz	NA	27 / 67 / 6	73	26 / 36 (10)	ML	33.4 - 34.1	0.89 - 0.91	8354 psf / 8354 psf (1)	1019
W_03	WS SR-99, Alaskan Way Viaduct / Seattle, WA	Tidal Silt / Marine Estuarine	S&W (2004)	SDC-001, S-18 (71 ft)	1 CDSS at average γc = 0.29%	0.01 Hz to 0.05 Hz	0.05 / 0.004	28 / 66 / 6	72	NP	ML	38.4	0.879	4178 psf / 4178 (1)	NA
				SDC-001, S-24 (86 ft)	1 CDSS at average γc = 0.1%	0.01 Hz to 0.1 Hz	0.07 / 0.006	46 / 48 / 6	54	23 / 28 (5)	ML	35.6	0.825	4658 psf / 4658 psf (1)	NA
				SDC-001, S-24 (86 ft)	1 CDSS at average γc = 0.075%	0.05 Hz to 0.1 Hz	0.03 / 0.002	29 / 66 / 5	71	NP	ML	35.2	0.781	8356 psf / 8356 psf (1)	NA
				SDC-002, S-19 (52 ft)	1 CDSS at average γc = 0.165%	0.05 Hz to 0.1 Hz	0.05 / 0.004	37 / 60 / 3	63	NP	ML	38.7	0.957	3134 psf / 3134 psf (1)	NA
W_08	I-5 Puyallup River Bridge	Fluvial Silt	CH2M Hill (2008)	5/456-H-19vwp, ST-4 (16 ft)	3 strain-controlled CDSS at γc = 0.1%, 0.4%, 1.6%	0.1 Hz	.05 / 0.003	39 / 48 / 13	61	33 / 43 (10	ML	42.6	1.14	1086 psf / 1086 psf (1)	385

Project ID	Project / Location	Soils	Reference	Boring, Sample ID / Depth	Tests	Cyclic loading rate	D50 / D10 (mm)	Sand / Silt / Clay (%)	FC (%)	PL / LL (PI)	USCS classification	Natural water content (%)	Void ratio	Consolidation vertical stress / Vertical stress prior to cyclic loading (OCR)	Bender element Vs (ft/sec)
	/ Tacoma, WA			WR-12-H-1p-08, ST-16 (67 ft)	3 strain-controlled CDSS at γc = 0.1%, 0.4%, 1.6%	0.1 Hz	0.07 / 0.009	46 / 47 / 7	54	NP	ML	24.8	0.66	4595 psf / 4595 psf (1)	696
				WR-12-H-1p-08, ST-20 (84 ft)	3 strain-controlled CDSS at γc = 0.1%, 0.4%, 1.6%	0.1 Hz	0.045 / 0.004	23 / 66 / 11	77	21 / 27 (6)	CL-ML	31.7	0.82	10025 psf / 10025 psf (1)	821

Table 5.2. Calibrated V&D parameters

Soil Unit	Soil Properties	f	P	γ_{tvp}	F	s
O_15: SR18 Newberg-Dundee (Willamette Silt / Missoula Flood FF)	CL-ML, PI=16, FC=100%, OCR=1, Vs=797 ft/sec	1	0.94	0.03	1.10	1.90
	CL-ML, PI=9, FC=99%, OCR=1, Vs=1149 ft/sec	1	0.95	0.020	1.00	2.00
	ML, PI=5, FC=54%, OCR=1.5, Vs=1629 ft/sec	1	0.94	0.015	0.56	2.20
	ML, PI=6, FC=97%, OCR=2.5, Vs=2632 ft/sec	1	0.80	0.020	0.04	3.10
W_01: WS SR-532, General Mark W. Clark Bridge (Estuarine/Tidal Silt)	ML, PI=8, FC=61%, OCR=1, Vs=840 - 924 ft/sec	1	1	0.020	1.05	1.50
	CL-ML, PI=10, FC=87%, OCR=1, Vs=1876 - 2044 ft/sec	1	1	0.020	0.90	1.60
	SP (ST-1), PI=NP, FC=1%, OCR=1, Vs=889 ft/sec	1	1	0.015	2.6	1.5
	SM (ST-4), PI=NP, FC=32%, OCR=1, Vs=862 ft/sec	1	1	0.015	1.4	1.6
O_01: Warenton, OR (Columbia River Silt)	ML, PI=10 to 12, FC=73% to 99%, OCR=1, Vs=1019 ft/sec to 1086 ft/sec	1	1.00	0.06	0.49	1.76
W_03: WS SR-99, Alaskan Way Viaduct (Estuarine/Tidal Silt)	ML, PI=NP to 5, FC=54% to 72%, OCR=1	1	1.00	0.015	0.80	1.60
W_08: I-5/Puyallup River Bridge (Fluvial Silt)	ML, PI=10, FC=61%, OCR=1, Vs=385 ft/sec	1	0.80	0.020	0.30	1.30
	ML, PI=NP, FC=54%, OCR=1, Vs=696 ft/sec	1	1.00	0.015	0.40	1.30
	CL-ML, PI=6, FC=77%, OCR=1, Vs=821 ft/sec	1	1.00	0.020	0.30	1.60

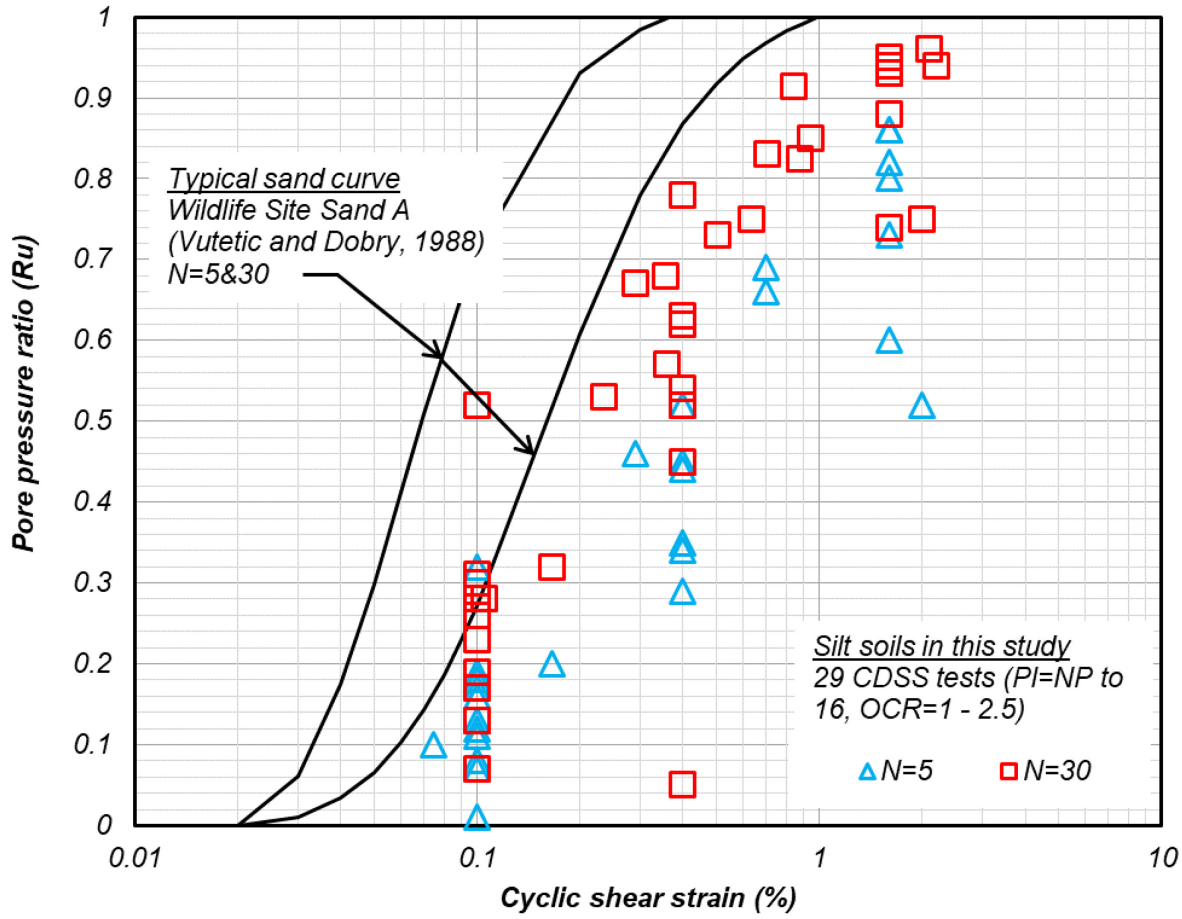

Figure 5.1a: Comparison of cyclically induced excess pore pressure ratios in sands and silts

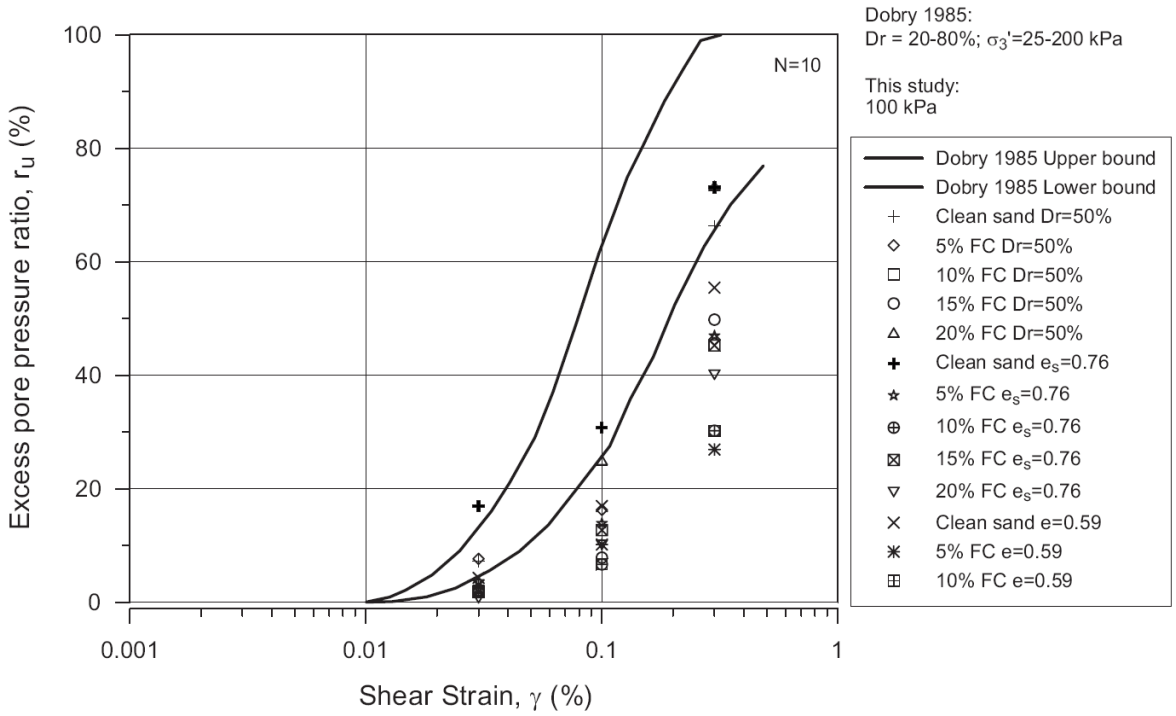

Figure 5.1b: Effects of fines content on cyclically induced excess pore pressure ratios in sand (form Hazirbaba and Rathje, 2009)

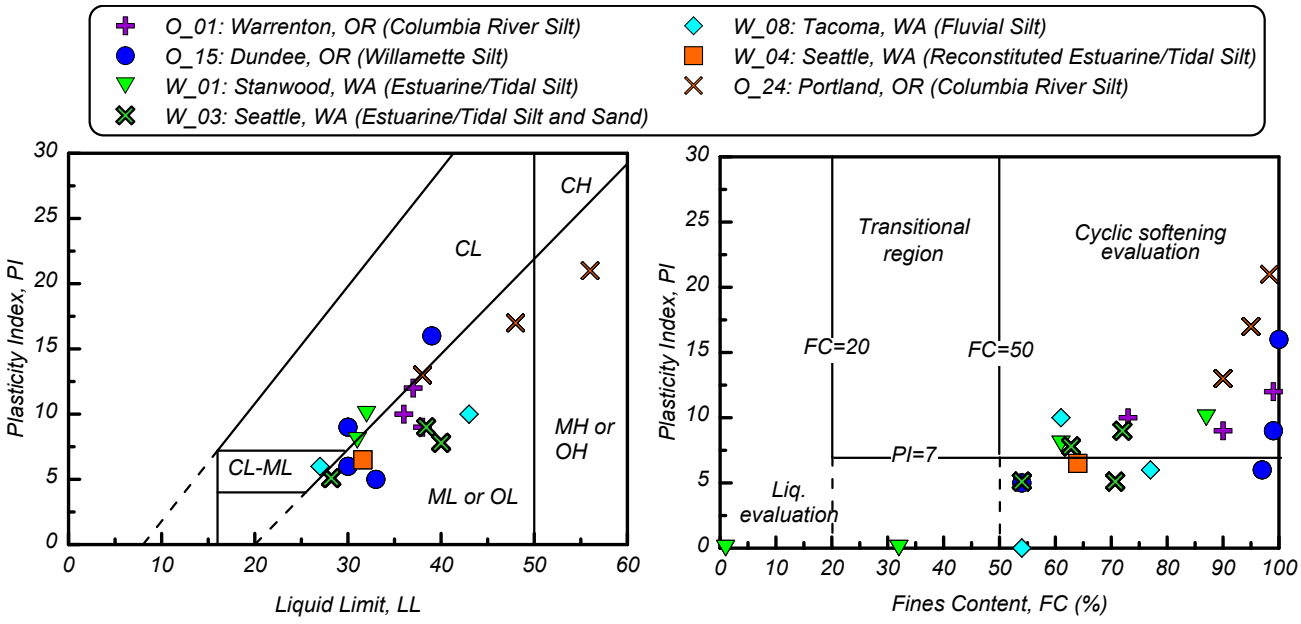

Figure 5.2: Atterberg limits and fines contents of the test specimens used in this database and screening liquefaction and cyclic softening criteria by Idriss and Boulanger (2008) as summarized by Armstrong and Malvick (2015)

(a) OCR=1 **(b) OCR=1.5** **(c) OCR=2.5**

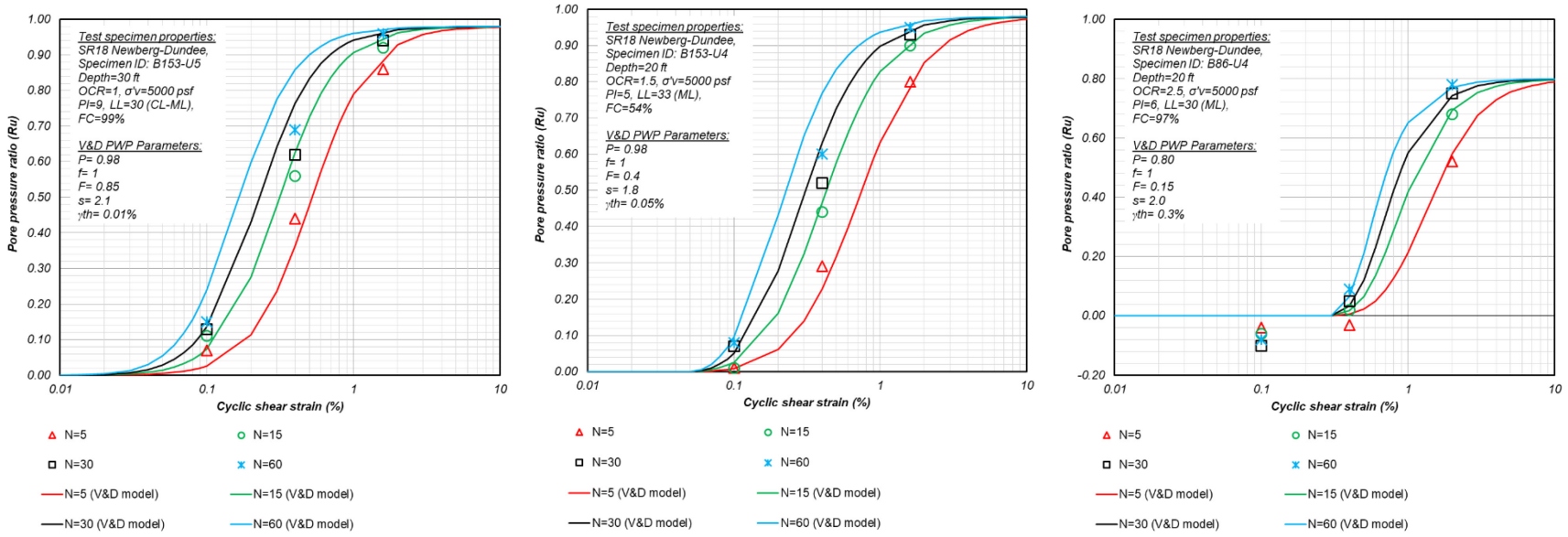

Figure 5.3: Excess pore pressure ratios versus cyclic shear strain from strain-controlled CDSS tests and calibrated V&D models for Willamette Silt samples from SR18 Newberg-Dundee Project (ID: O_15): (a) OCR=1, (b): OCR=1.5, (c) OCR=2.5

(a) OCR=1 **(b) OCR=1.5** **(c) OCR=2.5**

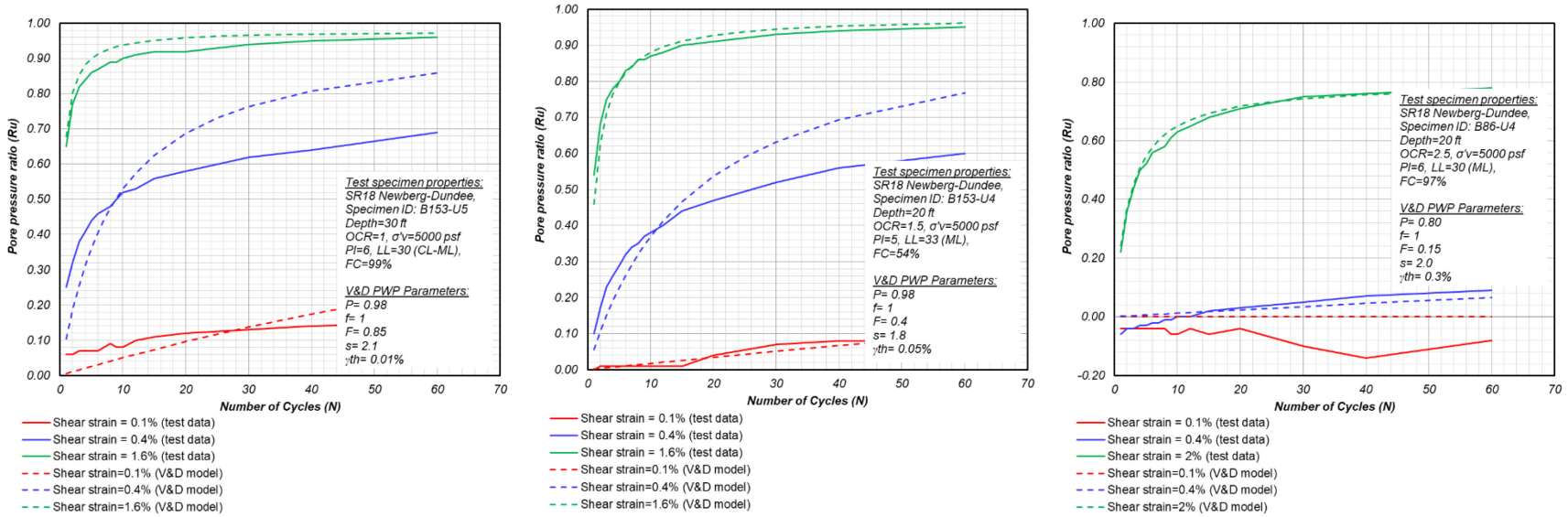

Figure 5.4: Excess pore pressure ratios versus loading cycles from strain-controlled CDSS tests and calibrated V&D models for Willamette Silt samples from SR18 Newberg-Dundee Project (ID: O_15): (a) OCR=1, (b): OCR=1.5, (c) OCR=2.5

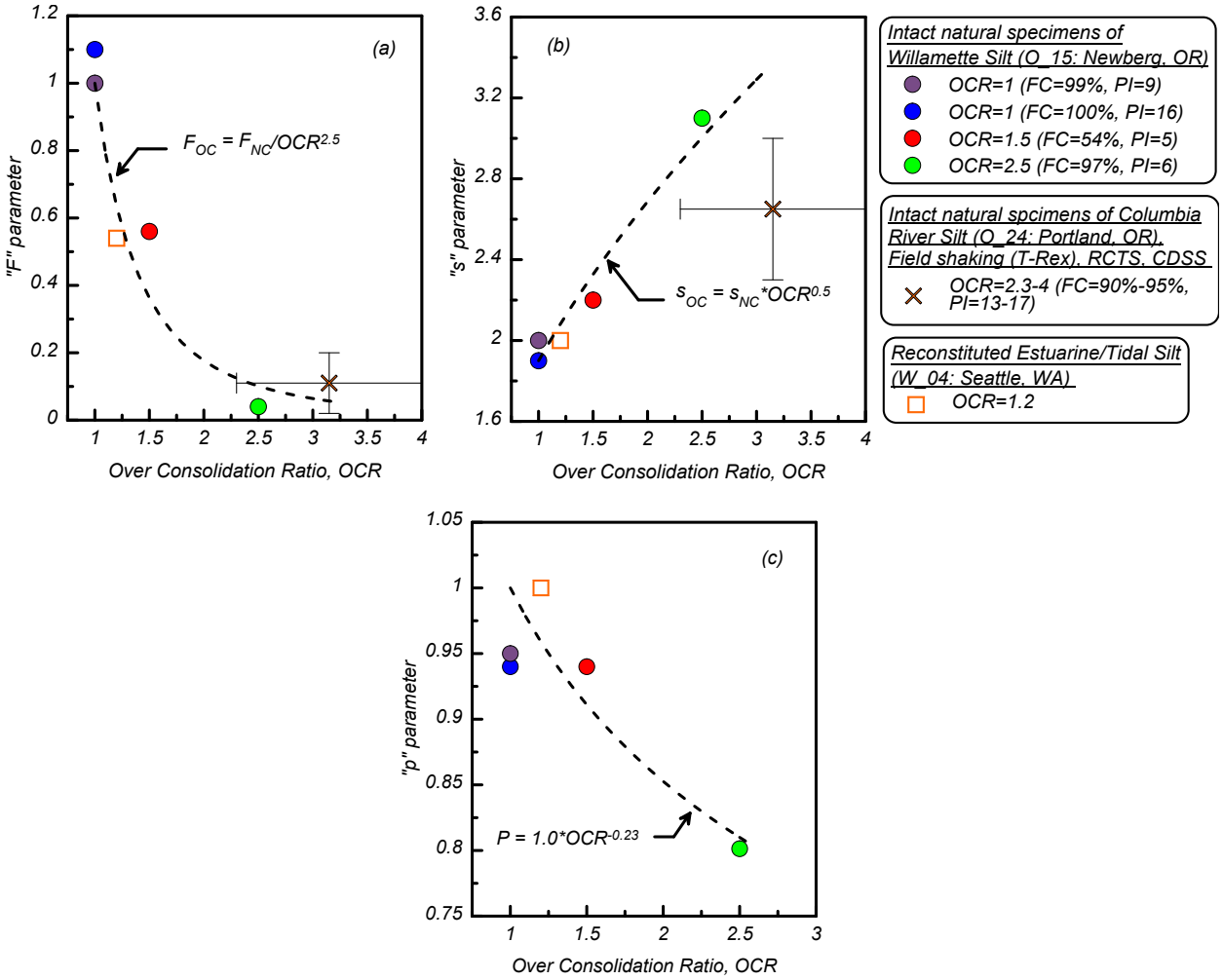

Figure 5.5: Effects of overconsolidation ratio (OCR) on (a) "F" parameter, (b) "s" parameter, and (c) "P" parameter in Vucetic and Dobry model

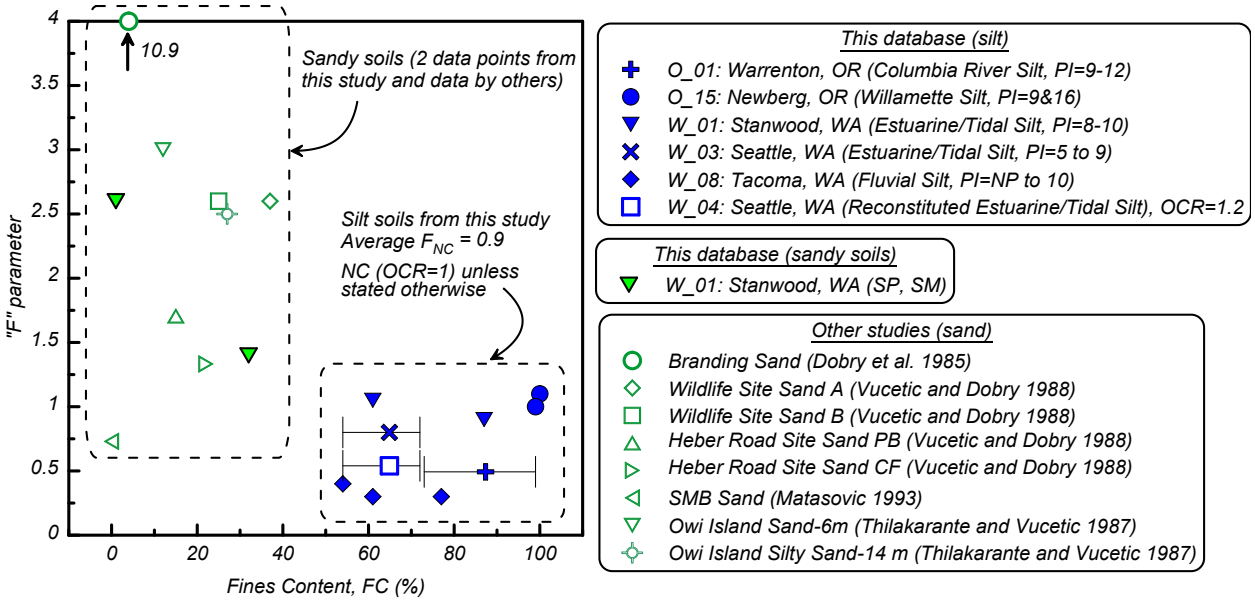

Figure 5.6: Variation in "F" parameter in Vucetic and Dobry model with fines content for silt and sand soils included in this study and sand soils in other studies.

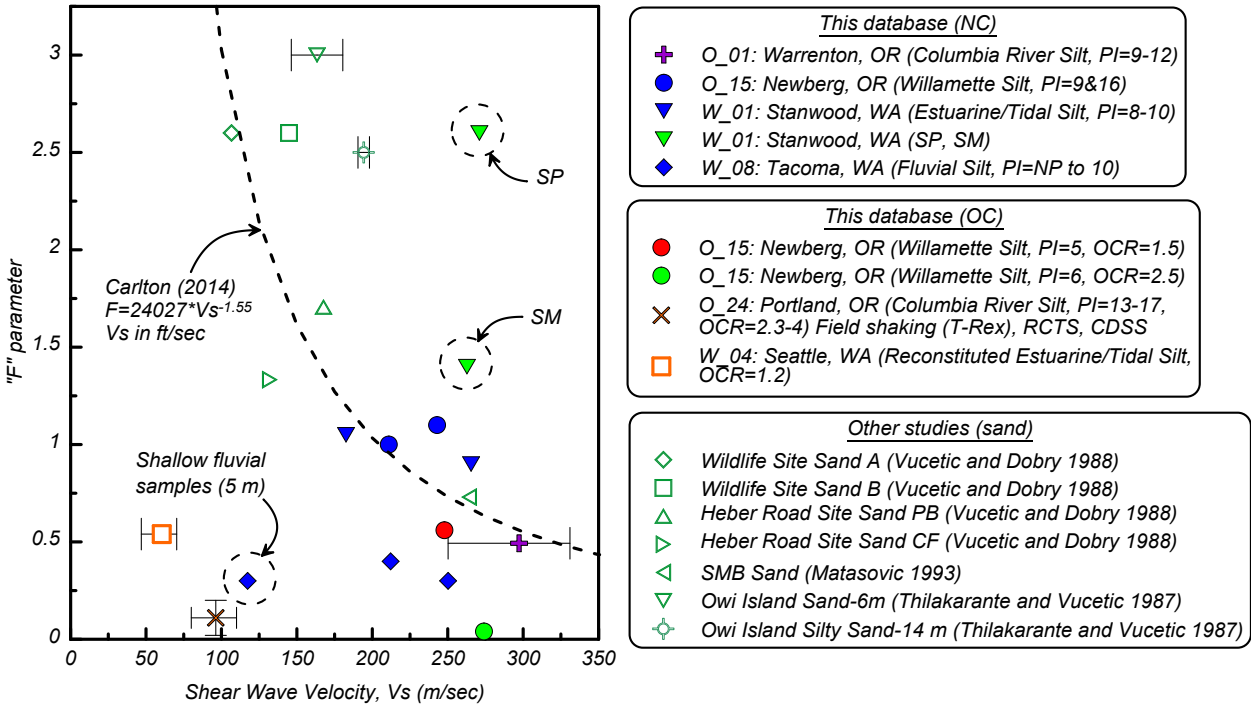

Figure 5.7: Variation between "F" parameter in Vucetic and Dobry model and shear wave velocity (Vs)

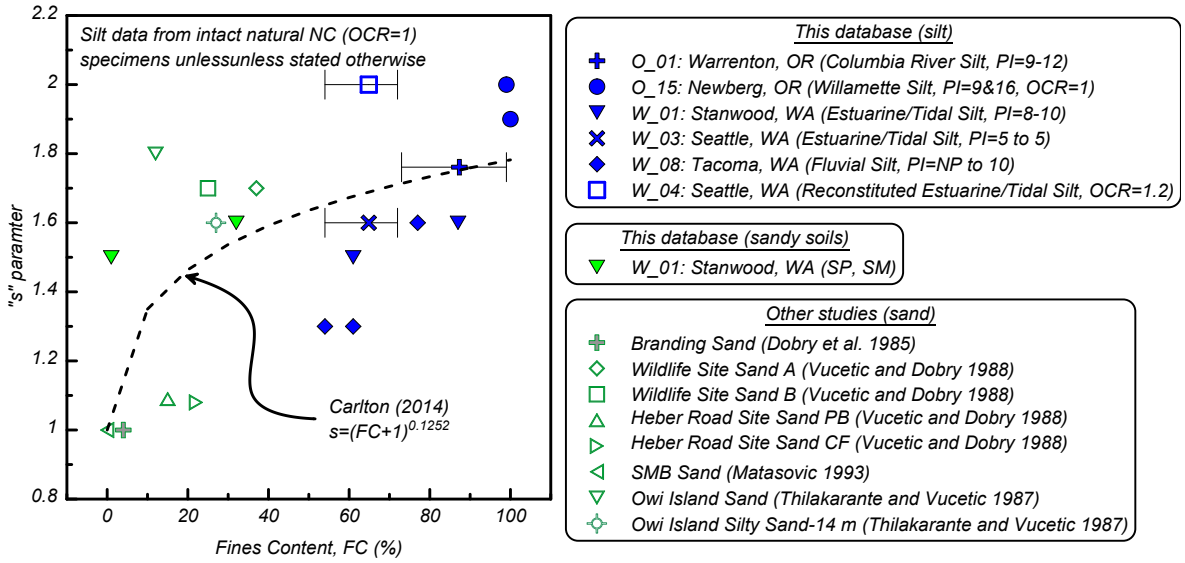

Figure 5.8: Variation in "s" parameter in Vucetic and Dobry model and fines content (FC)

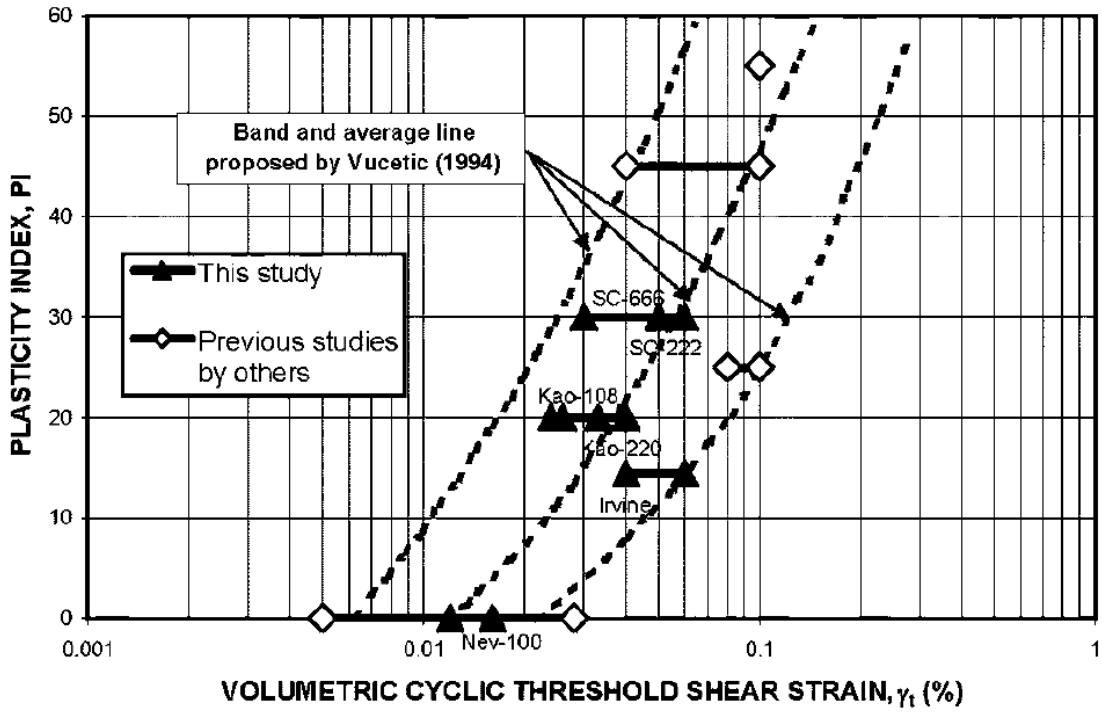

Figure 5.9a: Correlations between threshold shear strain for volumetric change (γ_{tvp}) and plasticity index (from Hsu and Vucetic 2006)

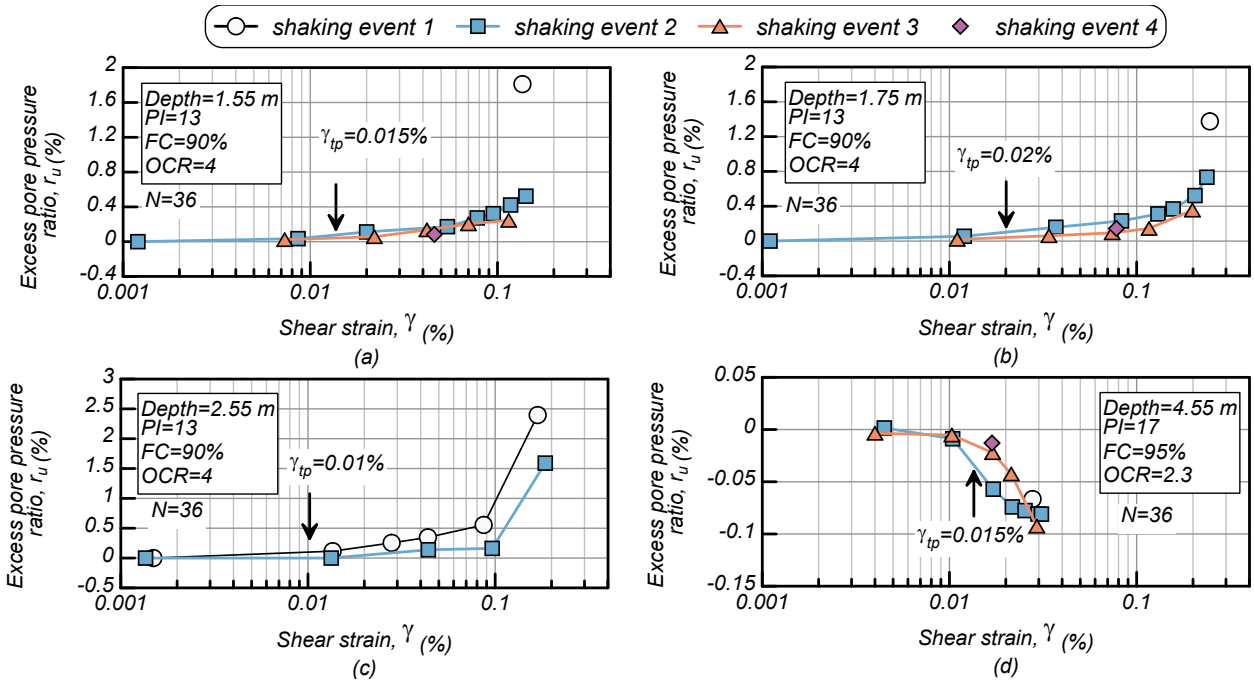

Figure 5.10a: Excess pore pressure ratio versus cyclic shear strain from field shaking using truck-mounted shakers from NHERI@UTexas on Columbia River Silt from Portland, OR (Preciado et al., 2021) and threshold shear strains for cyclic pore water pressure generation (γ_{tp})

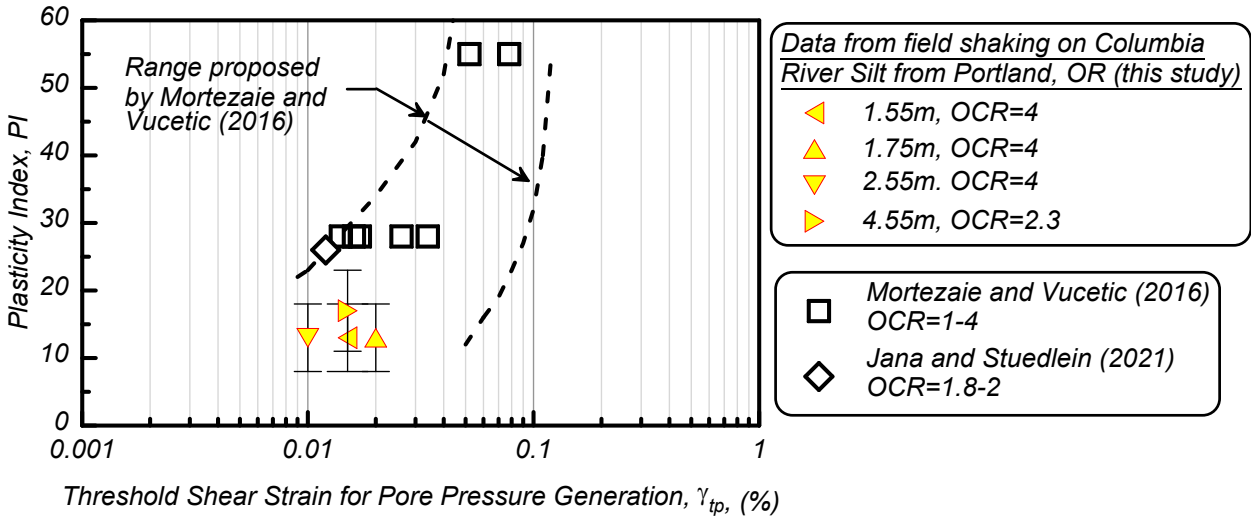

Figure 5.10b: Comparison of threshold shear strain for cyclic pore water pressure generation (γ_{tp}) from this study and data reported by Mortezaie and Vucetic (2016) and Jana and Stuedlein (2021)

CHAPTER 6

Cone Penetration Test and Cyclic Shear Resistance Data

CHAPTER 6 CONTENTS

6-1 INTRODUCTION 105
6-2 ESTIMATING Q_{C1N} RANGE FOR SOIL SPECIMENS 106
6-3 CRR VS. Q_{C1N} DATA POINTS 107
6-4 DISCUSSION & CONCLUSIONS 108
6-5 REFERENCES 110
6-6 CHAPTER 6 TABLES AND FIGURES 111

6-1 INTRODUCTION

Cone penetration test-based relationships to cyclic strength for sands are reasonably well established in engineering practice. These relationships between cyclic strength and cone penetration test (CPT) cone tip resistance (q_c) were primarily developed from earthquake and liquefaction case histories (e.g., Boulanger and Idriss 2015; Youd et al., 2001; Robertson and Wride 1998). However, engineering practice lacks a comprehensive case history database of fine-grained soils behavior in strong earthquake shaking, although recent efforts are addressing this gap in case-histories (Saye et al., 2021). Consequently, there is little guidance for CRR-q_c relationships that account for fine-grained soil properties such as fines content and soil plasticity.

Researchers used data from laboratory testing and cone penetration to study CRR-q_c relationships when case history data were limited. Mitchell and Tseng (1990) developed triggering relationships for four different sands by combining the CRR from laboratory tests and q_c from cavity expansion simulations. Then the relationships were independently evaluated with laboratory testing on undisturbed field samples from sites where q_c profiles were measured. Carraro et al. (2003) developed CRR-q_c relationships for clean and silty sands with cyclic triaxial (CTX) tests and cylindrical cavity expansion simulations; the developed relationships were compared to case history-based correlations for the appropriate range of fines contents. Kokusho et al. (2006) directly developed CRR-q_c curves for sand with varying fines content by preparing specimens in a CTX apparatus and measuring q_c with a mini cone penetrometer before the specimens were cyclically loaded. Moug et al. (2019) developed CRR-q_c relationships for clean sand with data from cyclic direct simple shear tests (CDSS) and an axisymmetric numerical cone penetration model. These relationships were validated with geotechnical centrifuge models. These studies demonstrate that data from laboratory cyclic tests and CPT profiles can inform CRR-q_c relationships.

This chapter presents a preliminary analysis of CRR-q_c relationships for fine-grained soils in Oregon and Washington. The analysis is performed with data from stress-controlled laboratory cyclic shear tests on intact samples and field-measured normalized cone tip resistance (q_{c1N}) profiles performed near sampling locations. The dataset is from twelve engineering projects in Oregon and Washington at predominately fine-grained soil sites. Cyclic laboratory testing included stress-controlled constant volume CDSS and stress-controlled undrained CTX. The CRR for CDSS was defined as the shear loading ratio to reach 3% double amplitude shear strain in 15 uniform loading cycles ($CRR_{N=15}$). The $CRR_{N=15}$ for CTX was defined as the shear loading ratio to reach 5% single amplitude axial strain in 15 uniform loading cycles. It should be noted that normalization to 30 uniform cycles is generally used to represent equivalent magnitude 7.5 earthquake loading for clay-like soils from laboratory testing, while 15 uniform cycles is typically used for sand-like soils (e.g., Idriss and Boulanger, 2008). Soils included in this data report likely include sand-like and clay-like behavior, and distinction between these behaviors remains a challenge for engineering practice, therefore $CRR_{N=15}$ was used for all data points. Cyclic loading rates were between 0.1 and 2.0 Hz for CDSS and 0.1 and 1.0 Hz for CTX. CRR values were uniformly strain-rate adjusted for equivalent 1.0 Hz cyclic loading with a 9% increase per log cycle of loading frequency (Lefebvre & Pfendler, 1996); future analysis of the dataset

will evaluate possible refinement of the strain-rate adjustment for specimens that exhibit transitional behavior, based on correlation to parameters such as FC, PI, or I_c. Table 6.1 summarizes the relevant CPT data, $CRR_{N=15}$, and key soil properties for each project. The process for estimating a representative range of CPT-based soil parameters for the tested soil specimens is described herein.

The dataset in this chapter includes estimated soil behavior type (SBT) through the I_c parameter (Robertson 2009) interpreted from CPT measurements; as well as plasticity index (PI) and fines content (FC) if available for the laboratory specimens. The I_c values ranged from 2.47 (silty sand to sandy silt) to 3.4 (clay to silty clay); PI values ranged from 0 (non-plastic) to 32, FC ranged from 22% to 100%.

Data points are plotted as $CRR_{N=15}$ vs. q_{c1N} with groupings to look at ranges of PI, I_c, and FC. These data are compared with published $CRR_{N=15}$-q_{c1N} relationships for a typical clay that undergoes cyclic softening (Boulanger and Idriss 2004) and for sand with fines that undergoes liquefaction triggering (Boulanger and Idriss 2016). The $CRR_{N=15} - q_{c1N}$ relationship for clay soils is estimated using a τ_{cyc}/s_u for N=15 of 0.92. This τ_{cyc}/s_u ratio is based on an empirical value of 0.80 for N=30 from Boulanger and Idriss (2004) that includes a correction from 1D laboratory loading to 2D field loading conditions. The equivalent τ_{cyc}/s_u for N=15 cycles was estimated with a factor b = 0.20. The undrained shear strength (s_u) relates to corrected cone tip resistance (q_t) with an assumed cone factor (N_{kt}) of 15 as:

$$s_u = \frac{q_t - \sigma_{vo}}{N_{kt}}$$

This analysis is intended as a basis to direct future investigation and study of CRR-q_{c1N} relationship in fine-grained soils of the Pacific Northwest. Discussion of implications of the results for engineering practice to assess CRR or cyclic soil behavior from CPT data is included.

6-2 ESTIMATING Q_{C1N} RANGE FOR SOIL SPECIMENS

The data presented in this chapter are from engineering projects in Oregon and Washington with (i) cyclic laboratory tests performed on specimens prepared from intact Shelby tube samples, and (ii) at least one CPT profile in the same soil unit from which the Shelby tube sample was obtained. Based on the site stratigraphy and the distance from the sampled borehole to CPT profile(s), a representative q_{c1N} value was estimated for the laboratory-tested soil. For projects with digital CPT data or projects where CPT profiles could be digitized, a range of q_{c1N} values were estimated for the soil unit (further described below). For projects where a range of q_{c1N} values could not reasonably be estimated from CPT data profiles (i.e., the image quality of available data profiles is very low), a single value was estimated at approximately the same depth as the sample was obtained.

The general approach to estimate a representative range of q_{c1N} values was:

1. Examine CPT profiles, borehole logs, site geology and additional project data to determine the soil unit from which a Shelby tube sample was obtained.
2. Select one or more CPT profiles near the sampled borehole for analysis and delineate the depth interval of the sampled soil unit in the CPT profiles. The CPT profile(s) and depth interval selected for each Shelby tube sample is provided in Table 6.1.

3. Calculate q_{c1N} and I_c profiles from CPT data of the sampled soil unit. An example of the CPT data and depth interval for project O-05 CPT-3C is shown in Figure 6.1a.
4. Analyze the frequency distribution of q_{c1N} and I_c of the sampled soil unit to provide a best-estimate (median value) of q_{c1N} and I_c, as well as lower-estimate (15th percentile) and upper-estimate (85th percentile) of q_{c1N}. An example of the frequency distribution with determination of the median, lower-estimate, and upper-estimate from the data from 41 to 49 feet of CPT-3C is shown in Figure 6.1b.

The median values of q_{c1N} and I_c for each sample are provided in Table 6.1, as well as the lower-estimate and upper-estimate of q_{c1N} if available.

6-3 CRR VS. Q_{C1N} DATA POINTS

The laboratory-characterized $CRR_{N=15}$ values are compared against the estimates of q_{c1N} from nearby CPT profiles in Figures 6.2 to 6.5. The data in Table 6.1 are presented in figures in this section to evaluate trends. Data points where in-situ over consolidation ratio (OCR) was inconsistent with the OCR for cyclic laboratory testing are indicated on the figures, otherwise the two OCR values were considered to agree. In cases where the two OCR levels are not consistent, they could still be considered to represent a reasonable range of in situ OCR values since lab testing OCR levels are often specified to bracket the range of possible in situ OCR values given depositional history and aging even when the range is not indicated by CPT or lab data It should be noted that in-situ OCR values were estimated from Casagrande analysis of 1D consolidation lab test data and/or CPT data analyzed with relationships to q_t from Chen & Mayne (1994). Estimates of in-situ OCR may change if laboratory test data are re-evaluated with energy-based methods.

The data points are plotted for ranges of PI, I_c and FC to study preliminary trends in the data. The q_{c1N} values are plotted at the median value along with a range spanning from the lower-estimate to the upper-estimate. All data plots include the Boulanger and Idriss (2015) $CRR_{N=15}$-q_{c1N} relationship for liquefaction triggering of sand with 70% FC, and the approximate relationship of $CRR_{N=15}$-q_{c1N} for typical cyclic softening clay behavior from Boulanger and Idriss (2004).

FC were reported as the percent of soil by weight passing the standard number 200 sieve. The $CRR_{N=15}$ and q_{c1N} data points were plotted for FC ranges of less than 70%, 71% to 80%, 81% to 90%, and greater than 90%. The data points for all FC are plotted in Figure 6.2, including separate plots for the FC ranges.

The data points with a reported PI value are plotted in Figure 6.3, including separate plots with specific PI ranges. The $CRR_{N=15}$ and q_{c1N} data points are plotted for PI ranges of PI = 0 to 1, 2 to 5, 6 to 12, and greater than 12.

An estimate of I_c was obtained from CPT data and summarized in Table 6.1. The $CRR_{N=15}$ and q_{c1N} data points are plotted for I_c ranges of: $I_c \leq 2.5$, $2.5 < I_c \leq 2.9$, $2.9 < I_c \leq 3.1$, and $I_c > 3.1$. All data points are plotted in Figure 6.4, including separate plots for I_c ranges.

6-4 DISCUSSION & CONCLUSIONS

This data report presents cyclic strength and CPT data from projects in fine-grained soils in Oregon and Washington. Data points of laboratory-estimated $CRR_{N=15}$ from intact Shelby tube specimens were compared with q_{c1N} values measured near the sampling boreholes. The data points were plotted across a range of FC, PI and I_c and compared with standard $CRR_{N=15}$-q_{c1N} relationships for cyclic softening (clay-like behavior) and liquefaction triggering (sand-like behavior). This data report is intended to develop observations that provide a basis for future research work to investigate development and validation of CRR-q_{c1N} relationships for Oregon's fine-grained soils.

Observations of the data presented herein include:

- There is a range of $CRR_{N=15}$-q_{c1N} relationships that are applicable for fine-grained soils in Oregon and Washington, including relationships for clay and sand soils. Additionally, the data indicate that several projects involved soils with $CRR_{N=15}$-q_{c1N} relationships that transitioned between the relationship for sands with fines and clays.
- Data points presented herein tend to fall to the right of the $CRR_{N=15}$ – q_{c1N} relationship for clays. This $CRR_{N=15}$ – q_{c1N} relationship has a large increase in CRR over a relatively small range of q_{c1N} values compared to the relationship for sands. Therefore, a small over-estimation of q_{c1N} could lead to under-conservative estimates of CRR if the soil is assumed to be clay-like. Cyclic laboratory testing of high-quality intact samples for a project should be performed to inform site-specific CRR estimates and interpretation of CPT data.
- FC does not appear to be a strong indicator of whether CRR relates to q_{c1N} with sand relationships, clay relationships, or neither. For example, from Figure 6.2, data points of $CRR_{N=15}$ vs. q_{c1N} fall between the two $CRR_{N=15}$ – q_{c1N} relationships. However, additional data over a range of FC may provide further insight to these relationships.
- PI appears to correlate with whether CRR relates to q_{c1N} with relationships for sand or clay. Based on data in Figure 6.3, soil with PI < 6 might be reasonably and conservatively characterized with a CRR – q_{c1N} relationship for sand soils with high FC; soil with PI > 12 might be reasonably characterized with a CRR-q_{c1N} relationship for clay soils; soils with PI between 6 and 12 appear to transition between clay and sand relationships. These observations are based on a limited number of projects and data points, particularly for PI < 6. Therefore, additional investigation would provide insight to CRR-q_{c1N} relationships for low PI soils.
- I_c appears to be an indicator of whether CRR relates to q_{c1N} with relationships for sand or clay soils. Based on data presented in Figure 6.4, soil with I_c > 3.1 might be reasonably characterized with a CRR – q_{c1N} relationship for clay; soil with $I_c \leq 2.5$ might be reasonably characterized with a CRR-q_{c1N} relationship for sand soils with high FC; soil with $2.5 < I_c \leq 3.1$ appear to be transitional where data fall between CRR – q_{c1N} relationships for sand and clay. For fine-grained soils that fall in the transition values of I_c, conservative estimates of CRR could be made from CPT data with the liquefaction triggering CRR-q_{c1N} relationship for FC > 70%. These observations are based on a limited number of data points for I_c < 2.9. Additional investigation over a wider range of I_c values would inform whether sand or clay CRR-q_{c1N} relationships are appropriate based on I_c for fine-grained soil.

- This study did not investigate whether PI, FC, or I_c values correlated to sand-like, clay-like, or transitional cyclic behavior. Clay-like soils are characterized by cyclic softening behavior with some excess porewater pressure generation, while sand-like soils are characterized by a loss of shear stiffness and significant excess porewater pressure generation during cyclic loading. This type of investigation may provide further insight into whether soils exhibiting these cyclic behaviors also correlate to sand or clay CRR-q_{c1N} relationships.
- Standard soil behavior relationships have established that q_t and CRR increase as OCR increases. However, it has not been established whether these increases are implicitly accounted for in CRR-q_{c1N} relationships, or if CRR-q_{c1N} should be adjusted as OCR changes. Future studies might investigate the role of OCR on CRR-q_{c1N} relationships on fine-grained soils in Oregon and Washington.

Additional soil data and investigation will be required to build upon these preliminary observations. A comprehensive study might include laboratory testing, CPT profiles, and numerical modeling for soils over a range of I_c, PI, FC, and OCR values for major soil units in Oregon and Washington (e.g., Columbia River silt, Willamette silt, Willamette River silt). Objectives of this study might include: (i) characterizing region-specific CRR-q_{c1N} relationships for fine-grained soils in the Pacific Northwest, including relationships that represent the transition between clay and sand soils, and (ii) investigating soil index properties (e.g., I_c, PI, or FC) as indicators of clay-like, sand-like, or transitional soil behavior in cyclic loading and how CRR-q_{c1N} relationships correspond to these behaviors.

6-5 REFERENCES

Boulanger, R. W., and Idriss, I. M. (2015). "CPT-based liquefaction triggering procedure." Journal of Geotechnical and Geoenvironmental Engineering, ASCE, 142(2), 04015065, 10.1061/(ASCE)GT.1943-5606.0001388.

Boulanger, R.W., and Idriss, I.M. (2004). "Evaluating the potential for liquefaction or cyclic failure of silts and clays". Davis, California: Center for Geotechnical Modeling. Report No. UCD/CGM-04/01.

Carraro, J. A. H., Bandini, P., and Salgado, R. (2003). "Liquefaction resistance of clean and nonplastic silty sands based on cone penetration resistance." *Journal of Geotechnical and Geoenvironmental Engineering,* 129(11), 965-976. 10.1061/(ASCE)1090-0241(2003)129:11(965).

Kokusho, T., Tadashi, H., and Murahata, K. (2006). "Liquefaction strength of sands containing fines compared with cone resistance in triaxial specimens." *Geomechanics II: Testing, Modeling, and Simulation,* 356-373. 10.1061/40870(216)24.

Lefebvre G, Pfendler P. Strain rate and preshear effects in cyclic resistance of soft clay. *Journal of Geotechnical Engineering* 1996, 122(1), 21-26.

Mitchell, J.K., and Tseng, D.J. (1990). "Assessment of liquefaction potential by cone penetration resistance." *Proc. HB Seed Memorial Symp.* Vol. 2.

Moug, D.M., Price, A.B., Parra Bastidas, A.M., Darby, K.M., Boulanger, R.W., DeJong, J.T. (2019). "Mechanistic development of CPT-based cyclic strength correlations for a clean sand." ASCE *Journal of Geotechnical and Geoenvironmental Engineering*, 145(10): 04019072.

Robertson, P.K. (1990). "Soil classification using the CPT." *Canadian Geotechnical Journal*, 27(1): 151 - 158.

Robertson, P.K. and Wride, C.E. (1998). "Evaluating cyclic liquefaction potential using the cone penetration test." *Can. Geotech. J.,* 35(3), 442-459.

Saye SR, Olson SM, Franke KW. Common-origin approach to assess level-ground liquefaction susceptibility and triggering in CPT-compatible soils using ΔQ. *Journal of Geotechnical and Geoenvironmental Engineering*. 2021, 147(7):04021046.

Youd, T.L., Idriss, I.M., Andrus, R.D., Arango, I., Castro, G., Christian, J.T., Dobry, R., Finn, W.D., Harder, L.F., Hynes, M.E., Ishihara, K., Koester, J.P., Liao, S.S.C., Marcuson, W.F., Martin, G.R., Mitchell J.K., Moriwaki, Y., Power, M.S., Robertson, P.K., Seed, R.B., and Stokoe, K.H. (2001). "Liquefaction resistance of soils: summary report from the 1996 NCEER and 1998 NCEER/NSF workshops on evaluation of liquefaction resistance of soil. *J. Geotechnical and Geoenvironmental Eng.,* 10.1061/(ASCE)1090-0241(2001)127:10(817), 817-833.

6-6 CHAPTER 6 TABLES AND FIGURES

Table 6.1. Cyclic laboratory tests and associated cone penetration test data

Project ID	Project / Location	Soils	Reference	Boring, Sample ID / Depth	Associated CPT Profile(s) / Depth Interval	q_{c1N} median	q_{c1N} lower estimate	q_{c1N} upper estimate	I_c	FC (%)	USCS classification	PI	CRR DSS 3% SA, N=15	CRR CTX 5% DA, N=15	In-Situ OCR	Lab OCR
O_05	Portland – N. Marine Drive	Columbia River Silt	Dickenson et al. (2000)	3C-9-T (45 ft)	CPT-3C (41 ft to 49 ft)	13	8	29	3.0	1.8	ML	-	-	0.24	1.0 to 1.5	1.0
				3C-9-M (46 ft)	CPT-3C (41 ft to 49 ft)	13	8	29	3.0	35.4	ML	4	-	0.24	1.0 to 1.5	1.0
				1C-5-TM (23.5 ft)	CPT-1C (22 ft to 32 ft)	8	5.7	14	3.2	71.4	ML	5	-	0.24	1.0 to 1.5	1.0
				4E-8-T (33.5 ft)	CPT-4E (33.5 ft to 47 ft)	8.3	6.3	10.5	3.2	-	MH	14	-	0.24	1.0 to 1.5	1.0
				3C-8-M (41 ft)	CPT-3C (41 ft to 49 ft)	13	8	29	3.0	-	ML	1	-	0.36	1.0 to 1.5	2.0
				3C-8-B (42 ft)	CPT-3C (41 ft to 49 ft)	13	8	29	3.0	67.8	ML	1	-	0.36	1.0 to 1.5	2.0
O-07	Tri-Met Bridge, Willamette River	Willamette River Silt	Northwest Geotech Inc. (2011)	WRTB 1, B-1 (30.5 ft)	P-1 (27 ft to 65 ft); P-2 (31 ft to 55 ft); P-4 (26.2 ft to 50 ft)	9.1	6.7	16.4	3.1	56	ML	10	0.21	-	1.0 to 1.5	1.0
				WRBT 2, B-1 (43.2 ft)		9.1	6.7	16.4	3.1	51	ML	6	0.21	-	1.0 to 1.5	1.0
				WRBT 3, B-1 (42.8 ft)		9.1	6.7	16.4	3.1	70	ML	10	0.21	-	1.0 to 1.5	1.0
				WRBT 4, B-1 (43.4 ft)		9.1	6.7	16.4	3.1	18	SM	0	0.21	-	1.0 to 1.5	1.3
				WRBT 5, B-1 (41 ft)		9.1	6.7	16.4	3.1	90	ML	8	0.21	-	1.0 to 1.5	1.0
O-08	Port of Portland, Willamette River	Willamette River Silt	Geocon Northwest Inc. (2012)	B16, S6 (30 ft)	CPT-5 (30 ft)	12	-	-	1.17	22	SM	NA	0.28	-	1.0 to 1.5	2.0
O-10	Swan Island, Willamette River	Willamette River Silt	Geocon Northwest Inc. (2012)	B1-10 (30 ft)	CPT-1 (30 ft)	12	-	-	2.9	98	MH	32	0.28		1.5 to 2.0	2.4
O-11	Lake Oswego	High PI lacustrine clays / organics	Pyrch (2003)	B-10, S-6 (60 ft)	CPT-3 (60 ft)	9	-	-	3.4	85	MH/OH	18	-	0.37	1.0	1.0
				B-10, S-8 (76 ft)	CPT-3 (76 ft)	7	-	-	3.2	-	ML	12	-	NA	1.0	
				B-9, S-3 (60 ft)	CPT-2 (60 ft)	10	-	-	3.0	100	ML	6	-	0.37	1.0	1.0
				B-9, S-4 (86 ft)	CPT-2 (86 ft)	29	-	-	2.5	64	ML	0	-	0.24	1.0	1.0
				B-13, S-7 (66 ft)	CPT-6 (66 ft)	7	-	-	3.3	-	ML	13	-	NA	1.0	
O-12	Forest Grove	Willamette silt	Geocon Northwest Inc. (2011)	B3-7 (21 ft)	P-1 (15 ft to 31 ft)	50	26	80	2.3	94	ML	5	0.25	-	2.9	3.0

Project ID	Project / Location	Soils	Reference	Boring, Sample ID / Depth	Associated CPT Profile(s) / Depth Interval	q_{c1N} median	q_{c1N} lower estimate	q_{c1N} upper estimate	I_c	FC (%)	USCS classification	PI	CRR DSS 3% SA, N=15	CRR CTX 5% DA, N=15	In-Situ OCR	Lab OCR
O-15	Newberg-Dundee	Willamette silt	ODOT	09320-086-U3 (15 ft)	CPT-1 (1 ft to 26 ft), CPT-2 (1.5 ft to 47 ft), CPT-3 (0.5 ft to 32.5 ft), CPT-4 (1.5 ft to 59 ft), CPT-5 (1.5 ft to 44.5 ft)	23	13	37	2.7	100	CL/ML	16	-	-		1.0
				09320-086-U4 (20 ft)		23	13	37	2.7	97	ML	6	-	-		1.0
				09320-153-U4 (20 ft)		23	13	37	2.7	54	ML	5	-	-		1.0
				09320-153-U5 (30 ft)		23	13	37	2.7	99	CL/ML	9	-	-		1.0

Table 6.1. Cyclic laboratory tests and associated cone penetration test data (continued)

Project ID	Project / Location	Soils	Reference	Boring, Sample ID / Depth	Associated CPT Profile(s) / Depth Interval	q_{c1N} median	q_{c1N} lower bound	q_{c1N} upper bound	I_c	FC (%)	USCS classification	PI	CRR DSS 3% SA, N=15	CRR CTX 5% DA, N=15	In-Situ OCR	Lab OCR
O-18	Newport	Yaquina Bay silt	GRI (2019)	B-3, S-16 (101 ft)	CPT-1 (100 ft), CPT-2 (100 ft), CPT-3 (100 ft), CPT-6 (100 ft)	10	-	-	3.3	-	CH	47	0.38	-	1.6	1.6
				B-1, S-16 (100.5 ft)		10	-	-	3.3	-	MH	22	0.38	-	1.6	1.6
W-01	Stanwood/ Camano Island	Tidal / estuarine silt	CH2M Hill (2009)	GMWC-1C-08 ST2 (33 ft)	GMWC-1D-08 (31.5 ft to 34.5 ft)	2.6	0.8	5.2	3.69	61	ML	8	0.19	-	1.0	1.0
				GMWC-1A-08-ST5 (87 ft)	GMWC-1D-08 (85.5 ft to 88.5 ft)	23	11	39	2.73	87	CL	10	0.19	-	1.0	1.0
W-02	Marysville – SR-529, Ebey Slough	Tidal / estuarine silt	Shannon & Wilson (2008), (2010)	H16p-07, S-16 (51.5 ft)	CPT-08-07 (47 ft to 114.5 ft)	11.5	7.5	30	2.93	88	ML	11	0.19	-	1.0	1.0
				H16p-07, S23 (73 ft)	CPT-08-07 (47 ft to 114.5 ft)	11.5	7.5	30	2.93	71	ML	10	0.19	-	1.0	1.0
				H16p-07,S25 (81.5 ft)	CPT-08-07 (47 ft to 114.5 ft)	11.5	7.5	30	2.93	85	ML	8	0.19	-	1.0	1.0
				H16p-07, S31 (101 ft)	CPT-08-07 (47 ft to 114.5 ft)	11.5	7.5	30	2.93	100	ML	15	0.19	-	1.0	1.0
				H16p-07, S34 (111 ft)	CPT-08-07 (47 ft to 114.5 ft)	11.5	7.5	30	2.93	84	ML	7	0.19	-	1.0	1.0
				H18p-07, S10 (31.5)	CPT-9a-07 (30 ft to 42 ft), CPT-9b-07 (22 ft to 42 ft)	5.2	3.5	7.9	3.2	69	ML	9	0.19	-	1.0	1.0
W-07	Tacoma, Port of Tacoma	Tidal / estuarine silt	GeoEngineers (2007)	B-4, S29 (123 ft)	CPT10-07 (66 ft to 164 ft)	38	14	95	2.64	75	ML	NA	0.17	-	1.0	1.0
				B-5, S30 (97 ft)	CPT10-07 (66 ft to 164 ft)	38	14	95	2.64	60	ML	NA	0.17	-	1.0	1.0

Project ID	Project / Location	Soils	Reference	Boring, Sample ID / Depth	Associated CPT Profile(s) / Depth Interval	q_{c1N} median	q_{c1N} lower bound	q_{c1N} upper bound	I_c	FC (%)	USCS classification	PI	CRR DSS 3% SA, N=15	CRR CTX 5% DA, N=15	In-Situ OCR	Lab OCR
				B-11, S37 (151.75 ft)	CPT10-07 (66 ft to 164 ft), CPT7-07 (66 ft to 174 ft)	60	28	107.5	2.47	70	ML	NA	0.17	-	1.0	1.0
W-09	Vancouver: I-5, I-205, NE 139th St./ Salmon Creek Interchange	Lacustrine silt	WSDOT (2010)	H-30-07, S-13 (5 ft)	CPT7-07 (33 ft to 50 ft), CPT8-07 (30 ft to 50 ft)	28	17.25	41	2.905	90	ML	5	0.20	-	1.0	1.0
				H-35-07, S-17 (52 ft)	CPT9-07 (30 ft to 48 ft), CPT10-07 (33 ft to 55 ft), CPT11-07 (39 ft to 49 ft)	24	15	34	2.92	99	ML	4	0.18	-	1.0	1.0
				H-45-08, S-3 (9 ft)	CPT26-07 (10' to 20')	35.5	10	80	2.48	37	SM	0	0.15	-	1.0	1.0
				H-45-08, S-14 (40 ft)	CPT26-07 (39.5 ft to 52.5 ft)	17.4	9.45	24.5	3.13	99	ML	6	0.24	-	1.0	1.0

Table 6.1. Cyclic laboratory tests and associated cone penetration test data (continued)

Project ID	Project / Location	Soils	Reference	Boring, Sample ID / Depth	Associated CPT Profile(s) / Depth Interval	q_{c1N} median	q_{c1N} lower bound	q_{c1N} upper bound	I_c	FC (%)	USCS classification	PI	CRR DSS 3% SA, N=15	CRR CTX 5% DA, N=15	In-Situ OCR	Lab OCR
W-10	Vancouver gravel pit	Wash tailings	GeoDesign Inc. (2009)	G-34, S3 (14 ft to 16 ft)		10.9	6.4	25.8	3.0	-	ML	12	0.29	-	1.5 to 2.0	2.0
				G-34, S3 (14 ft to 16 ft)		10.9	6.4	25.8	3.0	-	ML	12	0.14	-	1.5 to 2.0	1.0
				G-35A, S1 (25 ft to 27 ft)	P1 (5 ft to 30 ft), P2, 7 ft to 32 ft), P3 (5 ft to 29 ft), P4 (5 ft to 32 ft), P5 (8 ft to 34 ft)	10.9	6.4	25.8	3.0	-	MH	19	0.39	-	1.0 to 1.5	2.0
				G-36, S6 (14 ft to 16 ft)		10.9	6.4	25.8	3.0	-	ML	13	0.29	-	1.5 to 2.0	2.0
				G-37, S8 (25 ft to 27 ft)		10.9	6.4	25.8	3.0	-	MH	28	0.39	-	1.0 to 1.5	2.0

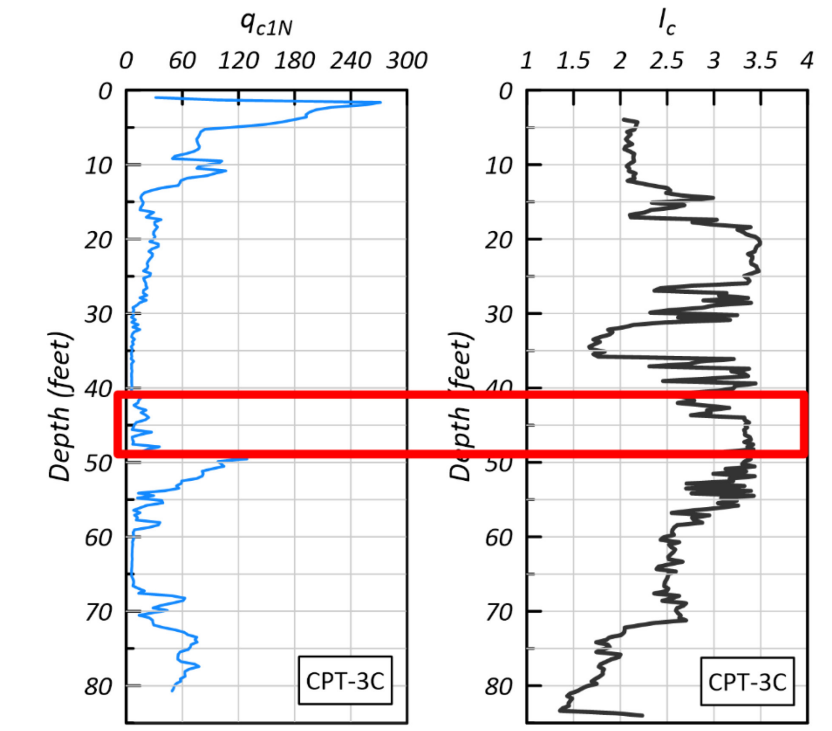

(a)

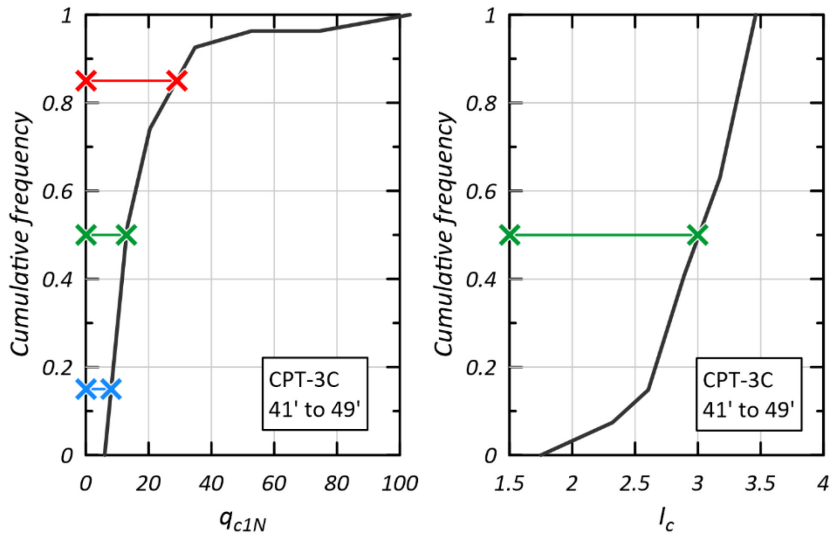

(b)

Figure 6.1: (a) Project O-05 CPT-3C profiles and representative interval for samples 3C-9-T, 3C-9-M, 3C-9-M, 3C-9-B, and (b) cumulative frequency of q_{c1N} and I_c from representative interval.

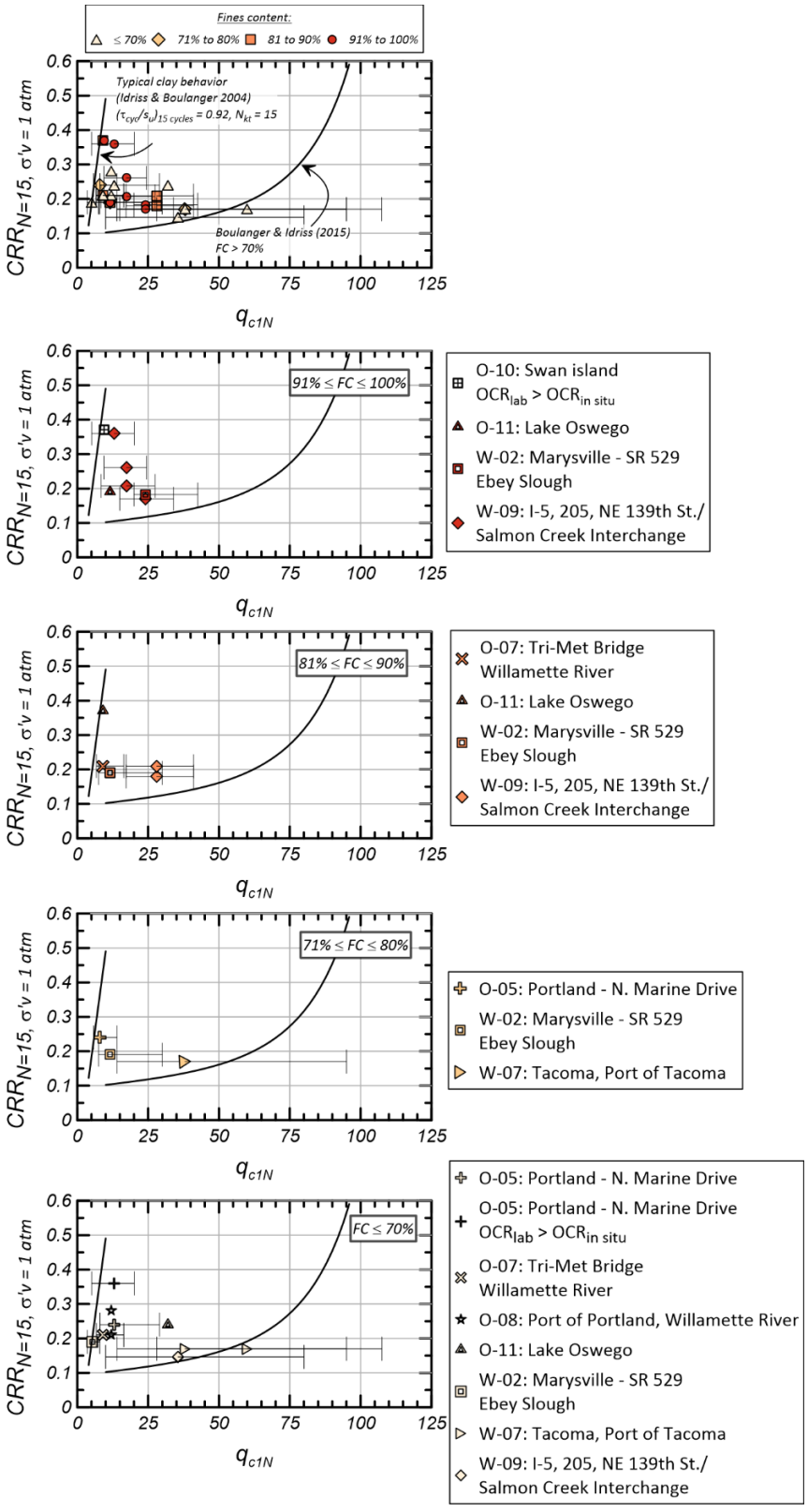
Fines content:
≤ 70%
71% to 80%
81 to 90%
91% to 100%
Typical clay behavior
(Idriss & Boulanger 2004)
$(\tau_{cyc}/s_u)_{15\ cycles}$ = 0.92, N_{kt} = 15
Boulanger & Idriss (2015)
FC > 70%
$CRR_{N=15,\ \sigma'v\ =\ 1\ atm}$
q_{c1N}
91% ≤ FC ≤ 100%
O-10: Swan island
$OCR_{lab} > OCR_{in\ situ}$
O-11: Lake Oswego
W-02: Marysville - SR 529
Ebey Slough
W-09: I-5, 205, NE 139th St./
Salmon Creek Interchange
81% ≤ FC ≤ 90%
O-07: Tri-Met Bridge
Willamette River
O-11: Lake Oswego
W-02: Marysville - SR 529
Ebey Slough
W-09: I-5, 205, NE 139th St./
Salmon Creek Interchange
71% ≤ FC ≤ 80%
O-05: Portland - N. Marine Drive
W-02: Marysville - SR 529
Ebey Slough
W-07: Tacoma, Port of Tacoma
FC ≤ 70%
O-05: Portland - N. Marine Drive
O-05: Portland - N. Marine Drive
$OCR_{lab} > OCR_{in\ situ}$
O-07: Tri-Met Bridge
Willamette River
O-08: Port of Portland, Willamette River
O-11: Lake Oswego
W-02: Marysville - SR 529
Ebey Slough
W-07: Tacoma, Port of Tacoma
W-09: I-5, 205, NE 139th St./
Salmon Creek Interchange

Figure 6.2: CRR and q_{c1N} data points categorized by fines content (FC).

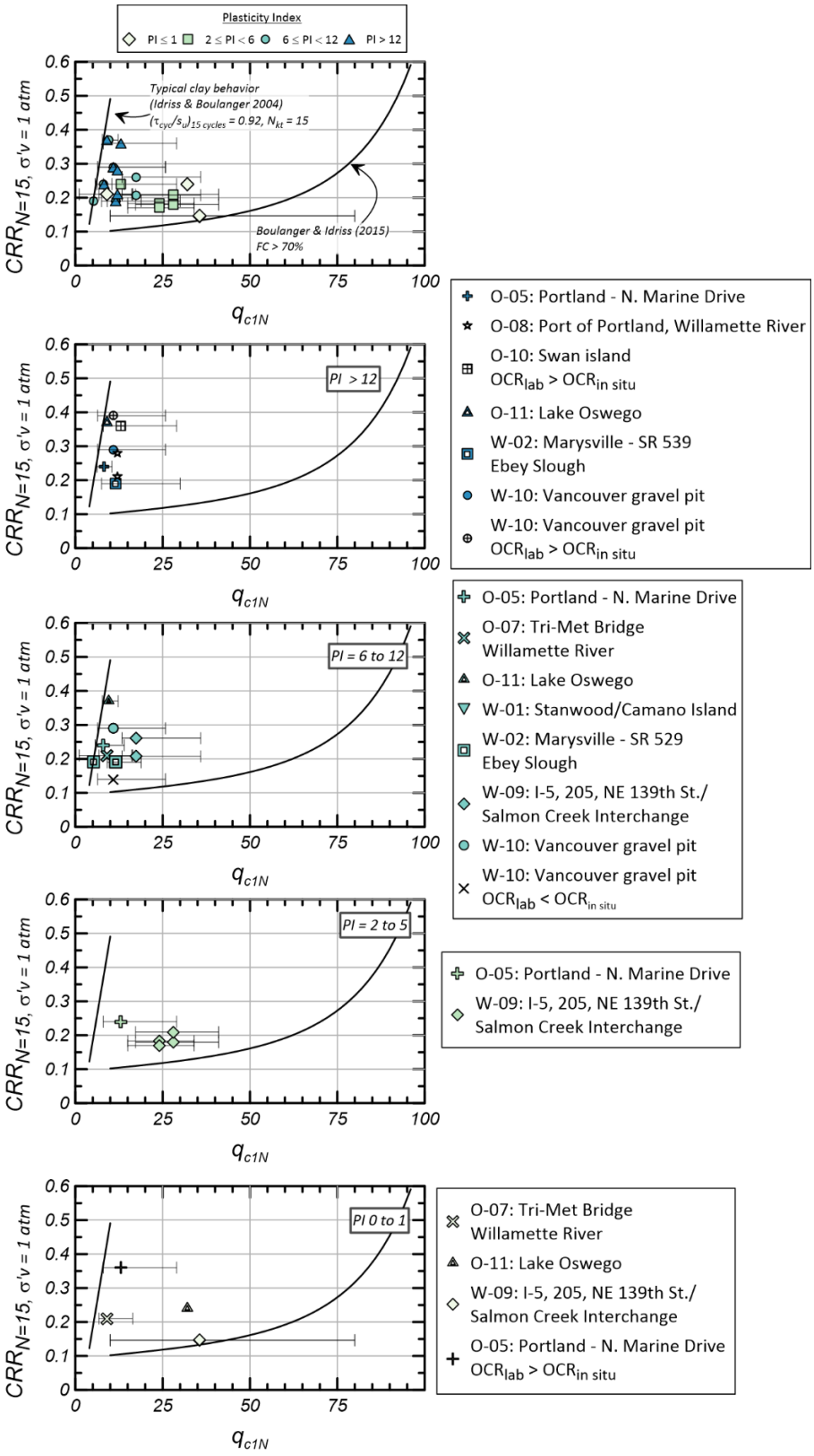
Plasticity Index
PI ≤ 1
2 ≤ PI < 6
6 ≤ PI < 12
PI > 12
Typical clay behavior
(Idriss & Boulanger 2004)
$(\tau_{cyc}/s_u)_{15\ cycles}$ = 0.92, N_{kt} = 15
Boulanger & Idriss (2015)
FC > 70%
$CRR_{N=15,\ \sigma'v\ =\ 1\ atm}$
q_{c1N}
PI > 12
PI = 6 to 12
PI = 2 to 5
PI 0 to 1
O-05: Portland - N. Marine Drive
O-08: Port of Portland, Willamette River
O-10: Swan island
$OCR_{lab} > OCR_{in\ situ}$
O-11: Lake Oswego
W-02: Marysville - SR 539
Ebey Slough
W-10: Vancouver gravel pit
W-10: Vancouver gravel pit
$OCR_{lab} > OCR_{in\ situ}$
O-05: Portland - N. Marine Drive
O-07: Tri-Met Bridge
Willamette River
O-11: Lake Oswego
W-01: Stanwood/Camano Island
W-02: Marysville - SR 529
Ebey Slough
W-09: I-5, 205, NE 139th St./
Salmon Creek Interchange
W-10: Vancouver gravel pit
W-10: Vancouver gravel pit
$OCR_{lab} < OCR_{in\ situ}$
O-05: Portland - N. Marine Drive
W-09: I-5, 205, NE 139th St./
Salmon Creek Interchange
O-07: Tri-Met Bridge
Willamette River
O-11: Lake Oswego
W-09: I-5, 205, NE 139th St./
Salmon Creek Interchange
O-05: Portland - N. Marine Drive
$OCR_{lab} > OCR_{in\ situ}$

Figure 6.3: CRR and q_{c1N} data points categorized by plasticity index (PI).

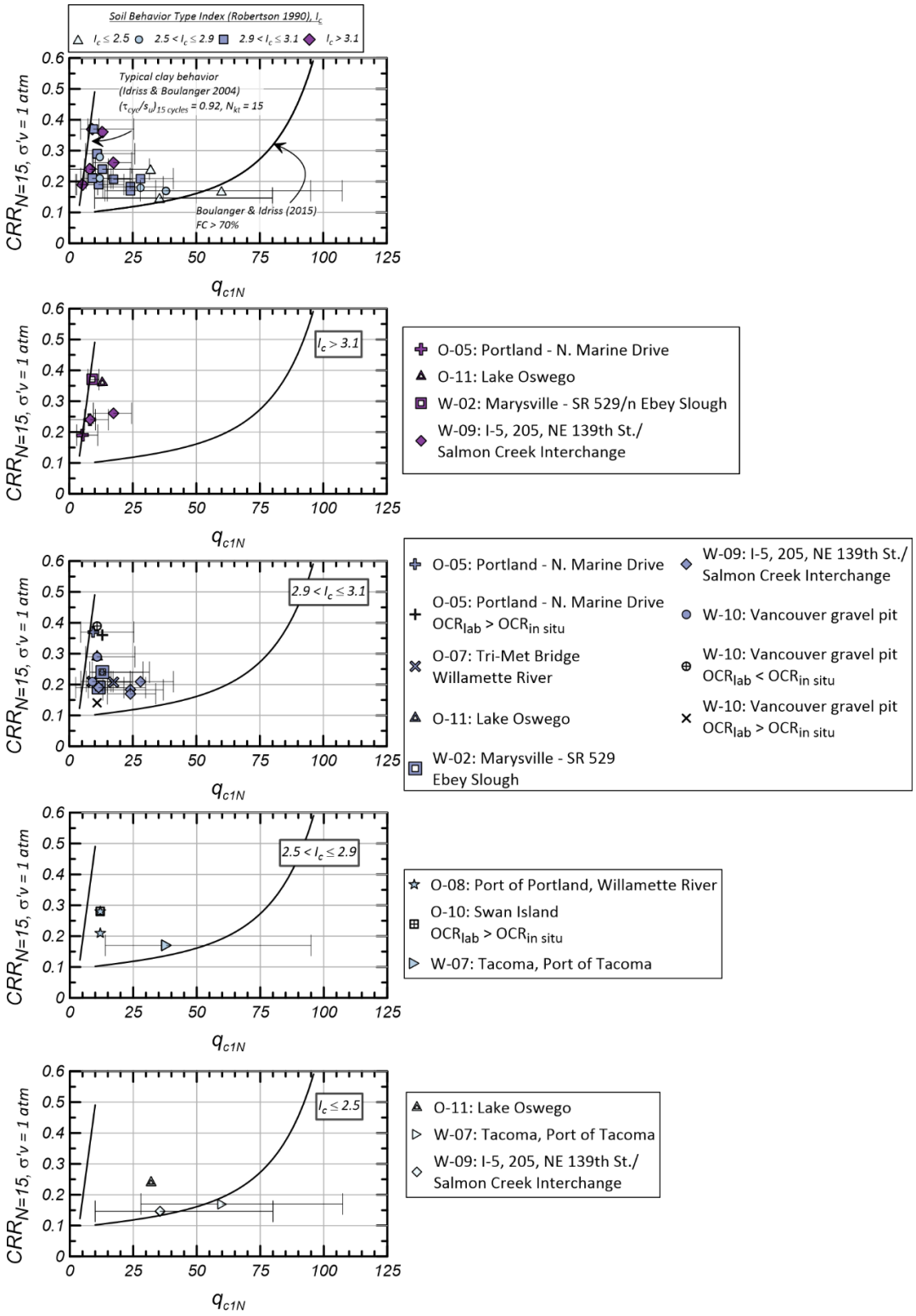

Figure 6.4: CRR and q_{c1N} data points categorized by soil behavior type index (I_c).

APPENDIX A

Alaska Project Sites

APPENDIX B

British Columbia Project Site

APPENDIX C

Oregon Project Sites

APPENDIX D

Washington Project Sites

APPENDIX E

Considerations for Testing and Interpretation of Data on Reconstituted Specimens of Silt

APPENDIX E CONTENTS

E-1 INTRODUCTION E-2
E-2 PROJECT SUMMARY E-3
E-3 CHARACTERIZATION OF THE SILT E-5
E-3.1 Supplementary Testing and Imaging E-5
E-4 PREPARATION OF THE RECONSTITUTED SPECIMENS E-7
E-4.1 Slurry Preparation E-7
E-4.2 Consolidation Procedure E-8
E-4.3 Sampling Procedure E-9
E-5 RESULTS OF STATIC DSS TESTING OF RECONSTITUTED SILT E-10
E-6 RESULTS OF CYCLIC DSS TESTING OF RECONSTITUTED SILT E-10
E-7 RESULTS OF POST-CYCLIC DSS TESTING OF RECONSTITUTED SILT E-12
E-8 COMPARISON OF DSS TESTS ON RECONSTITUTED AND UNDISTURBED SPECIMENS E-15
E-8.1 Cyclic Excess Pore Pressure Generation E-15
E-8.2 Post-Cyclic Strength E-17
E-9 PRIMARY FINDINGS AND CONSIDERATIONS FOR PRACTICE E-19
E-10 REFERENCES E-22
E-11 ACKNOWLEDGEMENTS E-24

APPENDIX E

CONSIDERATIONS FOR TESTING AND INTERPRETATION OF DATA ON RECONSTITUTED SPECIMENS OF SILT

E-1 INTRODUCTION

The use of reconstituted specimens of silt has been suggested on several regional projects known to the project team. This approach to project-specific characterization of the cyclic behavior of foundation soil has generally been considered in cases where there is a limited number of high-quality samples and it is necessary to balance the need for cyclic testing with other laboratory tests necessary for adequate characterization of the silt (e.g., particle size distribution, Atterberg Limits, consolidation, static undrained shear strength). Testing of reconstituted specimens for project-specific applications may facilitate the "re-use" of material with the goal of maximizing limited sampling of silt; however, this procedure is not without potential challenges and limitations (Blaker et al., 2020; Wang et al, 2006; Wijewickreme et al., 2019). This appendix provides a summary of one investigation that included cyclic Direct Simple Shear (DSS) testing of reconstituted specimens of an estuarine silt and comparison with test results on high-quality samples of relatively undisturbed soil. The cyclic resistance and excess pore pressure generation in four independent test sequences are provided, and primary lessons learned with the preparation and testing of reconstituted specimens are listed.

Testing of reconstituted specimens of soil is not uncommon on larger projects involving sandy soils that cannot be sampled, transported, and prepared for testing without significant disturbance. The limitations inherent with interpretation of the laboratory data and application to field behavior have been well established in the geotechnical literature and will not be summarized here for the sake of brevity. These limitations notwithstanding, the testing of reconstituted specimens can be worthwhile for evaluating the relative influence of parameters such as confining stress (K_σ), static stress bias (K_α), stress history (OCR), and initial stiffness (V_s or G_{max}) on the cyclic and post-cyclic behavior of the soil. The primary benefits being the uniformity of carefully prepared specimens and the repeatability of the testing results. Testing of reconstituted specimens can be advantageous for developing trends in the cyclic resistance and post-cyclic behavior over project-specific ranges of the parameters listed; however, the direct application of lab test results to the field conditions must be made judiciously. This consideration has been well addressed in the Washington State Department of Transportation Geotechnical Design Manual (WSDOT GDM, 2021) as it applies to sandy soils:

> *Laboratory cyclic simple shear or cyclic triaxial testing may also be used to evaluate liquefaction susceptibility of and effects on sandy soils from reconstituted soil samples. However, due to difficulties in creating soil test specimens that are representative of the actual in-situ soil, liquefaction testing of reconstituted soil may be conducted only if approved by the State Geotechnical Engineer. Requests to test reconstituted soil specimens will be evaluated based on how well the proposed specimen preparation procedure mimics the in-situ soil conditions and geologic history.*

The same requirement is also warranted for silt-rich soils.

The importance of fabric and microstructure on cyclic and post-cyclic behavior of silt has been highlighted by Wijewickreme and his coworkers, and others making use of his data on low-plasticity silt from the lower Fraser River region of British Columbia (e.g., Dahl, 2011; Soysa, 2015; Wijewickreme et al., 2019). The effects of fabric have been evaluated by comparison of the behavior of intact, relatively undisturbed specimens to that of reconstituted specimens. The following general observations pertaining to the behavior of reconstituted specimens have been noted in the references listed:

1. The reconstituted specimens generally have a lower undrained strength ratio (s_{u_st} / σ_v') in static testing.
2. The reconstituted specimens tend to exhibit higher rates of excess pore pressure generation and cyclic shear strain accumulation.
3. In light of the behavior indicated in (2) it follows that the cyclic resistance for a given reference accumulated shear strain (e.g., 3.75%), is generally lower for the reconstituted specimens.
4. The degradation of shear stiffness due to mobilization of shear strain and excess pore pressure generation is generally greater with reconstituted specimens.
5. The degradation of shear strength, simply evaluated in terms of the ratio τ_{f_cyc} / s_{u_st}, tends to be less pronounced in reconstituted specimens. This is likely related to fabric and aging effects, given the initially "remolded" fabric of reconstituted specimens prepared and consolidated as a slurry.

This brief overview of observations associated with a low-PI fluvial, deltaic silt is provided to highlight potential differences in the stress-strain behavior of reconstituted specimens of fine-grained soil. This is an important consideration for situations involving calibration of constitutive models in dynamic analysis for project-specific use. The limitations associated with testing and interpretation of data from test on reconstituted specimens for applications involving intact, native soil requires careful consideration.

E-2 PROJECT SUMMARY

The comparison of static, cyclic, and post-cyclic behavior of relatively undisturbed and reconstituted specimens is made for an estuarine silt deposit located along the Seattle waterfront at Elliott Bay. This deposit has been very well characterized for several major projects and it provides an extensive set of cyclic DSS data. The testing of reconstituted specimens was completed as a part of an applied research project modeling the dynamic behavior of deep silt deposits using the large-scale geotechnical centrifuge at the University of California, Davis (PI: S. Dickenson). Fabrication of the centrifuge model required placement of the silt as a reconstituted

slurry in the box used for testing, therefore static and cyclic testing of reconstituted specimens of the silt was performed to provide engineering parameters for use in numerical analysis of the centrifuge modeling.

The silt obtained for centrifuge testing was sampled in the field as continuous sonic cores along the alignment of the Alaskan Way Viaduct Replacement and Seawall Replacement Project. The sonic samples were stored in a warehouse and made available for the research investigation by Shannon & Wilson (Seattle). A collection of approximately 2,000 lbs of silt was transported by van to the U.C. Davis Center for Geotechnical Modeling Large Centrifuge Facility. Once at the U.C. Davis lab, a large composite sample of the silt was blended, mixed to a prescribed water content, placed as a slurry in layers in one of the flexible testing boxes (i.e., ESB), and consolidated to a prescribed vertical stress prior to placement in the centrifuge. In order to evaluate differences in the cyclic behavior of the reconstituted silt in the centrifuge model and the field a suite of cyclic DSS tests was performed on reconstituted specimens. The testing of reconstituted specimens facilitated comparison with both the cyclic behavior of reconstituted soil in the centrifuge and the intact, relatively undisturbed specimens. The method of specimen preparation commonly used for sand-like soils (e.g., dry- or moist-tamping, air- or water-pluviation) has been demonstrated to influence the stress-strain behavior in cyclic testing. For this investigation a method of mixing the soil in a slurry consistency then consolidating to a prescribed stress was followed for both the DSS and centrifuge testing. The cyclic resistance and post-cyclic behavior were then evaluated as functions of effective confining stress, stress history, and low-strain stiffness (V_s) for both intact, relatively undisturbed specimens and reconstituted specimens.

Geotechnical investigations for major projects adjacent to the Elliott Bay waterfront provide a large base of in situ and laboratory data on the local soil deposits. General overviews of these projects have been prepared by Perkins, Chang, and Mitchell (2006); Bayrack et al. (2019); and Perkins and Malinak (2019). The project team has drawn from cyclic testing data sets obtained during the following specific projects:

1. SR 99: Alaskan Way Viaduct and Seawall Replacement Project (UCLA for Shannon & Wilson, 2004).
2. Alaskan Way Viaduct & Seawall Replacement Program (Shannon & Wilson, 2008a, b), and Elliott Bay Seawall Project (Shannon & Wilson, 2013).
3. Seattle Multimodal Terminal at Colman Dock, King County, WSDOT / Washington State Ferries (Golder Associates, 2015).

A summary of laboratory index tests on specimens of the estuarine silt specimens tested in the previously listed projects is provided in Table E.1.

E-3 CHARACTERIZATION OF THE SILT

The silt used for this comparison of testing procedures has been described (Shannon & Wilson, 2004, 2008a, 2008b, 2013) as representative of Holocene estuarine deposits (He) that were deposited in the relatively quiet waters of the ancient Duwamish River estuary and Elliott Bay. Along the Elliott Bay seawall, these estuarine deposits typically consist of very soft to medium stiff, low-plasticity silt and clayey silt to silty clay with minor amounts of fine sand. Interbeds of organic-rich soils exist within this unit.

The silt deposits are generally found underlying several feet to several tens of feet of fill and interlayered within and above beach (Hb) deposits. These sediments have not been glacially overridden and are normally consolidated to slightly over-consolidated.

E-3.1 SUPPLEMENTARY TESTING AND IMAGING

Samples of the estuarine silt were provided for Scanning Electron Microscopy (SEM) and X-Ray Diffraction (XRD) analysis in support of the research. Selected SEM images provided in Figures E.1a to E.1c highlight the general grain shapes, the inclusion of biogenic material such as shells (tests) of microorganisms, and fine, decomposed roots, which likely originated as marsh grass on exposed tidal flats. Platy and prismatic grains are prevalent in many of the SEM images of this silt. The results and description of the XRD analysis on specimens of silt from four different boreholes included the following summary addressing the mineralogy and genesis of the soil (Glasmann, 2008):

> *"Mineralogically, the clay assemblage includes smectite, chlorite, minor amounts of biotite/muscovite, and kaolinite. Non-clay minerals also included in the clay-size material consist of zeolite (heulandite), amphibole, calcic to intermediate plagioclase, pyroxene, quartz, and amorphous glass. These minerals are consistent with a dominance of Cascadian sediments. The silt fraction is generally dominated by plagioclase and amorphous material. The quartz/plagioclase ratio is very characteristic of andesitic/basaltic volcanics."*

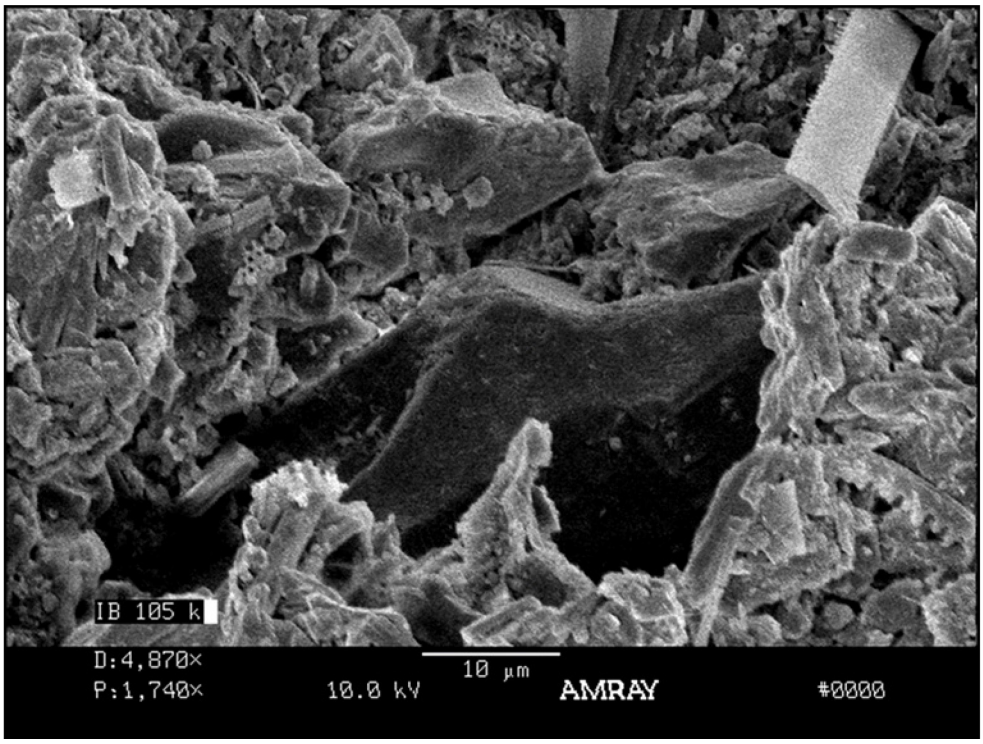

Figure E.1a: SEM image of Holocene Elliott Bay Estuarine (He) Silt, showing mixture of mineral grains and biogenic particles.

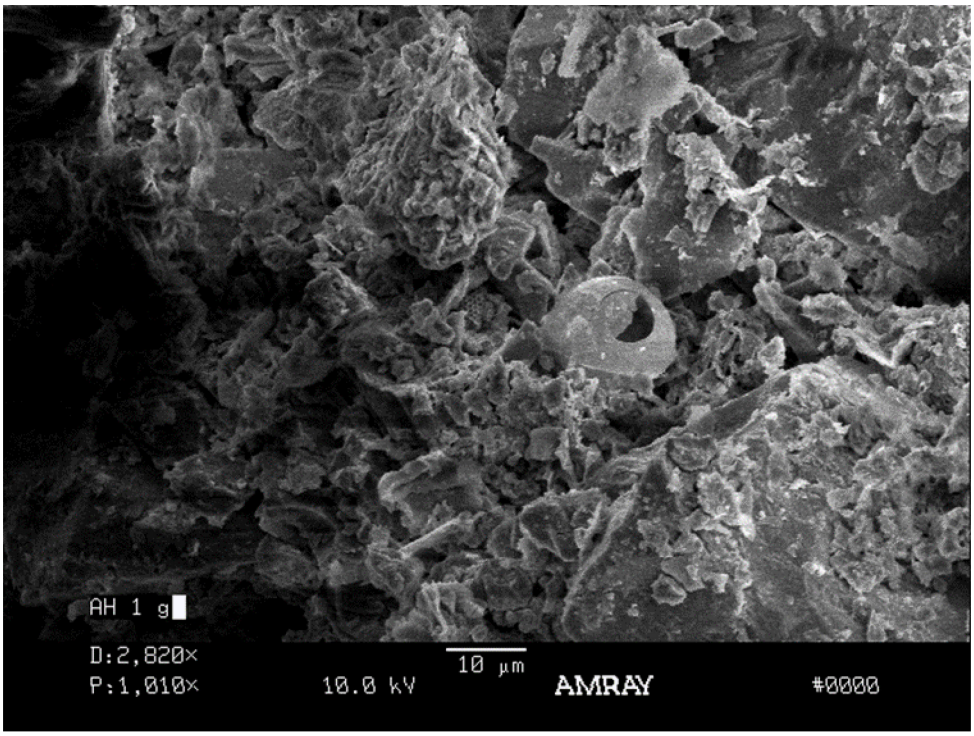

Figure E.1b: SEM image of Holocene Elliott Bay Estuarine (He) Silt, showing fabric of mineral grains and biogenics.

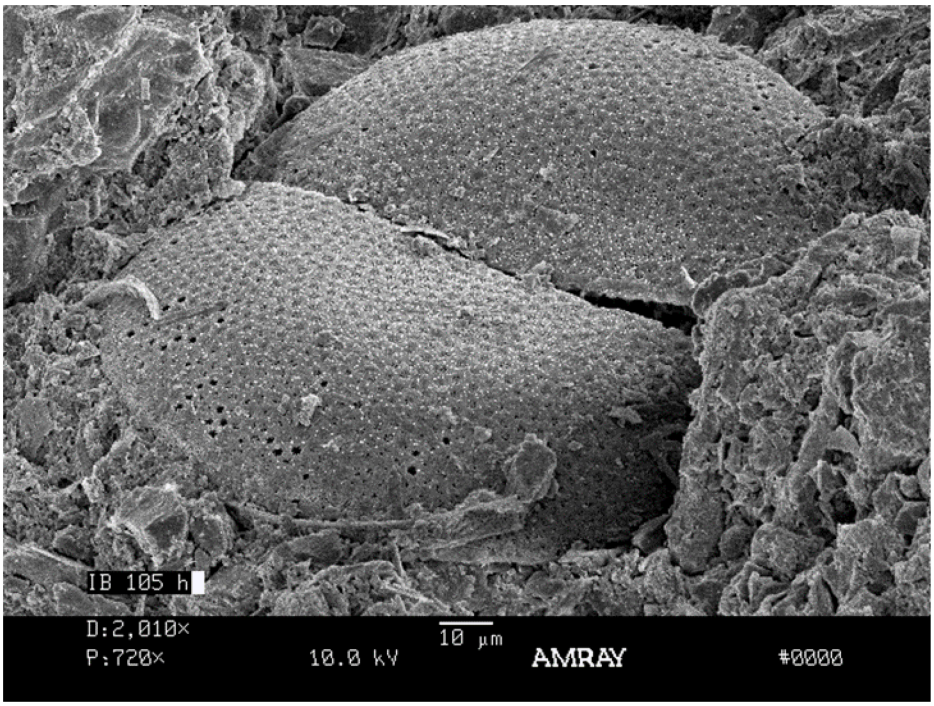

Figure E.1c: SEM image of Holocene Elliott Bay Estuarine (He) Silt, focusing on biogenic material.

E-4 PREPARATION OF THE RECONSTITUTED SPECIMENS

E-4.1 SLURRY PREPARATION

Grab samples of the silt tested at the U.C. Davis geotechnical centrifuge were obtained for transport to the laboratory. The volume of the moist soil was roughly 2.5 ft^3 and the average water content of four specimens from the sample was 25.8% (range 24.3 to 26.9%). The target water content for the slurry was defined as 1.75 times the Liquid Limit of the silt to ensure a consistency and workability conducive to placement in the large diameter consolidometer used for this application. De-aired water was used, and mixing was achieved with a large ribbon mixer. Once the silt had been thoroughly mixed it was transferred into the consolidometer (Figure E.1).

Establishing the volume of slurry to be transferred into the consolidometer required estimation of the initial height of slurry in the cell that would provide an adequate height of silt after consolidation. The following information was necessary to complete this estimation:

1. The target final height after consolidation: 7.5-inch minimum.
2. Specific Gravity, Gs: 2.60 assumed.
3. Liquid Limit, LL: 31.6% from the average of three Atterberg Limits tests.
4. Consolidation Pressure, σ'_{v_con}: 200 kPa (29 psi).
5. Compression Index, C_c: 0.60 assumed.
6. Initial void ratio, e_o: 1.46 based on water content of 1.75 * LL.

It was estimated that the change of sample height due to primary consolidation would be approximately 52% of the original height, thus the initial target height of the slurry was set at 17 inches. The volume of slurry required to fill the consolidometer and the limited volume of the ribbon mixer required that the sample be mixed in several batches then combined. It is instructive to note that the laboratory research team reported the following in their daily notes:

> *"As expected, the soil was not the easiest to mix. With the combination of the stiffness of the soil clumps and the large amount of water used, it made a mess."*

It was also noted; however, that after 30 minutes of mixing the soil was thoroughly mixed with the exception of a few small clumps. These clumps and any particles larger than the No. 40 sieve were screened out before placement into the consolidometer.

Specimens for water content determinations were collected at three locations within the slurry immediately after mixing. The average water content was 58%, slightly above the target value of 56%, but suitable for continuing to the consolidation stage of the sample preparation.

E-4.2 CONSOLIDATION PROCEDURE

The mixed slurry was immediately placed into the consolidometer with care to minimize the trapping of air bubbles during pouring. After slurry placement the top plate was installed, and bottom and top drainage lines were connected. A vacuum pressure of 24-inches Hg was applied for approximately 30 minutes to remove any air between the soil and the top plate. The slurry was then prepared for consolidation.

The target consolidation pressure was 200 kPa (29 psi). The consolidation stress was applied in ten increments of approximately 3.0 psi, each increment added within a 2-minute period until 29 psi was achieved. The time at which consolidation was considered to have been initiated was at the application of the full consolidation stress of 29 psi. Vertical displacement was recorded from this time forward. The consolidation stress was applied until the sample was determined to have passed an average degree of consolidation of 90% (t_{90}). This was tracked by plotting the vertical displacement versus the square root of time (i.e., Taylor's method). The consolidation process took approximately five days.

The initial height of slurry in the consolidometer was 19.94-inches. The total consolidation settlement was 5.69-inches, which indicates a Compression Index, C_c, of 0.31, roughly half the initially estimated value of 0.60. This result was fortuitous as the final height of the consolidated sample was 14.25-inches, roughly twice the target height.

The time-rate of consolidation characteristics of the slurry were also computed from the data obtained during loading in the consolidometer. The coefficient of consolidation, c_v, for the slurry

was 0.012 in^2/min (42.4 ft^2/year). The final water content after consolidation was 31.7%, very closely matching the Liquid Limit of the material (Liquidity Index ≈ 1.0).

E-4.3 SAMPLING PROCEDURE

The final step in the preparation process involved sampling from the consolidometer using a 3-inch diameter Shelby tube. An apparatus was prepared to sample the soil by applying pressure to the base plate of the consolidometer and pushing the soil upward into a 14-inch-long Shelby tube, which was braced from lateral and vertical movement (Figure E.2). The soil was pushed up into the Shelby tube, with the soil surrounding the outside of the tube trimmed in small increments. The extra soil (trimmings) was saved in a 5-gallon bucket. The total height of the consolidated soil was approximately 14-½ inches, with a total of 13-inches filling the Shelby tube. The roughly 1-inch void in the Shelby tube was filled with paraffin wax, then capped and taped. The sample tube was then prepared for shipping to MEG Consulting, Inc. (Richmond, B.C.) for cyclic DSS testing. The sample was shipped in a well-padded and sturdy box by overnight courier.

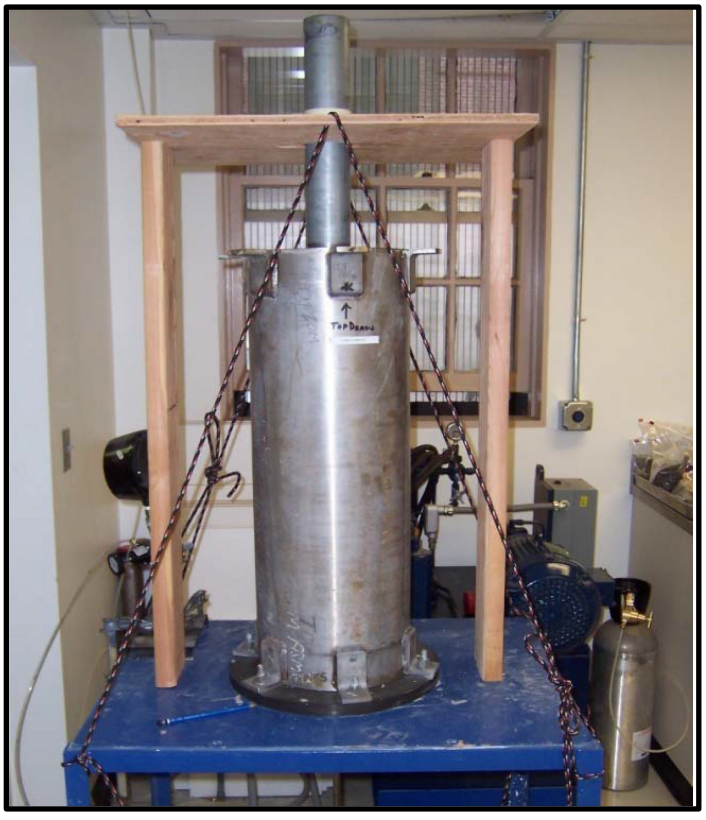

Figure E.2: Sampling Apparatus and Large-Diameter Consolidometer

E-5 RESULTS OF STATIC DSS TESTING OF RECONSTITUTED SILT

The DSS test was performed under constant volume conditions by deforming the specimen at a controlled rate of strain after the specimen is consolidated to the specified vertical stress and OCR. Detailed testing procedures for the DSS tests are described in ASTM D 6528.

The specimen was initially consolidated to a vertical stress of 480 kPa. The consolidation process was allowed to continue for about one log cycle of time or 24 hours, whichever occurred first, past the time for the end of primary consolidation (t_{100}) to ensure that the K_o condition is developed. The specimen was then unloaded to a vertical stress of 400 kPa to produce an OCR of 1.2.

The peak shear stress ($s_{\_st}$) of 88 kPa was mobilized at roughly 7.5% shear strain. The test was continued to a shear strain of 20%, at which the shearing resistance was approximately 77 kPa representing a roughly 12% reduction in shearing resistance with moderate strain. The resulting normalized strength ratio at failure (s_{u_st} / σ'_v) was 0.22. This value is consistent with trends of residual, or "mobilized", strength developed for normally consolidated soft clays and silts. This correlation suggests that the peak strength mobilized by the slurry consolidated specimen is similar to the residual strength of the soil in the field. The difference in the stress-strain-strength behavior of the reconstituted silt relative to specimens of undisturbed specimens is considered to be due, in large part, to the influence of fabric, aging, and cementation, and to a lesser, yet not unimportant, degree pore water chemistry and thixotropic hardening.

Static DSS tests on high quality specimens of silt obtained for the Alaskan Way Viaduct and Seawall Replacement Program (Shannon & Wilson 2008b) and other projects involving estuarine silt in the Puget Sound region have provided ranges of undrained strength ratios for normally consolidated to lightly-overconsolidated specimens of 0.21 to 0.28 and 0.24 to 0.29, respectively. The strength of the reconstituted silt is at the lower bound of the DSS lab data for undisturbed specimens of the same, and similar, deposits.

The undrained strength of the reconstituted specimen is approximately 25% less than values observed for native specimens of fluvial silt in the Pacific Northwest. The following relationship is provided for the sake of comparison (Beaty et. al. 2014):

$$s_{u\_st} / \sigma'_v = 0.25 \times (OCR)^{0.9} \qquad \text{Equation E-1}$$

For OCR of 1.2 the normalized undrained strength ratio is 0.295.

E-6 RESULTS OF CYCLIC DSS TESTING OF RECONSTITUTED SILT

Strain-controlled CDSS tests were performed on three specimens of the reconstituted silt. The objective of this testing was to monitor the progressive increase in excess pore pressure generation during cyclic loading at three different uniform shear strains. This procedure provides

data for the curve-fit parameters in the Vucetic-Dobry constitutive model for cyclic pore pressure generation, as outlined in Chapter 5 of this report. These pore-water pressure generation parameters (PPPs) were used to simulate the dynamic behavior of the reconstituted silt in the centrifuge model. The tests were performed under constant volume conditions according to the ASTM D 6528, using the following general procedures (MEG 2008):

1. Each test specimen was consolidated to an effective vertical consolidation stress (σ'_{vc}) equal to the targeted vertical stress condition (σ'_v). This consolidation process was allowed to continue for about one log cycle of time or 24 hours, whichever occurred first, past the time for the end of primary consolidation (t_{100}) to ensure that the K_o condition is developed.
2. Each specimen was initially consolidated to a vertical stress of 480 kPa then unloaded to a vertical stress of 400 kPa to produce an OCR of 1.2, in the same process followed for the static undrained test.
3. Following the consolidation process, cyclic horizontal shear strains (γ_c) were applied sinusoidally at strain amplitudes of 0.1, 0.4 and 1.8 percent. The γ_c was applied at constant volume with a specified frequency (i.e., 0.1 Hz) for 60 strain cycles (N=60). Since the test is performed at constant volume, the pore pressure in the sample is estimated by monitoring the changes in the vertical stress (σ_v) applied to the specimen during cycling.

The accumulation of excess pore pressure during cyclic loading was monitored and plotted as Excess Pore Pressure Ratio (R_u) versus Cyclic Shear Strain (Figure E.3). and Excess Pore Pressure Ratio versus Loading Cycles (Figure E.4). The contours for the Number of Cycles were developed using the Vucetic – Dobry constitutive model, with the PPP's provided in the legend.

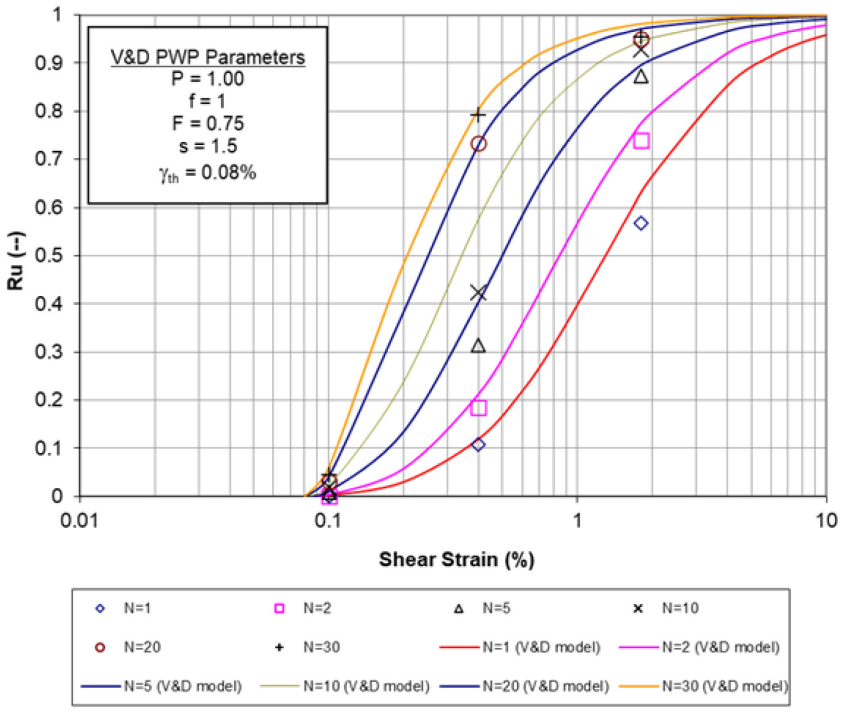

Figure E.3: Excess pore pressure ratios versus cyclic shear strain from strain-controlled CDSS tests and calibrated V&D models for reconstituted lightly overconsolidated (OCR = 1.2) specimens of Holocene, estuarine silt from the Seattle waterfront (ID W_04).

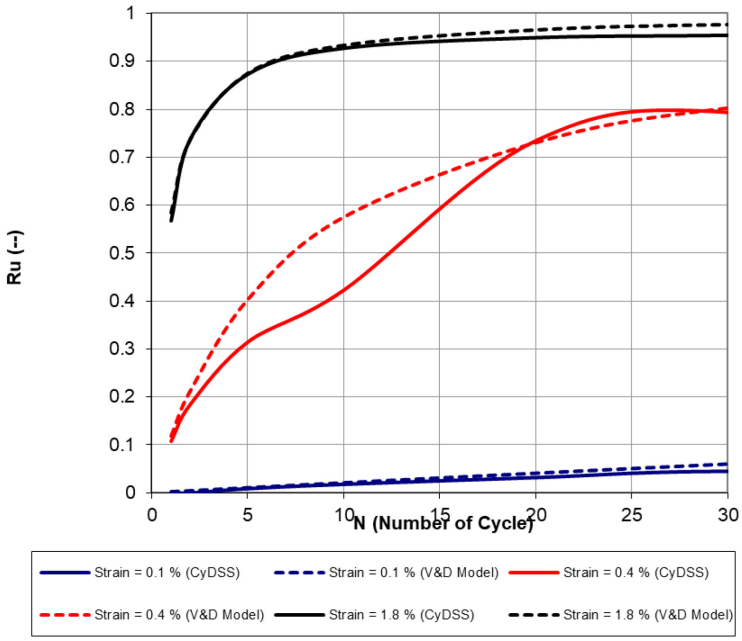

Figure E.4: Comparison of measured and predicted Ru from CDSS tests and calibrated V&D model for lightly overconsolidated (OCR = 1.2) reconstituted samples of estuarine silt from the Seattle Waterfront – Elliott Bay (ID WA_04).

E-7 RESULTS OF POST-CYCLIC DSS TESTING OF RECONSTITUTED SILT

Post-cyclic, monotonic (static) shear tests were performed on each specimen immediately after the cyclic loading stage of the test sequence in order to assess the influence of cyclic loading on the strength and stiffness of the reconstituted silt. The softening, or degradation, of the specimens was evaluated for three important aspects of stiffness, stress-strain, and post-cyclic shearing resistance; (i) low-strain shear stiffness (V_s) immediately after cyclic loading, (ii) monotonic stress-strain behavior after cyclic loading normalized by the initial static stress-strain behavior, and (iii) the ratio of the post-cyclic peak shearing resistance to the static undrained shear strength. Each of these metrics for cyclic softening were found to be correlated with the excess pore pressure generated at the end of cyclic loading. All of the cyclic tests were conducted to 60 cycles therefore the influence of duration of the cyclic loading was not directly evaluated in this suite of tests.

The test procedure was conducted as follows (MEG 2008); once the sample had been tested under cyclic loading and without allowing any consolidation or dissipation of the final excess pore pressure condition, the sample was statically sheared at constant volume and at a constant strain rate (i.e., 5%/hour) in accordance with the general procedure described in ASTM D 6528.

As presented in Chapter 3, the influence of cyclic loading on undrained shearing resistance can be simply evaluated by the ratio of the post-cyclic shear strength to the static shear strength ($\tau_{f\text{-}post\ cyclic}$ / s_{u_st}). This ratio is often used in post-seismic slope stability analysis using Limit Equilibrium methods. The reduction, or degradation, of shear strength has been found to be a function of excess pressure generation during cyclic loading, which is directly linked to the number of cycles of loading and accumulated cyclic shear strain. The reduction in shear strength due to cyclic loading obtained in the three tests is provided in Table E-1.

It is noted that for the tests at cyclic shear strains of 0.10% and 0.40% the post-cyclic strength was greater than the static undrained strength. This apparent increase in strength may be due to inherent variability in the specimens and testing procedures. The small data set should not be interpreted to suggest that a nominally 7% increase in undrained strength is expected after cyclic loading at low- to moderate-strain. An important observation can be made; however, that cyclic degradation of shear strength appears to be negligible for cyclic loading at shear strain reaching 0.4% and R_u of approximately 70%. This finding must also be tempered by the limited data set. The test at 1.8% cyclic shear strain resulted in much greater R_u and associated reduction in post-cyclic shear strength, and clearly demonstrates the influence of high cyclic pore pressure generation on the post-cyclic shear strength.

TABLE E-1: Summary of Cyclic Direct Simple Shear Testing of the Holocene Estuarine Silt from the Seattle Waterfront – Elliott Bay

Project	BH	Specimen	Soil Description	Depth, ft	In Situ		Consistency		Cyclic DSS Testing			
					w_n	V_s	LL	PI	Control	σ'v[a]	OCR	V_s
					%	ft/sec				lb/ft^2		ft/sec
Dickenson (2008)	Composite	Reconstituted	Brown to Dark gray SILT (ML)	--	30.0[b]	--	31.6[c] 35.3[d]	-- 8.5	Strain	8356	1.2	791[e]
AWV (2004)	SDC-001	S-18	--	71	38.4	500	36	4	Stress	4032	1.0	--
	SDC-001	S-24	--	86	35.6	525	28.2	5.1	Stress	4658	1.0	--
	SDC-001	S-24	--	86	35.2	525	*36*	*14*	Stress	8356	1.0	--
	SDC-002	S-19	--	52	38.7	550	34	9	Stress	3134	1.0	--
AWV&SRP (2008)	IB-213	S-17	Blackish Brown SILT (ML)	54	36.8	*480*	37	9	Stress	3592	1.0	--
	IB-222	S-19	Blackish Brown SILT (ML)	64	34.2	*490*	37	10	Stress	4104	1.0	--
Colman Dock (2012)	BH04-11	S-5	Dark gray SM & CL/ML	16	22	--	22	6	Stress	459	1.0	--
	BH01-11	S-9	Dark gray CLAY (CL)	24	50	--	45	20	Stress	668	1.0	--
	BH05A-11	S-3	Dark gray SILT (ML)	14	56	--	44	16	Stress	459	1.45	--
	BH05-11	S-5	(CL)	19	46	--	39	16	Stress	459	1.5	--
	BH04-11	S-6	(ML-CL)	18	49	--	40	15	Stress	480	1.48	--

Notes:

a. Vertical Effective Stress at the initiation of cyclic loading.

b. Average water content of 4 specimens prepared for DSS testing (i.e., prior to consolidation in the DSS apparatus).
c. Liquid Limit testing of specimen from the composite sample of silt (Laboratory #1 tested during preparation of the reconstituted slurry).
d. Atterberg Limits testing of specimen from the composite sample of silt (Laboratory #2 tested during cyclic testing program).
e. Average of Bender Element V_s tests made on 4 specimens after consolidation to 480 kPa and unloading to a vertical stress of 400 kPa (OCR = 1.2).

E-8 COMPARISON OF DSS TESTS ON RECONSTITUTED AND UNDISTURBED SPECIMENS

The test sequence on reconstituted silt provides a worthwhile comparison with the DSS test results for high-quality, relatively undisturbed specimens from the same deposit. The generation of excess pore pressure and post-cyclic stress-strain behavior of the soil are summarized as follows.

E-8.1 CYCLIC EXCESS PORE PRESSURE GENERATION

The cyclic DSS data obtained by Vucetic (2004) has been selected for comparison and the Vucetic – Dobry pore pressure algorithm applied for both data sets. Two important differences in the test sequences are noted; (i) the reconstituted specimens were tested at an OCR of 1.2 and the intact, relatively undisturbed specimens were tested at OCR of 1.0, and (ii) the tests on reconstituted specimens and intact specimens were performed using strain-controlled and stress-controlled procedures, respectively.

The progressive increase in excess pore pressure with cyclic shear strain and number of load cycles for four intact specimens are plotted in Figures E.5 and E.6, respectively.

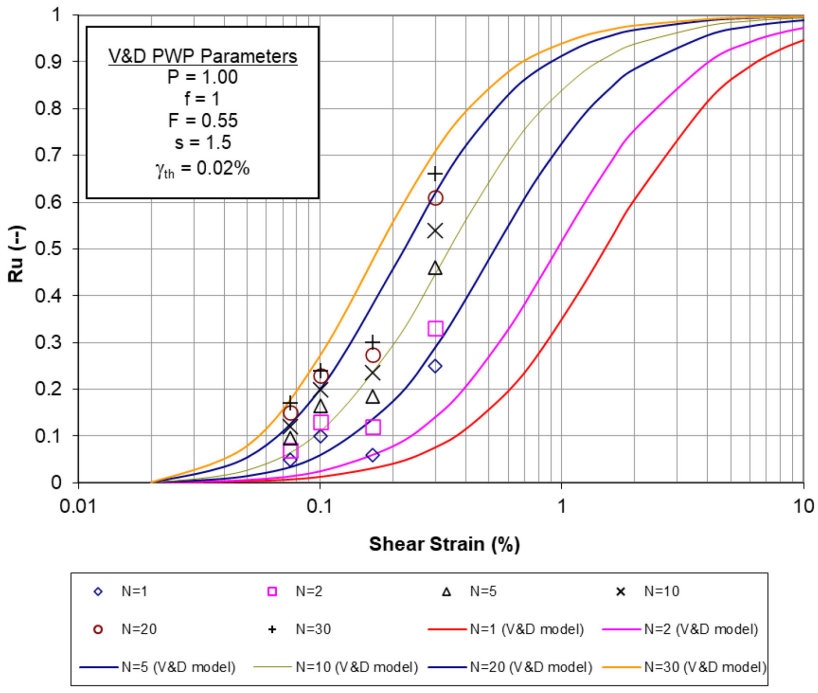

Figure E.5: Excess pore pressure ratios versus cyclic shear strain from CDSS tests and calibrated V&D models for intact, relatively undisturbed, normally consolidated specimens of Holocene, estuarine silt from the Seattle waterfront (after Vucetic 2004).

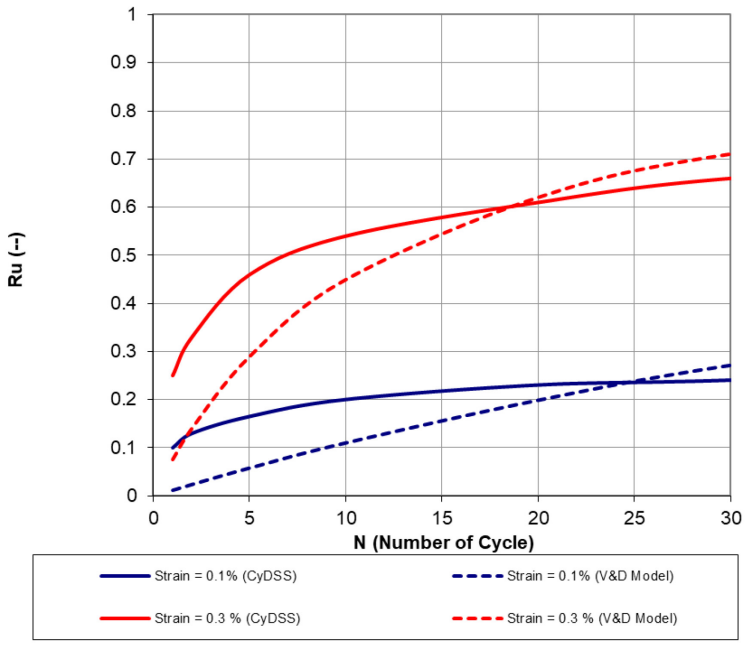

Figure E.6: Comparison of measured and predicted Ru from CDSS tests and calibrated V&D model for intact, relatively undisturbed, normally consolidated samples of estuarine silt from the Seattle Waterfront – Elliott Bay (after Vucetic 2004).

The comparison of trends in excess pore pressure generation for the undisturbed and reconstituted specimens, as simulated using the Vucetic-Dobry (V&D) pore pressure model, is provided in Figure E.7. The rate of pore pressure development at 5 cycles of loading is very similar for both the reconstituted and intact specimens, suggesting similar cyclic resistance; however, the difference in stress history (i.e., OCR) must be taken into consideration. The effect of OCR on the pore pressure parameters used in the Vucetic-Dobry algorithm is addressed in Chapter 5 of this report. It appears in this instance that the any inherent decrease in cyclic resistance to excess pore pressure development in reconstituted specimens may be offset, in part, to the greater OCR as tested (1.2 as opposed to 1.0 for the intact specimens). The rate of pore pressure development at 30 cycles of loading is greater for the intact specimens at smaller cyclic shear strains (≤ 0.20%), although the trends for both intact and reconstituted specimens converge at greater cyclic shear strain. Again, this similarity may be attributed to the shear histories of the specimens.

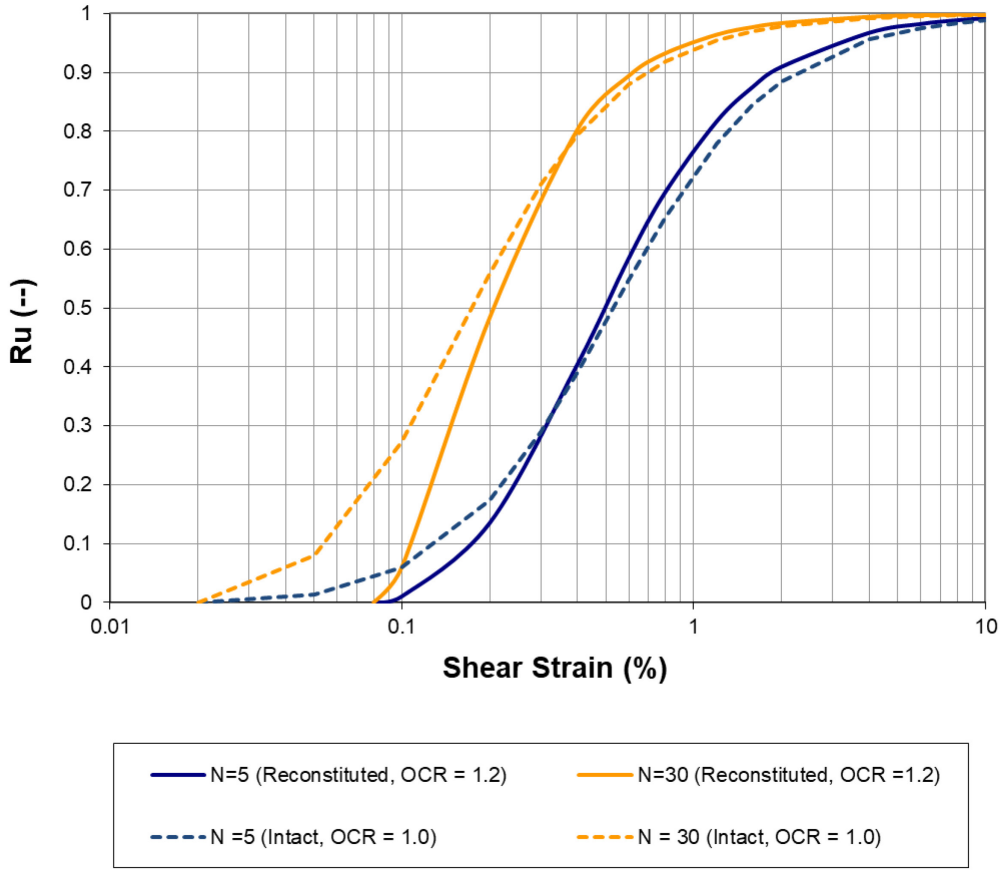

Figure E.7: Comparison in trends of excess pore pressure ratio development for intact and reconstituted specimens of the Holocene, estuarine silt as a function of cyclic shear strain and number of load cycles.

E-8.2 POST-CYCLIC STRENGTH

As addressed in Chapter 3 of this data report, the post-cyclic shear strength of fine-grained soils is reported in the form of a post-cyclic strength ratio $(\tau_{cyc} / S_{u\text{-}st})_{Y=x}$, where:

τ_{cyc} : Shearing resistance at a reference shear strain in the post-cyclic monotonic test,
S_{u_st} : Static undrained shear strength at the same reference shear strain

This convention as an index to post-cyclic behavior is followed in this appendix. A suite of four DSS tests was performed on specimens of the reconstituted silt to evaluate the influence of cyclically induced pore pressure generation on the post-cyclic behavior. The assessment of post-cyclic testing of shear strength was limited to three specimens, the results of which were normalized by the results of a single static undrained (constant volume) test. In light of the small data set, the resulting trend and interpretation should be tempered by uncertainties associated with inherent variability in test

results. A lower bound static undrained strength, for example, would bias the post-cyclic strength ratio toward larger values (i.e., less apparent cyclic degradation and potentially unconservative results). This bias could be evaluated with a larger data set and mean static shear strength.

The post-cyclic strength ratios from three tests are plotted in Figure E.8 as a function of the maximum pore pressure generated in the cyclic stage of the test. Note that this figure is modified from Figure 3.10, with an explanation for the trends provided in Section 3-3.3. In general, cyclic degradation of shear strength was negligible to cyclically induced excess pore pressure ratios in the range of 0.6 to 0.7. This exhibits significantly less cyclic reduction in undrained strength (i.e., degradation) than observed for the other soils in the Ru range of 0.4 to 0.7. The trend in the post-cyclic strength ratio with excess pore pressure then decreased at a rate that is in general agreement with DSS testing of other reconstituted fine-grained specimens (Ajmera et al., 2019), although the absolute value of the strength ratio is significantly greater.

The comparison of the limited data for reconstituted specimens of a Holocene estuarine silt with data trends for various intact specimens is provided to illustrate potential differences in post-cyclic strength due to specimen preparation. Quantification of the influence of potentially important factors (e.g., fabric, pore water chemistry, composition, consistency, and aging) was not investigated for inclusion in this data report. Instead, general lessons learned from this assessment are summarized in the following section.

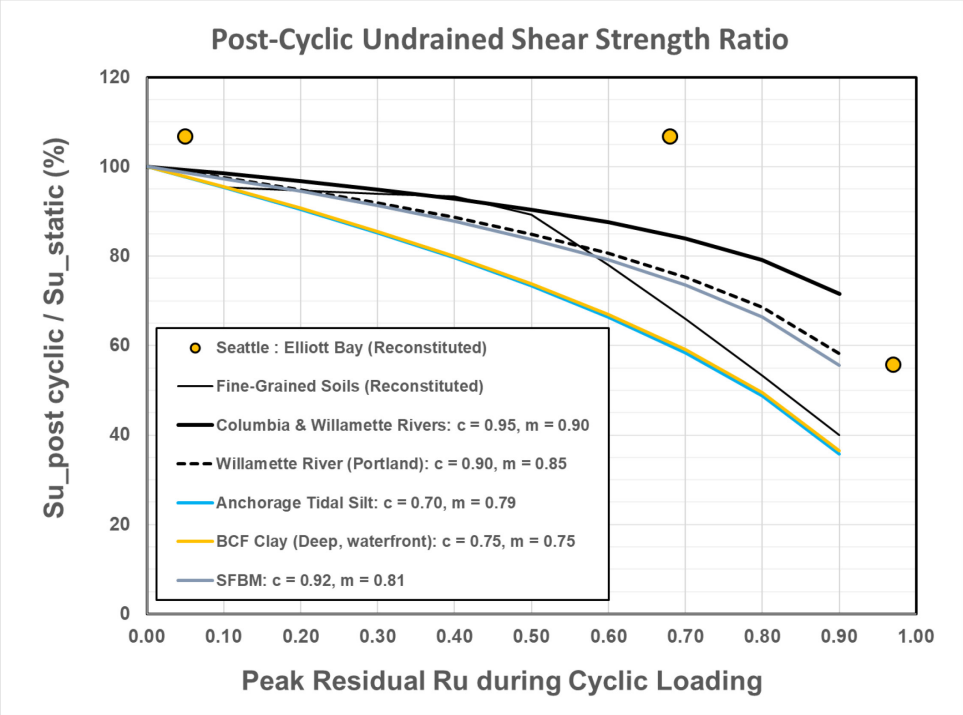

Figure E.8: Post-cyclic strength ratio for three reconstituted specimens of the Seattle – Elliott Bay Holocene estuarine silt and comparison to trends for other intact and reconstituted specimens of fine-grained soils.

E-9 PRIMARY FINDINGS AND CONSIDERATIONS FOR PRACTICE

The testing of reconstituted specimens of silt summarized in this appendix was performed for a research application involving large-scale centrifuge testing. Fabrication of the centrifuge model required the use of reconstituted silt prepared as a slurry, which was poured into place then consolidated using a large press. This procedure warranted the application of a similar procedure, at a smaller scale, to provide specimens for complementary testing in DSS. The primary objective was the direct comparison of cyclic behavior of the reconstituted silt in both series of tests (centrifuge and CDSS), and the calibration of constitutive models that could be applied to simulate the dynamic response of the centrifuge model. This testing program also facilitated the comparison of cyclic and post-cyclic behavior of relatively undisturbed specimens of silt from the same deposit for the sake of identifying the strengths and limitations inherent in testing reconstituted specimens.

The complete remolding of the silt during the mixing process is considered the primary shortcoming of testing reconstituted specimens for project-specific applications involving native, intact soil units. The in-situ fabric cannot be replicated in the lab; thus, the void ratio, stiffness, and stress-strain behavior of the reconstituted specimen will not match that of the in-situ soil under the same effective confining stresses and stress history (i.e., OCR). The influence of variations in pore water chemistry, aging, and cementation can also significantly impact the behavior of the silt. For these reasons, the direct application of DSS results on reconstituted specimens must be made with considerable engineering judgment.

It is noted that for research applications the use of reconstituted specimens may be useful, and perhaps advantageous due to sample uniformity, for examining the relative influence of various parameters on cyclic and post-cyclic behavior. The ability to test a suite of uniform specimens under controlled conditions may provide useful trends for the influence of various external conditions (e.g., depth-effects and confining stress, static shear bias, stress history, stress path) on the characterization of cyclic resistance, rate of strain accumulation, excess pore pressure generation and post-cyclic strength

The following general findings and considerations for practice have been compiled on the basis of the testing summarized in this appendix.

1. The preparation of moderate to large volume silt specimens from a slurry is labor and time intensive.
2. The following aspects of sample preparation warrant project-specific application:
    a. Batch mixing at water contents greater than 1.5 x Liquid Limit,

b. Method of consolidation of the slurry (i.e., size of sample, method for application of vertical load, estimation of void ratio at the end of primary consolidation, and time to completion of consolidation),
c. Method of obtaining specimens of the consolidated silt from the bulk sample,
d. Specimen preparation for testing in DSS follows routine procedures apply for undisturbed specimens.

3. The consolidation stress applied in the DSS apparatus should be selected with the following in mind:
    a. Determination of vertical stress that is consistent and reasonable for the post-construction conditions at the project site.
    b. The final vertical effective stress and OCR prior to the shearing phase of the test (i.e., static monotonic or cyclic loading).
    c. The target void ratio of the specimen prior to the shearing phase
    d. The target low-strain stiffness of the specimen prior to the shear phase
4. Shear wave velocity (V_s) measurements in static and post-cyclic lab tests provide necessary data for evaluating the variation in shear stiffness between soil in the field and in the lab.
5. Use of cyclic laboratory data on reconstituted specimens for element-level calibration of constitutive models used in practice (e.g., PM4Sand, PM4Silt, Vucetic - Dobry Pore Pressure Parameters), should be judiciously applied for project applications involving initially undisturbed soil units.
6. In this investigation the peak static undrained shear strength ratio of reconstituted silt was representative of residual strength in DSS testing, or "mobilized" strength back-calculated from slope failures in fine-grained soils. This static strength ratio is less than ranges applicable for undisturbed specimens the Holocene estuarine silt in the lower Duwamish – Elliott Bay region and other estuarine, coastal, and fluvial silt deposits in the Pacific Northwest.
7. The rate of pore pressure development was similar for the reconstituted and intact, relatively undisturbed specimens. The similarity in pore pressure generation may have been due, in part, to offsetting influence of the following; (i) fabric, aging and minor cementation that would have acted to decrease the rate of pore pressure generation in the intact specimens relative to the reconstituted specimens at the same OCR, (ii) the slightly greater OCR of the reconstituted specimens, which would have resulted in a greater cyclic resistance (i.e. lower rate of pore pressure generation), and (iii) the possible influence of geostatic stress on the rate of pore pressure generation. The latter issue was not evaluated for this data report and is the focus on on-going investigation by the project team.
8. Cyclic degradation of undrained shear strength was evaluated with DSS testing a one static test (the benchmark) and three post-cyclic monotonic tests. The three post-cyclic tests were performed on specimens loaded for 60 cycles at uniform shear strains of 0.1%, 0.4% and 1.8%, and the resulting excess pore pressure ratios at the end of the cyclic stages of the three tests were 5%, 69%, and 97%, respectively. The reduction in undrained shear strength, at 10% shear strain, was negligible for the tests resulting in Ru values of 5% and 69%. This trend

of post-cyclic strength indicated a significantly smaller influence of Ru on cyclic degradation than observed in many intact, native soils (refer to Chapter 3). The trend in post-cyclic strength inferred from data for the third test (1.8% and Ru = 97%) suggests significant reduction in shear strength for Ru greater than 0.7, with a rate of degradation that is consistent with other data sets for reconstituted soils (e.g., Ajmera et al., 2019). It is noted that the post-cyclic strength ratio for the third test, at high Ru, was within the range for intact specimens of the five silts and clays plotted in Figure E.8.

9. Testing for post-cyclic volumetric strain was not performed in this investigation therefore no guidance is provided for interpretation and application of one-dimensional reconsolidation of reconstituted silt.

E-10 REFERENCES

Ajmera, B., Brandon, T., & Tiwari, B. (2019). Characterization of the reduction in undrained shear strength in fine-grained soils due to cyclic loading. *Journal of Geotechnical and Geoenvironmental Engineering*, *145*(5), 04019017.

Bayrak, M.B., Mikhail, R., Wray, M., Mjelde, J., and Hegge, W.S. (2019). Geotechnical and Structural Challenges: New Seattle Multimodal Terminal at Colman Dock Project, Proc. of ASCE Ports '19, pp. 216 -226.

Beaty, M., Schlechter, S., Greenfield, M., Bock, J., Kempner Jr., L., and Cook, K. (2014). Seismic Evaluation of Transmission Tower Foundations at River Crossings in the Portland – Columbia River Region, Proc. of the Tenth U.S. National Conference on Earthquake Engineering, Frontiers of Earthquake Engineering.

Blaker, O. and DeGroot, D.J. (2020). Intact, Disturbed, and Reconstituted Undrained Shear Behavior of Low-Plasticity Natural Silt, Journal of Geotechnical and Geoenvironmental Engineering, ASCE, 146(8).

Dahl, K.R. (2011). Evaluation of Seismic Behavior of Intermediate and Fine-Grained Soils, Dissertation, Civil & Environmental Engineering, Univ. of California, Davis.

Glasmann, R.J. (2008). Letter report to S. Dickenson; "XRD Analysis of Silt Samples from Alaskan Way Viaduct Excavation," Willamette Geological Service, Philomath, Oregon.

Golder Associates (2015). Seattle Multimodal Terminal at Colman Dock, King County, WSDOT / Washington State Ferries, 30% Geotech Recommendations Report, Appendix A; Dynamic Laboratory Tests on Samples from Seattle Ferries project, report prepared by MEG Consulting Ltd. (January 9, 2012).

MEG (2008). Letter report: Dynamic Laboratory Tests, CycDSS testing on SILT, prepared for S. Dickenson, MEG Consulting Limited, 24 December 2008.

Perkins, W.J., Chang, S.W., Mitchell, R.A. (2006). The Alaskan Way Viaduct Project: An Example of Geologic and Geotechnical Earthquake Engineering Practice in the Pacific Northwest, GEOSTRATA, ASCE, Vol. 7, Issue 6, Nov/Dec, pp. 30 – 34.

Perkins, W. and Malinak, A. (2019), Ground Improvement Design and Construction for Seattle's Elliott Bay Seawall Replacement and Retrofit, *DFI Journal*, v. 13, no. 2, p. 1 – 11.

Shannon & Wilson, Inc. (2004). SR 99: Alaskan Way Viaduct and Seawall Replacement Project, Seismic Ground Motion Study Report, prepared for WSDOT, Urban Corridors Office, Seattle, WA, October.

Shannon & Wilson, Inc. (2008a). Alaskan Way Viaduct & Seawall Replacement Program, Geotechnical and Environmental Data Report – S. Holgate Street to S. King Street Viaduct Replacement Project, Volume 1 of 2, prepared for WSDOT Urban Corridors Office, Seattle, WA, December.

Shannon & Wilson, Inc. (2008b). Alaskan Way Viaduct & Seawall Replacement Program, Geotechnical and Environmental Data Report – S. Holgate Street to S. King Street Viaduct Replacement Project, Volume 2 of 2, prepared for WSDOT Urban Corridors Office, Seattle, WA, December.

Shannon & Wilson, Inc. (2013). Elliott Bay Seawall Project, Geotechnical Engineering Report, prepared for City of Seattle, Department of Transportation, Seattle, WA, July.

Soysa, A.N. (2015). Monotonic and Cyclic Shear Loading Response of Natural Silts, Thesis, Civil Engineering, Univ. of British Columbia, Vancouver.

Vucetic, M. (2004). Results of Seven Cyclic Simple Shear Tests on Five Soils Conducted for Shannon & Wilson, Inc., provided as Appendix J "Laboratory Testing - Dynamic Soil Tests by University of California at Los Angeles, August" in Shannon & Wilson (October 2004).

Wang, J-H., Moran, K., and Baxter, C.D.P. (2006). Correlation between Cyclic Resistance Ratios of Intact and Reconstituted Offshore Saturated Sands and Silts with the Same Shear Wave Velocity, Jrnl. of Geotechnical and Geoenvironmental Engineering, ASCE, 132(12), 1574-1580.

Wijewickreme, D., Soysa, A., and Verma, P. (2019). Response of natural fine-grained soil for seismic design practice: A collection of research findings from British Columbia, Canada, Soil Dynamic and Earthquake Engineering, 124, 280-296.

WSDOT (2021). Geotechnical Design Manual, M 46-03.12, Section 6-4.2.6 Assessment of Liquefaction Potential and Effects Using Laboratory Test Data, page 6-38.

E-11 ACKNOWLEDGEMENTS

The centrifuge testing program was sponsored by the USGS National Earthquake Hazard Reduction Program. The first author greatly appreciates the interest in dynamic silt behavior and encouragement provided by Art Frankel (USGS).

Considerable in-kind support was provided by the Center for Geotechnical Modeling (CGM), Civil & Environmental Engineering, University of California, Davis. The project greatly benefitted from the insights and numerous contributions provided by; Prof. Ross Boulanger, Dr. Dan Wilson, and Prof. Bruce Kutter.

Significant in-kind support was also provided by Shannon & Wilson, Inc. (Seattle, WA). This support was crucial for the centrifuge testing and included the following: geotechnical and geophysical project reports for the Alaskan Way Viaduct & Seawall Replacement Program, recommendations for characterization and testing of the silt, and most importantly, providing approximately 2,000-lb of the Holocene estuarine silt used in the centrifuge.

The following individuals are also acknowledged for their tremendous contributions to the investigation:

- Ben Haines, FHWA (formerly S&W, Seattle, WA), for his efforts to secure the silt for testing at the UCD CGM, transport of the silt to Corvallis, and his assistance in providing project reports.
- Michael Eller, Kleinschmidt Associates. This appendix was developed as an expanded reporting of his efforts in the lab: preparation of the reconstituted silt, consolidation testing, index tests, sampling, and coordination of the cyclic testing with MEG Consulting, Ltd.
- Drs. John Sully and Ender Parra, MEG Consulting, Ltd., who oversaw the cyclic and post-cyclic testing, and provided insights on the behavior of the reconstituted specimens relative to native, undisturbed silt.